January 2009

Role And Regulation Of ESCRT-III In Multivesiculr Body Biogenesis

Soomin Shim
Washington University in St. Louis

WASHINGTON UNIVERSITY IN ST. LOUIS

Division of Biology and Biomedical Sciences

Program in Molecular Cell Biology

Dissertation Examination Committee:
Dr. Phyllis Hanson, Chair
Dr. Kendall Blumer
Dr. Valeria Cavalli
Dr. Maurine Linder
Dr. Robert Mecham
Dr. Alan Shiels

ROLE AND REGULATION OF ESCRT-III IN MULTIVESICULR BODY BIOGENESIS

by

Soomin Shim

A dissertation presented to the
Graduate School of Arts and Sciences
of Washington University in
partial fulfillment of the
requirements for the degree
of Doctor of Philosophy

August 2009

St. Louis, Missouri

ACKNOWLEDGEMENTS

First of all, I would like to thank my advisor, Phyllis Hanson for her excellent mentoring and wonderful support throughout my thesis study. I also would like to thank my committee: Drs. Robert Mecham, Maurine Linder, Ken Blumer, Alan Shiels and Valeria Cavalli for their wonderful advice and support.

I could not have made it this far without support from the members of the Hanson Lab. I would like to thank current and former members of the Hanson lab for their help and support. In particular, I would like to give special thanks to Teri Naismith for her wonderful advice on lab work and life. I also feel absolutely lucky to have wonderful friends as well as scientific colleagues, Sam Merrill and Abby Buchwalter Vander Hyden.

There are many people outside of the lab who helped me during graduate school. First, I would like to thank Dr. Douglas Berg in the Dept. of Molecular Microbiology for encouraging me to apply to the Ph.D. program at Washington University, and giving me advice whenever I asked. I would like to thank many Korean students in DBBS for being wonderful friends in particular, Seol-Hee Im, Jae-Eun Kang, Hyungjin Kim, Gyusang Jung, Jung-Eun Shin and Myung-Jin Yoon. I also want to give special thanks to Dr. Abdul Waheed at St. Louis University for his tremendous help including all the food he made for me. I also deeply appreciate Dr. Matt Riordan for wonderful support over the past two years. Finally, I am really grateful to my family for their endless love and support.

TABLE OF CONTENTS

LIST OF FIGURES AND TABLES

Chapter 1

Chapter 2

Chapter 3

Chapter 4

Chapter 5

ABSTRACT

Endosomal sorting complex required for transport (ESCRT) machinery responsible for multivesicular body (MVB) biogenesis is essential for receptor downregulation, viral budding and cytokinesis. ESCRT-III is a large polymer built from related ESCRT-III proteins that is thought to help generate intralumenal vesicles (ILVs) within the MVB. How ESCRT-III functions is poorly understood. Although ESCRT-III assembles on the endosomal membrane, its components are predominantly soluble in the cytoplasm. I found that the transition between these two states is controlled by autoinhibitory domains within ESCRT-III proteins, which I identified by structure/ function analysis in four human ESCRT-III proteins – Charged multivesicular body protein2A (CHMP2A), CHMP3, CHMP4A, and CHMP6. Biochemical and functional assays confirmed that the C-terminally located autoinhibitory domains control cycling between a "closed" state in which they are soluble monomers and an "open" state in which they assemble into membrane associated complexes. While searching for cellular factor(s) that might regulate transition between these states, I found that LIP5, a proposed cofactor of the ATPase VPS4, binds efficiently to the autoinhibitory domains of a subset of ESCRT-III proteins including CHMP1B, 2A and 3. Because VPS4 disassembles ESCRT-III complexes, this direct interaction between its cofactor LIP5 and ESCRT-III proteins can enhance VPS4 mediated ESCRT-III disassembly. To ask when and how individual ESCRT-III proteins and VPS4 contribute to ILV formation in cultured cells, I established reagents to detect and manipulate these proteins including antibodies and effective small interfering RNAs. I used these tools to show that representatives of two classes of cell surface receptors, epidermal growth factor receptor (EGFR), a tyrosine kinase receptor and delta-opioid receptor (DOR), a G-protein coupled receptor, use ESCRT-III and VPS4 to undergo downregulation via lysosomal degradation. Taken

together, the studies in this thesis provide insights into the role and regulation of ESCRT-III in MVB biogenesis.

CHAPTER ONE

INTRODUCTION

1. Membrane trafficking pathways

1.1 Intracellular compartments

Eukaryotic cells contain highly specialized membrane-bound compartments (or organelles) essential for fundamental cellular processes. These include the nucleus, the endoplasmic reticulum (ER), the Golgi apparatus, endosomes, lysosomes, peroxisomes, mitochondria, chloroplasts (plant only) and a variety of transport vesicles (1). Each membrane-bound organelle has a unique set of proteins and lipids; at the same time, it dynamically exchanges materials with other organelles. Therefore, cells have developed specific transport mechanisms to selectively transfer materials to different compartments while maintaining the identity of the individual organelles (2, 3). Intracellular membrane trafficking occurs via two main pathways - the biosynthetic-secretory pathway (outbound) and the endocytic pathway (inbound) (Fig. 1-1). Transport at each step of both pathways requires highly regulated multi-step processes in which numerous proteins and lipids participate. The critical steps include concentrating a specific set of cargo proteins, generating transport vesicles by coat proteins, packaging cargo into the vesicles, transporting these vesicles between compartments, and fusion between vesicles and target membranes (2, 3).

1.2 The secretory pathway

The secretory pathway is involved in secreting proteins out of cells or and delivering newly synthesized proteins to the plasma membrane (Fig. 1-1). Newly synthesized proteins from ribosomes are first incorporated into the lumen or membranes of the ER and scrutinized by quality control processes. Correctly folded proteins are packaged into coat protein complex II (COPII) coated vesicles and delivered to the ER-Golgi intermediate compartment (ERGIC) (2-4). The COPII coat consists of the small GTPase Sar1p and the coatomer complex (Sec23/24 and Sec13/31). Activated Sar1p

recruits soluble coat complexes onto the membrane which initiate membrane deformation to generate vesicles (5). Proteins leaving the ERGIC are transported through the Golgi apparatus (cis, medial and trans Golgi) and finally arrive in the trans-Golgi network (TGN), where they are sorted into secretory granules targeted to either plasma membrane or endosomes (2, 3).

Resident proteins in the secretory pathway sometimes escape from their own compartments but can be retrieved by retrograde transport which is mediated in most cases by COPI coated vesicles. Similar to COPII, the COPI coat consists of a coatomer complex and the small GTPase, ADP-ribosylation factor (Arf)1. The coatomer complex contains α-, β-, β'-, γ-, δ-, ε-, and ζ- COP. Activated Arf1 binds membranes and recruits the coatomer complex which provides a mechanical force for membrane deformation as it polymerizes on the membrane surface (6).

1.3 The endocytic pathway

The endocytic pathway is the inward membrane trafficking pathway from the plasma membrane to the lysosome (Fig. 1-1). As endocytic compartments mature, their lumenal pH becomes progressively lower. The lysosome, a final destination of the endocytic pathway, has the lowest pH (pH 4-5) and contains hydrolytic enzymes that are active at the low pH and degrade internalized materials (2, 7).

Cells internalize material from outside the cell or the cell surface by several distinct mechanisms: clathrin-mediated endocytosis (including most receptor mediated endocytosis), caveolar endocytosis, clathrin- and caveolin-independent endocytosis, macropinocytosis (cell drinking) and phagocytosis (cell eating) (8). The most well understood endocytic process is clathrin dependent endocytosis of receptors. In this process, a specific receptor on the plasma membrane binds to a ligand and then both are internalized via clathrin coated pits, which progress to form clathrin coated vesicles

(7, 9). Clathrin is a large protein composed of three heavy and three light chains, and self-assembles to form a basket-like clathrin lattice. The clathrin lattice serves as a scaffold to generate vesicles from the plasma membrane as well as the TGN and endosomes. Clathrin is recruited to the membrane by various adaptor proteins which bind to the cytoplasmic domains of transmembrane proteins (e.g. surface receptors). For example, clathrin coated vesicles from the plasma membranes are generated by clathrin together with adaptor protein 2 (AP2) (10, 11).

Once clathrin coated vesicles pinch off from the plasma membrane, they lose their coats and fuse with early endosomes. Many ligands internalized by receptor-mediated endocytosis dissociate from their receptors in early endosomes as a consequence of the lower pH in these compartments. Once ligands have disassociated, unoccupied receptors are often recycled back to the plasma membrane (7, 12). There are two distinct subpopulations of early endosomes– the sorting endosome and endocytic recycling compartments (ERC). Some molecules are delivered directly back to the plasma membrane from the sorting endosome (fast recycling), while others are delivered to a long-lived organelle, the ERC, before recycling to the plasma membrane (slow recycling) (Fig.1-1). Both the sorting endosome and the ERC can communicate with the TGN. Sorting endosomes remove recycling proteins by concentrating them in vesicles that bud from their tubular domains. As sorting endosomes mature into late endosomes, they move from the cell periphery to the center, and gradually become more spherical. Mature late endosomes no longer directly communicate with the plasma membrane, but still exchange proteins with the TGN (12, 13). Maturation from early to late endosomes is accompanied by the formation of intralumenal vesicles (ILVs), leading them to also be called multivesicular bodies (MVBs). Late endosomes/MVBs eventually become lysosomes by fusing with preexisting lysosomes (7, 14, 15).

1.4 Different routes in the endocytic pathway

Different proteins take different routes in the endocytic pathway. For example, transferrin receptor (TfR) bound to transferrin is endocytosed by receptor-mediated endocytosis, releases iron in the early endosome, and returns to the cell surface as a transferrin-bound form without iron. Low-density lipoprotein (LDL) receptor dissociates from its ligand, LDL, in the endosome and is recycled back to the plasma membrane as an unoccupied receptor (7). TGN38, a protein enriched in the TGN, continuously cycles between the TGN and the plasma membrane via the ERC. Mannose-6-phosphate receptor (M6PR) cycles between the TGN and late endosome, releasing lysosomal enzymes in the acidic milieu of the late endosome (7, 13). Some receptors bound to ligands are not recycled efficiently, but instead are delivered into ILVs of the MVB and eventually to the lysosome where they are degraded. One of the best studied receptors in this context is epidermal growth factor receptor (EGFR). EGFR is a receptor tyrosine kinase and an important regulator of cell proliferation, angiogenesis, migration and tumorigenesis (16). Lysosomal delivery of a signaling receptor functions to terminate signaling, thereby preventing cells from inappropriately responding to signal input until new receptors are synthesized (7, 17, 18).

2. Molecular mechanism for multivesicular body biogenesis

2.1 The multivesicular body (MVB)

The MVB is an intermediate endosome *en route* to the lysosome which was originally identified in early electron microscopy studies in the 1950s as a unique membranous structure with internal vesicles (19, 20). The MVB is characterized by proteins and lipids including Rab7, CD63 and lysobisphosphatidic acid (LBPA) which distinguish it from other organelles with internal membranes such as the autophagic body (21, 22). The MVB in yeast is a spherical structure with a diameter of ~200nm filled

with ~24nm ILVs (23). In mammalian cells, the MVB with a diameter of 400-500nm contains 50-100nm ILVs (15, 24, 25).

The MVB plays critical roles in various cellular functions. Sorting into the MVBs followed by delivery to the lysosome serves as a major mechanism for degrading transmembrane proteins and lipids (18, 21). Transmembrane proteins destined for lysosomal degradation are first sorted into the limiting membrane of the endosome, which is subsequently invaginated into the endosomal lumen to form ILVs. Proteins and lipids in the ILVs are eventually degraded by lysosomal hydrolases inside the lysosome.

Sorting ligand-activated receptors into MVB vesicles function to sequester the receptor, thus abgorating signal transduction. Some newly synthesized proteins are also sorted into ILVs of the MVB as part of the process delivering them to the lysosome (21, 26, 27). Finally, in certain cells, the MVB can fuse with the plasma membrane to release ILVs into the extracellular space. These secreted vesicles are called exosomes and are important for intercellular communication and some aspects of the immune response (28).

An intriguing feature of MVB vesicle formation is the topology of budding. To generate MVB vesicles, the limiting membrane must invaginate into the lumen of the endosome (21). This process requires generating negative curvature from the cytoplasmic side (i.e. budding away from the cytoplasm), which is opposite from the curvature involved in COP- and clathrin-mediated vesicle formation. COPs or clathrin proteins bind to the cytoplasmic side of the membrane and induce positive membrane curvature (i.e. budding towards the cytoplasm) to generate vesicles (29). Therefore, MVB vesicle formation requires a budding mechanism distinct from those for formation of other cytoplasmic vesicles.

2.2 Ubiquitin as a sorting signal to MVB

The most well-defined signal for sorting transmembrane proteins (cargo) to the MVB is ubiquitination (26, 27). Ubiquitin is a 76 amino acid protein which is covalently attached to proteins through the formation of an isopeptide bond between the C-terminus of ubiquitin and the ε-amino group of lysine residues on target proteins. Ubiquitin itself contains seven lysine residues that can serve as acceptor sites for additional ubiquitin molecules (30). Polyubiquitin chains can be generated by attachment of the C-terminus of one ubiquitin to lysine 48 or lysine 63 of the adjacent ubiquitin. Proteins with polyubiquitin chains linked at lysine 48 are efficiently targeted to proteasomes for degradation. Attachment of a single ubiquitin (monoubiquitin), multiple monoubiquitins or polyubiquitin linked at lysine 63 acts as a signal for endocytosis and/or MVB sorting (26, 27).

The attachment of ubiquitins to substrate proteins is carried out by the sequential activity of three enzyme classes: E1 (ubiquitin-activating enzyme), E2 (ubiquitin-conjugating enzyme), and E3 (ubiquitin ligase). The E3 ubiquitin ligase provides specificity to the reaction by recognizing substrate proteins. The E3 ubiquitin ligases are subdivided into two classes containing either a HECT (homologous to E6-AP C-terminus) domain or a RING (really interesting new gene) finger domain (30). Among different E3 ligases, Nedd4 E3 ligases, a subfamily of HECT E3 ligases are notably involved in MVB sorting. Rsp5 is the only Nedd4 ligase in yeast and is required for sorting of Sna3 and carboxypeptidase S (CPS) into the MVB (31, 32). In mammalian cells, AIP4, a Nedd4 ligase, was shown to be essential for lysosomal degradation of the chemokine receptor CXCR4, a G protein-coupled receptor (GPCR) (33). RING E3 ligases also contribute to MVB sorting: c-Cbl in mammalian cells is essential for lysosomal degradation of EGFR, whereas Tul1 in yeast is involved in sorting CPS to the MVB (34, 35).

Deubiquitinating enzymes are proteases that cleave the isopeptide bonds between two ubiquitins or between ubiquitin and a substrate protein (30). Several deubiquinating enzymes function during cargo sorting into the MVB, presumably allowing for recycling of ubiquitin. These include Doa4 in yeast, AMSH (associated-molecule with the SH3 domain of STAM), and UBPY (ubiquitin specific processing protease Y) in mammalian cells (36). Deubiquitinating enzymes are recruited to the endosome by interaction with proteins responsible for MVB biogenesis, which will be described in the next section.

2.3 Protein machinery responsible for MVB biogenesis

Elegant genetic screens in *S. cerevisiae* identified proteins involved in MVB biogenesis as a subset of vacuolar protein sorting (Vps) proteins, termed the class E Vps proteins (37). Functional loss of any of the class E Vps genes in yeast results in accumulation of enlarged prevaculoar compartments lacking internal vesicles, called class E compartments, and defects in delivering cargo to the endosomal and ultimately vacuolar lumen (38, 39). Class E Vps proteins are conserved throughout eukaryotes (Table 1-1). In mammalian cells, these proteins are also important for other topologically related budding processes including viral budding and cell abscission during cytokinesis (Figure 1-2) (40). Most class E Vps proteins assemble to form four separate protein complexes - Endosomal Sorting Complex Required for Transport-0 (ESCRT-0), ESCRT-I, ESCRT-II and ESCRT-III (Table 1-1 and Fig. 1-3). In the current model, ESCRTs in the cytoplasm are thought to be sequentially recruited to the endosomal membrane where they act together to sort ubiquitinated cargo and generate ILVs (39, 41) (Figure 1-3). ESCRT-0, I and II complexes can be purified *in vitro* with defined stoichiometry, and their structures have been mostly described based on high resolution structural studies

(22, 40, 42). Less is known about the nature of ESCRT-III complex, which will be discussed in more detail in Section 3.

2.4 Roles of lipids in MVB biogenesis

In addition to protein machinery, some phosphoinositides - phosphorylated derivatives of phosphatidylinositol - are important for MVB biogenesis. Phosphatidylinositol 3-phosphate (PI(3)P) is concentrated on the early endosome and also found on internal MVB membranes. (43, 44). The class III PI 3-kinase, Vps34 produces PI3P, and functional loss of yeast and human Vps34 results in missorting of cargo and impairing formation of internal vesicles in MVBs (45, 46). Another endosomal phosphoinositide, phosphatidylinositol 3,5 bisphosphate ($PI(3,5)P_2$), has also been implicated in MVB biogenesis. This phosphoinositide is generated through the phosphorylation of PI(3)P by the PI(3)P 5-kinase PIKfyve and Fab1 in mammals and yeast, respectively. Inhibiting function of these enzymes causes accumulation of abnormal MVBs and missorting of cargo (47-50).

One major contribution of phosphoinositides to MVB biogenesis is recruiting ESCRT machinery to endosomes. For example, Hrs/Vps27 (ESCRT-0) contains a FYVE domain that specifically binds to PI(3)P, and the GLUE domain in Vps36/Eap45 (ESCRT-II) can bind to several phospinositides (51-56). Components of ESCRT-III, CHMP3 and CHMP4A, were shown to have a weak specificity to $PI(3,5)P_2$ (57, 58).

Some lipids are proposed to more directly contribute to ILV formation. Lysobisphosphatidic acid (LBPA) is an inverted, cone-shaped phospholipid that is concentrated on the MVB in mammalian cells and can promote formation of MVB-like structures *in vitro* (59, 60). This lipid, however, has not been found in yeast (38). Because MVB biogenesis is highly conserved throughout eukaryotes, LBPA may not be a major mechanism facilitating MVB vesicle formation. Ceramide, another cone-shaped

lipid, was recently shown to be required for generating ILVs containing proteolipid protein (PLP) which are secreted as exosomes (61). Spontaneous formation of ILVs is triggered by ceramides which are generated by addition of sphingomyelinase to sphingomyelin-containing giant unilamellar vesicles (GUV). Furthermore, inhibition of ceramide synthesis in cells blocks sorting of PLP to the endosomal lumen and greatly reduces release of PLP-containing exosomes (61).

2.5 Roles of ESCRT machinery in cargo sorting and MVB vesicle formation

The current model for how the ESCRT machinery operates to sort cargo and generate ILVs is depicted in Figure 1-3 (39). In detail, ESCRT-0 is first brought to the endosomal membrane through interactions with membranes and ubiquitinated cargo. ESCRT-0 recruits both ESCRT-I and ESCRT-II to the endosomal membrane. ESCRT-II in turn recruits ESCRT-III, which engages the deubiquitinating enzymes that remove ubiquitin from cargo and the ATPase Vps4 that disassembles ESCRTs (39). The ESCRT machinery probably dissociates from membranes before MVB vesicles pinch off because ESCRT proteins are not present in high copy number in exosomes, viral particles or MVB vesicles (62, 63).

The model assumes that ESCRTs act sequentially; in other words, that ESCRT-0, I, II and III assemble in a specific order and hand off ubiquitinated cargo to the next ESCRT. For this reason, this model is often called the conveyor belt model (64, 65). There are numerous structural and interaction data that support this model. First, ESCRTs can interact directly with other ESCRTs. Briefly, Hrs/Vps27 (human name/yeast name; ESCRT-0) contains the P(S/T)AP motif that binds to the ubiquitin E2 variant (UEV) domain of Tsg101/Vps23 (ESCRT-I) (66-68). The C-terminal domain of Vps28/VPS28 (ESCRT-I) interacts with the N-terminus of Vps36/Eap45 (ESCRT-II) while Vps25/EAP20 (ESCRT-II) binds to the N-terminus of Vps20/CHMP6 (ESCRT-III)

(69-72). These data explain how upstream ESCRT can recruit the next downstream ESCRTs.

Second, components of ESCRTs interact with specific phosphoinositides concentrated on the endosomal membrane as described in Section 2.3, explaining how the machinery is directed to endosomes. Finally, ESCRTs can interact with ubiquitin on cargo (Table 1-1). Vps27/Hrs (ESCRT-0) and Vps23/Tsg101 (ESCRT-I) bind to ubiquitin via their ubiquitin interacting motif (UIM) and UEV respectively (73-76). In addition, Vps36/Eap45 (ESCRT-II) can interact with ubiquitin via their NZF or GLUE domain (77, 78) (Fig. 1-3). Unlike upstream ESCRTs, ESCRT-III does not contain ubiquitin binding motifs. Therefore, cargo may be fully committed to the MVB sorting pathway by the time it arrives at ESCRT-III. The idea of sequential recruitment of ESCRTs in the conveyor belt model is largely based on yeast genetic data. Briefly, overexpression of ESCRT-II in *S. cerevisiae* compensates for loss of ESCRT-I while ESCRT-I and II are required for appropriate assembly of ESCRT-III (79, 80).

Although most data available are consistent with this model, there are some data that do not agree with it. For example, ESCRT-I can be directly connected to ESCRT-III without ESCRT-II, which does not fit the sequential recruitment model. Vps28/VPS28 (ESCRT-I) binds to Vps20/CHMP6 (ESCRT-III), and Alix, an adaptor protein in mammalian cells, may bridge Tsg101 (ESCRT-I) to CHMP4 (ESCRT-III) (81-83). Furthermore, although there is evidence for the sorting of ubiquitinated cargo by ESCRTs, the data do not necessarily support “sequential transfer” of ubiquitinated cargo. Finally, yeast genetic data supporting sequential recruitment of ESCRTs were obtained using mutants lacking MVB function, and therefore, whether ESCRTs are sequentially recruited under physiological conditions remains unclear. To solve these issues, an alternative model has been proposed: ESCRTs could co-assemble around cargo (39, 64,

84). However, it should be noted that the current and alternative models are not mutually exclusive because ESCRTs might be clustered after they are sequentially recruited.

Once ESCRTs concentrate ubiquitinated cargo on the microdomain of the limiting membrane, they are thought to generate vesicles that contain the cargo. How ESCRTs drive ILV formation is one of the important questions yet to be answered in the ESCRT field. Current thinking is that ESCRT-III subunits may assemble into an array or lattice on the endosomal membrane and thus provide a driving force to generate ILVs (39, 41, 85, 86).

2.6 Non-endosomal functions of ESCRT machinery - viral budding and cytokinesis

At least part of the ESCRT machinery is important for viral budding from the cell surface, which is topologically equivalent to MVB vesicle formation (40, 87, 88) (Fig 1-2). The most extensively studied virus in this context is human immunodeficiency virus (HIV) that causes acquired immunodeficiency syndrome (AIDS). In fact, the involvement of the ESCRT machinery in the budding of HIV has been a major motivation for pursuing ESCRT research. The sequences in the C-terminal region of Gag protein (a structural protein of retroviruses) are required for efficient viral particle release, and these sequence motifs were termed the late domain because virus assembly arrested at a late stage when mutated (88, 89). The late domain of HIV Gag protein interacts with Tsg101 (ESCRT-0) and Alix via its PS/TAP motif and LYPXP motif, respectively (82, 90-92). Both Tsg101 and Alix likely engage ESCRT-III and Vps4 to complete viral budding. ESCRT-I, which contains Tsg101, probably recruits ESCRT-III via ESCRT-II or perhaps direct interaction with ESCRT-III (87-89). Virus interaction with Alix can be used to recruit ESCRT-III since Alix binds directly to a component of ESCRT-III, (93, 94).

Viral budding is an attractive therapeutic target distinct from other conventional drug targets, and therefore there have been efforts to develop drugs to interfere with

interaction between ESCRTs and HIV Gag protein. In fact, a recent report has identified a cyclic peptide which disrupts the Gag-Tsg101 interaction, and thereby effectively reduces virus release without compromising normal endocytic function in cells (95).

In mammalian cells, ESCRT machinery is also essential for the abscission step during cytokinesis, another budding process topologically equivalent to MVB vesicle formation (40) (Fig 1-2). For cytokinesis, ESCRT machinery is recruited through the interaction of centrosome protein 55 (Cep55) with Tsg101 or Alix that occurs at midbodies (96, 97). Whether Cep55 interacts with Tsg101 or Alix, the final stage probably involves recruitment of ESCRT-III and Vps4 to the midbody to achieve abscission (40). Recent evidence suggests that Vps2/Vps4 related factors play roles in cytokinesis in Archaea, supporting highly conserved roles of ESCRT-III and Vps4 in this process (98).

3. ESCRT-III

3.1 ESCRT-III family

Subunits of ESCRT-III are structurally related, small (~200 – 250 amino acids long) proteins with N-terminal basic and C-terminal acidic halves (79, 99). There are six ESCRT-III proteins in yeast (Vps2, Vps20, Vps24, Snf7, Did2 and Vps60) and these extend to 11 members in humans called charged multivesicular body proteins (CHMPs) (39-41) (Table1-1). ESCRT proteins are subdivided into two groups: Vps2, Vps20, Vps24 and Snf7 are core ESCRT-III proteins while Did2 and Vps60 are ESCRT-III-like proteins (note that these are all yeast names) (79, 99). Core ESCRT-III proteins are essential in MVB biogenesis while ESCRT-III-like proteins are proposed regulators of the ESCRT pathway. This classification is mostly based on the severity of the mutant phenotypes in yeast (79).

ESCRT-III proteins consist of a common set of 6 helices (α1 – α6), as will be discussed in Chapter 2 (100). Based on the crystal structure of a partial fragment of CHMP3, the first two helices (α1 and α2) of the protein form a 70Å long helical hairpin that constitutes a four-helical bundle together with two other helices (α3 and α4). The ability to bind to membranes and form polymers generally lies in this N-terminal helical bundle of the protein (α1-α4). A fifth helical segment (α5) is positioned perpendicularly to the helical bundle core. The last helix (α6) and its surrounding linker sequences are missing from the crystal structure but appear to extend from one side of the core (101). Because ESCRT-III proteins are homologous to each other, the crystal structure of CHMP3 is likely to be representative of all ESCRT-III proteins.

ESCRT-III proteins interact with themselves, other ESCRT-III proteins, upstream ESCRTs and a number of other cellular factors. One of the most important interacting partners is the AAA ATPase Vps4, which has been shown to bind to most ESCRT-III proteins (82, 102-105). This is not surprising because Vps4 is required for disassembly of ESCRT-III. Unlike Vps4, many other interactions involving ESCRT-III appears to be specific to one or a subset of ESCRT-III proteins. For example, CHMP1B interacts with spastin, a microtubule severing enzyme linked to hereditary spastic paraplegia (106). AMSH, a mammalian deubiquinating enzyme, shows distinct selectivity for CHMP3 while UBPY, another mammalian deubiquitinating enzyme, interacts strongly with CHMP1 and CHMP7 (107-110). Vps4, AMSH, UBPY and spastin all have a *M*icrotubule *I*nteracting and *T*ransport (MIT) domain, which is responsible for binding to ESCRT-III proteins (104, 110-112). Snf7/CHMP4 interacts with Bro1 domain containing proteins including Bro1, Alix and HD-PTP (His domain phosphotyrosine phosphatase) (83, 93, 94, 113, 114). In yeast, a deubiquinating enzyme, Doa4, is recruited to the endosomal membrane via the interaction of Bro1 with Snf7 (115).

3.2 Assembly of ESCRT-III polymers on the endosomal membrane

ESCRT-III proteins cycle on and off endosomal membranes and function as membrane-associated polymers. How ESCRT-III proteins are targeted to the endosomal membrane is poorly understood. Yeast genetic studies suggest that core ESCRT-III consists of two distinct subcomplexes, the Vps20-Snf7 (membrane-proximal subcomplex) and the Vps2-Vps24 (soluble subcomplex) (79). The Vps20-Snf7 subcomplex is thought to bind to the endosomal membrane through binding to ESCRT-II and myristolylation of Vps20. The Vps20-Snf7 subcomplex may recruit Vps2-Vps24 subcomplex which in turn may bring the AAA ATPase Vps4 to endosomes (39).

ESCRT-III proteins recruited to the endosomal membrane assemble into large polymers which may facilitate MVB vesicle formation. While upstream ESCRTs can be purified as stable complexes with defined stoichiometry, ESCRT-III polymers were originally identified as Triton X-100 insoluble complexes with unknown stoichiometry and size in mutant yeast cells lacking Vps4 (79). Recently, Teis et al. have identified a ~450kDa membrane associated complex containing Snf7 in yeast after crosslinking. Whether the complex represents ESCRT-III polymers in cells requires further investigation (116).

Although still largely unknown, several recent studies provide some clues on the structure of ESCRT-III polymers. First, our group recently reported deep-etch electron microscopy of ESCRT-III polymers formed by human orthologs of Snf7, CHMP4A and CHMP4B (86). When CHMP4 proteins were overexpressed in mammalian cells, they assembled into 5nm filaments that form circular arrays on the plasma membrane. Furthermore, in the presence of the ATPase defective mutant VPS4B, the circular scaffolds of the ESCRT polymers turned into buds and tubules emanating from the cell surface that could bend the membrane away from the cytoplasm. This data suggests

that ESCRT-III proteins may form circular polymers that promote or stabilize negative curvature and outward budding.

Several other studies reconstituted assembly of ESCRT-III polymers *in vitro* using purified ESCRT-III proteins. One study showed that yeast Vps24 could form helical filaments with diameters of ~15nm (two stranded) or 20nm (three stranded) in solution (117). Vps4 induced curved bundling of two stranded filaments and could disassemble the filaments in a nucleotide dependent fashion when the C-terminal region of Vps24 was replaced by the C-terminal end of Vps2. An alternative structure of ESCRT-III polymers, a helical tubule, was also reported. CHMP2A and CHMP3 could be assembled into helical tubular structures with ~ 40nm diameter which also could bind to liposomes (118). Interestingly, the membrane interaction sites were exposed on the outside of the tubule, while the ATPase VPS4 bound on the inside of the tubule. It is possible that such helical polymer structures assemble within the neck of a vesicle, catalyzing budding reactions under the control of Vps4.

Two recent studies reconstituted assembly of ESCRT-III polymers on synthetic liposomes using four core yeast ESCRT-III proteins, and demonstrated that ESCRT-III can induce membrane deformation and vesicle formation *in vitro.* One study observed the invagination about ~40nm in diameter in ~80-100nm liposomes after treating with four core ESCRT-III proteins (119). The other showed that ESCRT-III proteins were concentrated on the periphery of giant unilamellar liposomes and could induce formation of ILVs (120). Among four ESCRT-III proteins, Vps20, Snf7 and Vps24 but not Vps2 were required for completing vesicle formation and scission of vesicles from the limiting membranes.

All of these data support the idea that ESCRT-III proteins can assemble into stable polymers with regular organization and perhaps these polymers may mediate vesicle formation. However, these studies were carried out under non-physiological

conditions. Therefore, further investigation will be required to determine the extent to which of these studies reflects actual ESCRT-III polymers in cells.

3.3 Regulation of ESCRT-III polymer assembly

Although ESCRT-III proteins function as membrane-associated complexes, they exist predominantly as soluble monomers in the cytoplasm. ESCRT-III proteins in the cytoplasm are in a closed conformation in which their autoinhibitory domains keep the proteins from binding to membranes and forming polymers. ESCRT-III proteins assemble on the endosomal membrane when the autoinhibition is relieved (i.e. open/activated) (58, 100, 108). A recent study provides structural evidence for these two conformations of ESCRT-III proteins. Based on small-angle X-ray scattering data, an ESCRT-III protein, CHMP3, can adopt two conformations in solution. A globular form in a low salt condition most likely represents the closed state of the ESCRT-III protein whereas an extended conformation in a high salt condition may represent the open/activated state (121). Conformational changes of Snf7 protein was also examined by fluorescence spectroscopy (119). To do this, probes at several different positions of Snf7 were monitored spectroscopically in aqueous solution and in the presence of different ESCRT-III proteins and membranes. In solution, Snf7 was soluble monomer but then oligomerized in the presence of Vps20 and liposomes. Upon membrane binding and oligomerization, the loop between α5 and α6 of Snf7 underwent the most dramatic changes, presumably representing a conformational transition from a closed to open form. Autoinhibition of ESCRT-III proteins will be further discussed in Chapter 2.

3.4 Disassembly of ESCRT-III polymers

ESCRT-III polymers do not disassemble spontaneously, but require the ATPase activity of Vps4. Vps4 is an essential factor in ILV formation and functional loss of Vps4

blocks ILV formation and results in accumulation of cargo and other ESCRT proteins in class E compartments near vacuoles (79, 80, 122-124). In mammals, there are two isoforms, VPS4A and VPS4B (41). Vps4 belongs to the ATPase family associated with various cellular activities (AAA) family that functions in the unfolding and disassembly of protein complexes. Members of the AAA ATPase family contain conserved AAA domains which oliogomerize to form single or dual hexameric rings required for ATP hydrolysis (125). There are two subtypes in the AAA ATPase family – type I and type II. Vps4 is a type I AAA ATPase with a single AAA domain per monomer. Unlike type II AAA proteins that form stable rings, Vps4 is oliogermized in an ATP dependent manner (125). Additionally, Vta1/LIP5, a proposed cofactor of Vps4, may promote ATPase activity of Vps4 in part through promoting or stabilizing Vps4 oligomerization (126, 127). Vta1/LIP5 binds to the beta domain of Vps4, beta sheets inserted in the AAA domain of Vps4. Vta1/LIP5 can also interact directly with a subset of ESCRT-III proteins, which will be discussed in greater detail in Chapter 3.

Vps4 interacts with ESCRT-III proteins via its N-terminal MIT domain. Structure determination of the Vps4 MIT domain revealed a three-helix bundle reminiscent of an incomplete tetratricopeptide-like repeat (TPR) (104). The C-terminal regions of many ESCRT-III proteins contain motifs called MIT domain interacting motifs (MIMs) responsible for binding to the Vps4 MIT domain (102, 103). It is fairly clear that Vps4 plays a critical role in the dissociation of ESCRT-III from the endosomal membrane, considering the phenotypes of cells lacking functional Vps4 (58, 79). More direct evidence came from a series of recent studies on ESCRT-III polymers built *in vitro* showing that they could be disassembled by purified Vps4 (117-120). Whether Vps4 is actively required for the budding/fission reaction of ILV formation is still a matter of debate in the field. Recent data from an *in vitro* budding assay, however, favors the idea

that Vps4 plays a role in disassembling the machinery after the budding reaction is complete (120).

3.6 Implications of ESCRT-III in human diseases

ESCRT-III proteins are essential in numerous critical cellular processes including receptor downregulation and viral budding (39, 40). Dysfunction of ESCRT-III proteins may contribute to pathophysiology of cancer because abnormal activity of signaling receptors can lead to tumorogenesis (17, 128). Roles of ESCRT-III are also linked to life threatening infectious diseases such HIV and Ebola (88, 91). Additionally, it appears that disrupting function of ESCRT-III impairs autophagosome formation, which may lead to dysfunction and death of neurons (129). In fact, mutations in CHMP2B have been associated with frontotemporal dementia (FTD; the second most common form of familial dementia after Alzheimer's disease) and amyotrophic lateral sclerosis (ALS) (130, 131). Both of these neurodegenerative diseases are characterized by accumulation of ubiquitin-positive protein aggregates in the central nervous system, perhaps because of impaired autophagocytosis (129, 132, 133). Finally, mutations in CHMP4B are linked to familial cataracts although exactly how the ESCRT machinery contributes to lens transparency is not known (134). Note that I contributed to this work which resulted in the publication attached as Appendix 1 to this thesis.

4. Summary

The field has learned much about the structures and interactions of the ESCRT machinery, and the mechanism of cargo recruitment by ESCRTs. ESCRT-III still remains one of the least understood players in the ESCRT pathway, and the mechanism for MVB vesicle formation is still a matter of conjecture. Knowledge about ESCRT-III was far less extensive at the time I started my thesis work. In fact, most of the information regarding

ESCRT-III described in this introduction came from work carried out over the past four years while I was working on this thesis.

Four years ago, ESCRT-III polymers were defined as Triton X-100 insoluble material which could be seen only in cells lacking functional Vps4 (79). Deletion of yeast ESCRT-III proteins led to defects in ability to sort cargo to the vacuolar lumen (79, 99). Because the size, structure and stoichiometry of ESCRT-III polymers were undetermined, it was difficult to understand whether and how ESCRT-III polymers contributed to formation of MVB vesicles. While ESCRT-III proteins are expected to function as polymers on the endosomal membrane, they exist predominantly as soluble monomers in the cytoplasm (79). Precise mechanisms by which ESCRT-III is targeted to the endosomal membrane and assembles to polymers on the membrane remain poorly understood.

A hypothesis to explain the transition between soluble monomers and membrane associated complexes was that ESCRT-III proteins might have autoinhibitory domains that keep the proteins from binding to membranes and forming polymers (58). Based on the data from our lab and others with half fragments of CHMP3 and CHMP4A, an autoinhibitory domain was thought to be present within the C-terminal half of ESCRT-III protein (57, 58). Because ESCRT-III proteins are structurally related to each other, such a domain was expected to be present in all ESCRT-III proteins. To determine whether this was the case and to identify a common autoinhibitory domain that controls conformational changes of ESCRT-III proteins, I performed a structure/function analysis of four representative human ESCRT-III proteins (CHMP2A, CHMP3, CHMP4A and CHMP6). This work is described in Chapter 2 and was published in Traffic (100).

While searching for cellular factor(s) that might regulate conformational changes in ESCRT-III proteins, I found that LIP5, a proposed cofactor of Vps4, could bind efficiently to the autoinhibitory domain of CHMP2A. Through further analyses, I identified

novel connections between LIP5 and a subset of ESCRT-III proteins (CHMP1B, 2A and 3) that have been implicated in Vps4 mediated ESCRT-III disassembly. In Chapter 3, I describe these protein interactions as well as their involvement in the disassembly of ESCRT-III. This work was published in Molecular Biology of the Cell (135).

Recent work from our group and others provides insight into structures and possible function of ESCRT-III polymers in generating ILVs. Specific roles for individual ESCRT-III proteins have emerged from some of the studies. This will be discussed in Chapter 5 in greater detail. Overall, however, it has yet to be determined precisely how ESCRT-III polymers generate ILVs in cells under physiological conditions and differential contributions of each ESCRT-III protein to ILV formation. One of the ultimate goals of my thesis is to study the roles of mammalian ESCRT-III in ILV formation. In Chapter 4, I describe tools developed for this purpose. Using these tools, I explore the role of ESCRT-III and interacting proteins in trafficking of two receptor proteins, epidermal growth receptor (EGFR) and δ-opioid receptor (DOR).

In Chapter 5, I discuss remaining questions to be addressed regarding the role and regulation of ESCRT-III and describe my preliminary data and future directions.

REFERENCES

1. Lodish H, Berk A, Kaiser CA, Krieger M, Scott MP, Bretscher A, Ploegh H, Matsudaira P. Molecular Cell Biology. W H Freeman & Co. 2003 5th edition (Chapter 5):p165-173.

2. Derby MC, Gleeson PA. New insights into membrane trafficking and protein sorting. Int Rev Cytol 2007;261:47-116.

3. van Vliet C, Thomas EC, Merino-Trigo A, Teasdale RD, Gleeson PA. Intracellular sorting and transport of proteins. Prog Biophys Mol Biol 2003;83(1):1-45.

4. Appenzeller-Herzog C, Hauri HP. The ER-Golgi intermediate compartment (ERGIC): in search of its identity and function. J Cell Sci 2006;119(Pt 11):2173-2183.

5. Lee MC, Miller EA. Molecular mechanisms of COPII vesicle formation. Semin Cell Dev Biol 2007;18(4):424-434.

6. Bethune J, Wieland F, Moelleken J. COPI-mediated transport. J Membr Biol 2006;211(2):65-79.

7. Mukherjee S, Ghosh RN, Maxfield FR. Endocytosis. Physiol Rev 1997;77(3):759-803.

8. Conner SD, Schmid SL. Regulated portals of entry into the cell. Nature 2003;422(6927):37-44.

9. Roth MG. Clathrin-mediated endocytosis before fluorescent proteins. Nat Rev Mol Cell Biol 2006;7(1):63-68.

10. Spang A. The life cycle of a transport vesicle. Cell Mol Life Sci 2008;65(18):2781-2789.

11. Stagg SM, LaPointe P, Balch WE. Structural design of cage and coat scaffolds that direct membrane traffic. Curr Opin Struct Biol 2007;17(2):221-228.

12. Gruenberg J. The endocytic pathway: a mosaic of domains. Nat Rev Mol Cell Biol 2001;2(10):721-730.

13. Maxfield FR, McGraw TE. Endocytic recycling. Nat Rev Mol Cell Biol 2004;5(2):121-132.

14. Piper RC, Luzio JP. Late endosomes: sorting and partitioning in multivesicular bodies. Traffic 2001;2(9):612-621.

15. Gruenberg JS, H. The biogenesis of multivesicular endosomes. Nat Rev Mol Cell Biol 2004;5(4):317-323.

16. Grandal MV, Madshus IH. Epidermal growth factor receptor and cancer: control of oncogenic signalling by endocytosis. J Cell Mol Med 2008;12(5A):1527-1534.

17. Eden ER, White IJ, Futter CE. Down-regulation of epidermal growth factor receptor signalling within multivesicular bodies. Biochem Soc Trans 2009;37(Pt 1):173-177.

18. Woodman PG, Futter CE. Multivesicular bodies: co-ordinated progression to maturity. Curr Opin Cell Biol 2008;20(4):408-414.

19. Palade GE. A small particulate component of the cytoplasm. J Biophys Biochem Cytol 1955;1(1):59-68.

20. Sotelo JR, Porter KR. An electron microscope study of the rat ovum. J Biophys Biochem Cytol 1959;5(2):327-342.

21. Piper RC, Katzmann DJ. Biogenesis and function of multivesicular bodies. Annu Rev Cell Dev Biol 2007;23:519-547.

22. Williams RL, Urbe S. The emerging shape of the ESCRT machinery. Nat Rev Mol Cell Biol 2007;8(5):355-368.

23. Nickerson DP, West M, Odorizzi G. Did2 coordinates Vps4-mediated dissociation of ESCRT-III from endosomes. J Cell Biol 2006;175(5):715-720.

24. White IJ, Bailey LM, Aghakhani MR, Moss SE, Futter CE. EGF stimulates annexin 1-dependent inward vesiculation in a multivesicular endosome subpopulation. Embo J 2006;25(1):1-12.

25. Murk JL, Humbel BM, Ziese U, Griffith JM, Posthuma G, Slot JW, Koster AJ, Verkleij AJ, Geuze HJ, Kleijmeer MJ. Endosomal compartmentalization in three dimensions: implications for membrane fusion. Proc Natl Acad Sci U S A 2003;100(23):13332-13337.

26. Piper RC, Luzio JP. Ubiquitin-dependent sorting of integral membrane proteins for degradation in lysosomes. Curr Opin Cell Biol 2007;19(4):459-465.

27. Raiborg C, Rusten TE, Stenmark H. Protein sorting into multivesicular endosomes. Curr Opin Cell Biol 2003;15(4):446-455.

28. Fevrier B, Raposo G. Exosomes: endosomal-derived vesicles shipping extracellular messages. Curr Opin Cell Biol 2004;16(4):415-421.

29. McMahon HT, Gallop JL. Membrane curvature and mechanisms of dynamic cell membrane remodelling. Nature 2005;438(7068):590-596.

30. Weissman AM. Themes and variations on ubiquitylation. Nat Rev Mol Cell Biol 2001;2(3):169-178.

31. Katzmann DJ, Sarkar S, Chu T, Audhya A, Emr SD. Multivesicular body sorting: ubiquitin ligase Rsp5 is required for the modification and sorting of carboxypeptidase S. Mol Biol Cell 2004;15(2):468-480.

32. Oestreich AJ, Davies BA, Payne JA, Katzmann DJ. Mvb12 is a novel member of ESCRT-I involved in cargo selection by the multivesicular body pathway. Mol Biol Cell 2007;18(2):646-657.

33. Marchese A, Raiborg C, Santini F, Keen JH, Stenmark H, Benovic JL. The E3 ubiquitin ligase AIP4 mediates ubiquitination and sorting of the G protein-coupled receptor CXCR4. Dev Cell 2003;5(5):709-722.

34. Dikic I. Mechanisms controlling EGF receptor endocytosis and degradation. Biochem Soc Trans 2003;31(Pt 6):1178-1181.

35. Reggiori F, Pelham HR. A transmembrane ubiquitin ligase required to sort membrane proteins into multivesicular bodies. Nat Cell Biol 2002;4(2):117-123.

36. Clague MJ, Urbe S. Endocytosis: the DUB version. Trends Cell Biol 2006;16(11):551-559.

37. Raymond CK, Howald-Stevenson I, Vater CA, Stevens TH. Morphological classification of the yeast vacuolar protein sorting mutants: evidence for a prevacuolar compartment in class E vps mutants. Mol Biol Cell 1992;3(12):1389-1402.

38. Babst M. A protein's final ESCRT. Traffic 2005;6(1):2-9.

39. Hurley JH, Emr SD. The ESCRT complexes: structure and mechanism of a membrane-trafficking network. Annu Rev Biophys Biomol Struct 2006;35:277-298.

40. Raiborg C, Stenmark H. The ESCRT machinery in endosomal sorting of ubiquitylated membrane proteins. Nature 2009;458(7237):445-452.

41. Saksena S, Sun J, Chu T, Emr SD. ESCRTing proteins in the endocytic pathway. Trends Biochem Sci 2007;32(12):561-573.

42. Hurley JH, Im YJ, Lee HH, Ren X, Wollert T, Yang D. Piecing together the ESCRTs. Biochem Soc Trans 2009;37(Pt 1):161-166.

43. Gillooly DJ, Morrow IC, Lindsay M, Gould R, Bryant NJ, Gaullier JM, Parton RG, Stenmark H. Localization of phosphatidylinositol 3-phosphate in yeast and mammalian cells. Embo J 2000;19(17):4577-4588.

44. Gillooly DJ, Raiborg C, Stenmark H. Phosphatidylinositol 3-phosphate is found in microdomains of early endosomes. Histochem Cell Biol 2003;120(6):445-453.

45. Schu PV, Takegawa K, Fry MJ, Stack JH, Waterfield MD, Emr SD. Phosphatidylinositol 3-kinase encoded by yeast VPS34 gene essential for protein sorting. Science 1993;260(5104):88-91.

46. Futter CE, Collinson LM, Backer JM, Hopkins CR. Human VPS34 is required for internal vesicle formation within multivesicular endosomes. J Cell Biol 2001;155(7):1251-1263.

47. Ikonomov OC, Sbrissa D, Yoshimori T, Cover TL, Shisheva A. PIKfyve Kinase and SKD1 AAA ATPase define distinct endocytic compartments. Only PIKfyve expression

inhibits the cell-vacoulating activity of Helicobacter pylori VacA toxin. J Biol Chem 2002;277(48):46785-46790.

48. Odorizzi G, Babst M, Emr SD. Fab1p PtdIns(3)P 5-kinase function essential for protein sorting in the multivesicular body. Cell 1998;95(6):847-858.

49. Jefferies HB, Cooke FT, Jat P, Boucheron C, Koizumi T, Hayakawa M, Kaizawa H, Ohishi T, Workman P, Waterfield MD, Parker PJ. A selective PIKfyve inhibitor blocks PtdIns(3,5)P(2) production and disrupts endomembrane transport and retroviral budding. EMBO Rep 2008;9(2):164-170.

50. Shisheva A. Regulating Glut4 vesicle dynamics by phosphoinositide kinases and phosphoinositide phosphatases. Front Biosci 2003;8:s945-946.

51. Komada M, Soriano P. Hrs, a FYVE finger protein localized to early endosomes, is implicated in vesicular traffic and required for ventral folding morphogenesis. Genes Dev 1999;13(11):1475-1485.

52. Misra S, Hurley JH. Crystal structure of a phosphatidylinositol 3-phosphate-specific membrane-targeting motif, the FYVE domain of Vps27p. Cell 1999;97(5):657-666.

53. Stahelin RV, Long F, Diraviyam K, Bruzik KS, Murray D, Cho W. Phosphatidylinositol 3-phosphate induces the membrane penetration of the FYVE domains of Vps27p and Hrs. J Biol Chem 2002;277(29):26379-26388.

54. Slagsvold T, Aasland R, Hirano S, Bache KG, Raiborg C, Trambaiolo D, Wakatsuki S, Stenmark H. Eap45 in mammalian ESCRT-II binds ubiquitin via a phosphoinositide-interacting GLUE domain. J Biol Chem 2005;280(20):19600-19606.

55. Teo H, Gill DJ, Sun J, Perisic O, Veprintsev DB, Vallis Y, Emr SD, Williams RL. ESCRT-I core and ESCRT-II GLUE domain structures reveal role for GLUE in linking to ESCRT-I and membranes. Cell 2006;125(1):99-111.

56. Im YJ, Hurley JH. Integrated structural model and membrane targeting mechanism of the human ESCRT-II complex. Dev Cell 2008;14(6):902-913.

57. Whitley P, Reaves BJ, Hashimoto M, Riley AM, Potter BV, Holman GD. Identification of mammalian Vps24p as an effector of phosphatidylinositol 3,5-bisphosphate-dependent endosome compartmentalization. J Biol Chem 2003;278(40):38786-38795.
58. Lin Y, Kimpler LA, Naismith TV, Lauer JM, Hanson PI. Interaction of the mammalian endosomal sorting complex required for transport (ESCRT) III protein hSnf7-1 with itself, membranes, and the AAA+ ATPase SKD1. J Biol Chem 2005;280(13):12799-12809.
59. Kobayashi T, Stang E, Fang KS, de Moerloose P, Parton RG, Gruenberg J. A lipid associated with the antiphospholipid syndrome regulates endosome structure and function. Nature 1998;392(6672):193-197.
60. Matsuo H, Chevallier J, Mayran N, Le Blanc I, Ferguson C, Faure J, Blanc NS, Matile S, Dubochet J, Sadoul R, Parton RG, Vilbois F, Gruenberg J. Role of LBPA and Alix in multivesicular liposome formation and endosome organization. Science 2004;303(5657):531-534.
61. Trajkovic K, Hsu C, Chiantia S, Rajendran L, Wenzel D, Wieland F, Schwille P, Brugger B, Simons M. Ceramide triggers budding of exosome vesicles into multivesicular endosomes. Science 2008;319(5867):1244-1247.
62. Pisitkun T, Shen RF, Knepper MA. Identification and proteomic profiling of exosomes in human urine. Proc Natl Acad Sci U S A 2004;101(36):13368-13373.
63. Olver C, Vidal M. Proteomic analysis of secreted exosomes. Subcell Biochem 2007;43:99-131.
64. Nickerson DP, Russell MR, Odorizzi G. A concentric circle model of multivesicular body cargo sorting. EMBO Rep 2007;8(7):644-650.
65. Hurley JH. ESCRT complexes and the biogenesis of multivesicular bodies. Curr Opin Cell Biol 2008;20(1):4-11.
66. Katzmann DJ, Stefan CJ, Babst M, Emr SD. Vps27 recruits ESCRT machinery to endosomes during MVB sorting. J Cell Biol 2003;162(3):413-423.

67. Bache KG, Brech A, Mehlum A, Stenmark H. Hrs regulates multivesicular body formation via ESCRT recruitment to endosomes. J Cell Biol 2003;162(3):435-442.
68. Bilodeau PS, Winistorfer SC, Kearney WR, Robertson AD, Piper RC. Vps27-Hse1 and ESCRT-I complexes cooperate to increase efficiency of sorting ubiquitinated proteins at the endosome. J Cell Biol 2003;163(2):237-243.
69. Gill DJ, Teo H, Sun J, Perisic O, Veprintsev DB, Emr SD, Williams RL. Structural insight into the ESCRT-I/-II link and its role in MVB trafficking. Embo J 2007.
70. Teo H, Perisic O, Gonzalez B, Williams RL. ESCRT-II, an endosome-associated complex required for protein sorting: crystal structure and interactions with ESCRT-III and membranes. Dev Cell 2004;7(4):559-569.
71. Kostelansky MS, Sun J, Lee S, Kim J, Ghirlando R, Hierro A, Emr SD, Hurley JH. Structural and functional organization of the ESCRT-I trafficking complex. Cell 2006;125(1):113-126.
72. Yorikawa C, Shibata H, Waguri S, Hatta K, Horii M, Katoh K, Kobayashi T, Uchiyama Y, Maki M. Human CHMP6, a myristoylated ESCRT-III protein, interacts directly with an ESCRT-II component EAP20 and regulates endosomal cargo sorting. Biochem J 2005;387(Pt 1):17-26.
73. Bilodeau PS, Urbanowski JL, Winistorfer SC, Piper RC. The Vps27p-Hse1p complex binds ubiquitin and mediates endosomal protein sorting. Nat Cell Biol 2002;4(7):534-539.
74. Hirano S, Kawasaki M, Ura H, Kato R, Raiborg C, Stenmark H, Wakatsuki S. Double-sided ubiquitin binding of Hrs-UIM in endosomal protein sorting. Nat Struct Mol Biol 2006;13(3):272-277.
75. Pornillos O, Alam SL, Davis DR, Sundquist WI. Structure of the Tsg101 UEV domain in complex with the PTAP motif of the HIV-1 p6 protein. Nat Struct Biol 2002;9(11):812-817.

76. Teo H, Veprintsev DB, Williams RL. Structural insights into endosomal sorting complex required for transport (ESCRT-I) recognition of ubiquitinated proteins. J Biol Chem 2004;279(27):28689-28696.

77. Hirano S, Suzuki N, Slagsvold T, Kawasaki M, Trambaiolo D, Kato R, Stenmark H, Wakatsuki S. Structural basis of ubiquitin recognition by mammalian Eap45 GLUE domain. Nat Struct Mol Biol 2006;13(11):1031-1032.

78. Alam SL, Sun J, Payne M, Welch BD, Blake BK, Davis DR, Meyer HH, Emr SD, Sundquist WI. Ubiquitin interactions of NZF zinc fingers. Embo J 2004;23(7):1411-1421.

79. Babst M, Katzmann DJ, Estepa-Sabal EJ, Meerloo T, Emr SD. Escrt-III: an endosome-associated heterooligomeric protein complex required for mvb sorting. Dev Cell 2002;3(2):271-282.

80. Babst M, Katzmann DJ, Snyder WB, Wendland B, Emr SD. Endosome-associated complex, ESCRT-II, recruits transport machinery for protein sorting at the multivesicular body. Dev Cell 2002;3(2):283-289.

81. Pineda-Molina E, Belrhali H, Piefer AJ, Akula I, Bates P, Weissenhorn W. The Crystal Structure of the C-Terminal Domain of Vps28 Reveals a Conserved Surface Required for Vps20 Recruitment. Traffic 2006.

82. von Schwedler UK, Stuchell M, Muller B, Ward DM, Chung HY, Morita E, Wang HE, Davis T, He GP, Cimbora DM, Scott A, Krausslich HG, Kaplan J, Morham SG, Sundquist WI. The protein network of HIV budding. Cell 2003;114(6):701-713.

83. McCullough J, Fisher RD, Whitby FG, Sundquist WI, Hill CP. ALIX-CHMP4 interactions in the human ESCRT pathway. Proc Natl Acad Sci U S A 2008;105(22):7687-7691.

84. Hurley JH, Ren X. The circuitry of cargo flux in the ESCRT pathway. J Cell Biol 2009;185(2):185-187.

85. Teis D, Saksena S, Emr SD. SnapShot: the ESCRT machinery. Cell 2009;137(1):182-182 e181.

86. Hanson PI, Roth R, Lin Y, Heuser JE. Plasma membrane deformation by circular arrays of ESCRT-III protein filaments. J Cell Biol 2008;180(2):389-402.

87. Usami Y, Popov S, Popova E, Inoue M, Weissenhorn W, H GG. The ESCRT pathway and HIV-1 budding. Biochem Soc Trans 2009;37(Pt 1):181-184.

88. Carlton JG, Martin-Serrano J. The ESCRT machinery: new functions in viral and cellular biology. Biochem Soc Trans 2009;37(Pt 1):195-199.

89. Bieniasz PD. Late budding domains and host proteins in enveloped virus release. Virology 2006;344(1):55-63.

90. Garrus JE, von Schwedler UK, Pornillos OW, Morham SG, Zavitz KH, Wang HE, Wettstein DA, Stray KM, Cote M, Rich RL, Myszka DG, Sundquist WI. Tsg101 and the vacuolar protein sorting pathway are essential for HIV-1 budding. Cell 2001;107(1):55-65.

91. Martin-Serrano J, Zang T, Bieniasz PD. HIV-1 and Ebola virus encode small peptide motifs that recruit Tsg101 to sites of particle assembly to facilitate egress. Nat Med 2001;7(12):1313-1319.

92. Strack B, Calistri A, Craig S, Popova E, Gottlinger HG. AIP1/ALIX is a binding partner for HIV-1 p6 and EIAV p9 functioning in virus budding. Cell 2003;114(6):689-699.

93. Fisher RD, Chung HY, Zhai Q, Robinson H, Sundquist WI, Hill CP. Structural and biochemical studies of ALIX/AIP1 and its role in retrovirus budding. Cell 2007;128(5):841-852.

94. Carlton JG, Agromayor M, Martin-Serrano J. Differential requirements for Alix and ESCRT-III in cytokinesis and HIV-1 release. Proc Natl Acad Sci U S A 2008;105(30):10541-10546.

95. Waheed AA, Freed EO. Peptide inhibitors of HIV-1 egress. ACS Chem Biol 2008;3(12):745-747.

96. Carlton JG, Martin-Serrano J. Parallels between cytokinesis and retroviral budding: a role for the ESCRT machinery. Science 2007;316(5833):1908-1912.

97. Morita E, Sandrin V, Chung HY, Morham SG, Gygi SP, Rodesch CK, Sundquist WI. Human ESCRT and ALIX proteins interact with proteins of the midbody and function in cytokinesis. Embo J 2007;26(19):4215-4227.

98. Samson RY, Obita T, Freund SM, Williams RL, Bell SD. A role for the ESCRT system in cell division in archaea. Science 2008;322(5908):1710-1713.

99. Kranz A, Kinner A, Kolling R. A Family of Small Coiled-Coil-forming Proteins Functioning at the Late Endosome in Yeast. Mol Biol Cell 2001;12(3):711-723.

100. Shim S, Kimpler LA, Hanson PI. Structure/Function Analysis of Four Core ESCRT-III Proteins Reveals Common Regulatory Role for Extreme C-Terminal Domain. Traffic 2007;8(8):1068-1079.

101. Muziol T, Pineda-Molina E, Ravelli RB, Zamborlini A, Usami Y, Gottlinger H, Weissenhorn W. Structural basis for budding by the ESCRT-III factor CHMP3. Dev Cell 2006;10(6):821-830.

102. Stuchell-Brereton MD, Skalicky JJ, Kieffer C, Karren MA, Ghaffarian S, Sundquist WI. ESCRT-III recognition by VPS4 ATPases. Nature 2007;449(7163):740-744.

103. Obita T, Saksena S, Ghazi-Tabatabai S, Gill DJ, Perisic O, Emr SD, Williams RL. Structural basis for selective recognition of ESCRT-III by the AAA ATPase Vps4. Nature 2007;449(7163):735-739.

104. Scott A, Gaspar J, Stuchell-Brereton MD, Alam SL, Skalicky JJ, Sundquist WI. Structure and ESCRT-III protein interactions of the MIT domain of human VPS4A. Proc Natl Acad Sci U S A 2005;102(39):13813-13818.

105. Kieffer C, Skalicky JJ, Morita E, De Domenico I, Ward DM, Kaplan J, Sundquist WI. Two distinct modes of ESCRT-III recognition are required for VPS4 functions in lysosomal protein targeting and HIV-1 budding. Dev Cell 2008;15(1):62-73.

106. Yang D, Rismanchi N, Renvoise B, Lippincott-Schwartz J, Blackstone C, Hurley JH. Structural basis for midbody targeting of spastin by the ESCRT-III protein CHMP1B. Nat Struct Mol Biol 2008;15(12):1278-1286.

107. Agromayor M, Martin-Serrano J. Interaction of AMSH with ESCRT-III and deubiquitination of endosomal cargo. J Biol Chem 2006;281(32):23083-23091.

108. Zamborlini A, Usami Y, Radoshitzky SR, Popova E, Palu G, Gottlinger H. Release of autoinhibition converts ESCRT-III components into potent inhibitors of HIV-1 budding. Proc Natl Acad Sci U S A 2006;103(50):19140-19145.

109. Ma YM, Boucrot E, Villen J, Affar el B, Gygi SP, Gottlinger HG, Kirchhausen T. Targeting of AMSH to endosomes is required for epidermal growth factor receptor degradation. J Biol Chem 2007;282(13):9805-9812.

110. Row PE, Liu H, Hayes S, Welchman R, Charalabous P, Hofmann K, Clague MJ, Sanderson CM, Urbe S. The MIT domain of UBPY constitutes a CHMP binding and endosomal localization signal required for efficient epidermal growth factor receptor degradation. J Biol Chem 2007;282(42):30929-30937.

111. Tsang HT, Connell JW, Brown SE, Thompson A, Reid E, Sanderson CM. A systematic analysis of human CHMP protein interactions: Additional MIT domain-containing proteins bind to multiple components of the human ESCRT III complex. Genomics 2006;88(3):333-346.

112. Reid E, Connell J, Edwards TL, Duley S, Brown SE, Sanderson CM. The hereditary spastic paraplegia protein spastin interacts with the ESCRT-III complex-associated endosomal protein CHMP1B. Hum Mol Genet 2005;14(1):19-38.

113. Kim J, Sitaraman S, Hierro A, Beach BM, Odorizzi G, Hurley JH. Structural basis for endosomal targeting by the Bro1 domain. Dev Cell 2005;8(6):937-947.

114. Doyotte A, Mironov A, McKenzie E, Woodman P. The Bro1-related protein HD-PTP/PTPN23 is required for endosomal cargo sorting and multivesicular body morphogenesis. Proc Natl Acad Sci U S A 2008;105(17):6308-6313.

115. Luhtala N, Odorizzi G. Bro1 coordinates deubiquitination in the multivesicular body pathway by recruiting Doa4 to endosomes. J Cell Biol 2004;166(5):717-729.

116. Teis D, Saksena S, Emr SD. Ordered assembly of the ESCRT-III complex on endosomes is required to sequester cargo during MVB formation. Dev Cell 2008;15(4):578-589.

117. Ghazi-Tabatabai S, Saksena S, Short JM, Pobbati AV, Veprintsev DB, Crowther RA, Emr SD, Egelman EH, Williams RL. Structure and disassembly of filaments formed by the ESCRT-III subunit Vps24. Structure 2008;16(9):1345-1356.

118. Lata S, Schoehn G, Jain A, Pires R, Piehler J, Gottlinger HG, Weissenhorn W. Helical structures of ESCRT-III are disassembled by VPS4. Science 2008;321(5894):1354-1357.

119. Saksena S, Wahlman J, Teis D, Johnson AE, Emr SD. Functional reconstitution of ESCRT-III assembly and disassembly. Cell 2009;136(1):97-109.

120. Wollert T, Wunder C, Lippincott-Schwartz J, Hurley JH. Membrane scission by the ESCRT-III complex. Nature 2009;458(7235):172-177.

121. Lata S, Roessle M, Solomons J, Jamin M, Gottlinger HG, Svergun DI, Weissenhorn W. Structural basis for autoinhibition of ESCRT-III CHMP3. J Mol Biol 2008;378(4):818-827.

122. Babst M, Wendland B, Estepa EJ, Emr SD. The Vps4p AAA ATPase regulates membrane association of a Vps protein complex required for normal endosome function. Embo J 1998;17(11):2982-2993.

123. Bishop N, Woodman P. ATPase-defective mammalian VPS4 localizes to aberrant endosomes and impairs cholesterol trafficking. Mol Biol Cell 2000;11(1):227-239.

124. Fujita H, Yamanaka M, Imamura K, Tanaka Y, Nara A, Yoshimori T, Yokota S, Himeno M. A dominant negative form of the AAA ATPase SKD1/VPS4 impairs membrane trafficking out of endosomal/lysosomal compartments: class E vps phenotype in mammalian cells. J Cell Sci 2003;116(Pt 2):401-414.

125. Hanson PI, Whiteheart SW. AAA+ proteins: have engine, will work. Nat Rev Mol Cell Biol 2005;6(7):519-529.

126. Azmi I, Davies B, Dimaano C, Payne J, Eckert D, Babst M, Katzmann DJ. Recycling of ESCRTs by the AAA-ATPase Vps4 is regulated by a conserved VSL region in Vta1. J Cell Biol 2006;172(5):705-717.

127. Scott A, Chung HY, Gonciarz-Swiatek M, Hill GC, Whitby FG, Gaspar J, Holton JM, Viswanathan R, Ghaffarian S, Hill CP, Sundquist WI. Structural and mechanistic studies of VPS4 proteins. Embo J 2005;24(20):3658-3669.

128. Stuffers S, Brech A, Stenmark H. ESCRT proteins in physiology and disease. Exp Cell Res 2008.

129. Lee JA, Gao FB. Roles of ESCRT in autophagy-associated neurodegeneration. Autophagy 2008;4(2):230-232.

130. Parkinson N, Ince PG, Smith MO, Highley R, Skibinski G, Andersen PM, Morrison KE, Pall HS, Hardiman O, Collinge J, Shaw PJ, Fisher EM. ALS phenotypes with mutations in CHMP2B (charged multivesicular body protein 2B). Neurology 2006;67(6):1074-1077.

131. Skibinski G, Parkinson NJ, Brown JM, Chakrabarti L, Lloyd SL, Hummerich H, Nielsen JE, Hodges JR, Spillantini MG, Thusgaard T, Brandner S, Brun A, Rossor MN, Gade A, Johannsen P*, et al.* Mutations in the endosomal ESCRTIII-complex subunit CHMP2B in frontotemporal dementia. Nat Genet 2005;37(8):806-808.

132. Rusten TE, Vaccari T, Lindmo K, Rodahl LM, Nezis IP, Sem-Jacobsen C, Wendler F, Vincent JP, Brech A, Bilder D, Stenmark H. ESCRTs and Fab1 regulate distinct steps of autophagy. Curr Biol 2007;17(20):1817-1825.

133. Filimonenko M, Stuffers S, Raiborg C, Yamamoto A, Malerod L, Fisher EM, Isaacs A, Brech A, Stenmark H, Simonsen A. Functional multivesicular bodies are required for autophagic clearance of protein aggregates associated with neurodegenerative disease. J Cell Biol 2007;179(3):485-500.

134. Shiels A, Bennett, T.M., Knopf, H.L.S., Yamada, K., Yoshiura, K., Niikawa, N., Shim, S., and Hanson, P.I. CHMP4B, a Novel Gene for Autosomal Dominant Cataracts Linked to Chromosome 20q. Am J Hum Genet 2007;81(3):596-606.

135. Shim S, Merrill S, Hanson PI. Novel Interactions of ESCRT-III with LIP5 and VPS4 and their implications for ESCRT-III disassembly. Mol Biol Cell 2008;19(6):2661-2672.

FIGURE LEGENDS

Figure 1-1 Membrane trafficking pathways with particular emphasis on the endocytic pathway.

Secretory pathway (outbound) and endocytic pathway (inbound) are shown. Organelles involved in the secretory pathway include the endoplasmic reticulum (ER), Golgi and trans-Golgi network (TGN). The endocytic pathway consists of endocytic vesicles, early and late endosomes, and lysosomes. A subset of endosomes containing internal vesicles is called the multivesicular body (MVB). Transmembrane proteins are internalized by endocytosis, and transported to early endosomes. Some proteins are recycled back to the plasma membrane, directly (step 1a) or indirectly through the recycling endosome (or ERC) (step 1b). Others are sorted to the TGN (step 2). Transmembrane proteins on the cell surface (e.g. receptors) are internalized and sorted into intralumenal vesicles (ILVs) of the MVB, which are eventually delivered to the lysosome lumen (step 3). In contrast, lysosomal membrane proteins remain on the limiting membrane of the MVB (step 4) (40).

Figure 1-2 Schematic diagram for MVB biogenesis and other topologically related processes.

Shown are three different cellular processes - MVB vesicle formation, viral budding from the cell surface and cell abscission during cytokinesis, all of which involve budding away from the cytoplasm.

Table 1-1 Class E Vps proteins and their mammalian orthologs.

Figure 1-3 Model for how ESCRT machinery functions in cargo sorting and MVB vesicle formation.

ESCRT-0, I and II complexes are sequentially recruited to the endosomal membrane by their interactions with membranes and ubiquitinated cargo. ESCRT-III is in turn recruited to the endosomal membrane, and engages deubiquitinating enzymes to remove ubiquitin from cargo and the AAA ATPase Vps4 to disassemble ESCRT complexes. During this process, the MVB vesicle is formed and cargo is sorted into the vesicle (39). PI3P – phosphoinositide-3-phosphate, Ub – ubiquitin

Figure 1-4 Structure of an ESCRT-III protein.

Partial crystal structure of an ESCRT-III protein, CHMP3 is shown in yellow (Protein Data Bank number:2GD5). The C-terminal end missing from the crystal structure is shown in gray. An ESCRT-III protein consists of 6 helices. The first four helices form a helical bundle responsible for dimerization and membrane binding. The fifth helix is positioned perpendicularly to the helical bundle. The last helix in the C-terminal end was separately crystallized together with the Vps4 MIT domain (101-103).

Figure 1-1

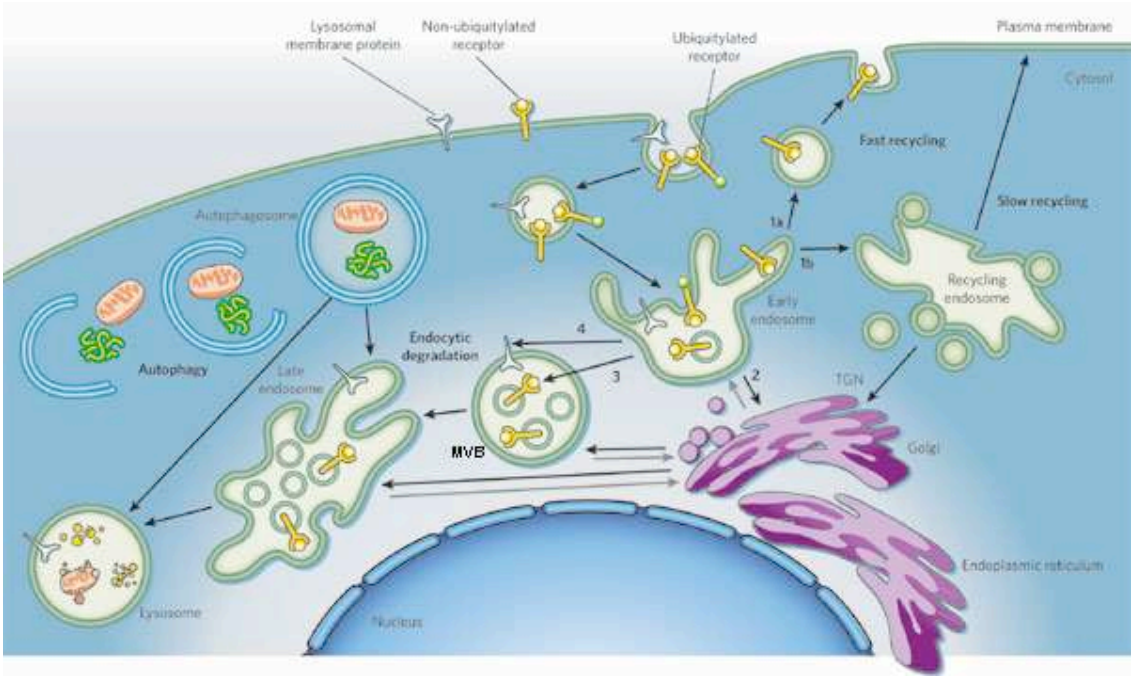

Adapted from Raiborg and Stenmark, 2009, Nature

Figure 1-2

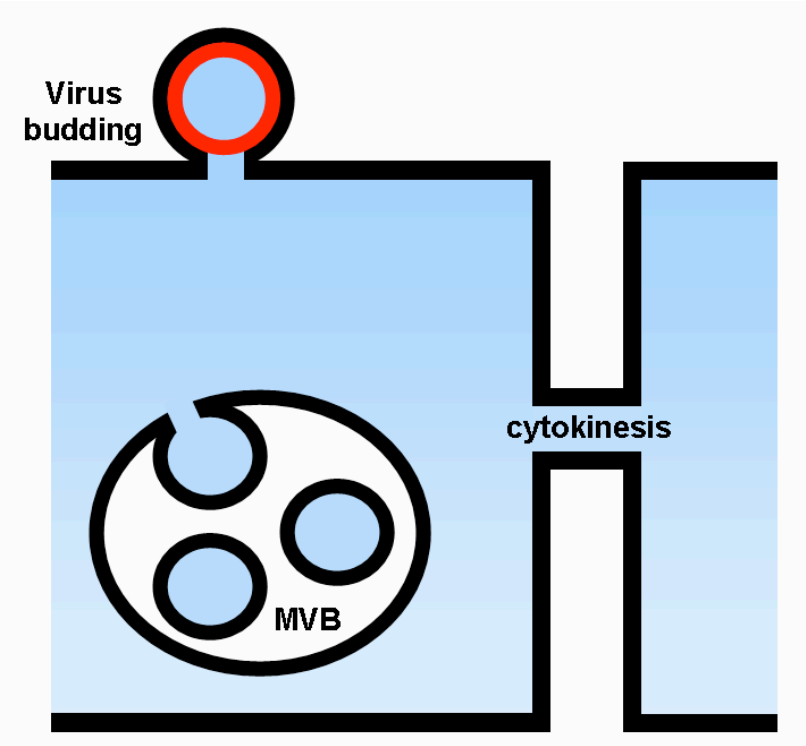

Modified from Hanson *et al.*, Curr Opin Cell Biol, 2009

Table 1-1

Complex	Sub-complex	Yeast name	Mammalian name	Ubiquitin binding motif	Selected interacting proteins (mammalian)
ESCRT-0		Vps27	HRS	UIM	TSG101
		Hse1	STAM1, 2	UIM	AMSH, UBPY
ESCRT-I		Vps23	TSG101	UEV	HRS, ALIX
		Vps28	VPS28		CHMP6
		Vps37	VPS37A, B, C, D		
		Mvb12	MVB12A, B		
ESCRT-II		Vps22	EAP30		
		Vps25	EAP20		CHMP6
		Vps36	EAP45	GLUE/NZF	
ESCRT-III	Core, Soluble	Vps2	CHMP2A, B		VPS4, LIP5
		Vps24	CHMP3		VPS4, AMSH, LIP5
	Core, Membrane proximal	Vps20	CHMP6		VPS4, ESCRT-II
		Snf7(Vps32)	CHMP4A, B, C		VPS4, ALIX
	ESCRT-III like	Vps60(Mos1)	CHMP5		LIP5
		Did2(Vps46)	CHMP1A, B		VPS4, LIP5, Spastin
		-	CHMP7		UBPY
Others		Vps4	VPS4A, B		LIP5, ESCRT-III
		Vta1	LIP5		VPS4, ESCRT-III
		Bro1	ALIX		CHMP4
		Ist1	IST1		VPS4, CHMP1

Figure 1-3

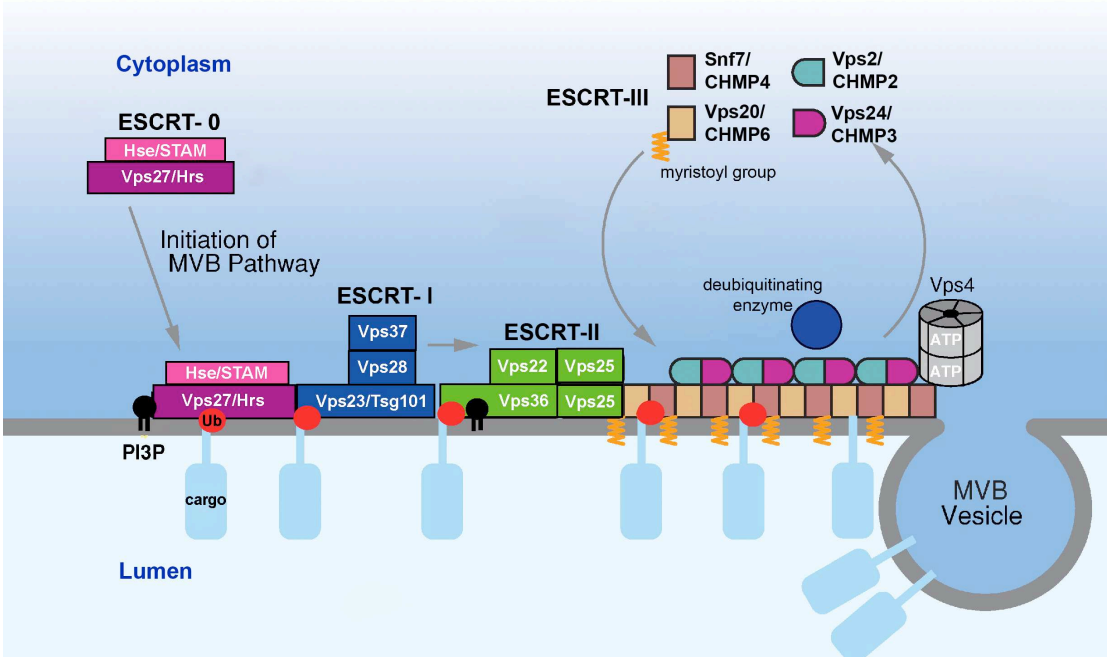

Modified from Hurley and Emr, Annu Rev Biophys Biomol Struct, 2006

Figure 1-4

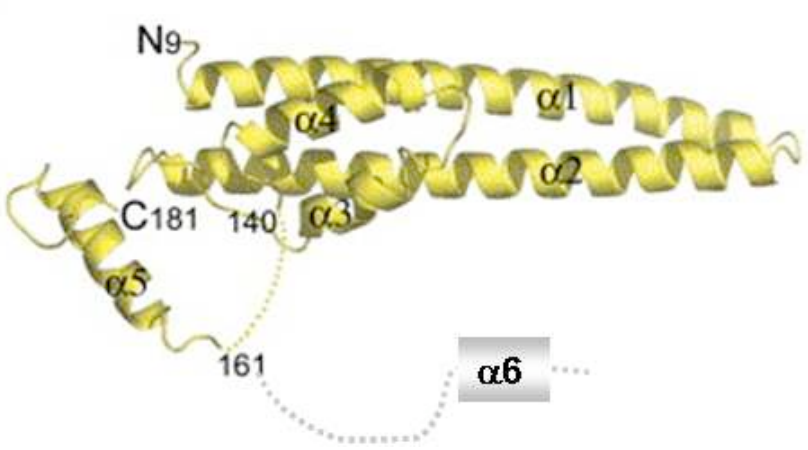

Modified from Muziol *et al.,* Dev Cell, 2006

CHAPTER TWO

Structure/function analysis of four core ESCRT-III proteins reveals common regulatory role for extreme C-terminal domain

ACKNOWLEDGEMENTS

I would like to thank Lisa Kimpler for general technical support and carrying out the immunofluorescence analysis which resulted in Figure 7A. I would also like to thank all members of the Hanson lab for helpful discussion. The work is published as Shim S, Kimpler LK, Hanson PI (2007). Structure/function analysis of four core ESCRT-III proteins reveals common regulatory role for extreme C-terminal domain. Traffic, 8:1068-79, which is reprinted here with permission of John Wiley & Sons Ltd.

INTRODUCTION

Multivesicular bodies (MVBs) are a subset of late endosomes that contain intralumenal vesicles (ILVs) generated by invagination from the endosomal membrane (1, 2). The MVB is an intermediate compartment *en route* to the lysosome; surface receptors destined for degradation and some newly synthesized lysosomal proteins are sorted into ILVs and delivered to the lysosome (1). In specialized cells, MVBs can instead fuse with the plasma membrane to secrete ILVs, also known as exosomes (3).

Genetic studies of vacuolar protein sorting (Vps) in *S. cerevisiae* have identified ~18 proteins specifically involved in creating the MVB, known as class E Vps proteins. Functional loss of any of these proteins leads to formation of an aberrant late endosome lacking internal vesicles, referred to as the 'class E compartment' (4, 5). Class E Vps proteins are conserved from yeast to human suggesting that the MVB pathway is universal (5, 6).

Most class E Vps proteins form heteromeric protein complexes called ESCRTs (endosomal sorting complexes required for transport) (6). Current thinking is that ESCRT complexes are intimately involved in both cargo sorting and ILV formation. In the most clearly defined pathway, ubiquitination marks cargo proteins for incorporation into a nascent ILV. Ubiquitinated cargo binds, possibly sequentially, to Vps27-Hse1, ESCRT-I, and ESCRT-II. These complexes in turn recruit ESCRT-III proteins to create ESCRT-III complex. ESCRT-III engages Bro1 and deubiquitinating enzymes that remove the initiating ubiquitin. ESCRT-III also recruits Vps4, which is an AAA+ (ATPases associated with a variety of cellular activities) protein that is thought to disassemble ESCRT complexes for recycling of the MVB machinery. How the sequential engagement of these complexes leads to ILV formation is unclear.

ESCRT-III appears to play a central coordinating role, bringing upstream (ESCRT-I, -II) and downstream (Bro1, deubiquitinating enzymes, and Vps4) factors

together. The specific composition, organization, and regulation of ESCRT-III is however not well understood. Components of ESCRT-III are related ~200-250 amino acid proteins that have characteristic basic N-terminal and acidic C-terminal halves (7). ESCRT-III proteins in *S. cerevisiae* include the core complex components Snf7p, Vps20p, Vps2p and Vps24p along with two additional members, Did2p and Vps60p (7, 8). Of the four core ESCRT-III proteins, two (Vps2p and Vps24p) require the other two (Snf7p and Vps20p) for recruitment to the membrane (7). Because of this, these pairs are referred to as cytosolic and membrane proximal ESCRT-III subcomplexes (7). The family is expanded to 10 proteins in humans (9). Human ESCRT-III proteins are referred to as human orthologues of their yeast counterparts or CHMPs (CHarged Multivesicular body Proteins) (6).

The discovery that at least some of the mammalian class E proteins are centrally involved in viral budding – a reaction topologically equivalent to ILV formation – has added new insight into the function of these proteins (10-12). Structural proteins of viruses (i.e. Gag in retrovirus) contain L domains (late assembly domains) in which mutations arrest viral release at a late stage (10, 13). Different L domains recruit different cellular factors; for example, P[T/S]AP sequences bind to an ESCRT-I protein, Tsg101, while YPxL sequences interact with Alix, the mammalian orthologue of Bro1 (9, 14-16). ATPase deficient VPS4 and ESCRT-III proteins fused to GFP inhibit release of viruses involving either type of L-domain (9, 16-18), suggesting a potential role for ESCRT-III proteins in the final steps of extracytoplasmic budding.

ESCRT-III proteins cycle on and off membranes in parallel with their incorporation into ESCRT-III complexes (5, 6). Yeast two-hybrid screens and biochemical studies have delineated interactions between ESCRT-III proteins in both yeast and higher eukaryotes that probably mediate complex assembly (9, 18-21). For a subset of these proteins, interactions with membranes as well as their ability to

assemble into complexes has been shown to require sequences within their N-terminal halves (22-24).

As a step toward understanding the role of ESCRT-III in MVB biogenesis and viral budding, we explored the functional roles of predicted helical domains within individual ESCRT-III proteins, including the core complex components hVps2-1/CHMP2A, hVps24/CHMP3, hVps20/CHMP6 and hSnf7-1/CHMP4A. Removing a short C-terminal domain from each protein promoted membrane binding and polymer assembly. These truncated ESCRT-III proteins were predominantly localized on enlarged vacuoles and potently inhibited both endosomal processing and viral budding. Our results suggest a model for ESCRT-III in which each individual protein cycles between a default closed and an activated open state under control of sequences at its extreme C-terminus. The transition between these states is likely to be controlled by other components of the ESCRT pathway.

EXPERIMENTAL PROCEDURES

Plasmids

The following constructs have been previously described (23): pcDNA3.1-FLAG-CHMP4A full-length (1-222), pcDNA3.1 CHMP4A full-length-myc/His6, pcDNA3.1-FLAG-CHMP4A 1-116, pcDNA3.1-CHMP3 full-length(1-222)-myc/His6, pHO4d VPS4B/SKD1(E235Q)-His6/myc and pGEX 4T-1 CHMP4A full-length. Dr. Lee Ratner (Washington University, St. Louis, MO) kindly provided pCMV55 encoding HIV Pr55(Gag).

To construct CHMP4A deletion mutants, DNA fragments corresponding to amino acids 1-80, 1-147, 1-181, 1-209, and 60-222 were amplified by polymerase chain reaction (PCR) using pcDNA3.1-FLAG-CHMP4A full-length as a template. Each fragment was inserted into pcDNA3.1-FLAG (a gift from Dr. Kenneth Johnson, Washington University, St. Louis, MO) between *BamHI* and *XhoI* sites to generate constructs with the FLAG epitope attached at the N-terminus. Additionally, 1-181 and 1-209 were inserted into pcDNA3.1-myc (a gift from Dr. Kenneth Johnson, Washington University, St. Louis, MO) between *BamHI* and *XhoI* sites to fuse a myc epitope to the N-termini.

To construct CHMP3 deletion mutants, DNA fragments corresponding to amino acids 1-119, 1-150 and 1-178 were amplified by PCR from pcDNA3.1 CHMP3-myc-His. Each fragment was inserted into pcDNA4/TO-myc (Invitrogen, Carlsbad, CA) via *BamHI* and *XhoI* sites to attach a myc epitope to the C-terminus.

cDNAs encoding CHMP6 full-length(1-201) and CHMP2A full-length(1-222) were amplified from HeLa cDNA (Clontech, Mountain View, CA). The CHMP6 cDNA and CHMP2A cDNA were cloned into pcDNA4/TO-myc.and pcDNA3.1-FLAG, respectively both via *BamHI* and *XhoI* sites. To make CHMP6 deletion constructs, DNA fragments of

CHMP6 corresponding to amino acids 1-115, 1-147 and 1-167 were amplified by PCR using pcDNA4/TO-CHMP6-full-length-myc as a template. These fragments were cloned into pcDNA4/TO-myc (Invitrogen, Carlsbad, CA) via *BamHI and XhoI* sites. To generate CHMP2A deletion mutants, DNA fragments of CHMP2A corresponding to amino acids 1-116, 1-144 and 1-180 were amplified by PCR using pcDNA3.1 FLAG-CHMP2A full-length as template. These fragments were inserted into pcDNA3.1-FLAG via *BamHI* and *XhoI* sites. All CHMP6 constructs were tagged with myc epitope at the C-termini while FLAG epitope was attached to the N-termini of all CHMP2A constructs.

To express CHMP2A in BL21(DE3) *E.coli*, DNA fragments of CHMP2A corresponding to amino acids 56-222 and 56-180 were amplified by PCR from pcDNA3.1 FLAG-CHMP2A and cloned into pGEX 4T-1 via *BamHI* and *XhoI* sites. DNA fragments corresponding to CHMP2A full-length and amino acids 1-144 were obtained by digesting pcDNA3.1 FLAG-CHMP2A full-length and 1-144 with *BamHI* and *XhoI* and inserted into pGEX 4T-1 between the two restriction sites.

All constructs were sequenced using ABI big dye reagents at the Nucleic Acid Chemistry Laboratory (Washington University, St. Louis, MO).

Immunofluorescence analysis

COS-7 cells were plated onto glass coverslips and transfected with plasmid(s) using Lipofectamine 2000 (Invitrogen, Carlsbad, CA) following the manufacturer's instructions. 18-24 hrs after transfection, cells were fixed with 3.5% paraformaldehyde in phosphate buffered saline (PBS) for 15 min and permeabilized with 0.2% Triton X-100 in PBS for 15min. Cells were stained with primary and secondary antibodies in blocking buffer (5% goat serum, 100mM NaCl, 30mM HEPES, 2mM $CaCl_2$, pH7.4). To visualize nuclei, cells were co-stained with 4'-6-diamidino-2-phenylindole (Molecular Probes, Eugene, OR). The following antibodies were used for immunostaining: mouse

monoclonal anti-FLAG, M2 (Sigma, St. Louis, MO, 1:2500), rabbit anti-FLAG (Sigma, St. Louis, MO, 1:500), mouse monoclonal anti-myc (from the 9E10 hybridoma cell line (40), 1:500), rabbit anti-myc (Cell Signaling Technology, Danvers, MA, 1:500), mouse monoclonal anti-ubiquitin, FK2 (Affiniti Research Products, Plymouth Meeting, PA 1:1000). Secondary antibodies, goat anti-mouse conjugated to Alexa Fluor 488 or Alexa Fluor 555 and goat anti-rabbit conjugated to Alexa Fluor 488 or Alexa Fluor 555 were purchased from Molecular Probes (Invitrogen, Carlsbad, CA). Microscopic images were obtained using a Leica Diaplan microscope and Zeiss Axiocam camera, processed in Adobe Photoshop (Adobe System, San Jose, CA) and assembled into figures in Adobe Illustrator (Adobe System, San Jose, CA).

Sedimentation assay

HEK (Human Embryonic Kidney) 293T cells in 6 cm dishes were transfected with the indicated plasmid(s) using Lipofectamine 2000. 18-24 hrs after transfection, cells were washed with PBS and solubilized in 350 μL lysis buffer (10mM Tris, 10% sucrose, 1mM ethylenediaminetetraacetic acid (EDTA), 1% Triton X-100, 0.1mg/ml phenylmethylsulfonyl fluoride (PMSF), complete protease inhibitor (Roche Diagnostics, Alameda, CA) and 4 μL benzonase (Novagen, San Diego, CA), pH 8.0) on ice for 40 min. Supernatant and pelletable fractions were separated by centrifuging samples at 10,000 x g for 15 minutes at 4^{o}C. Pellets were resuspended to the same volume as supernatant in lysis buffer. Equal volumes of fractions were analyzed by immunoblotting using rabbit anti-FLAG antibody (Sigma, St. Louis, MO, 1:5000), mouse monoclonal anti-myc (from the 9E10 hybridoma cell line, 1:3000) or rabbit anti-CHMP3 antibody ((23), 1:20).

Membrane flotation

COS-7 cells in 10 cm dishes were transfected with the indicated plasmid using Lipofectamine 2000. 18-24 hrs after transfection, cells were harvested in buffer (10mM Tris, 10% sucrose, 1mM EDTA, 0.1mg/ml PMSF and complete protease inhibitor, pH 8.0). Cells were frozen and thawed once followed by homogenization using a ball bearing cell cracker. Homogenate was brought to 73% sucrose (1.5ml) and overlaid with 65% sucrose (2.5ml) and 10% sucrose (1.5ml). After centrifugation at 34000 rpm in a SW55 Ti rotor (Beckman Coulter, Fullerton, CA) for 18 hrs at 4ºC, fractions were collected from the top and analyzed by western blotting using rabbit anti-FLAG (Sigma, St. Louis, MO, 1:5000), mouse anti-myc antibody (from the 9E10 hybridoma cell line, 1:3000), rabbit anti-caveolin antibody (BD Transduction Laboratories, San Jose, CA, 1:2500) or mouse anti-alpha-tubulin antibody (DM 1A, Sigma, St. Louis, MO, 1:5000).

VLP (Virus-like-particle) release assay

HEK 293T cells in 6 cm dishes were transfected using Lipofectamine 2000. Cells were transfected with 4 μg pCMV55 encoding HIV Gag alone or together with 1μg of the indicated ESCRT-III construct. These concentrations were chosen to avoid nonspecific effects. 18-24 hrs after transfection, media containing VLP was harvested and clarified by passing through a 0.45 μm filter. VLPs were pelleted by centrifugation through a 20% sucrose cushion at 26,000 rpm in a SW41 Ti rotor (Beckman Coulter, Fullerton, CA) for 3 hrs. VLPs and cell lysates were resuspended in SDS sample buffer and analyzed by immunoblotting using a rabbit antibody against p24, the capsid domain of HIV Gag (a gift from Dr. Lee Ratner, Washington University, St. Louis, MO, 1:5000).

GST (Glutathione-S-transferase) pull down assay

To express GST proteins, BL21(DE3) *E.coli* were transformed with pGEX 4T-1 constructs, grown at 37 ºC to $O.D._{600}$ ~ 0.8 and induced at room temperature for 4 hours with 0.5mM isopropyl-β-thiogalactopyranoside. Cells were lysed by sonication in buffer (20mM Tris, 250mM NaCl, 5% glycerol and 0.1mg/ml PMSF, pH 7.4) and GST proteins in lysates were immobilized on glutathione-Sepharose beads (Amersham Biosciences, Piscatawy, NJ). To prepare bacterial lysate containing VPS4B, BL21(DE3) *E.coli* were transformed with pHO4d VPS4B/SKD1(E235Q)-His6/myc, grown and induced as described above. The cells were sonicated in lysis buffer (30mM HEPES, 120mM NaCl, 2mM ATP, 5mM $MgCl_2$, 5% glycerol, 0.1mg/ml PMSF, pH 7.4) and the lysate was incubated with GST proteins immobilized on beads for 1 hr at 4 ºC in reaction buffer (20mM HEPES, 100mM NaCl, 2mM ATP, 4mM $MgCl_2$, pH7.4). Bound and unbound VPS4B/SKD1(E235Q) were analyzed by immunoblotting with anti-myc antibody (from the 9E10 hybridoma cell line 1:3000) while GST proteins were visualized by immunoblotting with a rabbit anti-GST antibody (Invitrogen, Carlsbad, CA, 1:5000).

Tissue Culture

COS-7 and HEK293T cells were grown in Dulbecco's modified Eagle's medium (Gibco-BRL, Gaithersburg, MD) containing 5% fetal bovine serum (Gibco-BRL, Gaithersburg, MD), 5% supplemented calf serum (Hyclone Laboratories, Logan, UT) and 2mM glutamine (Tissue culture center, Washington University, St. Louis, MO).

Western Blot Analysis

Samples were separated on SDS-PAGE gels and transferred to nitrocellulose membranes. Blots were incubated with indicated primary antibodies followed by secondary antibodies conjugated to horse radish peroxidase (HRP) in Tris-buffered

saline/0.1% Tween20 (TBST) buffer containing 5% nonfat milk. Proteins were detected using Super Signal West Pico (Pierce, Rockford, IL) according to the manufacturer's instruction.

RESULTS

Secondary structure of ESCRT-III proteins

To generate a framework to guide our structure/function analysis of ESCRT-III proteins, we used a neural-net based secondary structure prediction program to identify a common set of six predicted α-helices in human isoforms of the four core members of the ESCRT-III family, Vps2, Vps24, Vps20, and Snf7 (25). For Snf7 and Vps2, we focused on one each of the closely related human isoforms (CHMP4A/CHMP4a and hVps2-1/CHMP2a). Vps20 and Vps24 are present as only one isoform in humans, hVps20/CHMP6 and hVps24/CHMP3. As shown in Fig. 2-1, five predicted helices span most of the N-terminal two-thirds of each protein and are connected by a relatively long linker to a sixth short predicted helix near the C-terminus. The first five predicted helices correspond well with helices present in the recently published crystal structure of a hVps24/CHMP3 fragment (24). As has been previously noted, the N-terminal halves of ESCRT-III proteins are positively charged while the C-terminal halves are negatively charged. Correspondingly, $\alpha1 - \alpha3$ are basic while $\alpha4 - \alpha6$ are acidic (Fig. 2-1).

Removing C-terminal helices unmasks new properties in ESCRT-III proteins

Based on earlier proposals from us and others that the C-terminal acidic halves of ESCRT-III proteins might function as regulatory domains (6, 22, 23), we deleted one, two, or three predicted helices and flanking sequences from the C-terminal end of each ESCRT-III protein. To monitor the effects of these deletions, we transiently transfected constructs encoding FLAG- or myc-tagged mutant proteins into COS-7 cells and compared the distribution of each with that of its full-length counterpart by immunostaining and epifluorescence microscopy. Consistent with previous studies (19, 22, 23, 26-28), full-length CHMP2A and CHMP3 were diffusely distributed throughout

the cytosol and nucleus, while CHMP6 was associated with the plasma membrane and CHMP4A at least in part with endosomes (Fig. 2-1, column 1).

Surprisingly, removing only the most C-terminal helix (α6) along with flanking sequences dramatically changed the localization of all four proteins (Fig. 2-1, column 2). Unlike their full-length counterparts, CHMP2A (α1 – α5) and CHMP3 (α1 – α5) were found primarily on enlarged vacuoles. CHMP6 (α1 – α5) coalesced into discrete patches on the plasma membrane and internal vacuoles. CHMP4A (α1 – α5) was enriched on uniformly sized enlarged vacuoles.

Deleting additional helices (α5 and α4) from CHMP2A and CHMP3 reduced association of the protein fragments with vacuoles (Fig. 2-2, columns 3 & 4). CHMP3 (α1 – α4) accumulated on the plasma membrane, where it – like the CHMP6 mutants – was irregularly distributed in discrete patches. CHMP3 (α1 – α3) as well as both CHMP2A (α1 – α4) and CHMP2A (α1 – α3) accumulated primarily in the nucleus, presumably because of their positive charge (see Fig. 2-1). All CHMP6 deletion mutants (α1 – α5, α1 – α4, α1 – α3) formed patches along the plasma membrane. Finally, CHMP4A (α1 – α4) and (α1 – α3) were less apparent on vacuoles and instead present along the plasma membrane as well as diffusely throughout the cell.

The fact that removing the C-terminal α6 domain (35-45 amino acids including α6 and flanking sequences) changes the distribution of all four core ESCRT-III proteins led us to hypothesize that this short region may play a general role in regulating the engagement and activity of these proteins. To explore this idea, we compared full-length (α1 – α6) and C-terminally truncated (α1 – α5) proteins in more quantitative assays of localization and function.

Effects of removing ESCRT-III C-termini on membrane association and polymer assembly

To determine whether the striking differences in localization of full-length *vs.* truncated (α1 – α5) ESCRT-III proteins represent changes in their association with membranes, we floated cell lysates through sucrose step gradients to separate soluble or cytoskeletal proteins from those bound to membranes. Consistent with our immunofluorescence experiments (Fig. 2-2), CHMP2A and CHMP3 shifted from soluble to membrane-associated fractions following removal of α6 and flanking sequences (Fig. 2-3A). Full-length CHMP4A was already partially membrane associated (as previously shown (23)), but deleting its C-terminus enhanced this interaction such that all of CHMP4A (α1 – α5) was recovered in membrane-associated fractions (Fig. 2-3A). Both full-length and truncated CHMP6 cofractionated completely with membranes (Fig. 2-3A), presumably because of their myristoylation (19). Parallel immunoblots confirmed that the gradients cleanly separate membrane associated proteins such as caveolin from soluble and cytoskeletal proteins including α-tubulin (Fig. 2-3A, bottom). In all of these experiments, ESCRT-III proteins are highly overexpressed (>100 fold above endogenous levels, data not shown). It is therefore likely that the observed distributions reflect direct interactions between individual ESCRT-III proteins and membranes.

ESCRT-III proteins cycle on and off of membranes, and also assemble transiently into large complexes (5, 6). We wondered whether removing the C-terminal α6 domain would also enhance assembly into complexes. To detect complexes, we used a simple sedimentation assay (Fig. 2-3B). Transfected cells were incubated in buffer containing 1% Triton X-100 and then centrifuged at 10,000 x g. Pelleted material was resuspended in a volume equal to that of the soluble fraction, and the distribution of proteins between the two fractions was monitored by immunoblotting. While full-length

CHMP2A and CHMP3 were soluble, their α1 – α5 mutants were mostly (CHMP2A) or partially (CHMP3) insoluble (Fig. 2-3B). Full-length CHMP6 was already partially insoluble, but again its α1 – α5 mutant was even less soluble (Fig. 2-3B). Both full-length and truncated CHMP4A were insoluble (Fig. 2-3B). We conclude that removing α6 and flanking sequences promotes complex assembly. Once again, because individual proteins are highly overexpressed (>100 fold above endogenous levels), it is unlikely that formation of these insoluble protein complexes depends on other cellular proteins.

Requirements for ESCRT-III polymer assembly

To better understand how ESCRT-III proteins assemble into complexes, we used a series of deletion mutants to define the minimal structural requirements needed to form them. We chose CHMP4A for these experiments and compared the distribution of different fragments following sedimentation. As shown in Fig. 2-4, removing part of α1 or α2 (leaving residues 60-222, 1-80) shifted the protein entirely from insoluble to soluble fractions. α1 and α2 are therefore required for polymer assembly. A fragment containing the first three helices (α1 – α3, 1-116) was present to a small extent in the pellet (Fig. 2-4). Our earlier finding that adding a lipid modification to the α1 – α3 fragment increases its concentration on membranes and enhances its sedimentation (23) suggests that α1 – α3 retains the ability to polymerize, but does so only inefficiently without supplemental membrane targeting. A fragment also containing α4 (α1 – α4, 1-147) was found mostly in the pellet, and one further containing α5 (α1 – α5, 1-181) was entirely in the pellet (Fig. 2-4). These results show that α1 – α5 contains everything needed to efficiently bring the protein to the membrane and build ESCRT-III containing polymeric complexes.

Removing C-terminal α6 domains creates inhibitors of MVB biogenesis and viral budding: identification of a common regulatory domain?

To explore and compare the effects of truncating each of these ESCRT-III proteins on their function, we asked how expressing full-length (α1 – α6) or truncated (α1 – α5) proteins affects endosomes and viral particle release. To monitor protein handling on late endosomes, we took advantage of the fact that inhibiting the ESCRT pathway causes ubiquitinated proteins to accumulate on the rim of enlarged endosomes (23, 29, 30). We immunostained COS-7 cells expressing full-length or C-terminally deleted ESCRT-III proteins with an antibody that specifically recognizes conjugated ubiquitin (FK2). Cells expressing full-length ESCRT-III proteins had a level and distribution of ubiquitin conjugates indistinguishable from that of control cells (Fig. 2-5, left panel). In contrast, cells expressing any of the four α1 – α5 truncation mutants showed a striking accumulation of ubiquitin conjugates on large vacuoles (Fig. 2-5, left panel). In most but not all cases, the mutant ESCRT-III protein was also present on the vacuoles (Fig. 2-5, right panel). Note that typical cells expressing full-length CHMP4A did not have significantly elevated levels of ubiquitin conjugates, although as previously reported, at very high levels of expression, full-length CHMP4A did increase FK2 reactive proteins on enlarged endosomes (data not shown and (23)).

To compare the effect of full-length and truncated ESCRT-III proteins on release of HIV virus-like-particles (VLPs) from cells, we cotransfected full-length or mutant (α1 – α5 and α1 – α4) ESCRT-III proteins with a plasmid encoding Pr55 HIV Gag into HEK293T cells. Recovered VLPs were quantitated by immunoblotting with an antibody against its p24 capsid domain. Consistent with previous reports (9, 16, 18), expressing any of the full-length ESCRT-III proteins with small N- or C-terminal epitope tags had little effect on VLP production (Fig. 2-6 A-D). In contrast, deletion mutants (α1 – α5 and

α1 – α4) greatly reduced VLP release (Fig. 2-6 A-D). Cell lysates from cells expressing inhibitory mutants typically contained increased levels of Gag. All of the ESCRT-III proteins were expressed at similar levels (Fig. 2-6 A-D).

We were initially surprised to find that removing α6 and flanking sequences from CHMP4A created a protein that inhibited viral budding while full-length CHMP4A did not (Fig. 2-6D) because both forms of CHMP4A efficiently formed membrane associated polymeric complexes (Fig. 2-3). To confirm that expressing CHMP4A together with Gag did not change its behavior, we carried out a sedimentation assay with cells expressing both proteins (Fig. 2-6E). Full-length (α1 – α6) and truncated (α1 – α5) CHMP4A pelleted efficiently, indicating that both remained assembled in large complexes. As noted above, full-length CHMP4A also had substantially less effect than truncated (α1 – α5) protein on the distribution of ubiquitin conjugates in cells (Fig. 2-5). These findings suggest that there might be more than one step in the assembly and activation of CHMP4A (see Fig. 2-9 below for model).

CHMP4A (α1 – α5) mutant recruits full-length ESCRT-III proteins onto endosomes and into detergent insoluble complex

To determine if ESCRT-III (α1 – α5) mutants interact with full-length ESCRT-III proteins, we asked whether a mutant affects the distribution of other full-length ESCRT-III proteins. Coexpressing CHMP4A 1-181 (α1 – α5 mutant) with CHMP2A, CHMP3 or CHMP6 recruited each of these full-length proteins to the enlarged endosomes delineated by CHMP4A 1-181 (Fig. 2-7A). Comparable incorporation of cotransfected or endogenous CHMP3 into sedimentable complex was also seen (Figs. 2-7B & 7C). This ability of CHMP4A (α1 – α5) to bring other full-length ESCRT-III proteins into complexes suggests a mechanism for propagating ESCRT-III assembly on endosomes (see Fig. 2-

9 below for model). In contrast, full-length CHMP4A recruited neither cotransfected nor endogenous CHMP3 into its Triton X-100 insoluble complex (Figs. 2-7B & 7C).

Interaction of VPS4 with ESCRT-III C-terminal domain

From the above analysis, it is clear that removing the C-terminal α6 domain (α6 and flanking sequences, total of 35-45 residues) causes major changes in association of ESCRT-III proteins with membranes and each other. Therefore, anything that binds to this region is likely to have a role (positive or negative) in controlling membrane association and polymer assembly.

A number of proteins – including VPS4, Alix/AIP1, EAP20, AMSH and spastin – have shown bind to different ESCRT-III proteins (9, 19, 31-34). While most of these interactions are limited to a subset of ESCRT-III proteins, VPS4 has proven to bind all four core ESCRT-III proteins as well as CHMP1. Since our data suggest a general role for the C-terminal α6 domain of ESCRT-III proteins, we set out to further examine VPS4 interactions involving this domain.

To determine whether VPS4 binding to ESCRT-III proteins involves the C-terminal α6 domain, we used proteins produced in *E. Coli* to study interaction of VPS4B/SKD1 with an ESCRT-III protein, CHMP2A (Fig. 2-8). We chose to examine CHMP2A because its affinity for GST-CHMP2A was higher than that for other GST-ESCRT-III proteins (data not shown). To localize the VPS4B/SKD1 binding site within an ESCRT-III protein, we tested its interaction with a number of GST-CHMP2A deletion mutants (Fig. 2-8). Removing the C-terminal α6 domain abolished VPS4B/SKD1 binding while removing α1 from the N-terminus had no effect on binding. Together with previous work on CHMP1 (31, 33), these results suggest that ESCRT-III proteins bind VPS4 via sequences near their C-termini.

DISCUSSION

The interaction of ESCRT-III proteins with each other, membranes, and other factors is clearly a highly regulated process. Based on our present work with four ESCRT-III proteins, we propose a model to describe the assembly of individual ESCRT-III proteins into membrane-associated polymers (Fig. 2-9). Each protein has a default "closed" conformation in which it is soluble and not associated with other components of the ESCRT machinery (Fig. 2-9A). In the model shown, α1 – α4 corresponds to the α-helical bundle and α5 to the perpendicular helix observed in the recent crystal structure of CHMP3/CHMP3 (24). Correct positioning of α6 and surrounding sequences is important for maintaining this "closed" state. When the C-terminal α6 domain is removed or displaced, the ESCRT-III protein "opens" and moves to the membrane where it assembles into polymeric complexes and recruits other ESCRT-III proteins (Fig. 2-9C). Our experiments suggest that these complexes can be homo- or hetero-polymeric i.e. contain some or all of the ESCRT-III proteins. Finally, a subset of ESCRT-III proteins including CHMP4A and CHMP6 may have an intermediate stage of assembly in which they form "closed" polymers that do not recruit other ESCRT-III proteins (Fig. 2-9B).

Deletion of C-terminal α6 domain brings out common properties of membrane association and polymer assembly

There are clear differences in the way in which ESCRT-III proteins associate with other proteins and membranes and are regulated (5, 6). These differences include unique binding partners, i.e. CHMP6/CHMP6 binds to the ESCRT-II subunit EAP20 (19) and hSnf7 binds to Alix (9, 16), and distinct post-translational modifications, i.e. only CHMP6/CHMP6 is N-myristoylated (7, 19). In our experiments, differences between ESCRT-III proteins were apparent in the behavior of overexpressed full-length proteins,

with CHMP6 and hSnf7 assembled at least partially into membrane-associated complexes and hVps2 and CHMP3 entirely soluble. However, all four proteins were similarly incorporated into membrane-bound complexes after removing their C-terminal ~40 amino acid α6 domain, demonstrating that they share an underlying ability to assemble into complexes and associate with membranes.

We believe that the efficient localization of each α1 – α5 ESCRT-III mutant to membranes indicates that each of the core ESCRT-III proteins interacts directly with membranes, arguing against the idea that some (soluble) require others (membrane proximal) for this link. Binding of α1 – α5 fragments to the membrane may be mediated by different determinants than the spontaneous association of "closed" hSnf7 and CHMP6 with membranes. Because α1 – α5 mutants of CHMP3, CHMP2A, and CHMP4A localize to swollen endosomes more efficiently than do α1 – α4 mutants (Fig. 2-2), sequences within and around α5 may be particularly important for directing the proteins to endosomal membranes. The presence of one *vs*. two ways to interact with membranes might explain the difference between soluble (Vps2 and Vps24) and membrane-proximal (Vps20 and Snf7) ESCRT-III subcomplexes (7).

Intertwined with the accumulation of ESCRT-III proteins on membranes is their assembly into large Triton X-100 insoluble complexes (Fig. 2-3B). How closely these complexes resemble *bona fide* ESCRT-III complex will require a more precise understanding of native ESCRT-III complex than is currently available. (ESCRT-III complex has so far only been characterized in yeast cells lacking Vps4 activity and does not have a specifically defined size (7)). We believe that the detergent insoluble complexes formed by the individual overexpressed ESCRT-III proteins studied here represent specific polymers rather than aggregates for the following reasons: (1) the polymerized α1 – α5 fragments accumulate selectively on endosomal membranes (Fig.

2-2); (2) CHMP4A α1 – α5 recruits soluble full-length CHMP3 into the complexes it forms (Fig.2-7 B&C); (3) endogenous ESCRT-III proteins accumulate in similar complexes when Vps4 is inactivated (7, 23); and (4) the proteins can be seen in highly organized filaments along the membrane when examined by quick-freeze deep-etch electron microscopy (P.I. Hanson *et al.*, unpublished data).

Inhibiting function: all truncated ESCRT-IIIs are potent inhibitors of both MVB and viral budding pathways

Despite variations in the intracellular distribution of different full-length ESCRT-III proteins, none of them have much effect on either the MVB pathway or viral budding (Figs. 2-5 & 6) indicating that overexpressed full-length proteins retain normal regulation and function. In contrast, removing the C-terminal α6 domain converted each protein into a potent inhibitor of both pathways (Figs. 2-5 & 6). These data add to existing evidence implicating ESCRT-III and associated proteins in ILV formation (7, 19, 22, 23, 35, 36) and viral budding (9, 16, 18). We do not know whether the effects of α1 – α5 mutant ESCRT-III proteins on these pathways are direct or indirect. Sorting this out will require reconstituting ESCRT-III function on membranes *in vitro*.

The inhibitory effects of removing C-terminal α6 domains from ESCRT-III proteins are similar to previously described effects of fusing bulky GFP tags to the C-termini of the same proteins (9, 16, 18). This leads us to propose that disrupting the normal disposition of the α6 domain is what "opens" or activates ESCRT-III proteins. Proteins that bind to the C-terminal α6 domains are therefore likely to play critical roles in regulating these transitions.

Putative regulatory factors

It has been shown that deleting the extreme N-termini (~ 60 amino acids) of CHMP1 and CHMP2A did not disrupt interaction with Vps4 (31, 32). We found that CHMP2A bound well to VPS4B/SKD1 in an interaction that required the C-terminal α6 domain. Precisely how different ESCRT-III proteins engage the three helix structure of the VPS4 MIT domain remains to be determined (31, 37, 38). Reconstituting the disassembly of ESCRT-III containing complex(es) by VPS4 will be required to establish the precise relationship between this reaction and ESCRT-III function in vesicle biogenesis.

While this study was under revision, Gottlinger and coworkers (39) described inhibitory effects of truncated (α1 – α4) CHMP3/CHMP3 and hSnf7-2/CHMP4B on viral budding, proposing that the C-terminal acidic halves of ESCRT-III proteins are autoinhibitory domains. They further reported that CHMP3 is activated by binding to AMSH, and consistent with our results with CHMP2A found that CHMP3 binds to VPS4 via sequences near its C-terminus.

What do transient membrane associated ESCRT-III complexes contribute to ILV formation and viral budding? So far, it is clear that ESCRT-III serves as an organizational scaffold to bring up- and down-stream factors together presumably for the common purpose of generating a vesicle. Whether and if so how they contribute to actual vesicle biogenesis remains to be established. Understanding how ESCRT-III polymers affect membrane structure will be an important next step forward, as will establishment of an *in vitro* assay for ILV formation.

REFERENCES

1.Katzmann DJ, Odorizzi G, Emr SD. Receptor downregulation and multivesicular-body sorting. Nat Rev Mol Cell Biol 2002;3(12):893-905.

2.Gruenberg J, Stenmark H. The biogenesis of multivesicular endosomes. Nat Rev Mol Cell Biol 2004;5(4):317-323.

3. Fevrier B, Raposo G. Exosomes: endosomal-derived vesicles shipping extracellular messages. Curr Opin Cell Biol 2004;16(4):415-421.

4. Raymond CK, Howald-Stevenson I, Vater CA, Stevens TH. Morphological classification of the yeast vacuolar protein sorting mutants: evidence for a prevacuolar compartment in class E vps mutants. Mol Biol Cell 1992;3(12):1389-1402.

5. Babst M. A protein's final ESCRT. Traffic 2005;6(1):2-9.

6. Hurley JH, Emr SD. The ESCRT complexes: structure and mechanism of a membrane-trafficking network. Annu Rev Biophys Biomol Struct 2006;35:277-298.

7. Babst M, Katzmann DJ, Estepa-Sabal EJ, Meerloo T, Emr SD. Escrt-III: an endosome-associated heterooligomeric protein complex required for mvb sorting. Dev Cell 2002;3(2):271-282.

8. Kranz A, Kinner A, Kolling R. A Family of Small Coiled-Coil-forming Proteins Functioning at the Late Endosome in Yeast. Mol Biol Cell 2001;12(3):711-723.

9. von Schwedler UK, Stuchell M, Muller B, Ward DM, Chung HY, Morita E, Wang HE, Davis T, He GP, Cimbora DM, Scott A, Krausslich HG, Kaplan J, Morham SG, Sundquist WI. The protein network of HIV budding. Cell 2003;114(6):701-713.

10. Morita E, Sundquist WI. Retrovirus budding. Annu Rev Cell Dev Biol 2004;20:395-425.

11. Bieniasz PD. Late budding domains and host proteins in enveloped virus release. Virology 2006;344(1):55-63.

12. Demirov DG, Freed EO. Retrovirus budding. Virus Res 2004;106(2):87-102.

13.Gottlinger HG, Dorfman T, Sodroski JG, Haseltine WA. Effect of mutations affecting the p6 gag protein on human immunodeficiency virus particle release. Proc Natl Acad Sci U S A 1991;88(8):3195-3199.

14. Garrus JE, von Schwedler UK, Pornillos OW, Morham SG, Zavitz KH, Wang HE, Wettstein DA, Stray KM, Cote M, Rich RL, Myszka DG, Sundquist WI. Tsg101 and the vacuolar protein sorting pathway are essential for HIV-1 budding. Cell 2001;107(1):55-65.

15.Martin-Serrano J, Zang T, Bieniasz PD. HIV-1 and Ebola virus encode small peptide motifs that recruit Tsg101 to sites of particle assembly to facilitate egress. Nat Med 2001;7(12):1313-1319.

16.Strack B, Calistri A, Craig S, Popova E, Gottlinger HG. AIP1/ALIX is a binding partner for HIV-1 p6 and EIAV p9 functioning in virus budding. Cell 2003;114(6):689-699.

17.Martin-Serrano J, Zang T, Bieniasz PD. Role of ESCRT-I in retroviral budding. J Virol 2003;77(8):4794-4804.

18.Martin-Serrano J, Yarovoy A, Perez-Caballero D, Bieniasz PD. Divergent retroviral late-budding domains recruit vacuolar protein sorting factors by using alternative adaptor proteins. Proc Natl Acad Sci U S A 2003;100(21):12414-12419.

19.Yorikawa C, Shibata H, Waguri S, Hatta K, Horii M, Katoh K, Kobayashi T, Uchiyama Y, Maki M. Human CHMP6, a myristoylated ESCRT-III protein, interacts directly with an ESCRT-II component EAP20 and regulates endosomal cargo sorting. Biochem J 2005;387(Pt 1):17-26.

20. Tsang HT, Connell JW, Brown SE, Thompson A, Reid E, Sanderson CM. A systematic analysis of human CHMP protein interactions: Additional MIT domain-containing proteins bind to multiple components of the human ESCRT III complex. Genomics 2006.

21.Bowers K, Lottridge J, Helliwell SB, Goldthwaite LM, Luzio JP, Stevens TH. Protein-protein interactions of ESCRT complexes in the yeast Saccharomyces cerevisiae. Traffic 2004;5(3):194-210.

22. Whitley P, Reaves BJ, Hashimoto M, Riley AM, Potter BV, Holman GD. Identification of mammalian Vps24p as an effector of phosphatidylinositol 3,5-bisphosphate-dependent endosome compartmentalization. J Biol Chem 2003;278(40):38786-38795.

23. Lin Y, Kimpler LA, Naismith TV, Lauer JM, Hanson PI. Interaction of the mammalian endosomal sorting complex required for transport (ESCRT) III protein hSnf7-1 with itself, membranes, and the AAA+ ATPase SKD1. J Biol Chem 2005;280(13):12799-12809.

24. Muziol T, Pineda-Molina E, Ravelli RB, Zamborlini A, Usami Y, Gottlinger H, Weissenhorn W. Structural basis for budding by the ESCRT-III factor CHMP3. Dev Cell 2006;10(6):821-830.

25. Cuff JA, Clamp ME, Siddiqui AS, Finlay M, Barton GJ. JPred: a consensus secondary structure prediction server. Bioinformatics 1998;14(10):892-893.

26. Katoh K, Shibata H, Hatta K, Maki M. CHMP4b is a major binding partner of the ALG-2-interacting protein Alix among the three CHMP4 isoforms. Arch Biochem Biophys 2004;421(1):159-165.

27. Katoh K, Shibata H, Suzuki H, Nara A, Ishidoh K, Kominami E, Yoshimori T, Maki M. The ALG-2-interacting protein Alix associates with CHMP4b, a human homologue of yeast Snf7 that is involved in multivesicular body sorting. J Biol Chem 2003.

28. Peck JW, Bowden ET, Burbelo PD. Structure and function of human Vps20 and Snf7 proteins. Biochem J 2004;377(Pt 3):693-700.

29. McCullough J, Row PE, Lorenzo O, Doherty M, Beynon R, Clague MJ, Urbe S. Activation of the endosome-associated ubiquitin isopeptidase AMSH by STAM, a component of the multivesicular body-sorting machinery. Curr Biol 2006;16(2):160-165.

30. Mizuno E, Kawahata K, Kato M, Kitamura N, Komada M. STAM proteins bind ubiquitinated proteins on the early endosome via the VHS domain and ubiquitin-interacting motif. Mol Biol Cell 2003;14(9):3675-3689.

31. Scott A, Gaspar J, Stuchell-Brereton MD, Alam SL, Skalicky JJ, Sundquist WI. Structure and ESCRT-III protein interactions of the MIT domain of human VPS4A. Proc Natl Acad Sci U S A 2005;102(39):13813-13818.

32. Fujita H, Umezuki Y, Imamura K, Ishikawa D, Uchimura S, Nara A, Yoshimori T, Hayashizaki Y, Kawai J, Ishidoh K, Tanaka Y, Himeno M. Mammalian class E Vps proteins, SBP1 and mVps2/CHMP2A, interact with and regulate the function of an AAA-ATPase SKD1/Vps4B. J Cell Sci 2004;117(Pt 14):2997-3009.

33. Agromayor M, Martin-Serrano J. Interaction of AMSH with ESCRT-III and deubiquitination of endosomal cargo. J Biol Chem 2006.

34.Reid E, Connell J, Edwards TL, Duley S, Brown SE, Sanderson CM. The hereditary spastic paraplegia protein spastin interacts with the ESCRT-III complex-associated endosomal protein CHMP1B. Hum Mol Genet 2005;14(1):19-38.

35. Babst M, Wendland B, Estepa EJ, Emr SD. The Vps4p AAA ATPase regulates membrane association of a Vps protein complex required for normal endosome function. Embo J 1998;17(11):2982-2993.

36. Howard TL, Stauffer DR, Degnin CR, Hollenberg SM. CHMP1 functions as a member of a newly defined family of vesicle trafficking proteins. J Cell Sci 2001;114(Pt 13):2395-2404.

37. Scott A, Chung HY, Gonciarz-Swiatek M, Hill GC, Whitby FG, Gaspar J, Holton JM, Viswanathan R, Ghaffarian S, Hill CP, Sundquist WI. Structural and mechanistic studies of VPS4 proteins. Embo J 2005;24(20):3658-3669.

38.Takasu H, Jee JG, Ohno A, Goda N, Fujiwara K, Tochio H, Shirakawa M, Hiroaki H. Structural characterization of the MIT domain from human Vps4b. Biochem Biophys Res Commun 2005;334(2):460-465.

39. Zamborlini A, Usami Y, Radoshitzky SR, Popova E, Palu G, Gottlinger H. Release of autoinhibition converts ESCRT-III components into potent inhibitors of HIV-1 budding. Proc Natl Acad Sci U S A 2006;103(50):19140-19145.

40. Evan GI, Lewis GK, Ramsay G, Bishop JM. Isolation of monoclonal antibodies specific for human c-myc proto-oncogene product. Mol Cell Biol 1985;5(12):3610-3616.

FIGURE LEGENDS

Figure 2-1 Secondary structure of human ESCRT-III proteins.

Schematic aligned representations of predicted secondary structures of (A) CHMP2A, (B) CHMP3, (C) CHMP6 and (D) CHMP4A obtained using a neural network based algorithm (http://www.compbio.dundee.ac.uk/~www-jpred/submit.html). (E) Secondary structure of CHMP3 fragment (9 -183) based on the recently published crystal structure (24). The regions missing from the crystal structure (1 - 8 and 184 - 222) are indicated as light grey lines. Boxes correspond to predicted helices. Blue and red boxes represent helices with pI higher than 8 and lower than 6, respectively. A lighter blue or lighter red box indicates a helix with approximately neutral pI.

Figure 2-2 Subcellular localization of full-length and C-terminally deleted ESCRT-III proteins.

COS-7 cells expressing indicated constructs of FLAG-CHMP2A, CHMP3-myc, CHMP6-myc and FLAG-CHMP4A were immunostained using anti-FLAG or myc antibody and visualized by epifluorescence microscopy. FLAG or myc staining is shown in red, DAPI in blue. The images shown are representative of cells expressing each ESCRT-III construct.

Figure 2-3 ESCRT-III (α1- α5) mutants lacking α6 and flanking sequences form membrane-associated complexes.

(A) Flotation though sucrose step gradient of full-length and α1 – α5 ESCRT-III proteins. COS-7 cells were transfected with full-length and α1 – α5 mutants of FLAG-CHMP2A, CHMP3-myc, CHMP6-myc and FLAG-CHMP4A. Cell lysate in 73% sucrose was loaded

at bottom and overlaid with 65% and 10% sucrose. Protein distribution was visualized by immunoblotting.

(B) Sedimentation analysis of full-length and α1 – α5 ESCRT-III proteins. HEK293T cells transfected with full-length and α1 – α5 mutants of FLAG-CHMP2A, CHMP3-myc, CHMP6-myc and FLAG-CHMP4A were solubilized in 1% Triton X-100 and fractionated by centrifugation at 10,000 x g. The distribution of ESCRT-III proteins in the resulting supernatant (S) and pellet (P) was analyzed by immunoblotting. The data shown here are representative of three independent experiments.

Figure 2-4 Core domain required for CHMP4A polymer assembly.

293T cells transfected with indicated FLAG-CHMP4A constructs were analyzed by sedimentation as described in Fig. 2-3B (solubilization in 1% Triton X-100 and centrifugation at 10,000 x g). The CHMP4A mutants were visualized in the resulting supernatant (S) and pellet (P) by immunoblotting. The data shown here are representative of three independent experiments.

Figure 2-5 Cells expressing ESCRT-III (α1 – α5) mutants accumulate ubiquitin conjugates on enlarged endosomes.

COS-7 cells transfected with full-length and α1 – α5 mutants of FLAG-CHMP2A, CHMP3-myc, CHMP6-myc and FLAG-CHMP4A were analyzed by epifluorescence microscopy. The cells were co-stained with FK2 antibody for conjugated ubiquitin (left panel) and anti-FLAG or anti-myc antibody for ESCRT-III constructs (right panel). The images shown are representative cells expressing each ESCRT-III construct.

Figure 2-6 Expressing C-terminally deleted ESCRT-III mutants reduces VLP (virus-like-particle) production.

(A-D) Effect of full-length and C-terminally deleted ESCRT-III mutants (α1 – α4 and α1 – α5) on VLP release. VLPs were collected from culture media of HEK293T cells transfected with a plasmid encoding HIV Pr55 (Gag) and indicated ESCRT-III constructs including (A) FLAG-CHMP2A, (B) CHMP3-myc, (C) CHMP6-myc and (D) FLAG-CHMP4A. Gag protein (55KDa) in VLPs and cell lysates was visualized by immunoblotting using a polyclonal antibody against p24 capsid domain of Gag. ESCRT-III proteins in cell lysates were visualized by immunoblotting with anti-FLAG or anti-myc antibody. All bands in each panel were from one exposure of a single blot. Where necessary, lanes were rearranged as indicated by white lines. FL= full-length.

(E) Effect of co-expressing Gag on sedimentation of full-length CHMP4A and CHMP4A (α1 – α5) mutant. HEK293T cells transfected with a plasmid encoding HIV Pr55 (Gag) and FLAG-CHMP4A full-length or 1-181 were subjected to sedimentation analysis as described in Fig. 2-3B (solubilization in 1% Triton X-100 and centrifugation at 10,000 x g). The distribution of protein in the resulting supernatant (S) and pellet (P) were visualized by immunoblotting.

Figure 2-7 CHMP4A (α1 – α5) mutant recruits other ESCRT III proteins.

(A) *Left panel*: Subcellular localization of individual full-length ESCRT-III proteins. COS-7 cells transfected with CHMP6-myc, CHMP3-myc or FLAG-CHMP2A were immunostained with anti-FLAG or anti-myc antibody and visualized by epifluorescence microscopy.

Right panel: Changed distribution of full-length ESCRT-III proteins in the presence of CHMP4A(α1 – α5) mutant. FLAG-CHMP4A 1-181 or myc-CHMP4A 1-181 was co-

transfected with CHMP6-myc, CHMP3-myc or FLAG-CHMP2A into COS-7 cells. Cells were co-stained with anti-myc and anti-FLAG antibody and visualized by epifluorescence microscopy. CHMP4A 1-181 is shown in green while full-length CHMP6, CHMP3 and CHMP2A are in red.

(B) Differential recruitment of cotransfected full-length CHMP3 into detergent-insoluble complex formed by full-length and $\alpha 1 - \alpha 5$ mutant of CHMP4A. HEK293T cells transfected with CHMP3-myc alone or together with FLAG-CHMP4A full-length or 1-181 were subjected to sedimentation analysis as described in Fig. 2-3B (solubilized in 1% Triton X-100, centrifuged at 10,000 x g). The resulting supernatant (S) and pellet (P) were analyzed by immunoblotting with anti-myc antibody.

(C) Differential recruitment of endogenous CHMP3 into detergent-insoluble complex formed by full-length and $\alpha 1 - \alpha 5$ mutant of CHMP4A. Samples of HEK293T cells transfected with FLAG-CHMP4A full-length or 1-181 were prepared as in (B) and the distribution of endogenous CHMP3 analyzed by immunblotting with anti-CHMP3 antibody (23).

Figure 2-8 A candidate binding site for VPS4B/SKD1 in CHMP2A.

GST and GST-CHMP2A constructs immobilized on glutathione-Sepharose beads were incubated with *E.coli* lysate containing VPS4B/SKD1(E235Q)-His6/myc. Bound and unbound VPS4B/SKD1(E235Q) were detected by immunoblotting with anti-myc antibody. Unbound material loaded corresponds to 5% of bound. GST and GST-Vps2-1 proteins were detected by immunoblotting using anti-GST antibody.

Figure 2-9 Model of regulated ESCRT-III polymer assembly

(A) Representative monomeric ESCRT-III proteins in their closed conformation. The C-terminal region including α6 and flanking sequences (~40 amino acids) is responsible for maintaining this closed state.

(B) Intermediate assembly into "closed" ESCRT-III polymers. At high concentration, membrane proximal (CHMP4A and CHMP6) ESCRT-III proteins assemble into the noninhibitory polymers shown here. This state may be an intermediate in assembling fully activated ESCRT-III complex.

(C) "Open" ESCRT-III proteins assemble into polymeric complexes on the membrane. Polymer assembly can propagate by recruitment (and coincident opening) of additional ESCRT-III proteins. Opening may be regulated by proteins that bind to the C-terminal α6 domain.

Figure 2-1

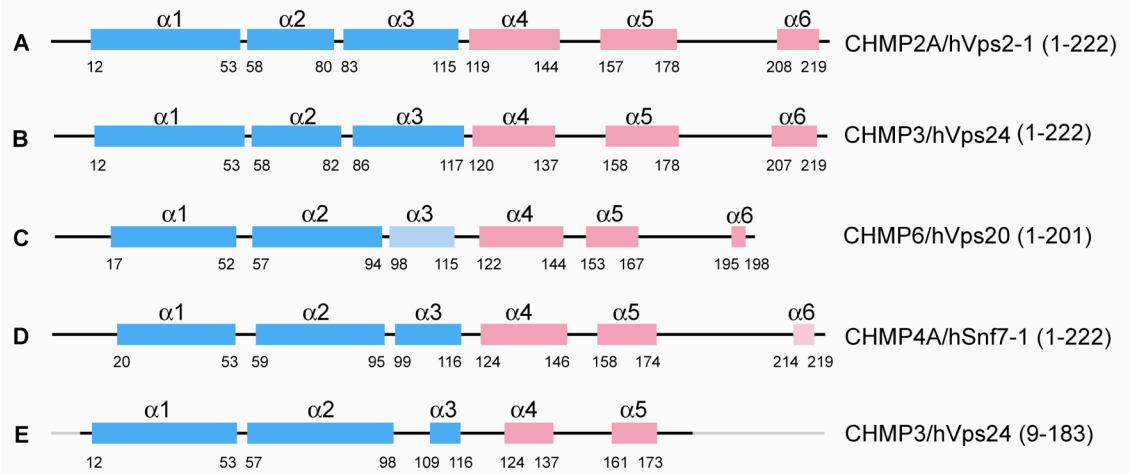
A
α1 α2 α3 α4 α5 α6
12 53 58 80 83 115 119 144 157 178 208 219
CHMP2A/hVps2-1 (1-222)
B
α1 α2 α3 α4 α5 α6
12 53 58 82 86 117 120 137 158 178 207 219
CHMP3/hVps24 (1-222)
C
α1 α2 α3 α4 α5 α6
17 52 57 94 98 115 122 144 153 167 195 198
CHMP6/hVps20 (1-201)
D
α1 α2 α3 α4 α5 α6
20 53 59 95 99 116 124 146 158 174 214 219
CHMP4A/hSnf7-1 (1-222)
E
α1 α2 α3 α4 α5
12 53 57 98 109 116 124 137 161 173
CHMP3/hVps24 (9-183)

Figure 2-2

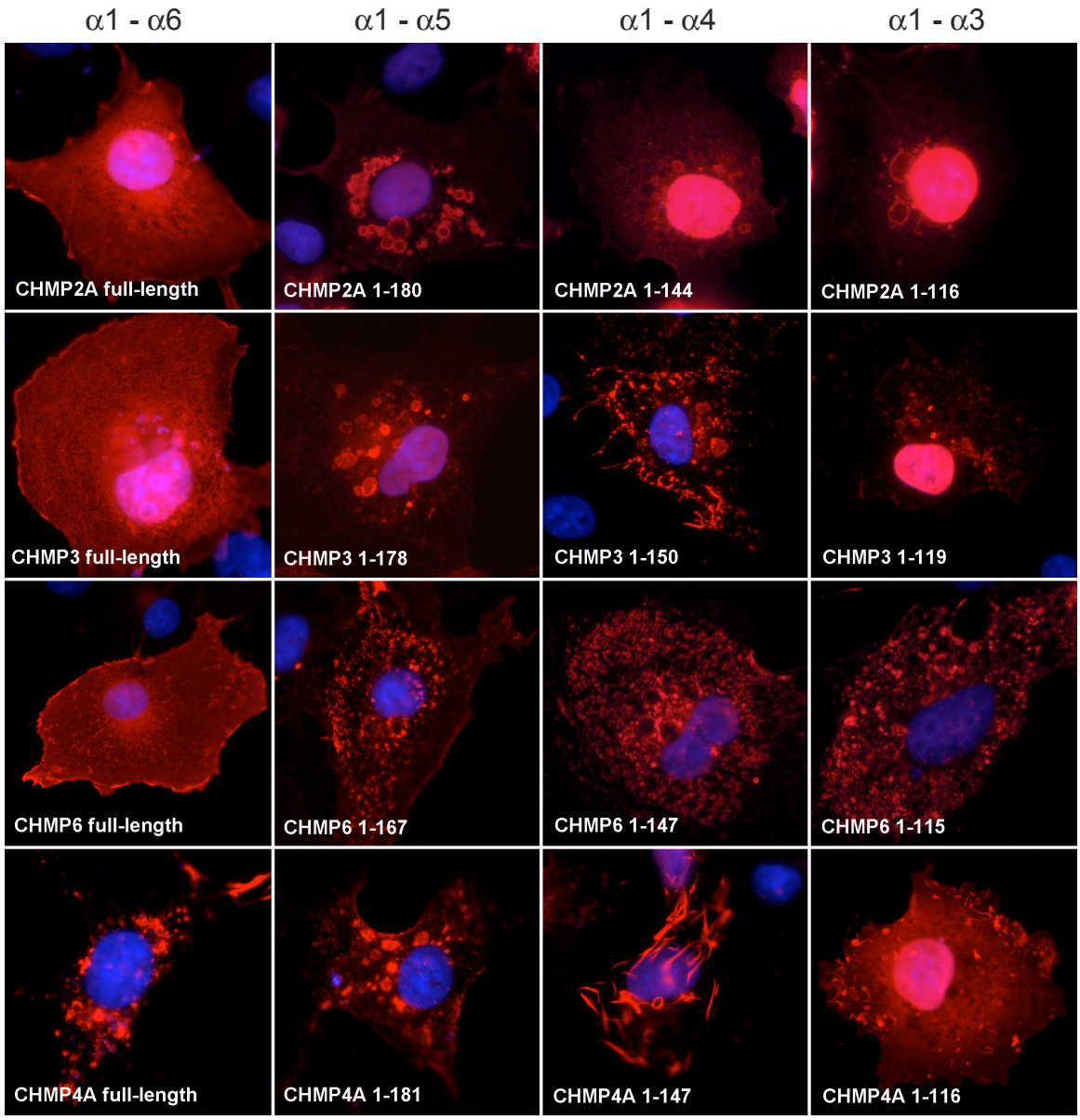
α1 - α6
α1 - α5
α1 - α4
α1 - α3
CHMP2A full-length
CHMP2A 1-180
CHMP2A 1-144
CHMP2A 1-116
CHMP3 full-length
CHMP3 1-178
CHMP3 1-150
CHMP3 1-119
CHMP6 full-length
CHMP6 1-167
CHMP6 1-147
CHMP6 1-115
CHMP4A full-length
CHMP4A 1-181
CHMP4A 1-147
CHMP4A 1-116

Figure 2-3

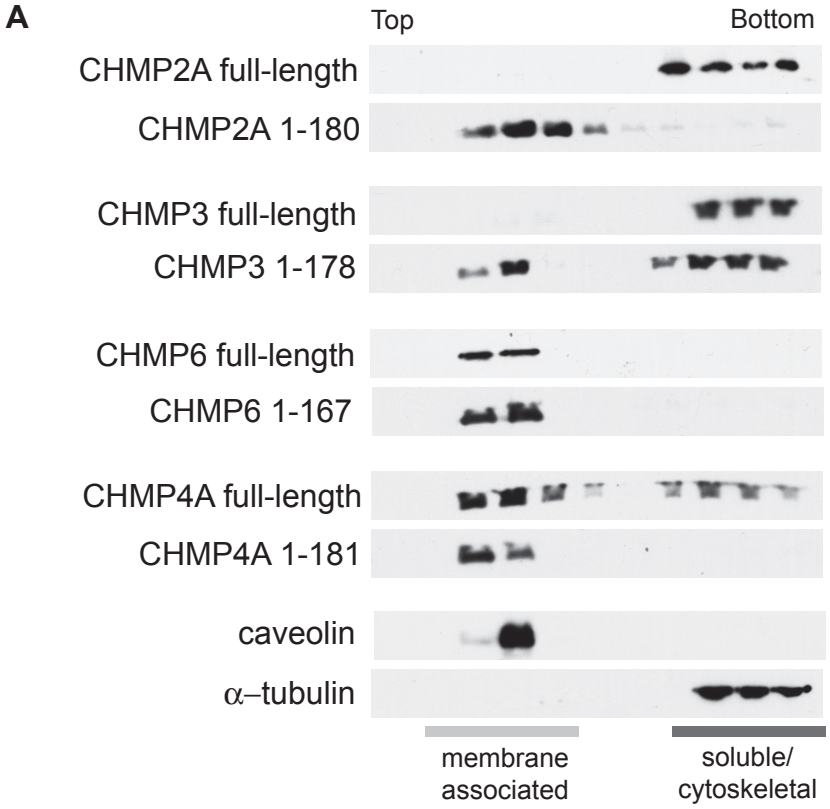
A
Top
Bottom
CHMP2A full-length
CHMP2A 1-180
CHMP3 full-length
CHMP3 1-178
CHMP6 full-length
CHMP6 1-167
CHMP4A full-length
CHMP4A 1-181
caveolin
α–tubulin
membrane associated
soluble/ cytoskeletal
B
S
P
CHMP2A full-length
CHMP2A 1-180
CHMP3 full-length
CHMP3 1-178
CHMP6 full-length
CHMP6 1-167
CHMP4A full-length
CHMP4A 1-181

Figure 2-4

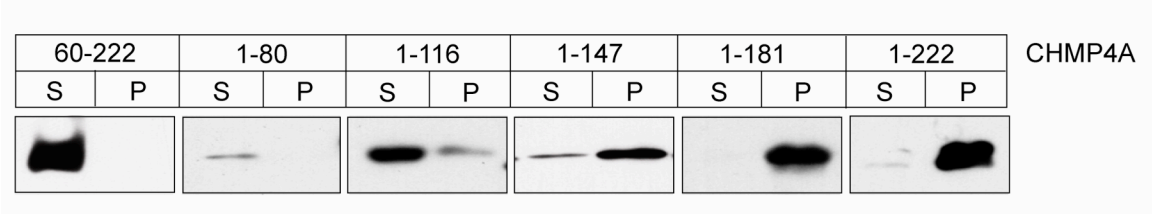

Figure 2-5

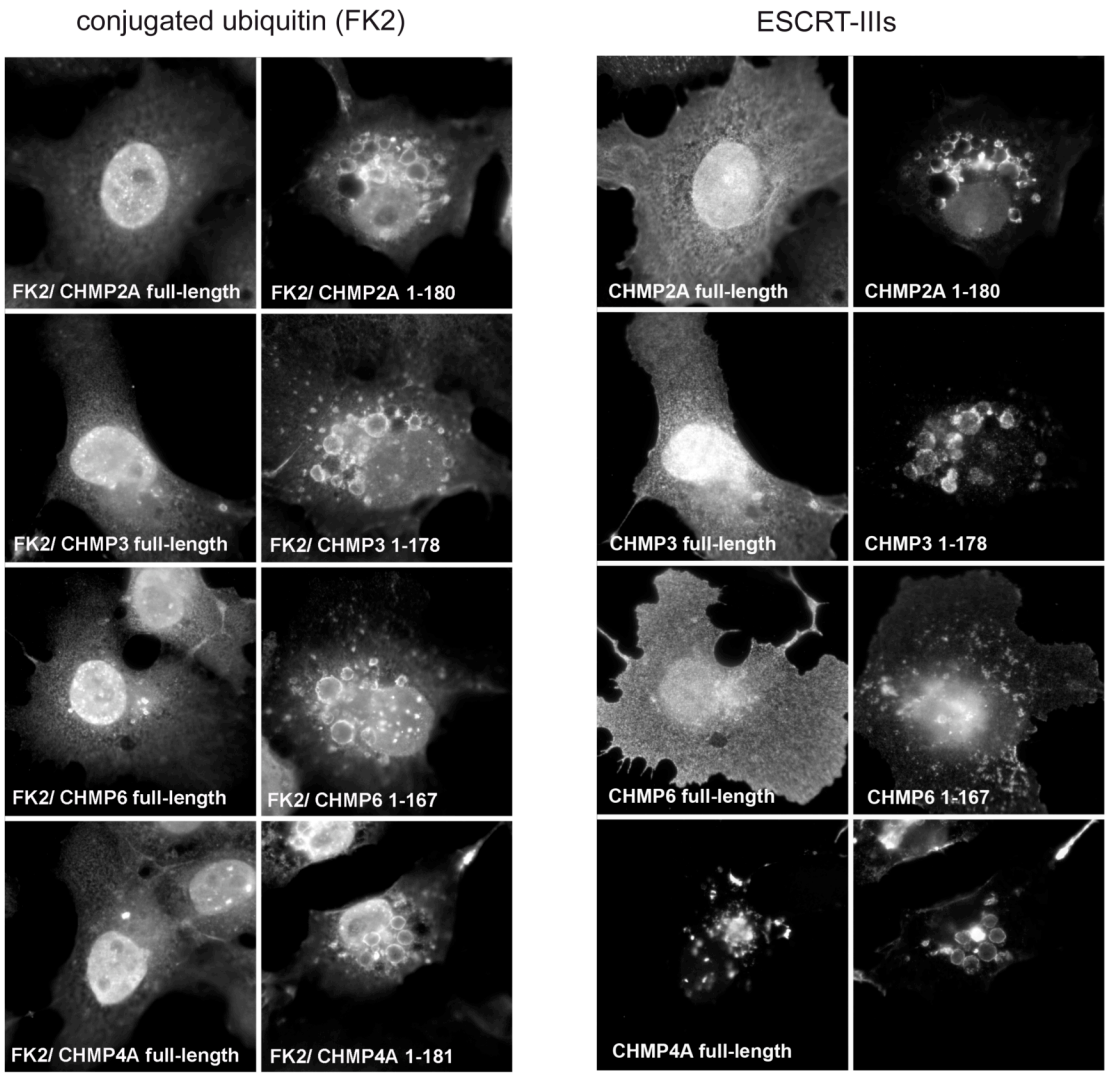
conjugated ubiquitin (FK2)
ESCRT-IIIs
FK2/ CHMP2A full-length
FK2/ CHMP2A 1-180
CHMP2A full-length
CHMP2A 1-180
FK2/ CHMP3 full-length
FK2/ CHMP3 1-178
CHMP3 full-length
CHMP3 1-178
FK2/ CHMP6 full-length
FK2/ CHMP6 1-167
CHMP6 full-length
CHMP6 1-167
FK2/ CHMP4A full-length
FK2/ CHMP4A 1-181
CHMP4A full-length

Figure 2-6

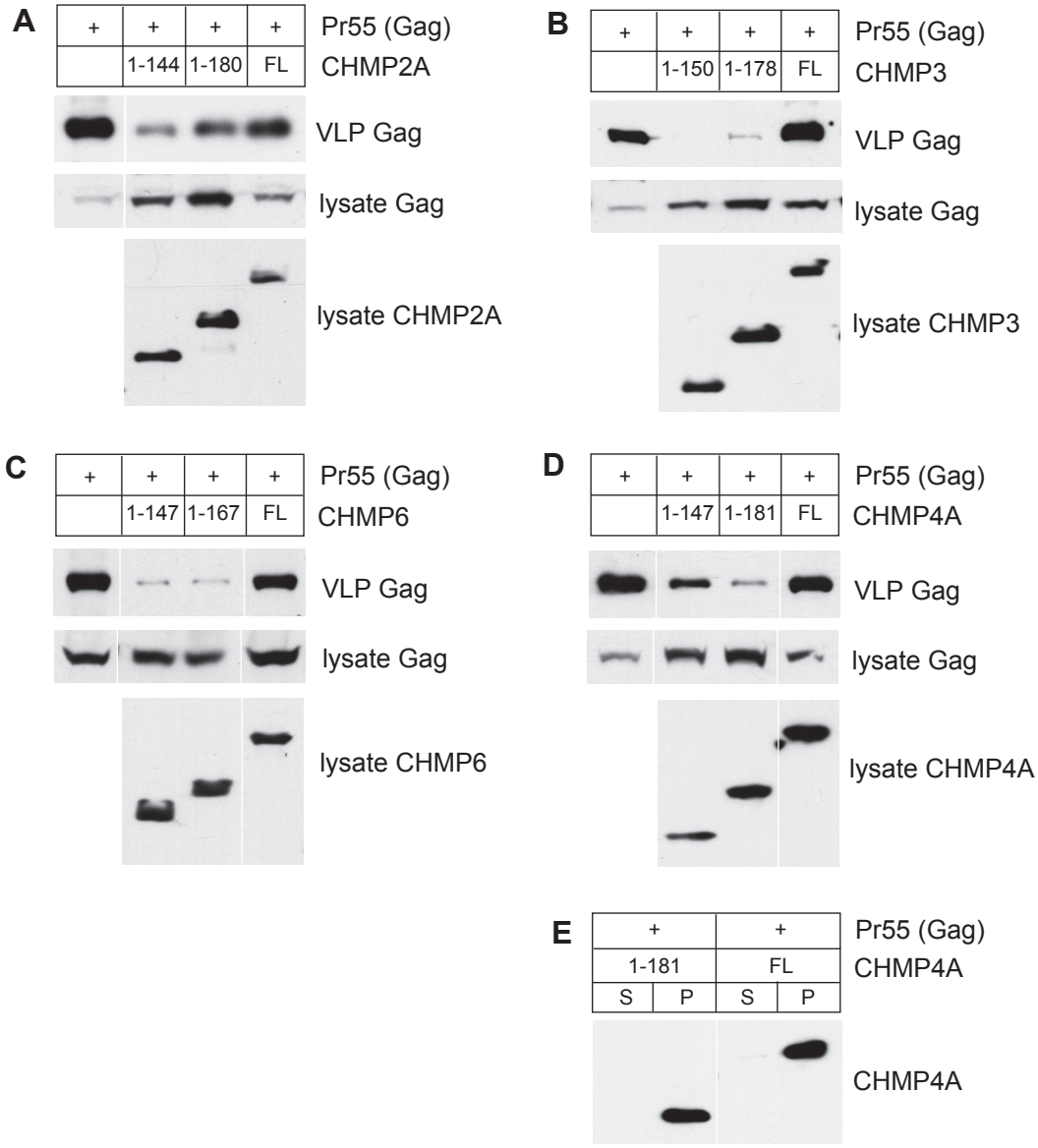
A
+ + + +
1-144 1-180 FL
Pr55 (Gag)
CHMP2A
VLP Gag
lysate Gag
lysate CHMP2A
B
+ + + +
1-150 1-178 FL
Pr55 (Gag)
CHMP3
VLP Gag
lysate Gag
lysate CHMP3
C
+ + + +
1-147 1-167 FL
Pr55 (Gag)
CHMP6
VLP Gag
lysate Gag
lysate CHMP6
D
+ + + +
1-147 1-181 FL
Pr55 (Gag)
CHMP4A
VLP Gag
lysate Gag
lysate CHMP4A
E
+ +
1-181 FL
S P S P
Pr55 (Gag)
CHMP4A
CHMP4A

Figure 2-7

A

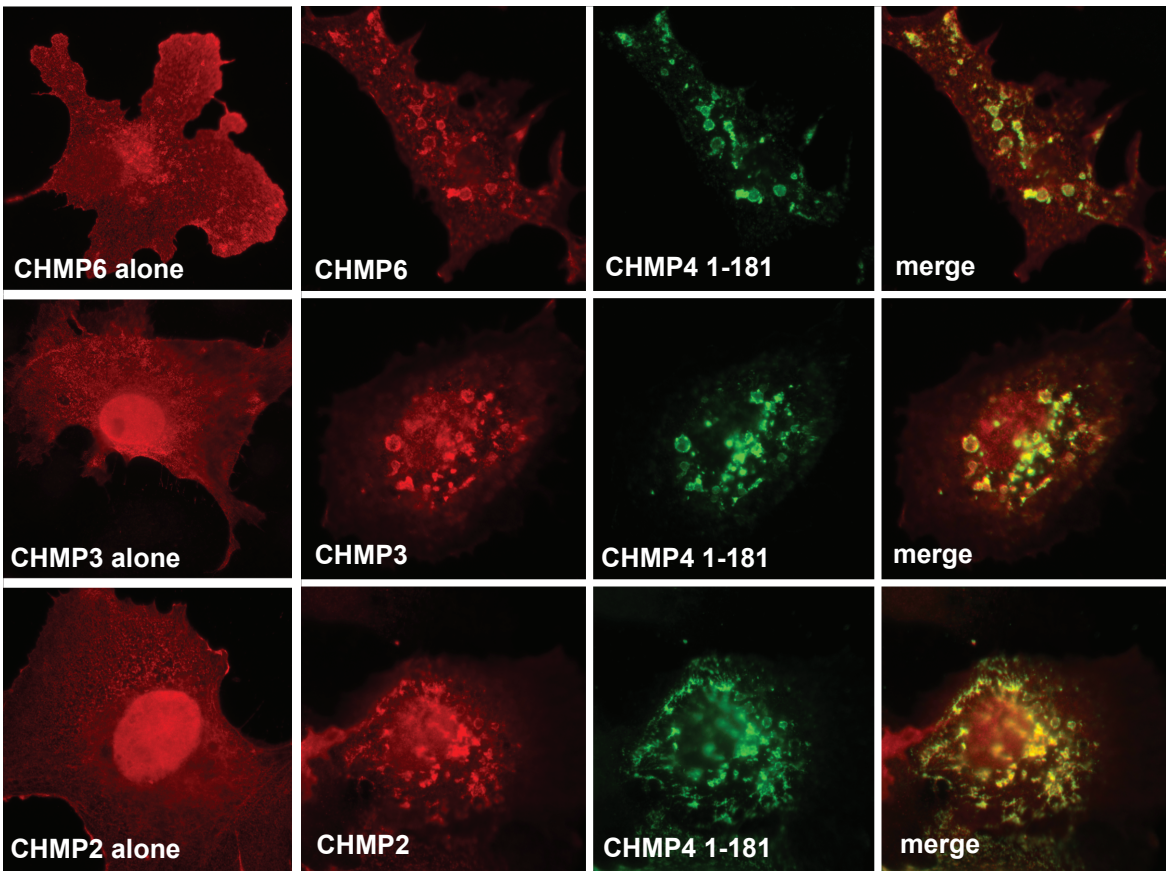
CHMP6 alone
CHMP6
CHMP4 1-181
merge
CHMP3 alone
CHMP3
CHMP4 1-181
merge
CHMP2 alone
CHMP2
CHMP4 1-181
merge

Figure 2-7

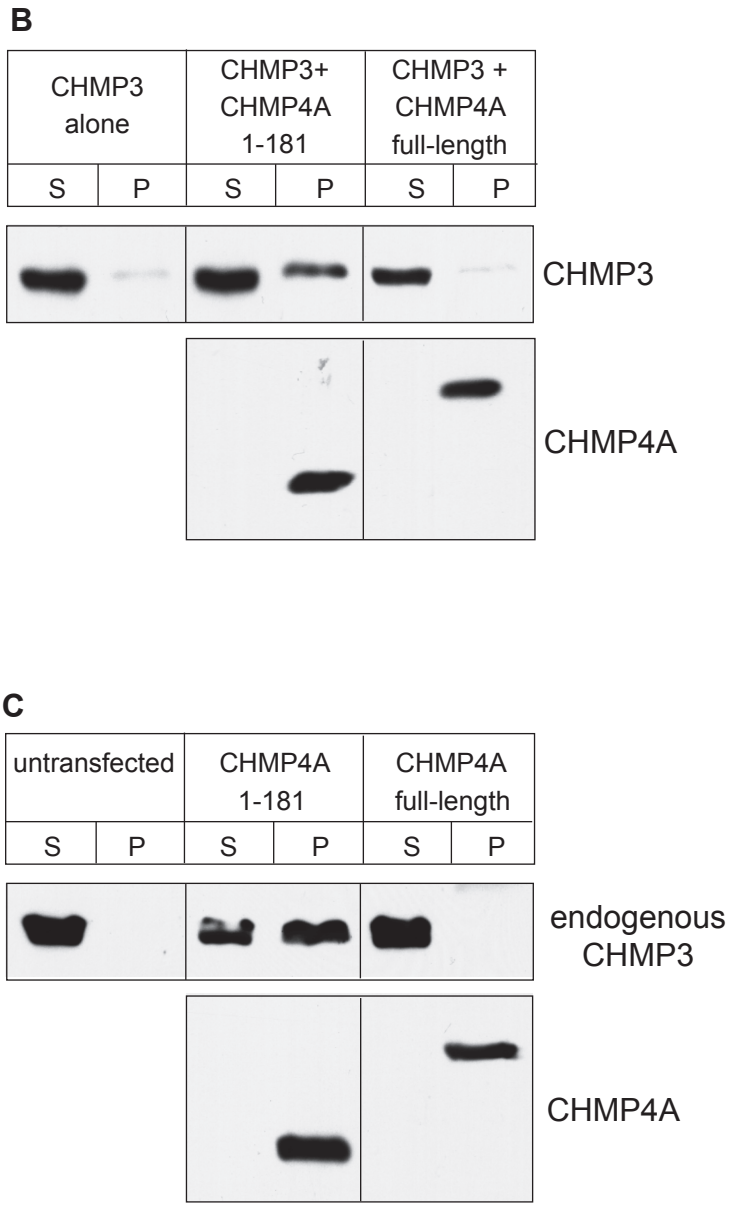
B
CHMP3 alone
CHMP3+ CHMP4A 1-181
CHMP3 + CHMP4A full-length
S
P
S
P
S
P
CHMP3
CHMP4A
C
untransfected
CHMP4A 1-181
CHMP4A full-length
S
P
S
P
S
P
endogenous CHMP3
CHMP4A

Figure 2-8

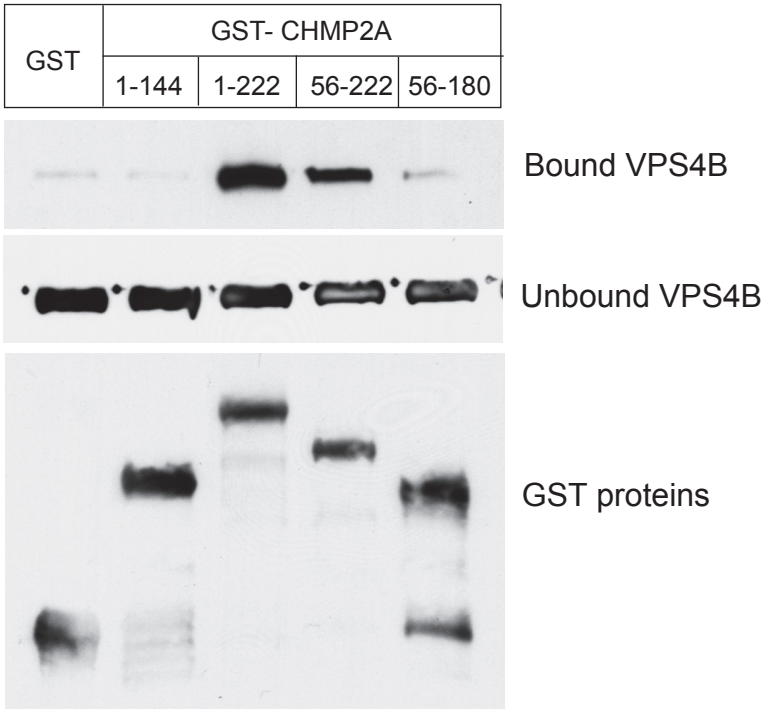
GST
GST- CHMP2A
1-144
1-222
56-222
56-180
Bound VPS4B
Unbound VPS4B
GST proteins

Figure 2-9

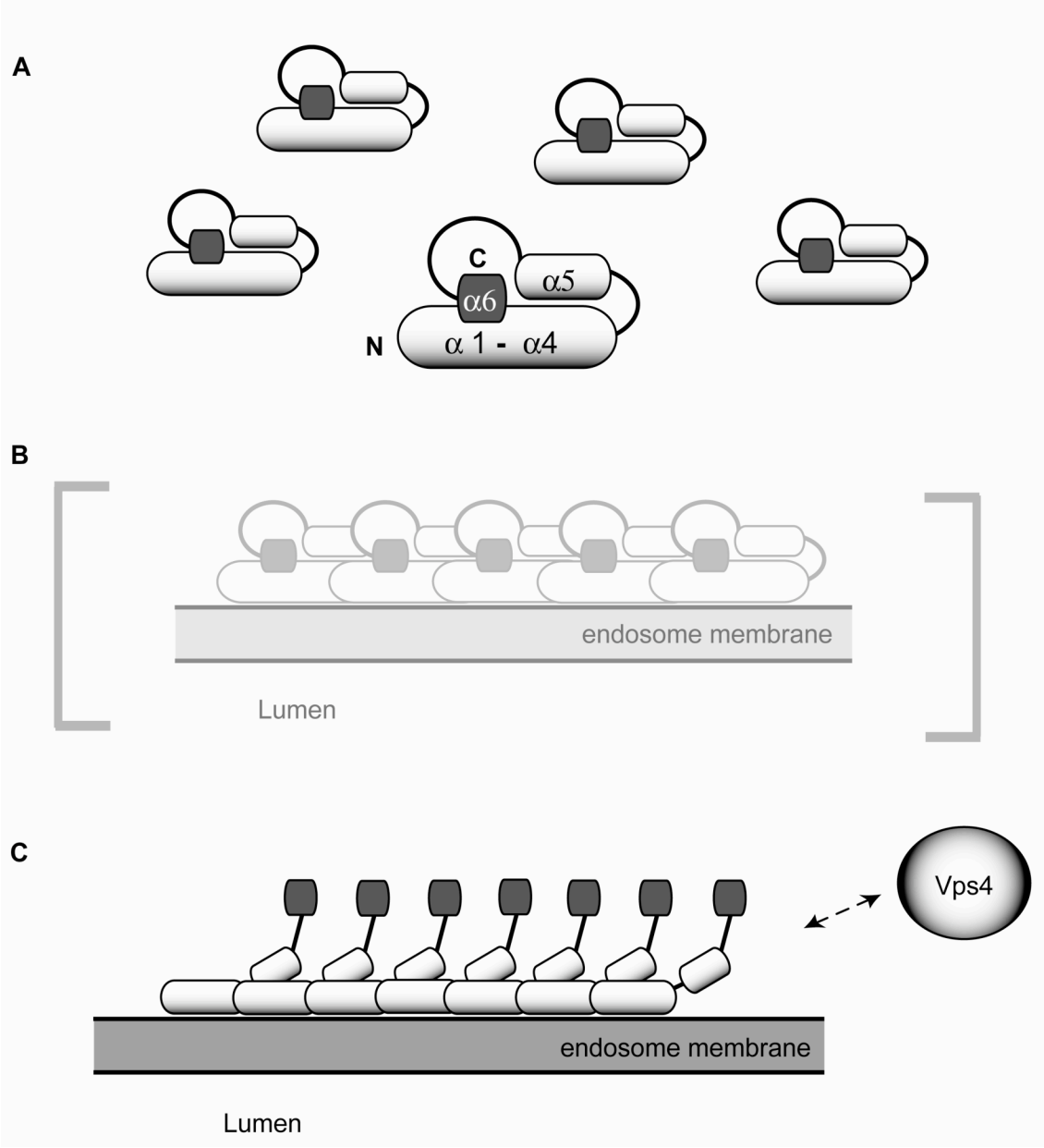
A
C
α5
α6
N
α 1 - α4
B
endosome membrane
Lumen
C
Vps4
endosome membrane
Lumen

CHAPTER THREE

Novel interactions of ESCRT-III with LIP5 and VPS4 and their implications for ESCRT-III disassembly

ACKNOWLEDGEMENTS

I would like to thank Sam Merrill for performing plate-based binding assays and an MIT domain competition assay which resulted in Figure 1B/C, Figure 3C, Figure 5B/C and Figure 8D. I would also like to thank Teri Naismith for technical help with site-directed mutagenesis, and all members of the Hanson lab for helpful discussion.

The work is published as Shim S, Samuel A. Merrill, Hanson PI (2008). Novel interactions of ESCRT-III with LIP5 and VPS4 and their implications for ESCRT-III disassembly. Mol Biol Cell, 19:2661-2672, which is reprinted here with permission of the American Society of Cell Biology.

INTRODUCTION

Multivesicular bodies (MVBs) are a subset of late endosomes morphologically characterized by the presence of intralumenal vesicles (ILVs) (1, 2). Signalling receptors destined for degradation as well as certain lysosomal proteins are sorted into ILVs *en route* to the lysosome (3). Protein machinery involved in MVB biogenesis was discovered in studies of protein sorting to the vacuole in *Saccharomyces cerevisiae*. Functional loss of what are termed the class E Vps (*v*acuolar *p*rotein *s*orting) proteins prevents delivery of cargo into the vacuole. Cargo accumulates instead on the limiting membrane of the vacuole and in an adjacent abnormal compartment referred to as the "class E compartment" (4). 18 class E Vps proteins have been identified in yeast and these proteins are highly conserved throughout evolution (5-7). Interestingly, several mammalian class E Vps proteins are also involved in viral budding and cytokinesis, demonstrating a conserved role in topologically similar membrane budding and fission reactions (8-12).

A majority of class E Vps proteins are components of four complexes that include Vps27/Hse (sometimes referred to as ESCRT-0), ESCRT-I, ESCRT-II and ESCRT-III where ESCRT is an acronym for Endosomal Sorting Complex Required for Transport. These complexes are recruited (possibly sequentially) to endosomal membranes where they function in sorting cargo and generating ILVs. The AAA+ ATPase Vps4 is recruited by ESCRT-III to disassemble and recycle the ESCRT machinery (5, 6, 13).

ESCRT-III components are small (200-250 amino acid) structurally related proteins. All have basic N-terminal and acidic C-terminal halves, and are thought to share a common set of six α-helices (14, 15). There are six ESCRT-III related proteins in yeast (Vps2, Vps24, Vps20, Snf7 – core members – and Did2/Vps46, Vps60 – proposed regulatory members) and these are extended to 11 proteins in humans (5, 16, 17).

Mammalian ESCRT-III proteins are referred to either as orthologs of their yeast counterparts or as CHMPs (*c*harged *m*ultivesicular *b*ody *p*roteins). To standardize our discussion of the large group of mammalian ESCRT-III proteins, we will primarily use the CHMP nomenclature in this paper.

Unlike ESCRT-I and -II that are stable heteropolymeric complexes, ESCRT-III proteins are monomers in the cytoplasm and only assemble into complex on the endosomal membrane (16). In current models, ESCRT-III proteins are maintained in a metastable "closed" conformation in the cytoplasm and "open" when they bind to the membrane and assemble into polymers (5, 6, 13, 15). These polymers may deform the membrane and participate in forming ILVs (18). Previously we defined ~40 amino acids at the extreme C-terminus of each core ESCRT-III protein as an autoregulatory domain that controls transition between these states (15). These 40 amino acids include a short C-terminal α-helix and a linker that connects it to the rest of the protein.

ESCRT-III does not spontaneously disassemble, but instead requires energy input from the AAA+ (ATPases associated with a variety of cellular activities) protein Vps4 (19), of which there are two isoforms in mammalian cells, VPS4A and VPS4B/SKD1. We will use VPS4 to refer generically to the different forms of this enzyme. VPS4 has recently been shown to bind via its N-terminal *M*icrotubule *I*nteracting and *T*rafficking (MIT) domain to a short motif present in a subset of ESCRT-III proteins, including CHMP1 (Did2 in yeast), CHMP2 (Vps2 in yeast), and CHMP3 (Vps24 in yeast) (20, 21). This VPS4 binding motif is in a short C-terminal α-helix and is referred to as the MIT domain interacting motif (MIM) (20). The C-termini of the remaining ESCRT-III proteins (CHMP4 (Snf7 in yeast), CHMP5 (Vps60 in yeast) and CHMP6 (Vps20 in yeast)) do not contain the conserved MIM despite the fact that some of them have

previously been shown to bind to VPS4 (22-24). How VPS4 interacts with these proteins remains to be determined.

Although VPS4 activity is essential for MVB biogenesis, little is known about how it works. The AAA+ domain of VPS4 is similar to other AAA+ domains with the exception of an inserted β-sheet motif (referred to as the β domain) and a C-terminal α-helix (24, 25). Like other AAA+ ATPases, VPS4 is thought to function as an oligomeric ring. VPS4 is primarily a monomer or dimer in the cytoplasm, and its assembly into a ring is enhanced by interaction of its β domain with the cofactor LIP5 (Vta1 in yeast) (25-29).

LIP5/Vta1 is a ~300 amino acid long highly charged protein. Deletion of Vta1 in yeast leads to defects in cargo sorting and vacuolar morphology (30) and knockdown of LIP5 in mammalian cells significantly impairs receptor downregulation and viral budding (31). A conserved domain at the C-terminus of LIP5 (the "VSL (Vta1/SBP1/LIP5) domain") mediates LIP5 dimerization and interaction with Vps4 (26).

In addition to binding to VPS4, LIP5/Vta1 has been found to interact with CHMP5/Vps60, one of the proposed regulatory ESCRT-III proteins (26, 30-32). This interaction is robust and has been documented in many systems. Less well explored connections between Vta1 and a few other ESCRT-III related proteins have been reported, primarily in yeast. In particular, Vta1 binds to Did2/Vps46 (yeast ortholog of CHMP1) (33) and the name Vta1 (*V*ps *t*wenty (Vps20) *a*ssociated 1) was originally derived from a connection between Vps20 and Vta1 although this interaction has not been reproduced (23, 26).

In the present study, we directly examine the ability of LIP5 to bind each of the six classes of ESCRT-III related proteins in order to determine whether ternary interactions between LIP5, VPS4 and ESCRT-III might play a role in ESCRT-III disassembly. We confirm that LIP5 binds to CHMP5, but also find that it binds to

CHMP1B, CHMP2A, and CHMP3 but not to CHMP4A or CHMP6. Mapping the binding sites reveals that LIP5 binds to the extreme C-terminal region of CHMP1B and CHMP2A and instead to an internal sequence in CHMP5. Complexes of LIP5 with CHMP5 are preferentially soluble, while those between LIP5 and CHMP2A are polymeric and insoluble. The C-terminal binding site for LIP5 in CHMP1B and CHMP2A overlaps with the previously defined "MIT interacting motif" or MIM responsible for recruiting Vps4. Surprisingly, we find evidence of a second binding site for VPS4 within these ESCRT-III proteins that may allow them to simultaneously interact with VPS4 and LIP5. These studies suggest that LIP5 is deeply intertwined with ESCRT-III and VPS4 in the pathway leading to multivesicular body formation.

EXPERIMENTAL PROCEDURES

Plasmids

The following ESCRT-III and VPS4 constructs have been previously described: pGEX4T-1 CHMP4A residues 1-222, pHO4d VPS4B(E235Q)-His_6/myc, pEGFP C1 VPS4B(E235Q), pcDNA3.1 FLAG-CHMP4A 1-222, 1-181, 1-147 and pGEX4T-1-CHMP2A 1-222, 1-180, and 1-144 (15, 34). ESCRT-III and VPS4 constructs prepared for this study include: pGEX4T-1-CHMP6 1-201; pGEX4T-1-CHMP3 1-222; pGEX4T-1-CHMP2A 1-219, 1-216, 1-203, 1-193, pGEX4T-1-CHMP1B 1-199, 1-181, 106-199, 106-181, 169-199; pGEX4T-1-CHMP5 1-219, 121-149, 121-158, 121-175, 121-219, 149-175, 149-183; pcDNA3.1-FLAG-CHMP2A 1-219, 1-206, 1-193; pcDNA3.1-FLAG-CHMP1B 1-199, 1-181, 1-168, 1-136; pcDNA3.1-FLAG-CHMP5 1-219; pcDNA4TO-CHMP5 1-219 His_6myc; pET28a-VPS4A MIT domain (1-75); pGEX4T-1-VPS4B(E235Q) and pGEX4T-1-VPS4B(E235Q, ΔGAI deletion of 390-396). cDNAs used to create these constructs were either from the Mammalian Genome Collection (human CHMP1B, CHMP2B, and CHMP5; IMAGE ID: 6165059, 3460712, and 4094210, respectively) or previously described (CHMP2A, CHMP3, CHMP4A, CHMP6) (15, 34). For insertion into pGEX4T-1, pcDNA3.1-FLAG, pcDNA4/TO- His_6myc or pET28a, *BamHI* and *XhoI* sites were added to the fragments as they were amplified by PCR. Quikchange (Stratagene, La Jolla CA) site directed mutagenesis was used to introduce point mutations into CHMP2A and CHMP1B as indicated in the text.

pEGFP C1-LIP5 was a kind gift from Dr. Jerry Kaplan (University of Utah, Salk Lake City, UT). For bacterial expression of His_6-LIP5, PCR amplified cDNA was inserted into pET28a between *NdeI* and *XhoI* sites. GFP-LIP5 ΔN contains residues 76-307 in pEGFP C1 between *BglII* and *HindIII* sites. All constructs were sequenced using ABI big

dye reagents at the Nucleic Acid Chemistry Laboratory (Washington University, St. Louis, MO).

Protein expression and purification

BL21(DE3) *E. coli* transformed with the indicated constructs were grown at 37 ºC to a 600nm optical density of ~1, transferred to room temperature, and brought to 0.4 μM IPTG for 3 hrs to induce expression. Pelleted bacteria were resuspended in buffer A (20mM Tris, 250mM NaCl, 5% glycerol, 1mM DTT, 1mM PMSF, pH 7.4) and lysed by sonication. Bacterial lysates were centrifuged at 66,000 x *g* for 20 minutes. Clarified lysates were bound to glutathione sepharose (Amersham Biosciences, Piscataway NJ) or Ni^{2+}-NTA agarose (Qiagen, Valencia CA) for 1 hr at 4ºC. Unbound material was removed by washes in buffer A, and proteins were eluted in buffer A containing either glutathione (50mM) or imidazole (160mM). Purified protein was quantitated using Bradford reagent with BSA as a standard. Proteins were snap frozen in liquid nitrogen and stored at -80ºC.

GST pull down assays

Where indicated, GST proteins immobilized on beads were combined with clarified bacterial lysate containing His_6-LIP5. This lysate was prepared from BL21(DE3) *E.coli* expressing pET28a-LIP5 grown as above. Bacteria were lysed in buffer B (30mM HEPES, 120mM NaCl, 5% glycerol, 1mM PMSF, pH 7.4), brought to 0.5% Triton X-100, and centrifuged at 66,000 x *g* for 20 min. Clarified bacterial lysate was incubated with immobilized GST fusion proteins for 1 hr at 4 ºC in buffer B. Beads were washed, and bound material was analyzed by SDS-PAGE and staining with Coomassie brilliant blue. For the experiment shown in Fig. 3-6B, GST proteins were combined with mammalian cell lysate containing GFP-LIP5. This was prepared from HEK293T cells transfected

with pEGFP C1-LIP5 solubilized in buffer B containing 0.5% Triton X-100 and centrifuged at 15,000 x *g* for 15min. After the binding reaction, bound and unbound material was detected by SDS-PAGE and immunoblotting with rabbit anti-GFP antibody ((34) (1:2500)).

To assess competition between LIP5 and the VPS4A MIT domain, GST proteins immobilized on glutathione sepharose were blocked in buffer C (20mm Tris pH 7.8, 100mM NaCl, 2mM $MgCl_2$, 2mM $CaCl_2$, 5mM DTT, 5% glycerol) also containing 1% casein for 1 hr. Beads were incubated with His_6-LIP5 (0.4 to 12.8 μM) with or without 300 μM His_6-VPS4A MIT domain (CHMP2A) and with or without 500 μM MIT domain (CHMP1B) for 1hr at 4 ºC. Control experiments were carried out with or without 300 μM ribonuclease A. Beads were then washed three times in buffer C. Bound proteins were analysed by SDS-PAGE. Gels were stained with colloidal Coomassie (G Biosciences, St. Louis MO) and visualized using an Odyssey Infrared imager (LiCor Biosciences, Lincoln NE). Bands were quantified with Odyssey 2.1 software and were within the experimentally determined linear range of detection.

Solid phase LIP5 binding assay

Microtiter plate wells containing immobilized antibody against GST (Pierce, Rockford IL or EMD Biosciences, Gibbstown NM) were incubated with 100 μl of the indicated GST-ESCRT-III or GST-VPS4B protein at 10 μg/ml for 1 hr in buffer D (20 mm Tris pH 7.4, 150 mM NaCl, pH7.4) (estimated to be ~60-100 times the binding capacity of the plate as per manufacturer data). For VPS4 binding assays, buffer D contained 100 mM KOAc in place of NaCl, 5 mM $MgCl_2$, and 1 mM ATP. Plates were washed three times in buffer D with 0.05% Tween-20 and blocked for 1 hr in buffer containing 1% casein (Pierce plates) or 1% casein + 0.5% BSA (EMD plates). Plates were then

washed, and 100 μl of His_6-LIP5 at the indicated concentration in buffer D was added and incubated for 1 hr. Plates were again washed with buffer D, and 100 μl of a 1:2000 dilution of NTA-HRP (Qiagen) was bound for 1 hr. After washing, 100 μl of TMB-Ultra (Pierce) was added to wells for ~3 min. Absorbance was read at 652 nm on a Bio-Tek plate reader. Background signal arising from non-specifically bound His_6-LIP5 (measured in parallel wells containing no GST protein or GST alone) was subtracted from each value. The background was concentration dependent and in a typical assay ranged from ABS of 0.1 for 4 nM His_6-LIP5 to 0.23 for 3 μM His_6-LIP5. Corrected absorbance data were analyzed using Prism (GraphPad, San Diego CA) to define an EC_{50} by nonlinear regression analysis using the formula ABS= (ABSmax*X)/(EC50+X).

Tissue Culture and transfection

HEK293T cells were grown in Dulbecco's modified Eagle's medium (Gibco-BRL, Gaithersburg MD) containing 5% fetal bovine serum (Gibco-BRL), 5% supplemented calf serum (Hyclone Laboratories, Logan UT) and 2mM glutamine. Cells were transfected with the indicated plasmid(s) using Lipofectamine 2000 (Invitrogen, Carlsbad CA) following the manufacturer's instructions and then used for experiments 18-24 hrs after transfection.

Sedimentation assay

Sedimentation assays were performed as described previously (15). Briefly, transiently transfected HEK293T cells in 6 cm dishes were solubilized in 1% Triton X-100 and centrifuged at 10,000 x *g* for 15 minutes at 4°C. Pellets were resuspended to the same volume as supernatant in lysis buffer and equal volumes of the fractions were analyzed by immunoblotting with rabbit anti-FLAG antibody (Sigma, St. Louis MO,

1:2500) or rabbit anti-GFP.

Immunoprecipitation

Transiently transfected HEK293T cells in 6 cm dishes were solubilized in 500μl buffer E (0.5% Triton X-100, 30mM HEPES, 120mM NaCl, 1mM PMSF and complete protease inhibitor (Roche Diagnostics, Alameda, CA)). Insoluble material was removed by centrifugation at 15,000 x g for 15 minutes. Soluble lysate was incubated with 20μl of protein A-sepharose^{TM} CL-4B (GE Healthcare, Piscataway, NJ) for 25 min to remove nonspecifically interacting material, then with 6μl of rabbit anti-GFP antibody for 2 hour, and finally with 30μl of protein A sepharose for 1 hour, all at 4^{o}C. Bound protein and lysate were analyzed by immunoblotting using mouse monoclonal anti-myc (Developmental Studies Hybridoma Bank, Iowa City IA, 1:2500) and rabbit anti-GFP.

RESULTS

LIP5 binds tightly to several ESCRT-III proteins in addition to CHMP5

The AAA+ ATPase VPS4 plays a key role in MVB biogenesis (19, 35-37), but precisely what it does and how this is regulated remains unclear. To gain new insight into this reaction, we explored connections between ESCRT-III and a known cofactor of VPS4, LIP5. A previous study demonstrated that LIP5 bound efficiently but apparently uniquely to the ESCRT-III like protein CHMP5 (31); this interaction was also found in a reciprocal immunoprecipitation of proteins that bind to CHMP5 (38). In yeast, Vta1p, the LIP5 orthologue, binds both to Vps60p (CHMP5 ortholog) (26, 30, 32) and to Did2p/Vps46p (CHMP1 ortholog) (33). Based on this, we asked whether LIP5 also interacts with other human ESCRT-III proteins. We expressed ESCRT-III proteins representing each of the ESCRT-III subfamilies as GST-fusion proteins in *E. coli* and carried out *in vitro* binding experiments. In a survey GST pulldown, we found that CHMP1B, CHMP2A/hVps2-1, and CHMP3/hVps24 all bound to His_6-LIP5 while CHMP4A/hSnf7-1 and CHMP6/hVps20 did not (Fig. 3-1A).

To quantitatively compare binding of LIP5 to these different proteins, we immobilized each GST-CHMP fusion protein on microtiter plates using anti-GST antibodies and measured binding of His_6-LIP5 across a range of concentrations using Ni^{2+}-NTA conjugated to horseradish peroxidase and a colored substrate to detect bound His_6-LIP5. EC_{50} values for LIP5 binding ranged from 10 - 20 nM for binding to GST-CHMP1B to 0.3 - 1 μM for binding to GST-CHMP3 (Fig. 3-1B). There was no binding above background to immobilized GST, GST-CHMP4A, or GST-CHMP6 (data not shown).

For comparison, we also quantitated the interaction of LIP5 with VPS4B. These two proteins have previously been shown to bind each other with an EC_{50} of 53 nM in

surface plasmon resonance experiments (39). We found that His_6-LIP5 bound to immobilized GST-VPS4B(E235Q) with an EC_{50} of 60 nM (Fig. 3-1C), and that this binding was abolished by a short deletion within the VPS4B β domain (Δ390-396) known to block interaction of yeast Vps4 and Vta1 (27) (Fig. 3-1C). We conclude that LIP5 binds with sub-micromolar affinity to both a subset of ESCRT-III proteins and to VPS4B. As will be described below, we confirmed in parallel studies that LIP5 also binds to CHMP5 with comparable or even higher affinity (see Fig. 3-8). The interaction of LIP5 with CHMP1B might have been anticipated based on earlier studies in yeast (33), but the association of LIP5 with the core ESCRT-III proteins CHMP2A and CHMP3 was unexpected and raises the possibility of a more intimate relationship between LIP5 and ESCRT-III than previously appreciated.

LIP5 binding to CHMP2A and CHMP1B is mediated by C-terminal sequences

To understand how LIP5 binds to ESCRT-III proteins, we began by looking for its binding site in the core ESCRT-III protein CHMP2A. We examined interaction between LIP5 and a series of CHMP2A deletion proteins that lack one or more of the protein's predicted six α-helices (Fig. 3-2A), as previously described (15). Because even the shortest deletion from the C-terminus (leaving an α1 – α5 protein, residues 1-180) abolished binding, we generated a series of smaller deletions from the C-terminus to determine whether binding required α6 or sequences within the long linker between α5 and α6. GST-CHMP2A fusion proteins were purified from *E. coli* and combined with His_6-LIP5 to assess their interaction (Fig. 3-2B). Removing three amino acids from the C-terminus of CHMP2A (leaving residues 1-219) was not expected to significantly affect α6, and did not change binding of LIP5. On the other hand, removing six or more amino acids (thus perturbing or removing α6) abolished interaction of CHMP2A with LIP5.

Deleting α1 from CHMP2A (leaving residues 56-222) did not perturb LIP5 binding, demonstrating that the interaction is independent of CHMP2A's N-terminus.

In further experiments, we found the same requirement for extreme C-terminal sequences for interaction of CHMP1B with LIP5 (Fig. 3-2C). Removing the predicted α6 from CHMP1B's C-terminus disrupted LIP5 binding while deleting the N-terminal half of the protein had no effect (Fig. 3-2D). These experiments demonstrate that sequences within α6 are needed for CHMP2A and CHMP1B to bind LIP5.

Because deleting sequences from ESCRT-III proteins significantly changes their conformation (15), there remained the possibility of deletions indirectly impairing binding to a site or sites located elsewhere in the protein. To rule this out, we carried out additional experiments. We started by changing a single conserved residue within α6 of CHMP2A from leucine to alanine (L216A). This mutation significantly decreased binding to LIP5 (Fig. 3-3A). A comparable leucine residue in other ESCRT-III proteins has previously been shown to be important for binding of VPS4B to CHMP1B (21) and binding of Alix to CHMP4 (22), pointing to a likely common role for the surface of α6 in binding between ESCRT-III proteins and other factors.

To ask whether the C-terminal region is by itself sufficient for interaction of these ESCRT-III proteins with LIP5, we expressed α6 and surrounding linker sequences from CHMP1B (169-199) as a GST fusion protein and asked if it could bind to LIP5. Indeed, LIP5 bound to this 31 amino acid fragment (Fig. 3-3B) with an EC_{50} of 25 nM (Fig. 3-3C), similar to what we observed above for full-length CHMP1B. These results argue that all of the determinants needed for LIP5 binding are encoded within the C-terminal regions of these ESCRT-III proteins.

Studies in mammalian cells suggest that ESCRT-III interaction with LIP5 may be regulated by ESCRT-III assembly status

As mentioned above, the high affinity binding of LIP5 to the core ESCRT-III protein CHMP2A was entirely unexpected. Indeed, this finding is at first glance inconsistent with a published report in which endogenous LIP5 was not immunoisolated with overexpressed CHMP2A from transfected mammalian cells (31). We therefore examined interaction of LIP5 with CHMP2A in HEK293T cells transiently transfected with tagged versions of each protein. When we immunoprecipitated FLAG-CHMP2A from the solubilized lysate of doubly transfected cells, we also did not recover significant amounts of LIP5 (data not shown). However, we noticed that overexpressed FLAG-CHMP2A had a strong tendency to form large complexes or aggregates that were insoluble in Triton X-100 and therefore pelleted during preparation of the solubilized lysate. Although LIP5-GFP expressed alone is soluble, we found that when coexpressed with CHMP2A it associated with this insoluble material (Fig.3-4A). LIP5 remained soluble when coexpressed with CHMP2A fragments lacking their α6 region despite the fact that the CHMP2A proteins still sedimented. In addition, LIP5 only associated with pelleted CHMP2A when its N-terminus – previously shown in yeast to mediate interaction with the ESCRT-III related protein Vps60 – was intact.

Parallel studies with cells transfected with CHMP1B and LIP5-GFP demonstrated that CHMP1B similarly recruited LIP5 to sedimentable complexes only when its α6 region was intact (Fig. 3-4B). These results are consistent with our analysis of recombinant proteins above and confirm that LIP5 binds to extreme C-terminal sequences in CHMP2A and CHMP1B. Based on our earlier study of ESCRT-III homopolymers (15), the preferential association of LIP5 with pelleted CHMP2A and

CHMP1B suggests that LIP5 may bind to these proteins in their "open" conformation and tend to stabilize this state.

LIP5 and VPS4 MIT binding sites overlap in CHMP2A and CHMP1B

Interestingly, the extreme C-terminal regions of CHMP2A and CHMP1B were recently shown to contain a short α-helix that binds to VPS4 *via* a twelve residue sequence referred to as the MIT interaction motif (MIM) (20, 21). The MIM helix largely coincides with the sequence we defined as α6 by secondary structure prediction (15). We found above (Fig. 3-3A) that mutating a conserved hydrophobic residue in this helix reduced binding of LIP5 to CHMP2A. This impairment is in accordance with the reported ten fold decrease in VPS4 binding when the equivalent change was made in CHMP1B (21). VPS4 and LIP5 may therefore share elements of a common binding site in these ESCRT-III proteins.

To determine if this is the case, we asked whether the VPS4 MIT domain competes with LIP5 for binding to CHMP2A and CHMP1B. We expressed and purified the His_6-tagged MIT domain of VPS4A from *E. coli* and added it to GST pulldown experiments (Fig. 3-5A). We found that high concentrations of the MIT domain reduced but did not abolish binding between LIP5 and both CHMP2A and CHMP1B (Fig. 3-5B). Parallel control experiments demonstrated that adding 300 μM ribonuclease A had no effect on LIP5 binding (Fig. 3-5A & C).

Given this apparent overlap in binding sites, the question of how the affinity of these ESCRT-III proteins for LIP5 compares to that for VPS4 becomes important. We were unable to quantitate VPS4B (full-length or MIT domain) binding to immobilized GST-ESCRT-III proteins because of high background in the microtiter plates. In recent studies of VPS4 MIT domain binding to ESCRT-III MIM fragments the observed EC_{50}

values were significantly higher (i.e. lower affinity) than those we measured between LIP5 and full-length ESCRT-III proteins (20, 21). For a first assessment of the relative ability of VPS4 and LIP5 to bind to their shared binding site, we compared binding of full-length proteins to GST-CHMP1B(169-199) (Fig. 3-5D). After incubating this α6 fragment with 5 μM His_6-VPS4B(E235Q) or His_6-LIP5, we recovered similar amounts of bound protein, suggesting that full-length VPS4B and LIP5 may have similar affinity for the MIM-containing ESCRT-III proteins.

A second binding site for VPS4 in ESCRT-III proteins

If VPS4 and LIP5 have overlapping binding sites in this subset of ESCRT-III proteins, how do they function together? One possibility is that the C-terminal α6 sequences, preferentially exposed when the proteins assemble into ESCRT-III complex, cooperate to bring VPS4 and LIP5 together. Another, not mutually exclusive, possibility is that the interaction between α6 sequences and these proteins is only one step in the reaction leading to ESCRT-III disassembly, with additional steps and interactions required. Based on what is known about other AAA+ proteins, we wondered whether there might be a second, yet unidentified, binding site for VPS4 within ESCRT-III proteins. If so, this might also enable simultaneous interaction of ESCRT-III with VPS4 and LIP5.

To search for such a binding site, we took advantage of the fact that the detergent insoluble polymers formed when CHMP proteins are overexpressed in mammalian cells (see Fig. 3-4) create a high avidity matrix for their binding partners. We carried out sedimentation assays using HEK293T cells coexpressing CHMP2A deletion mutants and VPS4B(E235Q). Similar to what we saw with LIP5, coexpressed VPS4B(E235Q) sedimented with full-length CHMP2A (Fig. 3-6A). Interestingly, however,

small C-terminal deletions (including the MIMs) that eliminated interaction between CHMP2A and LIP5 did not affect association of VPS4B(E235Q) with CHMP2A. On the other hand, further deleting α5 and surrounding sequences abolished the CHMP2A dependent recruitment of VPS4B(E235Q). Note that the basal association of VPS4B(E235Q) with the insoluble fraction is somewhat higher than that of LIP5, presumably because VPS4B(E235Q) traps and binds to polymerized endogenous ESCRT proteins (34). Similar results were obtained with CHMP1B and VPS4B(E235Q) (Fig. 3-6B), suggesting that there might be a secondary binding site for VPS4 around or within the predicted α5 helix of both proteins. The orthogonal and exposed position of α5 in the currently available crystal structure of CHMP3 (14) suggests that this helix may move as a function of ESCRT-III conformation, making it an attractive candidate for engaging VPS4. Our initial attempts to define this potential binding site more precisely using purified proteins in GST pulldown experiments failed, both because the affinity of this interaction appears to be low and because the nonspecific binding of VPS4B to truncated ESCRT-III proteins was variable and relatively high.

To gain additional insight into the nature of this binding site, we instead turned to site-directed mutagenesis in our cell-based sedimentation assay. We noted that the region within and around α5 is highly acidic in all ESCRT-III proteins, and contains a glutamic acid that is the only residue conserved among all ESCRT-III proteins (14) (Fig. 3-7A). To determine if this region is involved in the secondary association of VPS4B with ESCRT-III proteins, we replaced pairs of acidic residues within and around α5 in CHMP2A with alanines. One pair included the conserved glutamic acid (mut a) while the others (mut b and mut c) were nearby but less conserved pairs. We also replaced the conserved pair of acidic residues (mut a) in CHMP1B. We made these mutations in both full-length and α6-deleted proteins, with the prediction that association of VPS4B with

the full-length proteins would be mediated largely by their MIM and would therefore be independent of a secondary binding site, while association of VPS4B with the truncated (α6-deleted) proteins would instead be fully dependent on the secondary binding site. Strikingly, we found that mut a eliminated recruitment of VPS4B(E235Q) to α6-deleted but not full-length CHMP2A (Fig. 3-7B). Mut b and mut c had no effect. The fact that mut a did not affect recruitment of VPS4B to polymers of full-length CHMP2A confirms that the alanine replacements did not induce significant protein misfolding. In support of these results, we found the same effect of mut a replacements on the recruitment of VPS4B(E235Q) to CHMP1B (Fig. 3-7C). We conclude that conserved acidic residues at the center of α5 are an important component of the secondary VPS4 binding site. Because these experiments were carried out in cells that highly overexpress VPS4B and the ESCRT-III protein in question, we consider it unlikely but cannot exclude that an intermediate protein such as Ist1 (40) mediates this secondary interaction between VPS4 and the acidic α5 residues in ESCRT-III proteins.

LIP5 complex with CHMP5 is unique

Finally, we wondered how the previously described interaction between LIP5 and CHMP5 (31) compares to its binding to the MIM-containing ESCRT-III proteins studied above. The fact that LIP5 and CHMP5 have been reciprocally identified as binding partners in unbiased pulldowns from cultured mammalian cell cytosol (31, 38) while none of the other complexes have been detected suggests that there could be important differences. CHMP5 does not have a MIM, and in fact its predicted secondary structure does not include strong indication of a C-terminal helix comparable to α6 in the other ESCRT-III proteins (Fig. 3-8A). To characterize the interaction between LIP5 and CHMP5, we began by performing *in vitro* binding experiments. Our initial attempts to use

full-length GST-CHMP5 purified from *E. coli* were unsuccessful because the protein was not well behaved, forming aggregates that did not consistently bind to LIP5 (data not shown). The C-terminal half of the protein (GST-CHMP5 121-219), however, was readily soluble and reproducibly bound to LIP5 (Fig. 3-8B & C). In solid phase binding assays, we found that LIP5 bound to this C-terminal fragment with an EC_{50} of 1 - 2 nM (Fig. 3-8D), confirming an even tighter interaction between CHMP5 and LIP5 than between LIP5 and the other ESCRT-III proteins.

To define the structural requirements for interaction of CHMP5 with LIP5, we made a series of GST-CHMP5 fragments and tested their ability to bind to GFP-LIP5 present in a transfected cell extract (Fig. 3-8B). Deleting sequences C-terminal to the predicted α5 helix (GST-CHMP5 121-175) had little effect on binding while removing the predicted α5 region (GST CHMP5 121-158 and 121-149) abolished LIP5 binding, suggesting an important role for α5. Indeed, a 27 residue fragment containing only linker sequences and α5 (GST CHMP5 149-175) bound to LIP5 as efficiently as the longer fragments. Sequences within and around α5 are thus both necessary and sufficient for binding of LIP5. To confirm this result with purified proteins, we examined binding of His_6-LIP5 expressed in E. coli to the CHMP5 α4 + α5 or α5 fragments. As was the case with GFP-LIP5 from mammalian cell extracts, both fragments were able to bind efficiently to LIP5 confirming that sequences within and around α5 are responsible for high affinity binding between these two proteins (Fig. 3-8C).

To further compare the interaction of LIP5 with CHMP5 to that with CHMP1B or 2A, we again carried out a sedimentation assay in cotransfected HEK293T cells. As seen previously for CHMPs 1B and 2A, a substantial portion of overexpressed CHMP5 formed complexes or aggregates and ended up in the pellet. Interestingly, however, this insoluble material did not recruit LIP5, which was exclusively found in the soluble fraction

(Fig. 3-8E). To confirm that soluble CHMP5 actually interacts with LIP5 in these cells, we immunoprecipitated GFP-LIP5 and found that, as expected, FLAG-CHMP5 was efficiently recovered (Fig. 3-8F). Deleting the N-terminal 75 residues from LIP5 (LIP5ΔN) abolished this binding as it has been reported to do with the comparable proteins in yeast (26). Together, our data suggest that LIP5 interacts with CHMP5 in a distinct manner that may or may not be compatible with ESCRT-III polymer assembly.

DISCUSSION

LIP5 (Vta1 in yeast) emerged in recent years as a protein involved in late stages of MVB formation and viral budding. It participates in these events at least in part by binding *via* its C-terminal "VSL domain" to the AAA ATPase VPS4 to enhance oligomerization and ATPase activity (25-27, 33). At the same time, LIP5 also binds *via* its N-terminus to the ESCRT-III related protein CHMP5 (Vps60 in yeast) (30-32), and in yeast Vta1 has been shown to bind to Vps46, another ESCRT-III related protein (33). Whether, and if so how, these interactions affect VPS4 activity toward ESCRT-III complexes has been unclear. Here, we define new and unexpected relationships among these proteins, including a high affinity connection between LIP5 and the C-termini of a subset of ESCRT-III proteins and a second binding site for VPS4 further inside these proteins. In addition, comparison of LIP5's interaction with CHMP5 and the other ESCRT-III proteins revealed important differences in where and how the proteins bind to each other, suggesting the possibility of a unique role for CHMP5. These findings lead us to propose that there are at least two ways in which LIP5 is involved in ESCRT-III disassembly.

LIP5 has been clearly shown to be a positive modulator of the MVB sorting pathway. Reducing its expression by RNAi decreases degradation of the EGF receptor and blocks HIV viral particle release, while overexpressing it has no effect (31). In yeast, mutations in *VTA1* impair membrane protein degradation and create a weak class E phenotype, the severity of which may depend on the flux of cargo through the endosomal pathway (26, 30, 32). While LIP5's known role in VPS4 oligomerization might explain these effects, our results reveal that LIP5 also directly and efficiently engages a number of ESCRT-III proteins including in particular those that contain the C-terminal MIT interacting motif (MIM) known to bind VPS4 (Figs. 3-1 & 2) (20, 21).

How might LIP5 bound to ESCRT-III proteins modulate progress through the MVB pathway? Because LIP5 and ESCRT-III are already thought to be cofactor and substrate of VPS4, respectively, it is logical to think that their interaction will affect VPS4 function. This idea is supported by the fact that the same ESCRT-III proteins that bind well to VPS4 (CHMP1, CHMP2 and CHMP3) bind well to LIP5 (20, 21, 41-43). One possibility is that the extra link between LIP5 and ESCRT-III complex ensures that VPS4 oligomerizes only where it is needed. In the simplest scenario, this would predict that interactions between these three proteins would reinforce each other. Indeed, VPS4 interacts with ESCRT-III and LIP5/Vta1 *via* separate domains (26, 27). Similarly, LIP5/Vta1 binds to VPS4 and the ESCRT-III like protein CHMP5/Vps60 via its C-terminus and N-terminus, respectively (26). However, we found that the VPS4 MIT domain reduces LIP5 binding to both CHMP2A and CHMP1B, indicating that everything cannot happen simultaneously (Fig. 3-5).

At the same time, we found evidence for a second, more internal, binding site for VPS4 in these ESCRT-III proteins (Figs. 3-6 & 7), leading us to suggest that the interaction of VPS4 with the MIM motifs in α6 may represent only one step in ESCRT-III disassembly. Although we were unable to precisely define the second VPS4 binding motif *in vitro*, deletion and alanine scanning studies in both CHMP2A and CHMP1B indicated that this interaction depends on conserved sequences within these proteins' α5 helix and in particular on two acidic residues that are conserved across all ESCRT-III proteins. Interestingly, α5 occupies an exposed position in the crystal structure of CHMP3 (14), which probably represents the "open" form of these proteins (5). We propose that interaction of VPS4 – using its MIT domain, elements within its AAA+ domain such as the "pore loops" known to be important for its function (25), or possibly

an associated cofactor such as the recently described Ist1 (40) – with α5 in all ESCRT-III proteins is likely to be an important additional step in ESCRT-III complex disassembly.

While LIP5 is clearly established as a positive modulator of the MVB sorting pathway, the role played by CHMP5 (Vps60 in yeast) is less clear. CHMP5 binds with high affinity to LIP5 (Fig. 3-8), and deleting these two proteins in yeast has overlapping rather than additive effects (32). However, reducing or eliminating CHMP5 expression in mammalian tissues or cells does not prevent formation of MVBs (nor incorporation of TGF-β receptors into the internal vesicles) (44) and in fact enhances HIV budding from cells (31). These effects, together with the fact that LIP5's interaction with CHMP5 is fundamentally different from its interaction with the other ESCRT-III proteins, lead us to suggest that CHMP5 bound to LIP5 might negatively regulate LIP5 for engagement with other ESCRT-III proteins and VPS4. This possibility remains to be further explored.

A model that summarizes our results and how they impact thinking about the cooperation between LIP5 and VPS4 in regulating ESCRT-III is shown in Fig. 3-9. Binding sites for LIP5 (α5 in CHMP5, α6 in CHMP1B and CHMP2A) and for VPS4B (previously described primary site in α6, secondary binding site in α5) are shown in Fig. 3-9A. The relationship between ESCRT-III subunits, ESCRT-III complex, and LIP5 and VPS4 is depicted in Fig. 3-9B. ESCRT-III proteins are closed monomers in the cytosol. In this state, our results suggest that only CHMP5 binds to LIP5. When ESCRT-III proteins polymerize into complexes on the endosomal membrane (presumably nucleated by upstream factors that are connected to cargo) the subunits open, exposing sequences at their C-termini for binding to LIP5 and/or VPS4. How these two proteins share their overlapping binding sites remains to be determined, but their separate ability to bind each other (*via* domains that are not engaged with the ESCRT-III proteins, the β domain in VPS4 (25, 27) and the VSL domain in LIP5 (Azmi *et al.*, 2006)) is likely to

reinforce their association. Once some threshold is reached (perhaps full assembly of a VPS4 oligomer (28, 29), we hypothesize that VPS4 engages its secondary contact site. This in turn may allow VPS4 to unfold individual ESCRT-III subunits and release them into the cytoplasm, where they revert to their closed and monomeric states. While aspects of this model remain to be confirmed, and importantly any ESCRT-III disassembly reaction has yet to be reconstituted, the intricacies of this important step in MVB biogenesis are finally starting to come into focus.

While this paper was being reviewed and revised, two papers examining the structure and interactions of Vta1 (the yeast equivalent of LIP5) were published (45, 46). In one, the high-resolution crystal structure of the Vta1 N-terminus revealed two MIT-like domains, each consisting of three α-helices (46). This structure strongly supports our finding of a high affinity interaction between LIP5 and the MIM-containing ESCRT-III proteins CHMP1B and CHMP2A and suggests that one or both of LIP5's MIT domains binds to these proteins. In the second paper, the interaction between Vta1 and Vps60 (yeast CHMP5) was explored in more detail with results that largely agree with what we report here for mammalian proteins (45). Significant differences are the failure to see a high affinity interaction between Vta1 and Vps2 in the yeast system and mapping of the Vta1 binding site in Vps60 to α4 instead of α5 as found here for CHMP5 and LIP5. Whether these differences reflect differences in the protein interactions or in the conditions used to study them remains to be established.

REFERENCES

1. Gruenberg JS, H. The biogenesis of multivesicular endosomes. Nat Rev Mol Cell Biol 2004;5(4):317-323.

2. Piper RC, Katzmann DJ. Biogenesis and function of multivesicular bodies. Annu Rev Cell Dev Biol 2007;23:519-547.

3. Katzmann DJ, Odorizzi G, Emr SD. Receptor downregulation and multivesicular-body sorting. Nat Rev Mol Cell Biol 2002;3(12):893-905.

4. Raymond CK, Howald-Stevenson I, Vater CA, Stevens TH. Morphological classification of the yeast vacuolar protein sorting mutants: evidence for a prevacuolar compartment in class E vps mutants. Mol Biol Cell 1992;3(12):1389-1402.

5. Saksena S, Sun J, Chu T, Emr SD. ESCRTing proteins in the endocytic pathway. Trends Biochem Sci 2007;32(12):561-573.

6. Hurley JH, Emr SD. The ESCRT complexes: structure and mechanism of a membrane-trafficking network. Annu Rev Biophys Biomol Struct 2006;35:277-298.

7. Babst M. A protein's final ESCRT. Traffic 2005;6(1):2-9.

8. Bieniasz PD. Late budding domains and host proteins in enveloped virus release. Virology 2006;344(1):55-63.

9. Carlton JG, Martin-Serrano J. Parallels between cytokinesis and retroviral budding: a role for the ESCRT machinery. Science 2007;316(5833):1908-1912.

10. Demirov DG, Freed EO. Retrovirus budding. Virus Res 2004;106(2):87-102.

11. Morita E, Sundquist WI. Retrovirus budding. Annu Rev Cell Dev Biol 2004;20:395-425.

12. Morita E, Sandrin V, Chung HY, Morham SG, Gygi SP, Rodesch CK, Sundquist WI. Human ESCRT and ALIX proteins interact with proteins of the midbody and function in cytokinesis. Embo J 2007;26(19):4215-4227.

13. Williams RL, Urbe S. The emerging shape of the ESCRT machinery. Nat Rev Mol Cell Biol 2007;8(5):355-368.

14. Muziol T, Pineda-Molina E, Ravelli RB, Zamborlini A, Usami Y, Gottlinger H, Weissenhorn W. Structural basis for budding by the ESCRT-III factor CHMP3. Dev Cell 2006;10(6):821-830.

15. Shim S, Kimpler LA, Hanson PI. Structure/Function Analysis of Four Core ESCRT-III Proteins Reveals Common Regulatory Role for Extreme C-Terminal Domain. Traffic 2007;8(8):1068-1079.

16. Babst M, Katzmann DJ, Estepa-Sabal EJ, Meerloo T, Emr SD. Escrt-III: an endosome-associated heterooligomeric protein complex required for mvb sorting. Dev Cell 2002;3(2):271-282.

17. Kranz A, Kinner A, Kolling R. A Family of Small Coiled-Coil-forming Proteins Functioning at the Late Endosome in Yeast. Mol Biol Cell 2001;12(3):711-723.

18. Hanson PI, Roth R, Lin Y, Heuser JE. Plasma membrane deformation by circular arrays of ESCRT-III protein filaments. J Cell Biol 2008;180(2):389-402.

19. Babst M, Wendland B, Estepa EJ, Emr SD. The Vps4p AAA ATPase regulates membrane association of a Vps protein complex required for normal endosome function. Embo J 1998;17(11):2982-2993.

20. Obita T, Saksena S, Ghazi-Tabatabai S, Gill DJ, Perisic O, Emr SD, Williams RL. Structural basis for selective recognition of ESCRT-III by the AAA ATPase Vps4. Nature 2007;449(7163):735-739.

21. Stuchell-Brereton MD, Skalicky JJ, Kieffer C, Karren MA, Ghaffarian S, Sundquist WI. ESCRT-III recognition by VPS4 ATPases. Nature 2007;449(7163):740-744.

22. von Schwedler UK, Stuchell M, Muller B, Ward DM, Chung HY, Morita E, Wang HE, Davis T, He GP, Cimbora DM, Scott A, Krausslich HG, Kaplan J, Morham SG, Sundquist WI. The protein network of HIV budding. Cell 2003;114(6):701-713.

23. Yeo SC, Xu L, Ren J, Boulton VJ, Wagle MD, Liu C, Ren G, Wong P, Zahn R, Sasajala P, Yang H, Piper RC, Munn AL. Vps20p and Vta1p interact with Vps4p and function in multivesicular body sorting and endosomal transport in Saccharomyces cerevisiae. J Cell Sci 2003;116(Pt 19):3957-3970.

24. Xiao J, Xia H, Yoshino-Koh K, Zhou J, Xu Z. Structural Characterization of the ATPase Reaction Cycle of Endosomal AAA Protein Vps4. J Mol Biol 2007;374(3):655-670.

25. Scott A, Chung HY, Gonciarz-Swiatek M, Hill GC, Whitby FG, Gaspar J, Holton JM, Viswanathan R, Ghaffarian S, Hill CP, Sundquist WI. Structural and mechanistic studies of VPS4 proteins. Embo J 2005;24(20):3658-3669.

26. Azmi I, Davies B, Dimaano C, Payne J, Eckert D, Babst M, Katzmann DJ. Recycling of ESCRTs by the AAA-ATPase Vps4 is regulated by a conserved VSL region in Vta1. J Cell Biol 2006;172(5):705-717.

27. Vajjhala PR, Wong JS, To HY, Munn AL. The beta domain is required for Vps4p oligomerization into a functionally active ATPase. Febs J 2006;273(11):2357-2373.

28. Hartmann C, Chami M, Zachariae U, de Groot BL, Engel A, Grutter MG. Vacuolar protein sorting: two different functional states of the AAA-ATPase Vps4p. J Mol Biol 2008;377(2):352-363.

29. Yu Z, Gonciarz MD, Sundquist WI, Hill CP, Jensen GJ. Cryo-EM structure of dodecameric Vps4p and its 2:1 complex with Vta1p. J Mol Biol 2008;377(2):364-377.

30. Shiflett SL, Ward DM, Huynh D, Vaughn MB, Simmons JC, Kaplan J. Characterization of Vta1p, a class E Vps protein in S. cerevisiae. J Biol Chem 2004;279(12):10982-10990.

31. Ward DM, Vaughn MB, Shiflett SL, White PL, Pollock AL, Hill J, Schnegelberger R, Sundquist WI, Kaplan J. The role of LIP5 and CHMP5 in multivesicular body formation and HIV-1 budding in mammalian cells. J Biol Chem 2005;280(11):10548-10555.

32. Rue SM, Mattei S, Saksena S, Emr SD. Novel Ist1-Did2 Complex Functions at a Late Step in MVB Sorting. Mol Biol Cell 2008;19(2):475-484.

33. Lottridge JM, Flannery AR, Vincelli JL, Stevens TH. Vta1p and Vps46p regulate the membrane association and ATPase activity of Vps4p at the yeast multivesicular body. Proc Natl Acad Sci U S A 2006;103(16):6202-6207.

34. Lin Y, Kimpler LA, Naismith TV, Lauer JM, Hanson PI. Interaction of the mammalian endosomal sorting complex required for transport (ESCRT) III protein hSnf7-1 with itself, membranes, and the AAA+ ATPase SKD1. J Biol Chem 2005;280(13):12799-12809.

35. Babst M, Sato TK, Banta LM, Emr SD. Endosomal transport function in yeast requires a novel AAA-type ATPase, Vps4p. Embo J 1997;16(8):1820-1831.

36. Bishop N, Woodman P. ATPase-defective mammalian VPS4 localizes to aberrant endosomes and impairs cholesterol trafficking. Mol Biol Cell 2000;11(1):227-239.

37. Fujita H, Yamanaka M, Imamura K, Tanaka Y, Nara A, Yoshimori T, Yokota S, Himeno M. A dominant negative form of the AAA ATPase SKD1/VPS4 impairs membrane trafficking out of endosomal/lysosomal compartments: class E vps phenotype in mammalian cells. J Cell Sci 2003;116(Pt 2):401-414.

38. Ma YM, Boucrot E, Villen J, Affar el B, Gygi SP, Gottlinger HG, Kirchhausen T. Targeting of AMSH to endosomes is required for epidermal growth factor receptor degradation. J Biol Chem 2007;282(13):9805-9812.

39. Fujita H, Umezuki Y, Imamura K, Ishikawa D, Uchimura S, Nara A, Yoshimori T, Hayashizaki Y, Kawai J, Ishidoh K, Tanaka Y, Himeno M. Mammalian class E Vps proteins, SBP1 and mVps2/CHMP2A, interact with and regulate the function of an AAA-ATPase SKD1/Vps4B. J Cell Sci 2004;117(Pt 14):2997-3009.

40. Dimaano C, Jones CB, Hanono A, Curtiss M, Babst M. Ist1 regulates Vps4 localization and assembly. Mol Biol Cell 2008;19(2):465-474.

41. Howard TL, Stauffer DR, Degnin CR, Hollenberg SM. CHMP1 functions as a member of a newly defined family of vesicle trafficking proteins. J Cell Sci 2001;114(Pt 13):2395-2404.

42. Scott A, Gaspar J, Stuchell-Brereton MD, Alam SL, Skalicky JJ, Sundquist WI. Structure and ESCRT-III protein interactions of the MIT domain of human VPS4A. Proc Natl Acad Sci U S A 2005;102(39):13813-13818.

43. Nickerson DP, West M, Odorizzi G. Did2 coordinates Vps4-mediated dissociation of ESCRT-III from endosomes. J Cell Biol 2006;175(5):715-720.

44. Shim JH, Xiao C, Hayden MS, Lee KY, Trombetta ES, Pypaert M, Nara A, Yoshimori T, Wilm B, Erdjument-Bromage H, Tempst P, Hogan BL, Mellman I, Ghosh S. CHMP5 is essential for late endosome function and down-regulation of receptor signaling during mouse embryogenesis. J Cell Biol 2006;172(7):1045-1056.

45. Azmi IF, Davies BA, Xiao J, Babst M, Xu Z, Katzmann DJ. ESCRT-III family members stimulate Vps4 ATPase activity directly or via Vta1. Dev Cell 2008;14(1):50-61.

46. Xiao J, Xia H, Zhou J, Azmi IF, Davies BA, Katzmann DJ, Xu Z. Structural basis of Vta1 function in the multivesicular body sorting pathway. Dev Cell 2008;14(1):37-49.

FIGURE LEGENDS

Figure 3-1 LIP5 binds to ESCRT-III proteins.

(A) Interaction of LIP5 with a subset of ESCRT-III proteins. GST and GST-ESCRT-III proteins immobilized on glutathione-sepharose beads were incubated with *E.coli* lysate containing His_6-LIP5. Bound material was separated on a SDS-PAGE gel and stained with Coomassie Blue. Where necessary, lanes were rearranged as indicated by white lines. Immunoblotting with an anti-His_6 antibody confirmed that no His_6-LIP5 bound to GST-CHMP4A or GST-CHMP6 (not shown).

(B) Solid phase assay of LIP5 binding to GST-CHMP1B, 2A and 3. His_6-LIP5 bound to immobilized GST-CHMP proteins was detected with NTA-HRP and TMB colorimetric substrate. EC_{50} values determined by non-linear regression analysis ranged from 10-20 nM for CHMP1B (triangles, solid line), from 49-60nM for CHMP2A (open circles, dotted line), and from 0.3-1μM for CHMP3 (asterixes, alternating dashed line) in several independent experiments. Error bars show the SD from one experiment run in duplicate. Absorbance data was normalized to the B_{max} for CHMP1B.

(C) Binding of His_6-LIP5 to GST-VPS4B(E235Q) and GST-VPS4B(E235Q, ΔGAI) β domain mutant. EC_{50} for VPS4B(E235Q) (boxes, solid line) was 60nM. LIP5 binding to VPS4B(E235Q, ΔGAI) did not change as a function of LIP5 added (pyramids, dotted line). Error bars again show the SD from one experiment run in duplicate, and the absorbance data was normalized to the B_{max} for VPS4B(E235Q).

Figure 3-2 C-terminal sequences in CHMP2A and CHMP1B are required for LIP5 binding.

(A) Predicted CHMP2A secondary structure obtained using a neural network based algorithm (http://www.compbio.dundee.ac.uk/~www-jpred/submit.html). Pink and blue boxes correspond to predicted α-helices with pI higher than 8 and lower than 6, respectively.

(B) Effects of deleting N- and C-terminal sequences from CHMP2A on LIP5 binding. GST and GST-CHMP2A proteins with the indicated sequences immobilized on beads were incubated with *E.coli* lysate containing His_6-LIP5. Bound material was analyzed by staining with Coomassie Blue.

(C) Predicted CHMP1B secondary structure.

(D) Effects of deleting N- and C-terminal sequences from CHMP1B on LIP5 binding. GST and GST-CHMP1B proteins with the indicated sequences immobilized on beads were incubated with *E.coli* lysate containing His_6-LIP5. Bound material was analyzed by staining with Coomassie Blue (upper panel) and by immunoblotting with an anti-His_6 antibody (lower panel). Immunoblotting was needed because His_6-LIP5 migrates similarly to GST-CHMP1B(106-199).

Figure 3-3 CHMP2A and CHMP1B α6 region is responsible for LIP5 binding.

(A) Effect of CHMP2A L216A mutation on interaction with LIP5. GST and GST-CHMP2A proteins immobilized on beads were incubated with *E.coli* lysate containing His_6-LIP5. Bound material was analyzed by staining with Coomassie Blue. Where necessary, gel lanes were rearranged as shown by a white line.

(B) Binding of His_6-LIP5 to GST-CHMP1B(169-199). This CHMP1B fragment contains α6 and surrounding sequences but does not include α5.

(C) Solid phase assay of His_6-LIP5 binding to GST-CHMP1B(169-199) carried out as described in Fig. 3-1. The EC_{50} of 25 nM is similar to that of His_6-LIP5 for full-length CHMP1B. Absorbance data was normalized to the B_{max} for full-length CHMP1B measured in parallel.

Figure 3-4 LIP5 associates preferentially with polymerized CHMP2A and CHMP1B in transfected mammalian cells.

(A) Cosedimentation of LIP5 with CHMP2A. HEK293T cells cotransfected with GFP-LIP5 or GFP-LIP5ΔN and the indicated FLAG-CHMP2A constructs were solubilized in 1% Triton X-100 and centrifuged. The distribution of CHMP2A and LIP5 in the resulting supernatant (S) and pellet (P) was visualized by immunoblotting. LIP5ΔN is equivalent to a deletion in Vta1 that impairs binding to Vps60 (26). Experiments with LIP5ΔN were performed separately from those with full-length LIP5 and are therefore shown in a separate box.

(B) Cosedimentation of LIP5 with CHMP1B. The same experiments performed with FLAG-CHMP1B constructs.

Figure 3-5 Binding sites for VPS4 and LIP5 in CHMP2A and CHMP1B overlap.

(A) VPS4A MIT domain reduces LIP5 binding to GST-CHMP2A. GST-CHMP2A was incubated with His_6-LIP5 alone or together with 300μM His_6-VPS4A MIT domain or ribonuclease A as indicated. Bound LIP5 was visualized by staining with colloidal Coomassie blue and quantified by infrared fluorescence scanning. The bound MIT domain can be seen as an increased intensity in the dye front.

(B) Quantitation of the effect of MIT domain on binding of 3.2 μM LIP5 to CHMP2A or (in parallel experiments) CHMP1B.

(C) Quantitation of lack of effect of the same concentration (300 μM) of ribonuclease A on binding of 1.6 μM LIP5 to GST-CHMP2A.

(D) LIP5 and VPS4B(E235Q) bind similarly to GST-CHMP1B(169-199). Material retained on GST or GST-CHMP1B(169-199) after incubation with 5 μM of the indicated protein is shown on a gel stained with Coomassie Blue.

Figure 3-6 Effects of C-terminal deletions suggest existence of secondary binding site for VPS4B in CHMP2A and CHMP1B.

(A) HEK293T cells co-transfected with VPS4B(E235Q)-GFP and indicated FLAG-CHMP2A constructs were solubilized in 1% Triton X-100 and centrifuged. The resulting distribution of VPS4B(E235Q) and CHMP2A between supernatant (S) and pellet (P) was visualized by immunoblotting.

(B) Same experiment but with FLAG-CHMP1B constructs.

Figure 3-7 Conserved acidic residues in α5 are part of secondary VPS4 binding site.

(A) Sequences of predicted α5 and surrounding sequences in CHMP2 and CHMP1 proteins. Highly conserved acidic residues near the center of the helix are colored red, less conserved pairs of acidic residues in CHMP2A are colored blue. Pairs of alanine replacements in CHMP2A studied below are designated mut a, mut b, and mut c as indicated. The conserved central pair of acidic residues was also mutated in CHMP1B and designated as mut a.

(B) Effect of double alanine mutants on co-sedimentation of VPS4B(E235Q) with full-length (1-222) or α6-deleted (1-206) CHMP2A in cotransfected HEK293 cells. Cells were solubilized in 1% Triton X-100 and centrifuged. The resulting distribution of

VPS4B(E235Q) and CHMP2A between supernatant (S) and pellet (P) was visualized by immunoblotting.

(C) Effect of mut a on cosedimentation of VPS4B(E235Q) with full length (1-199) or α6-deleted α1 – α5 (1-181) CHMP1B.

Figure 3-8 Unique properties of CHMP5-LIP5 complex: LIP5 binds to CHMP5 α5 preferentially in the soluble fraction.

(A) Predicted secondary structure of CHMP5.

(B) GST and GST-CHMP5 proteins immobilized on beads were incubated with HEK293T cell lysate containing GFP-LIP5. Bound and unbound fractions were analyzed by immunoblotting with anti-GFP antibody. GST proteins were visualized by staining the immunoblot with Ponceau red.

(C) GST and GST-CHMP5 proteins on beads were incubated with *E.coli* lysate containing His_6-LIP5 and the bound material was analyzed by staining with Coomassie Blue. Where necessary, lanes were rearranged as indicated by white lines.

(D) Binding of His_6-LIP5 to immobilized GST-CHMP5(121-219), detected and analyzed as in Fig. 3-1B. EC_{50} values ranged from 1-2 nM. Error bars show SD from one experiment performed in duplicate.

(E) LIP5 does not cosediment with CHMP5. HEK293T cells co-transfected with GFP-LIP5 and FLAG-CHMP5 were solubilizated in 1% Triton X-100 and centrifuged. The resulting supernatant (S) and pellet (P) were analyzed by immunoblotting.

(F) Coimmunoprecipitation of CHMP5-myc with LIP5-GFP from co-transfected HEK293T cells. LIP5-GFP or LIP5ΔN-GFP was immunoprecipitated from the soluble lysate of cotransfected cells. Bound proteins and lysate were analyzed by immunoblotting.

Figure 3-9 Model showing proposed engagement of LIP5 with ESCRT-III proteins and VPS4.

(A) Binding sites for LIP5 and Vps4 in individual ESCRT-III subunits. Sites defined in this study in CHMP2A and CHMP1B are shown at left and in CHMP5 at right. The schematic structure of the ESCRT-III subunits is based on the crystal structure of CHMP3 (14). (B) Proposed model of ESCRT-III assembly, disassembly, and interaction with LIP5 and VPS4. Most ESCRT-III proteins are closed monomers in the cytoplasm and do not bind to LIP5, although CHMP5 interacts differently with LIP5 and can bind in the cytoplasm. As ESCRT-III complexes assemble on the endosomal membrane, individual subunits open and expose sequences at their C-termini for binding to LIP5 and/or VPS4. How these two proteins share their overlapping binding sites remains to be determined, but their separate ability to bind each other (*via* domains that are not engaged with the ESCRT-III proteins, the β domain in VPS4 (Scott *et al.*, 2005a; Vajjhala *et al.*, 2006) and the VSL domain in LIP5 (Azmi *et al.*, 2006)) is likely to reinforce their association. Once some threshold is reached (perhaps assembly of VPS4 rings), we propose that VPS4 engages its secondary contact site in α5 of the ESCRT-III proteins. Based on analogy to other AAA+ proteins, this may allow VPS4 to unfold individual ESCRT-III subunits and release them into the cytoplasm where they revert to their closed and monomeric state.

Figure 3-1

A

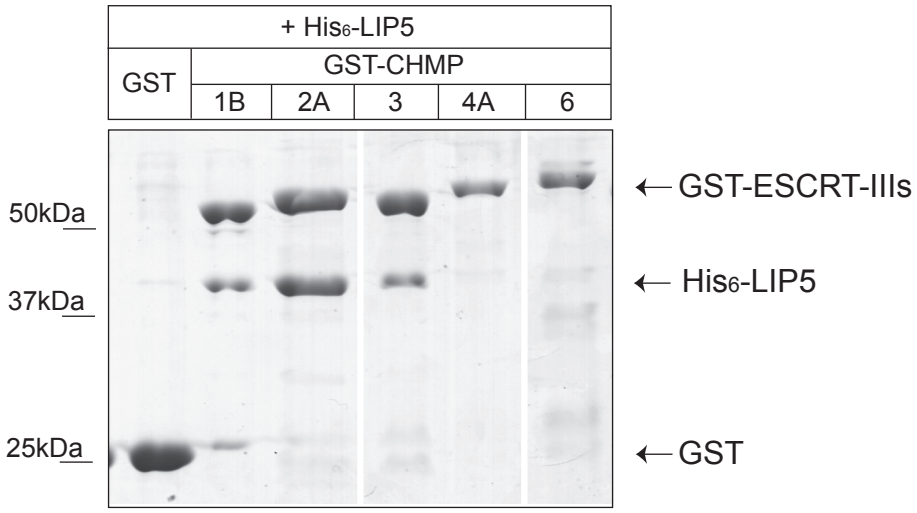
+ His6-LIP5
GST
GST-CHMP
1B
2A
3
4A
6
50kDa
37kDa
25kDa
← GST-ESCRT-IIIs
← His6-LIP5
← GST

Figure 3-1

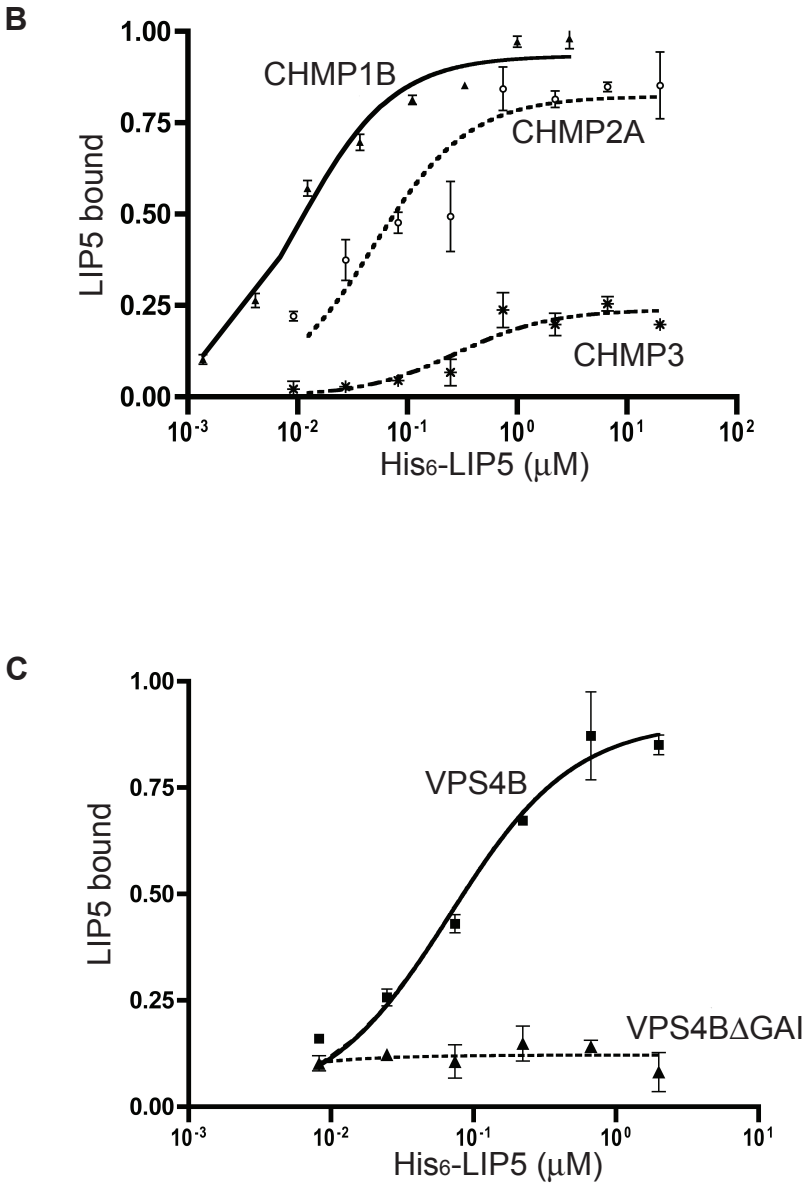
B
1.00
0.75
0.50
0.25
0.00
LIP5 bound
CHMP1B
CHMP2A
CHMP3
10-3
10-2
10-1
100
101
102
His6-LIP5 (μM)
C
1.00
0.75
0.50
0.25
0.00
LIP5 bound
VPS4B
VPS4BΔGAI
10-3
10-2
10-1
100
101
His6-LIP5 (μM)

Figure 3-2

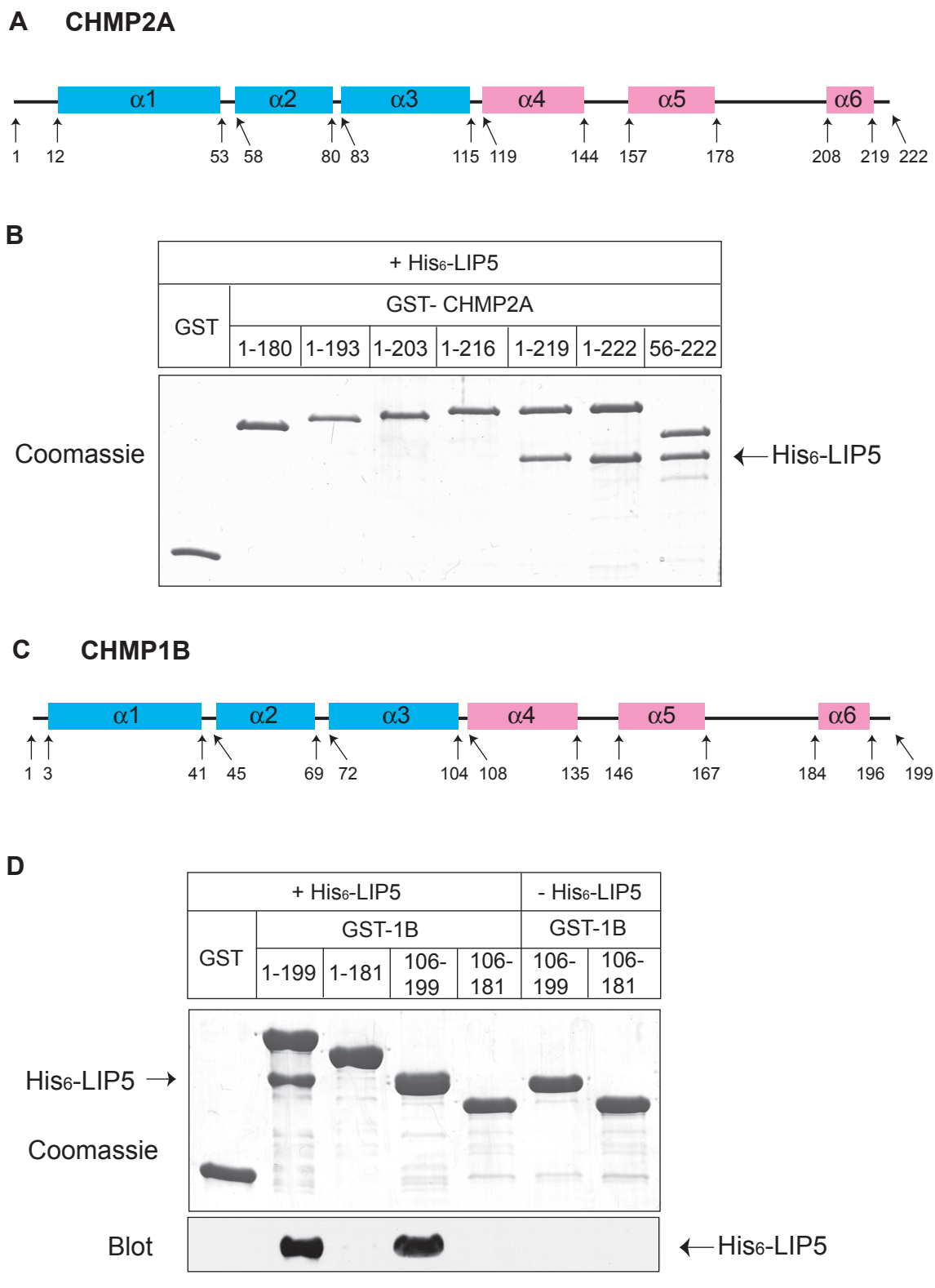
A
CHMP2A
α1
α2
α3
α4
α5
α6
1
12
53
58
80
83
115
119
144
157
178
208
219
222
B
+ His6-LIP5
GST
GST- CHMP2A
1-180
1-193
1-203
1-216
1-219
1-222
56-222
Coomassie
His6-LIP5
C
CHMP1B
α1
α2
α3
α4
α5
α6
1
3
41
45
69
72
104
108
135
146
167
184
196
199
D
+ His6-LIP5
- His6-LIP5
GST
GST-1B
GST-1B
1-199
1-181
106-199
106-181
106-199
106-181
His6-LIP5
Coomassie
Blot
His6-LIP5

Figure 3-3

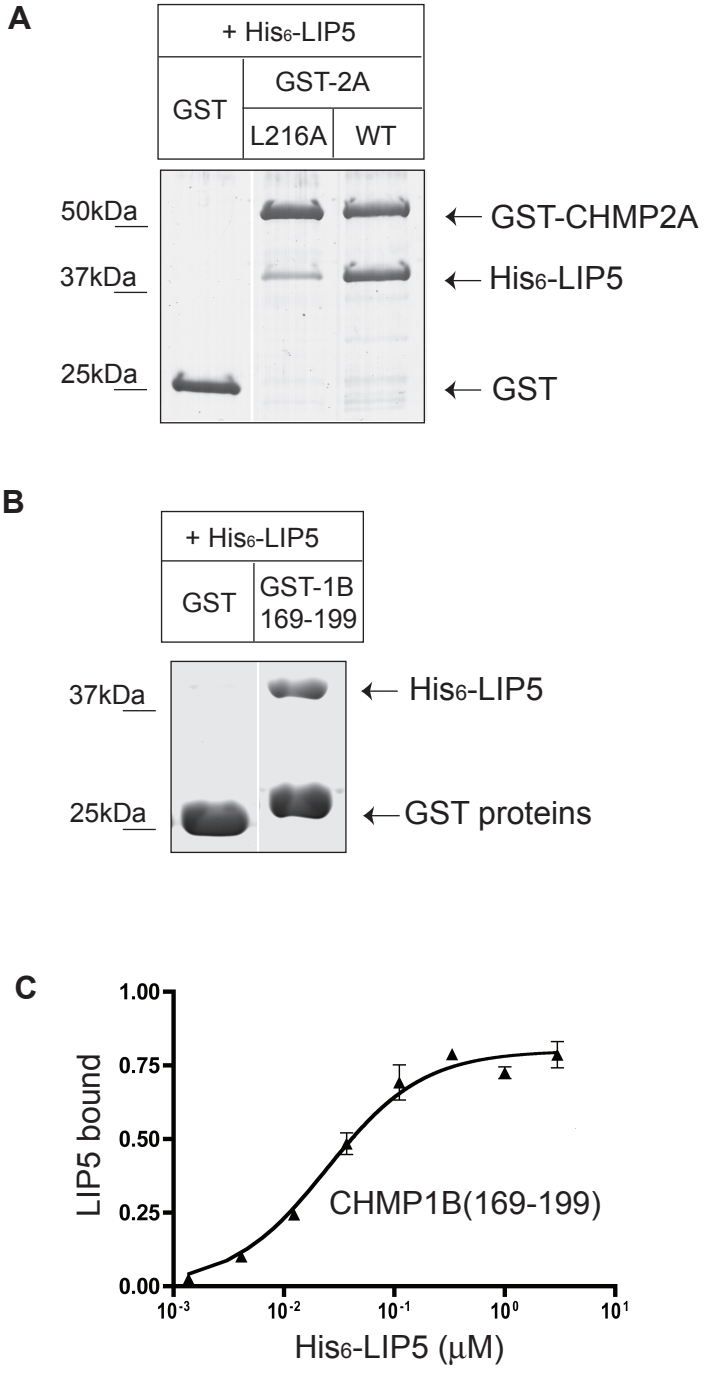
A
+ His6-LIP5
GST
GST-2A
L216A
WT
50kDa
37kDa
25kDa
← GST-CHMP2A
← His6-LIP5
← GST
B
+ His6-LIP5
GST
GST-1B 169-199
37kDa
25kDa
← His6-LIP5
← GST proteins
C
LIP5 bound
1.00
0.75
0.50
0.25
0.00
CHMP1B(169-199)
10-3
10-2
10-1
100
101
His6-LIP5 (μM)

Figure 3-4

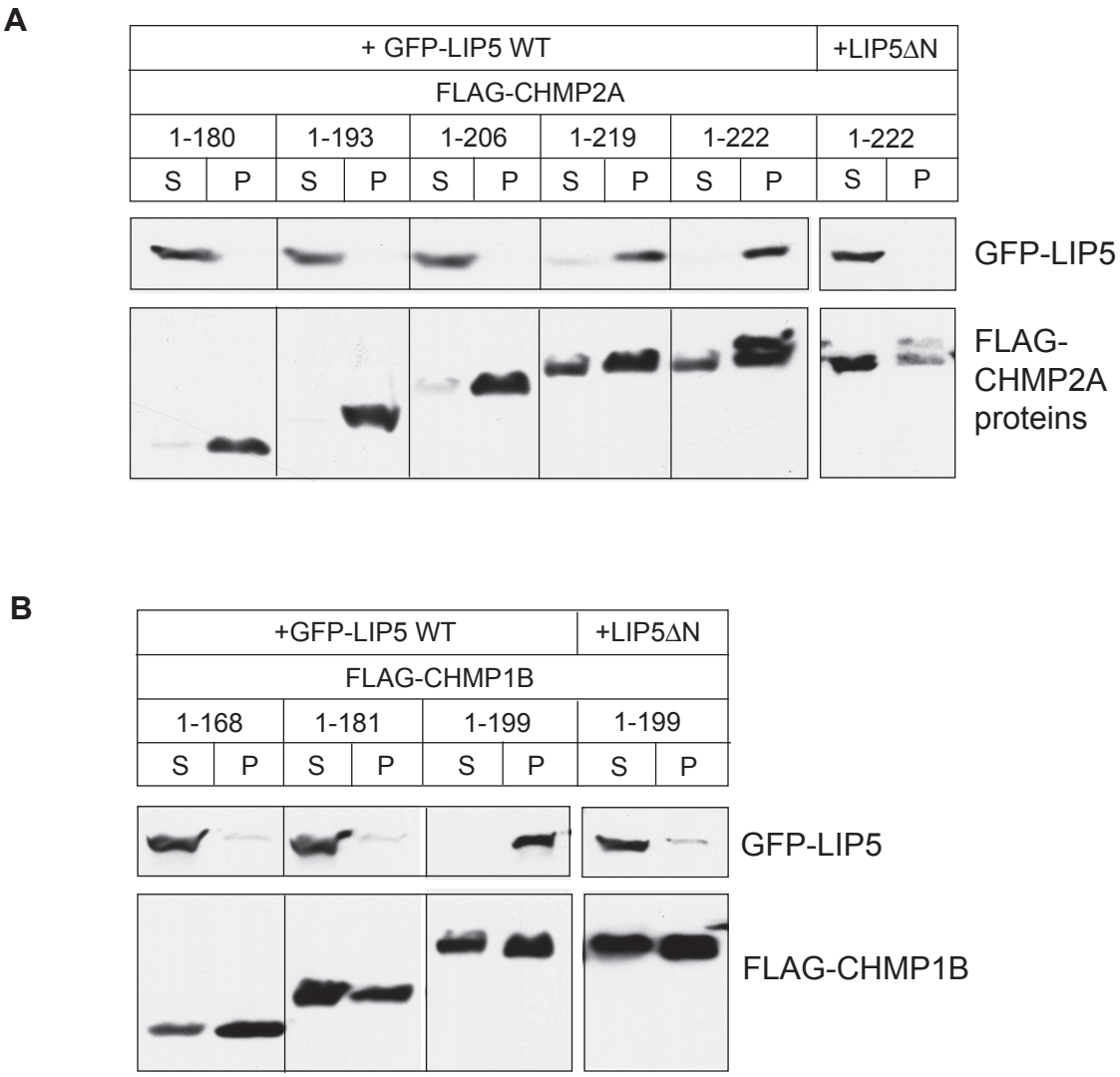
A
+ GFP-LIP5 WT
+LIP5ΔN
FLAG-CHMP2A
1-180
1-193
1-206
1-219
1-222
1-222
S
P
GFP-LIP5
FLAG-CHMP2A proteins
B
+GFP-LIP5 WT
+LIP5ΔN
FLAG-CHMP1B
1-168
1-181
1-199
1-199
GFP-LIP5
FLAG-CHMP1B

Figure 3-5

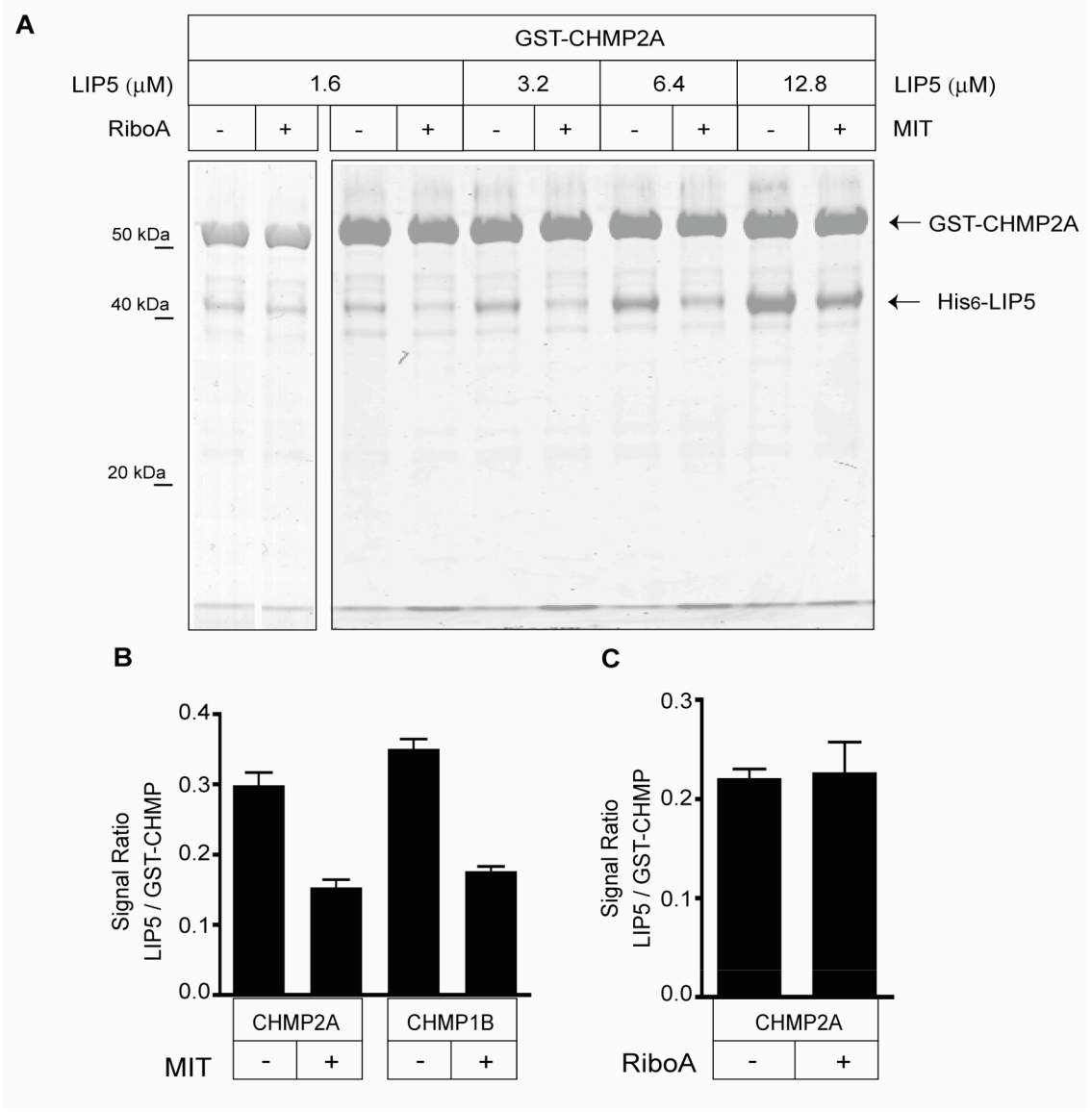
A
GST-CHMP2A
LIP5 (μM)
1.6
3.2
6.4
12.8
LIP5 (μM)
RiboA
- + - + - + - + - +
MIT
50 kDa
40 kDa
20 kDa
← GST-CHMP2A
← His6-LIP5
B
Signal Ratio
LIP5 / GST-CHMP
0.4
0.3
0.2
0.1
0.0
CHMP2A
CHMP1B
MIT
- + - +
C
Signal Ratio
LIP5 / GST-CHMP
0.3
0.2
0.1
0.0
CHMP2A
RiboA
- +

Figure 3-5

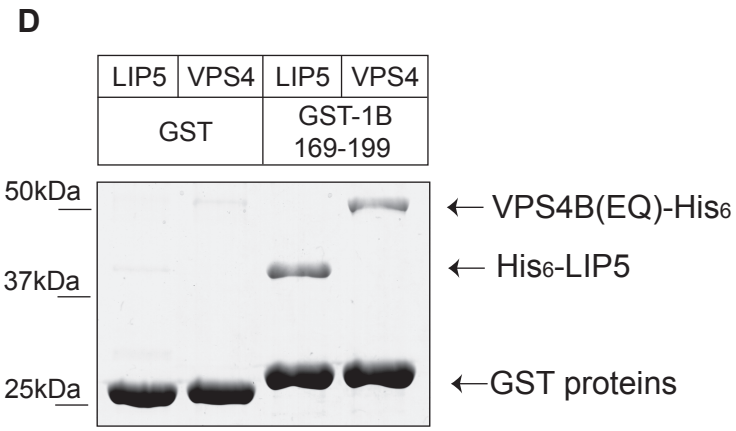
D
LIP5
VPS4
LIP5
VPS4
GST
GST-1B
169-199
50kDa
37kDa
25kDa
← VPS4B(EQ)-His6
← His6-LIP5
←GST proteins

Figure 3-6

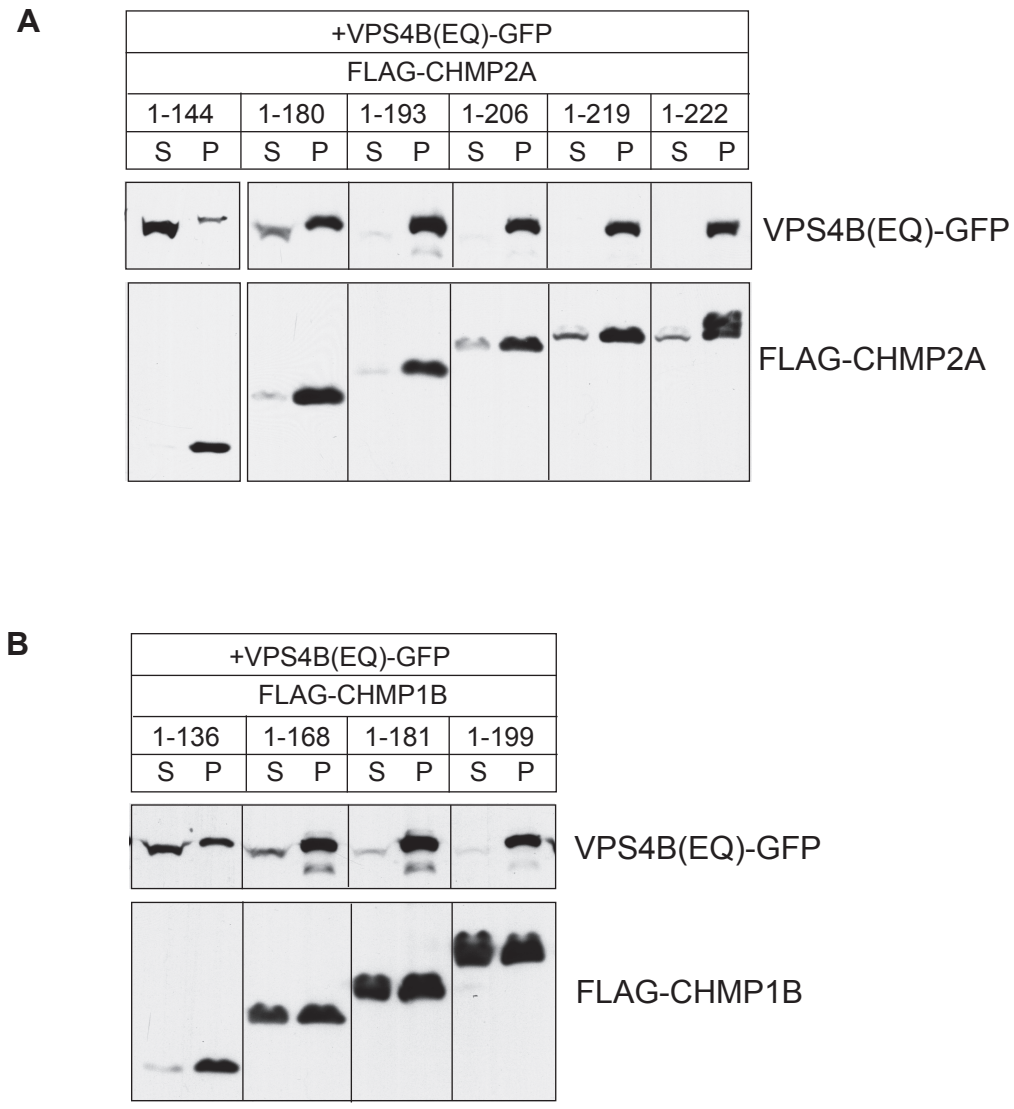
A
+VPS4B(EQ)-GFP
FLAG-CHMP2A
1-144
1-180
1-193
1-206
1-219
1-222
S P S P S P S P S P S P
VPS4B(EQ)-GFP
FLAG-CHMP2A
B
+VPS4B(EQ)-GFP
FLAG-CHMP1B
1-136
1-168
1-181
1-199
S P S P S P S P
VPS4B(EQ)-GFP
FLAG-CHMP1B

Figure 3-7

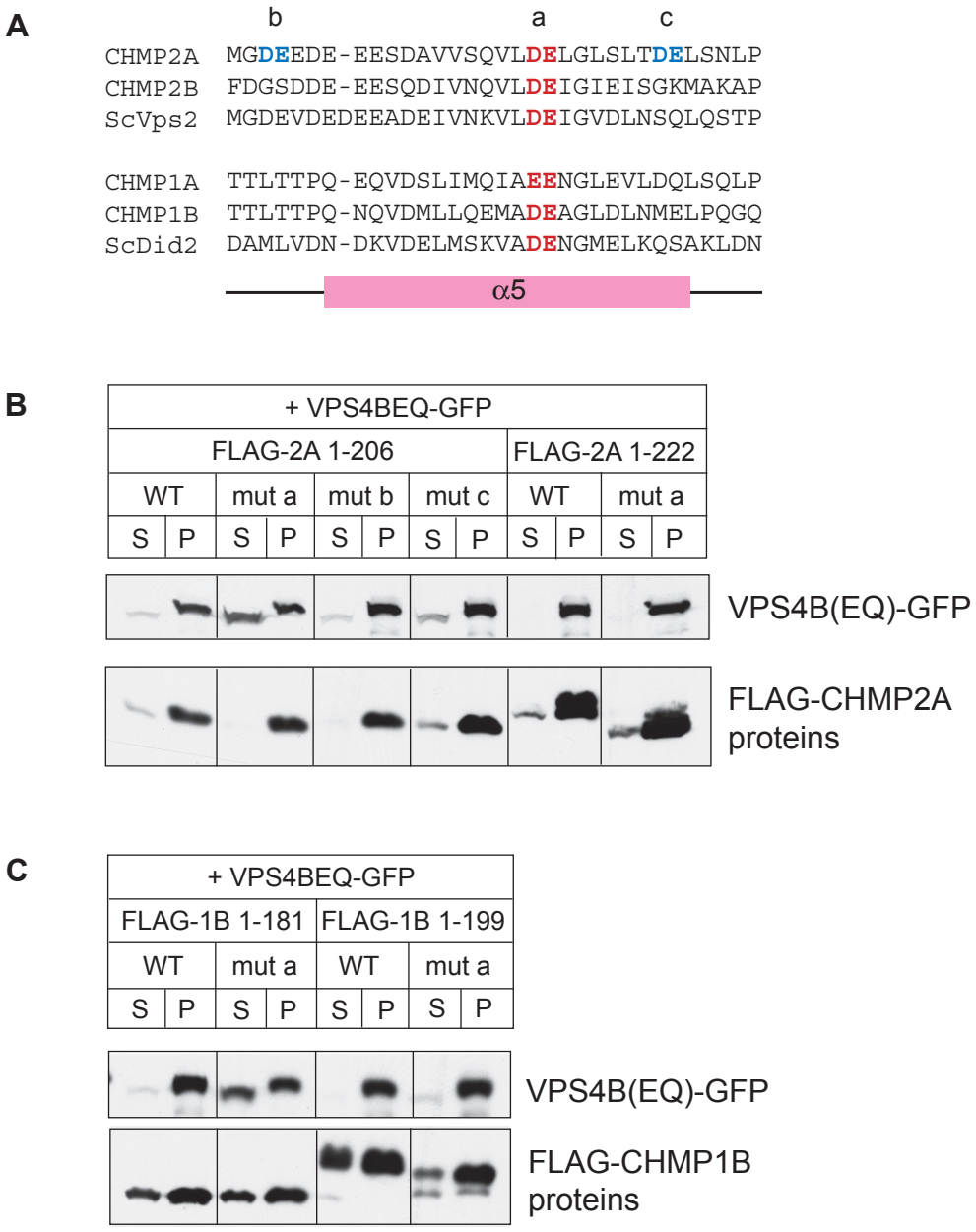
A
b
a
c
CHMP2A MGDEEDE-EESDAVVSQVLDELGLSLTDELSNLP
CHMP2B FDGSDDE-EESQDIVNQVLDEIGIEISGKMAKAP
ScVps2 MGDEVDEDEEADEIVNKVLDEIGVDLNSQLQSTP
CHMP1A TTLTTPQ-EQVDSLIMQIAEENGLEVLDQLSQLP
CHMP1B TTLTTPQ-NQVDMLLQEMADEAGLDLNMELPQGQ
ScDid2 DAMLVDN-DKVDELMSKVADENGMELKQSAKLDN
α5
B
+ VPS4BEQ-GFP
FLAG-2A 1-206
FLAG-2A 1-222
WT
mut a
mut b
mut c
WT
mut a
S
P
VPS4B(EQ)-GFP
FLAG-CHMP2A proteins
C
+ VPS4BEQ-GFP
FLAG-1B 1-181
FLAG-1B 1-199
WT
mut a
WT
mut a
S
P
VPS4B(EQ)-GFP
FLAG-CHMP1B proteins

Figure 3-8

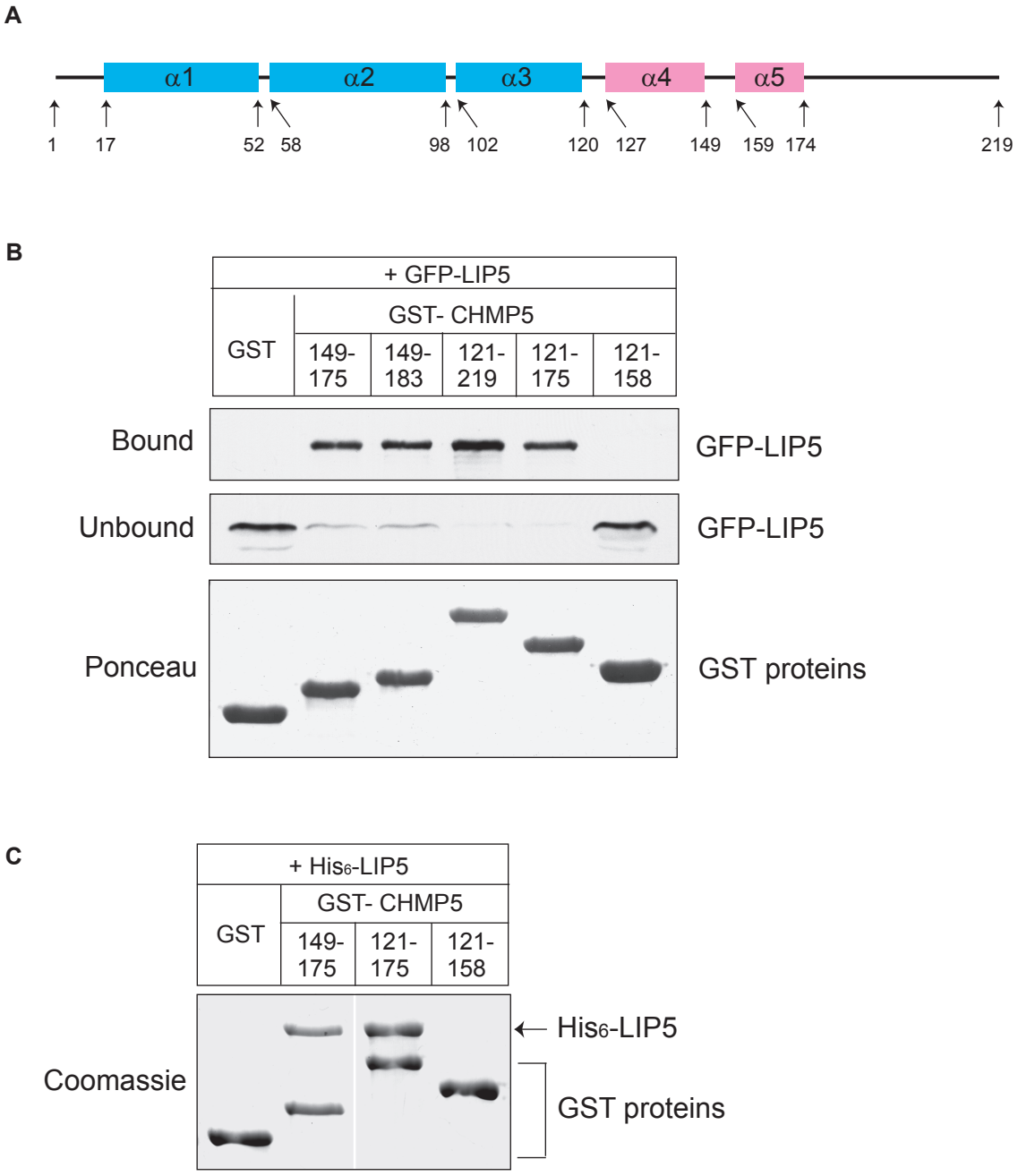
A
α1
α2
α3
α4
α5
1
17
52
58
98
102
120
127
149
159
174
219
B
+ GFP-LIP5
GST
GST- CHMP5
149-175
149-183
121-219
121-175
121-158
Bound
GFP-LIP5
Unbound
GFP-LIP5
Ponceau
GST proteins
C
+ His6-LIP5
GST
GST- CHMP5
149-175
121-175
121-158
Coomassie
His6-LIP5
GST proteins

Figure 3-8

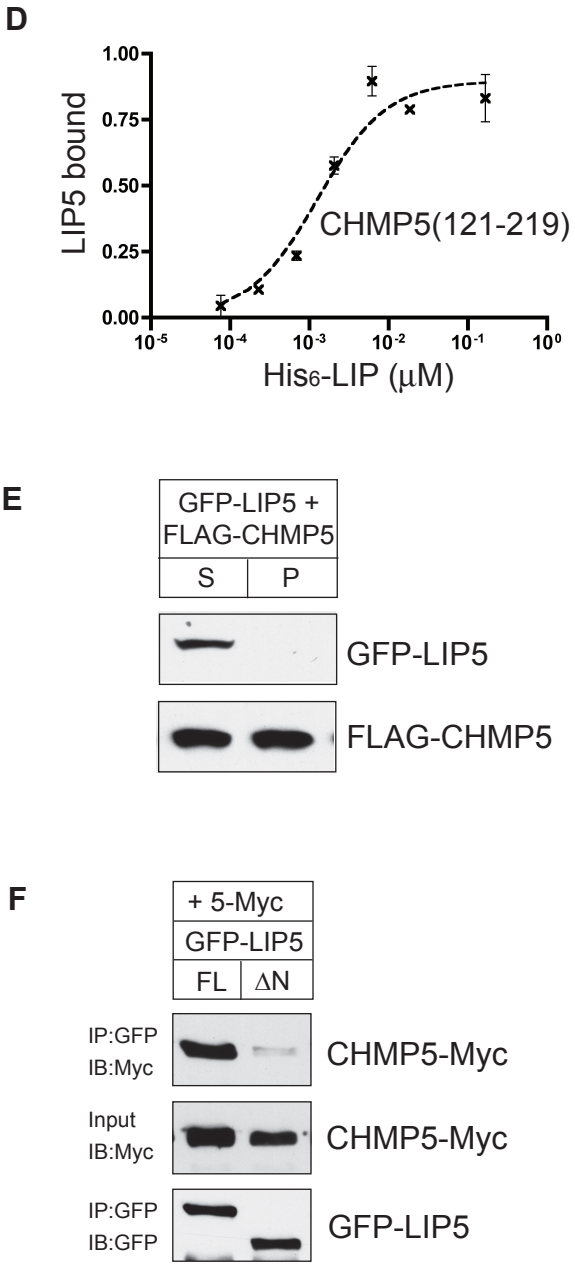
D
1.00
0.75
0.50
0.25
0.00
LIP5 bound
CHMP5(121-219)
10-5
10-4
10-3
10-2
10-1
100
His6-LIP (μM)
E
GFP-LIP5 +
FLAG-CHMP5
S
P
GFP-LIP5
FLAG-CHMP5
F
+ 5-Myc
GFP-LIP5
FL
ΔN
IP:GFP
IB:Myc
CHMP5-Myc
Input
IB:Myc
CHMP5-Myc
IP:GFP
IB:GFP
GFP-LIP5

Figure 3-9

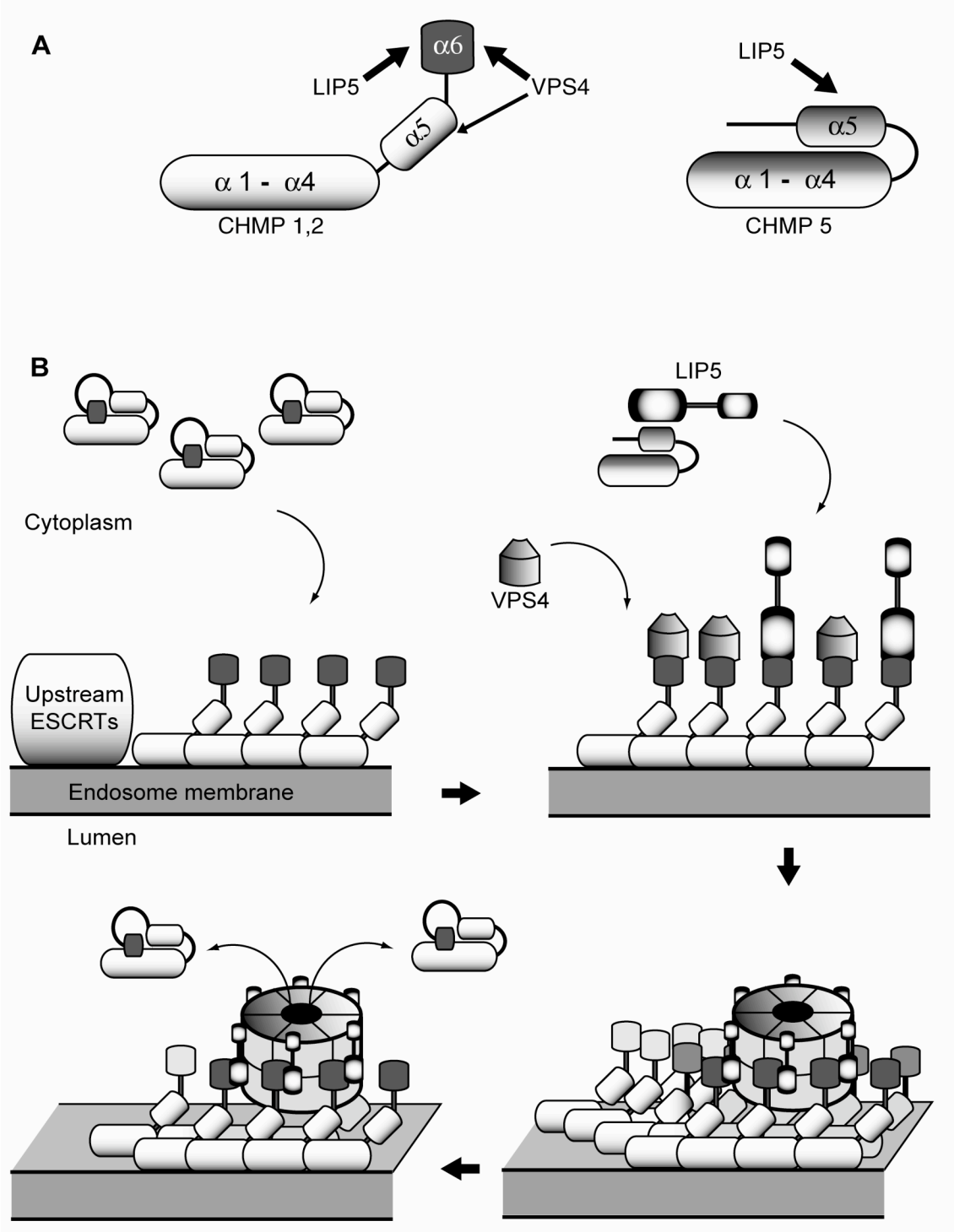
A
α6
LIP5
VPS4
α5
α 1 - α4
CHMP 1,2
LIP5
α5
α 1 - α4
CHMP 5
B
LIP5
Cytoplasm
VPS4
Upstream ESCRTs
Endosome membrane
Lumen

CHAPTER FOUR

Functional Analysis of ESCRT-III

ACKNOWLEDGEMENTS

I would like to thank Dr. von Zastrow at UCSF for providing cell lines and plasmids for δ-opioid receptor, and Dr. Alan Shiels for providing CHMP4B antibody. I would also like to thank the members of the Hanson lab for helpful discussion.

INTRODUCTION

One goal of my thesis is to better understand the role of ESCRT-III in mammalian cells. Recent studies from our lab and others provide some clues about the structure of ESCRT-III polymers and their effects on the membranes with which they associate. However, it is yet to be determined whether and precisely how such polymers play roles in ILV formation. The first *in vitro* reconstitution of intralumenal vesicle (ILV) formation by ESCRT-III and VPS4 was recently reported using giant unilamellar vesicles (GUVs) and a minimal set of yeast proteins (1). The next step will be reconstitution using endosomes containing cargo proteins in order to answer the questions of when and how individual ESCRT-III proteins and VPS4 contribute to ILV formation under more physiological conditions. To do this, we need to define relevant cargo that utilizes ESCRT-III machinery for entry into the MVB and establish reagents for manipulating and detecting endogenous components of the machinery. These tools and functional assays are described in this chapter.

To monitor incorporation of transmembrane protein cargo into the MVB and subsequent degradation in the lysosome, one typically follows the fate of specific signaling receptors destined for lysosomal degradation. Epidermal growth factor receptor (EGFR) has been extensively studied in this context (2-4). EGFR is a receptor tyrosine kinase that dimerizes upon ligand binding, inducing kinase activation and phosphorylation of tyrosine residues in the cytoplasmic tail. The phophorylated tyrosine resides interact with adaptors and effectors that activate various kinases including Ras/MAP kinase, phospholipase Cγ/protein kinase C and phosphatidylinositol 3-kinase (PI3-kinase)/Akt. Signal transduction pathways activated by these kinases lead to gene expression responsible for cellular responses including cell proliferation, adhesion and

migration (2, 5). Dysregulation of EGFR by overexpression or failure in downregulation is frequently associated with cancer, in particular carcinoma (6).

One functional assay using receptors is measurement of the degradation of the receptors or sometimes ligands after stimulation (7). A limitation of this assay is that lysosomal degradation of receptors is several steps away from sorting into ILVs within the MVB. A more direct assay is to monitor cargo sorting into the MVB vesicles. When the plasma membrane is disrupted, the cytoplasmic domain of a receptor on the limiting membrane of the endosome will be degraded by proteases (8). The receptor internalized into ILVs will be protected from protease treatment. Cargo sorting into the MVB can also be reconstituted and monitored *in vitro* using this protease protection assay (9). Finally, quantitative electron microscopy has also been used to observe ILV formation and EGFR sorting into ILVs (10).

In the current model, a receptor destined for lysosomal degradation engages ESCRT machinery via the interaction with ubiquitin at its cytoplasmic tail (11-13). EGFR destined for lysosomal degradation is ubiquitinated by the E3 ubiquitin ligase c-Cbl, and many components of the ESCRT machinery were shown to be involved in the degradation of EGFR (7-9, 14-18). Similar to EGFR, a number of surface receptors are efficiently degraded in the lysosome upon activation and ubiquitination of their cytoplasmic tails (11, 19). However, the involvement of the ESCRT machinery has been studied only in a small number of receptors with a subset of ESCRT components. Protease-activated receptor2 (PAR2), a G protein-coupled receptor (GPCR), is ubiquitinated by c-Cbl and subsequently degraded in the lysosome (20). Hrs (ESCRT-0) overexpression or knockdown resulted in formation of enlarged endosomes containing PAR2 and c-Cbl (21). The chemokine receptor CXCR4, another GPCR, is ubiquitinated by AIP4, an E3 Ub ligase, and also degraded in the lysosome. Its degradation is inhibited by overexpression of Hrs (ESCRT-0) and ATP hydrolysis defective VPS4 (22).

Finally, ferroportin, an iron transporter which is activated by binding to hepcidin, is similarly ubiquitinated and degraded in the lysosome. Its degradation was inhibited by knockdown of several components of ESCRTs (23, 24).

Interestingly, however, recent reports suggest that lysosomal degradation of some receptors does not require ubiquitin modification and may be independent of at least part of the ESCRT machinery. These include Protease-activated receptor1 (PAR1), δ opioid receptor (DOR) and Calcitonin receptor-like receptor (CLR), all of which belong to the GPCR family. Mutating all lysine residues in their cytoplasmic tails prevents them from being ubiquitinated but does not inhibit their degradation, indicating that ubiquitination of the receptors themselves is not necessary (25, 26). Lysosomal degradation of PAR1 was not affected by depletion of Hrs (ESCRT-0) and Tsg101 (ESCRT-I), leading to a proposal that PAR1 undergoes lysosomal degradation via an ESCRT-independent pathway (19, 27). CLR and DOR appeared to depend on Hrs (ESCRT-0), but DOR was not affected by Tsg101 (ESCRT-I) knockdown (21, 28). For the most part, the involvement of ESCRT-III and VPS4 has not been studied.

Because the ESCRT machinery engages cargo via the interaction with ubiquitin on cargo, it is possible that delivery of these receptors to the lysosome bypasses the ESCRT machinery. However, alternative routes have not been clearly identified. ESCRT-III and VPS4 do not have ubiquitin binding motifs, unlike upstream ESCRTs (ESCRT-0, I and II). Yet, ESCRT-III and VPS4 have been the most conserved ESCRT machinery throughout evolution, and are also required for other topologically related budding processes - viral budding and cytokinesis. Thus, I hypothesize that ESCRT-III and VPS4 are necessary for lysosomal degradation of all receptors whether or not the process requires upstream ESCRTs and ubiquitination.

I test this hypothesis using DOR as a model system. Although lysosomal degradation of DOR may be ESCRT-I-independent, dominant negative VPS4 can inhibit

its degradation, suggesting that ESCRT-III and VPS4 are likely involved in lysosomal degradation of DOR (28). DOR is a receptor expressed in neurons, and plays a role in opioid-mediated analgesia and opioid tolerance (29). Agonists of DOR were also shown to modulate T cell proliferation and cytokine production, suggesting that at least a subset of T cells may have DOR (30). Thus, studying the mechanisms for lysosomal degradation of DOR will provide insight into DOR mediated pain regulation and some aspects of the immune response. In summary, I test whether ESCRT-III and VPS4 are required for lysosomal degradation of DOR in order to provide evidence for their conserved roles in the lysosomal degradation of receptors. I also discuss how DOR together with EGFR can be used to determine the specific roles of individual ESCRT-III proteins and VPS4 in ILV formation.

EXPERIMENTAL PROCEDURES

Plasmids and siRNAs

The following plasmids are previously described: pcDNA4TO VPS4B wild type-GFP, pcDNA4TO VPS4B(E235Q)-GFP, pcDNA3.1 FLAG-CHMP2A full-length, pcDNA3.1 FLAG-CHMP2A 1-180 (Chapter 2 and (31)). FLAG-DOR plasmid was a gift from Dr. von Zastrow (UCSF, San Francisco, CA). pLKO shRNA plasmids were obtained from the Washington University Genome Sequencing Center (St. Louis, MO). siRNAs for Tsg101, VPS4A and VPS4B were purchased from Thermo Scientific (Chicago, IL). Sequences for shRNAs and siRNAs are listed in Table 4-2. Control siRNA is Accell Non-targeting siRNA #1 (Thermo Scientific, IL).

To make pcDNA4TO Myc-CHMP2A full-length or pcDNA4TO Myc-CHMP2A 1-180, CHMP2A, cDNAs for CHMP2A were cut from pcDNA3.1 FLAG-CHMP2A full-length and 1-180, and inserted into pcDNA 4TO -myc vector between *BamHI* and *XhoI* site. This generated constructs tagged with Myc at their N-termini. To make pcDNA4TO EGFR-GFP, cDNA for EGFR-GFP were cut from pEGFP-EGFR (a gift from Dr. Linda Pike Washington University, MO) and digested with *XhoI* and *NotI*. *XhoI* site was filled using Klenow (New England Biolabs, Ipswich, MA) to make a blunt end. The cDNA were subsequently ligated into pcDNA4TO vector (Invitrogen, Carlsbad, CA) between *EcoRV* and *NotI* sites.

Tissue culture

HEK293T and HeLa cells were grown in Dulbecco's modified Eagle's medium (DMEM) (Invitrogen-BRL, Gaithersburg, MD) supplemented with 10% fetal bovine serum (FBS) (Invitrogen –BRL or Atlanta Biologicals, Lawrenceville, GA) and 2mL glutamine (Washington University Tissue Culture Center, St. Louis, MO). HEK293 and HeLa cells stably expressing FLAG-DOR were obtained from Dr. Von Zastrow (UCSF) and

maintained in DMEM supplemented 10% FBS together with 2mL glutamine and 250μg/mL of G418 (Sigma, MO). TRex™-HEK293 cells (Invitrogen, CA) expressing tetracycline repressor were grown in DMEM supplemented with 10% tet-free FBS (Atlanta Biologicals), 2mL glutamine and 5μg/mL blasticidin (Invitrogen, CA). All cells were grown in a 5% CO_2 incubator at 37 ℃.

Establishing stable cell lines

TRex-HEK293 cells stably expressing EGFR-GFP were generated as described previously (32). Briefly, TRex-HEK293 cells were transfected with pcDNA4TO EGFR-GFP and selected in 125μg/mL Zeocin (Invitrogen, CA) containing media. One of the zeocin resistant clones was chosen and used for further analysis. 10ng/mL tetracycline was added to cells overnight to induce a low level of EGFR-GFP protein expression that can be degraded upon EGF treatment.

To establish TREx-HEK293 cell lines expressing FLAG-DOR together with VPS4B or CHMP2A, TRex-HEK293 cells were first transfected with FLAG-DOR and selected in 250μg G418 (Sigma, St. Louis, MO). One of G418 resistant clones was transfected again with pcDNA4TO VPS4B wild type-GFP, pcDNA4TO VPS4B(E235Q)-GFP, pcDNA4TO Myc-CHMP2A full-length or pcDNA4TO Myc-CHMP2A 1-180. Population cell lines were obtained by selection in 125μg/mL zeocin. These cell lines express FLAG tagged DOR constitutively but express VPS4 or CHMP2A in a tetracycline inducible manner. To express VPS4 and CHMP2A proteins, 1μg/mL tetracycline was added to cells overnight (Fig. 4-7B and 4-9B) or for 6 hours (Fig. 4-7C and 4-9C).

Transfection

For plasmid transfection, cells were transfected with indicated plasmids using Lipofectamine 2000 (Invitrogen, CA) following the manufacturer's instruction and typically assayed 18-24 hours after transfection. Cells transfected with shRNA expressing plasmids were assayed about 48 hours after transfection. For siRNA transfection, HEK293 derived cells and HeLa derived cells were seeded at $2x10^5$ cells/well and $8x10^4$ cells/well respectively in a 12 well plate. Next day, cells were transfected with indicated siRNAs using Dharmafect #1 (Thermo Scientific, IL), following the manufacturer's instruction, and assayed about 48 hours after transfection.

Transduction

$8x10^5$ HEK293T cells were plated in a 6cm dish a day before transfection, and were transfected with 1μg shRNA constructs together with 0.9μg pCMV 8.2 delta R (packaging construct) and 0.15μg pCMV VSV-G (envelope construct) (gifts from Dr. Sheila Stewart, Washington University in St. Louis, MO). Next morning, media was changed to DMEM containing 30% heat inactivated FBS and 2mL glutamine. About 26-28 hours later, media containing recombinant lentiviruses was collected by passing the media through a 0.45μm filter to remove cell debris, and was added to target cells together with 10μg/mL protamine sulfate. Target cells are typically prepared in a 6 well plate a day before transduction: $2.5x10^5$ cells/well and $8x10^4$ cells/well were seed for HEK293 derived cells and HeLa derived cells respectively. Production and transduction of recombinant lentiviruses were carried out in BL2+ facility in the Dept of Cell Biology and Physiology at Washington University in St. Louis, following BL2+ bio-safety criteria.

EGFR degradation assay

TRex-HEK293;EGFR-GFP cells were incubated with 10ng/mL tetracycline overnight. After incubating in tetracycline free media for 5 hours, cells were stimulated with 100ng/mL EGF for 0, 1 and 2 hours. Cells were then lyzed in sodium dodecyl sulfate (SDS) sample buffer and analyzed by immunoblotting with anti-GFP antibody (1:2500). HeLa cells were starved in serum free DMEM for 3 hours before stimulation with 100ng/mL EGF for 0, 1 and 2 hours. Treatment of 10μg/mL cycloheximide did not make noticeable differences in the level of EGFR and its degradation rate at least in this assay setting. The experiments presented in this chapter were carried out without cycloheximide. Cells stimulated with EGF were analyzed by immunoblotting with rabbit anti-EGFR antibody (Santa Cruz;1:500) after lysis in SDS sample buffer. Equal loading of proteins was confirmed by mouse anti-α-tubulin antibody (Sigma; 1:5000).

DOR degradation assay

HEK293 and HeLa cell lines expressing FLAG-DOR (HEK293;FLAG-DOR and HeLa;FLAG-DOR) were incubated with 10μM DADLE (enkephalin, D-Ala^2, D-Leu^5) (Sigma, MO) for 0, 2 and 4 hours. 10mg/mL cycloheximide was added to HeLa;FLAG-DOR cells 1 hour prior to treatment with DADLE and maintained during stimulation. HEK293;FLAG-DOR cells were not treated with cyloheximide. Stimulated cells were lyzed in SDS sample buffer and analyzed by immunoblotting with rabbit anti-FLAG antibody (Sigma; 1:5000). Equal loading of proteins was confirmed by mouse anti-α-tubulin antibody.

Immunofluorescence analysis

Cells grown on coverslips were fixed in 3.5% paraformaldehyde in PBS and permeabilized with 0.2% Triton X-100 in PBS. HeLa derived cell lines were grown on plain glass coverslips while HEK293 based cell lines were grown on poly-lysine coated coverslips. After blocking in 5% goat serum, cells were stained with indicated primary antibodies followed by secondary antibodies. To visualize nuclei, cells were costained with 4'-6'-diamidino-2-phenlindole (DAPI; 1:10000; Molecular Probes. Eugene, OR). The following antibodies were used for immunofluorescence analysis: rabbit anti-FLAG antibody (Sigma, MO, 1:500), mouse anti-myc ascities (1:500), anti-CD63 (Developmental Studies Hybridoma Bank, University of Iowa, IA; 1:1000), anti-early endosomal antigen1 (EEA1) (Developmental Studies Hybridoma Bank, 1:500). Staining conditions for CHMP2B, CHMP4A, CHMP4B and CHMP6 are described in Table 4-1.

For epifluorescence microscopy, images were obtained using a Leica Diaplan microscope and Zeiss Axiocam camera. For confocal microscopy, images were obtained using Zeiss Axioplan2 microscope coupled to a Radianceplus confocal laser system (Bio-Rad), and Zeiss Axioskop upright microscope coupled to Zeiss 2Photon LSM510 NLO system (Carl Zeiss, Maple Grove, MN) in the Bakewell NeuroImaging Laboratory at Washington University in St. Louis. Images are obtained using Laser and Images were processed using Image J (NIH image, Bethesda, MD) and Adobe Photoshop (Adobe, CA).

Fluorescence EGF uptake assay

HeLa cells grown on coverslips were starved in serum free DMEM for 3 hours and incubated with 200ng/mL of Alexa-555 EGF (Invitrogen, CA) in HEPES buffered DMEM containing 0.2% bovine serum albumin (BSA) for 30min on ice. After washing 3 times with ice-cold PBS, cells were incubated with pre-warm DMEM containing 10%

FBS in a 37ºC humidified incubator for 15min and 5 hours. Cells were then fixed and stained with DAPI and analyzed by epifluorescence microscopy.

RESULTS

Antibodies recognizing ESCRT-III proteins and other proteins in the ESCRT pathway

As a step towards studying the function of endogenous ESCRT-III proteins in mammalian cells, I first characterized antibodies that recognize human ESCRT-III proteins and other proteins in the ESCRT pathway. As shown in Fig. 4-1A and B, I was able to detect a number of ESCRT-III proteins (CHMP1A, CHMP2A, CHMP2B, CHMP3, CHMP4A, CHMP4B, CHMP5 and CHMP6), two VPS4 isoforms (VPS4A and VPS4B), Tsg101 (ESCRT-I), and LIP5 in HEK293 based cell lines by immunoblotting (Fig. 4-1A and B). Most antibodies visualized proteins of interest as specific bands near expected sizes. For CHMP2A, two bands appeared near the expected size, ~30 – 35 KDa (left lane). To determine which one of them represents endogenous CHMP2A, I took advantage of the fact that CHMP2A co-sediments with dominant negative mutant VPS4 following solubilization in Trinton X-100 (Fig. 3-4). When VPS4B(E235Q) was expressed, only the lower band appeared in the insoluble fraction, thereby identifying it as endogenous CHMP2A. The specificity of several antibodies including CHMP2A was confirmed by knockdown as shown in Fig. 4-2. The sources of antibodies and staining conditions are listed in Table 4-1. To further determine how specific the antibodies are, I tested antibodies for CHMP2, CHMP4 and VPS4 in HEK293T cells transiently transfected with isoforms of these proteins. Antibodies for CHMP2A, CHMP2B, CHMP4A, CHMP4B and VPS4B recognized their own proteins well but did not detect the related isoforms. VPS4A antibody cross-reacted with VPS4B at low efficiency (Table 4-1 and data not shown).

Importantly, several of these antibodies also detected endogenous proteins by immunofluorescence (Figure 4-1C and Table 4-1). Because ESCRT-III proteins are predominantly soluble in the cytoplasm, it is difficult to distinguish specific cytoplasmic

staining from non-specific staining. Thus, I tested antibodies in cells expressing dominant negative mutant VPS4B(E235Q). Because this mutant VPS4 interferes with ESCRT-III disassembly, one would expect ESCRT-III proteins to accumulate on the endosomal membrane. Our lab previously generated the TRex-HEK293 cell line that expresses VPS4B(E235Q)) following addition of tetracycline (33). The cells induced to express mutant VPS4B were stained for endogenous ESCRT-III proteins. CHMP4A is shown as an example (Fig. 4-1C). In a cell that did not express VPS4B (right), CHMP4A was present diffusely throughout the cell. In contrast, in a cell expressing VPS4B(E235Q) (left), enlarged endosomes were coated with both mutant VPS4B and CHMP4A. This different pattern of antibody staining confirms that the CHMP4A antibody specifically stains for endogenous CHMP4A. Similar staining patterns were observed with CHMP2B, CHMP4B and CHMP6 antibodies (Table 4-1 and data not shown). The differential distribution of ESCRT-III proteins with and without dominant negative mutant VPS4 indicates that endogenous ESCRT-III proteins indeed cycle between the endosomal membrane and cytoplasm, and that this dynamic transition can be inhibited by functional loss of VPS4.

Knockdown of ESCRT-III proteins and other proteins in the ESCRT pathway

To knock down ESCRT-III proteins and other proteins in the ESCRT pathway, I used two different approaches. The first was to express small hairpin RNA (shRNA) in cells. shRNA is a RNA molecule that forms a tight hairpin structure, which is cleaved by cellular machinery into a double stranded small interfering RNA (siRNA). This is then bound to the RNA-induced silencing complex (RISC) which cleaves its target mRNA and thereby reduces expression of a target protein (34). Another approach is to directly introduce synthesized siRNA into cells.

To express shRNAs, I obtained lentiviral constructs (pLKO) containing shRNAs targeting various ESCRT proteins from The RNAi Consortium (TRC) through Washington University Genome Sequencing Center. I screened 5 hairpins for each protein, and the most effective shRNAs are presented in Figure 4-2A. To produce recombinant virus to express shRNAs, I trasnsfected individual pLKO shRNA constructs into HEK293T cells with packaging and envelope constructs. It should be noted that some components of the ESCRT machinery are involved in lentiviral budding (35, 36). Thus, expressing shRNAs for those proteins may compromise production of recombinant virus. Because knockdown of Tsg101 and LIP5 has been shown to reduce viral budding, I transiently transfected shRNA constructs in HEK293T cells (Fig. 4-2A) (37, 38). Expression of Tsg101 and LIP5 was greatly reduced 48 hours after transfecting shRNAs. I tested the efficiency of knockdown of several ESCRT-III proteins by transducing cells with recombinant virus stocks containing shRNAs. 48-72 hours after transduction, ESCRT-III protein levels were decreased by more than 50%, implying that lentviruses were present in these stocks. Because shRNAs can be stably expressed in cell lines, I attempted to generate such knockdown cell lines for CHMP2A, CHMP6 and LIP5. However, expressing shRNAs for these proteins was toxic to cells and therefore I was not able to make the cell lines. Cells died 3 - 5 days after transduction. Because our lab had no problem generating comparable knockdown cell lines for unrelated proteins (Torsin A and LULL1) using the same system, the toxicity I encountered is likely to be a specific effect of knocking down the ESCRT proteins. It is conceivable that knocking down the ESCRT proteins could compromise cytokinesis, although I cannot completely rule out off-target effects of these shRNAs.

As a second knockdown approach, I transiently transfected siRNAs for VPS4A, VPS4B, and Tsg101. siRNA may be a better tool than viral packaged shRNAs for knocking down these proteins, which is clearly known to inhibit viral budding (23, 37).

The sequences for these siRNAs were all obtained from previous publications (23, 37) (Table 4-2). 48 hours after transfection of siRNAs, all three proteins were efficiently knocked down in HeLa cells (over 90%) and less efficiently in HEK293 derived cells (Fig. 4-2B).

EGFR/EGF degradation

To examine the effects of manipulating the ESCRT machinery on trafficking of a previously well studied cargo protein, EGFR, I monitored lysosomal degradation of EGFR. I first examined endogenous EGFR in HeLa cells before and at several time points after adding 100ng/mL EGF, and the level of undegraded EGFR was determined by immunoblotting. As expected, endogenous EGFR was efficiently degraded within 2 hours after EGF treatment (Fig. 4-3A). I also generated a TRex-HEK293 cell line expressing EGFR tagged with GFP in a tetracycline inducible manner. When I induced the expression of EGFR-GFP by treating a low concentration (10ng/mL) of tetracycline overnight, EGFR-GFP was efficiently degraded within 2 hours of 100ng/mL EGF treatment (Fig. 4-3B). Trafficking and degradation of EGFR-GFP was also analyzed by directly imaging the GFP signal with epifluorescence microscopy (Fig. 4-3C); EGFR-GFP was internalized upon 100ng/mL EGF treatment and most receptors disappeared 2 hours after stimulation. It should be noted that treating the EGFR-GFP cell line with a high concentration (1μg/mL) of tetracycline overnight resulted in a higher level of EGFR-GFP expression, which was not decreased by EGF treatment (data not shown). This suggests that something in the pathway, perhaps the ESCRT machinery, is saturated, and therefore maintaining expression of EGFR at a proper level is critical for targeting the receptor to the lysosome. Another way to detect EGFR degradation is measuring undegraded EGF bound to EGFR. Alexa-555 conjugated EGF bound to the surface of

HeLa cells on ice was internalized upon incubating at 37ºC and was mostly degraded 5 hours later (Fig. 4-3D).

To confirm a role for the ESCRT machinery in the lysosomal degradation of EGFR, I tested how manipulation of an upstream ESCRT component, Tsg101 (ESCRT-I), and a downstream ESCRT protein, VPS4, affects degradation of EGFR. When I expressed dominant negative mutant VPS4 (VPS4B (E235Q)) or knocked down Tsg101, EGFR degradation was greatly reduced as expected (Figure 4-4). This data confirms that lysosomal degradation of EGFR requires ESCRT machinery, and that EGFR is a good cargo for studying the roles of ESCRT-III and VPS4.

Requirement of ESCRT machinery for lysosomal degradation of DOR

To determine the involvement of the ESCRT machinery on DOR trafficking and delivery to the lysosome, I first examined DOR degradation in cell lines stably expressing FLAG tagged DOR before and after 10μM DADLE (D-Ala^2, D-Leu^5) treatment by immunoblotting. In both HEK and HeLa derived cell lines, most DOR was degraded within 4 hours after stimulation with DADLE (Fig. 4-5A and B). Trafficking and degradation of DOR were also analyzed by immunofluorescence and confocal microscopy. DOR in the HEK293 cell line was mostly present on the cell surface; however, the receptor was internalized upon agonist treatment and disappeared mostly 4 hours after stimulation (Fig. 4-5C). The internalized DOR colocalized well with CD63 30 min after stimulation, suggesting that DOR transits through late endosomes/MVBs, the compartment I am interested in (Fig. 4-6).

To test whether VPS4 is required for lysosomal degradation of DOR, I examined the effect of functional loss of VPS4 on DOR degradation. To do this, I transiently transfected the ATP hydrolysis defective mutant VPS4B (VPS4B(E235Q)) in the HEK293 derived DOR cell line. Similar to previously reported data, mutant VPS4B

greatly inhibited degradation of DOR while wild type VPS4B did not affect degradation (Fig.4-7A) (28). This inhibition was even greater in the cell line stably expressing mutant VPS4B in addition to DOR, presumably because VPS4B was expressed in all cells, unlike the transient transfection setting (Fig. 4-7B). I then used this cell line to determine colocalization of DOR and mutant VPS4B by immunofluorescence and confocal microscopy. As shown in Fig. 4-7C, DOR accumulated on enlarged endosomes generated by mutant VPS4B 1 hour after DADLE treatment, suggesting that DOR degradation was specifically inhibited by mutant VPS4B. Note that VPS4B(E235Q) protein was expressed in a tetracycline inducible manner because the sustained expression of this protein is toxic to cells. To further confirm whether DOR degradation is VPS4 dependent, I knocked down both VPS4A and VPS4B. Depleting both VPS4 isoforms reduced DOR degradation to some extent in both HEK and HeLa derived cell lines (Fig. 4-8). Incomplete knockdown of VPS4A may account for the smaller effect on DOR degradation by knockdown than that by expressing mutant VPS4. Nevertheless, this data further supports the requirement of VPS4 for lysosomal degradation of DOR.

Next, I tested whether ESCRT-III is also involved in DOR degradation. C-terminally deleted ESCRT-III proteins behave as inhibitors of MVB function and viral budding (Fig. 2-5 and 2-6). To examine the effect of manipulating the function of ESCRT-III proteins on DOR degradation, I transiently transfected C-terminally truncated and wild type CHMP2A or CHMP4A in the HEK293 derived DOR cell line and monitored the level of DOR. Interestingly, mutant ESCRT-III proteins inhibited DOR degradation while wild type ESCRT-III proteins had little effect (Fig. 4-9A and data not shown). Furthermore, stable expression of mutant CHMP2A inhibited DOR degradation to a greater extent, similar to that seen with the cell line expressing mutant VPS4 (Fig. 4-9B). Localization of DOR in the cell line expressing mutant CHMP2A was also examined by immunofluorescence followed by confocal microscopy. Similar to that seen in cells

expressing mutant VPS4, DOR and mutant CHMP2A co-accumulated on enlarged endosomes (Fig. 4-9C). Together, these data suggest that lysosomal degradation of DOR requires ESCRT-III. To further confirm this, I knocked down several ESCRT-III proteins. My first pass analyses suggest that knockdown of CHMP3 inhibits degradation of DOR but knockdown of CHMP2A and CHMP6 does not (data not shown). It is possible that certain ESCRT-III proteins (perhaps CHMP6) may not be required for lysosomal degradation of DOR, and the functions of CHMP2 isoforms (CHMP2A and CHMP2B) may be redundant. However, any conclusions should await further experiments.

Finally, I examined whether DOR degradation requires Tsg101. Surprisingly, knocking down Tsg101 inhibited DOR degradation, contrary to a previous report (28) (Fig. 4-10). Efficiency of knockdown could account for the discrepancy between these results. In fact, my knockdown appears to be more efficient than that previously reported based on the immunoblots for endogenous Tsg101 after knockdown. In conclusion, lysosomal degradation of DOR is required for Tsg101 (ESCRT-I), and therefore, DOR may be delivered to the lysosome via a pathway involving both upstream and downstream ESCRT machinery, similar to that seen with EGFR.

DISCUSSION

Precisely how ESCRT-III contributes to MVB biogenesis remains unclear. As a step toward understanding this process, I have described reagents to detect and manipulate ESCRT-III proteins and other proteins in the ESCRT pathway. I also showed that two different receptors, EGFR and DOR, use ESCRT machinery to undergo lysosomal degradation. These reagents and defined cargo will be used to study the specific roles of ESCRT-III proteins and VPS4 in ILV formation and cargo sorting into ILVs.

Detecting and knocking down ESCRT-III proteins

Using antibodies, I was able to detect a number of human ESCRT-III proteins, VPS4 and other proteins in the ESCRT pathway (CHMP1A, CHMP2A, CHMP2B, CHMP3, CHMP4A, CHMP4B, CHMP5 and CHMP6, VPS4A, VPS4B, LIP5 and Tsg101) by immunoblotting and some of them (CHMP2B, CHMP4A, CHMP4B and CHMP6) by immunofluorescence (Fig. 4-1 and Table 4-1). I also knocked down several of these proteins using shRNAs (for CHMP2A, CHMP2B, CHMP3, CHMP6, Tsg101 and LIP5) or siRNAs (for Tsg101, VSP4A and VPS4B) (Fig. 4-2 and Table 4-2). These tools were used to show the role of ESCRT machinery in lysosomal degradation of EGFR and DOR. I also attempted to generate cell lines expressing shRNAs for CHMP2A, CHMP6 and LIP5. However, these attempts were unsuccessful due to toxicity of the shRNAs. shRNAs for these proteins will need to be expressed transiently or expressed stably in an inducible manner.

Both upstream and downstream ESCRT machinery is required for lysosomal degradation of DOR

I found that degradation of DOR was inhibited by expressing mutant VPS4 and ESCRT-III proteins, and DOR co-accumulated on the endosomes with mutant VPS4 and mutant CHMP2A (Fig 4-7 and 4-9). Additionally, knocking down VPS4 and CHMP3 also decreased DOR degradation (Fig 4-8 and data not shown). These data suggest that lysosomal degradation of DOR requires ESCRT-III and VPS4. Surprisingly, Tsg101 knockdown did inhibit DOR degradation, contrary to a previous report (28). Taken together, I conclude that lysosomal degradation of DOR is mediated by both upstream (Hrs based on another report (28), and Tsg101) and downstream ESCRTs (ESCRT-III and VPS4) similar to that seen in lysosomal degradation of EGFR here and elsewhere (7-9, 15-17) (Fig. 4-4). Supporting this, my preliminary data indicates that trafficking of DOR is not noticeably different from that of the well characterized ESCRT-dependent EGFR. In fact, internalized DOR colocalized with EGFR 15min or 30min after treatment with both enkephalin (DADLE) and EGF (data not shown). Nevertheless, how DOR engages the ESCRT machinery without itself being ubiquitinated remains unclear. DOR could interact with ESCRT machinery via protein-protein interactions or by ubiquitin attached to a cellular factor binding to DOR.

One would be concerned that expressing dominant negative mutants or knocking down ESCRT proteins could block lysosomal targeting of transmembrane proteins nonspecifically by interfering with normal maturation of endosomes. However, there are situations in which compromising the ESCRT pathway does not affect ILV formation and sorting of transmembrane proteins into MVB vesicles. First, delivery of Pmel17 into the melamosome, a lysosome-related oraganelle, occurs via an MVB-like intermediate but distribution of Pmel17 is not affected by mutant VPS4, overexpressed Hrs and Tsg101, nor depletion of Hrs (39). Secondly, sorting of proteolipid protein (PLP) into the MVB and

release of PLP-containing exosomes (secreted ILVs) are not compromised by mutant VPS4 and overexpressed Tsg101, nor knockdown of Hrs and Tsg101 (40). These ESCRT independent pathways might have evolved for generation of special MVBs distinct from MVBs *en route* to the lysosome.

Requirement of ESCRT-III and VPS4 in lysosomal degradation of receptors independent of upstream ESCRTs

Because DOR appears to depend on upstream ESCRTs in addition to ESCRT-III and VPS4, my original hypothesis – that ESCRT-III and VPS4 are required for lysosomal degradation of receptors regardless of requirement of upstream ESCRTs or ubiquitin modification - should be tested using other receptors. PAR1 may be a good receptor on which to test this hypothesis since lysosomal degradation of PAR1 appears to be independent of Tsg101 and Hrs, yet the involvement of ESCRT-III and VPS4 has not been determined. If PAR1 degradation does not require ESCRT-III and VPS4, PAR1 may be delivered to the lysosome via an alternative route which deserves further investigation. If lysosomal degradation of PAR1 depends on ESCRT-III and VPS4, this will support my hypothesis, and PAR1 can be used as an additional cargo protein to study the roles of ESCRT-III and VPS4, complementing EGFR and DOR.

Studying specific roles of individual ESCRT-III proteins and VPS4

Growing evidence suggests that individual ESCRT-III proteins contribute differentially to ILV formation. For example, CHMP6/Vps20 is thought to connect ESCRT-III to ESCRT-II and initiate ESCRT-III polymer assembly (41-44). CHMP4/Snf7 is a main constituent of ESCRT-III polymers and might play a major role in generating ILVs (45, 46). CHMP2/Vps2 seems to be particularly critical for recruiting VPS4 disassembly machinery (1, 41, 47, 48). When each ESCRT-III protein is recruited to the

endosome may at least partly contribute to its specific function. Based on yeast genetic studies, a specific order of recruitment of core ESCRT-III proteins has been proposed (CHMP6/Vps20 → CHMP4/Snf7 → CHMP3/Vps24 → CHMP2/Vps2) (41, 45). In general, this order fits well with proposed roles of individual ESCRT-III proteins, although further investigation is required to determine whether and how this ordered ESCRT-III assembly occurs in mammalian cells.

To better understand specific roles of individual ESCRT-III proteins and VPS4 in ILV formation, it will be ideal to watch when and where these proteins are recruited to cargo (e.g. EGFR and DOR) on the endosome. However, if the machinery only stays on endosomes transiently, it may be difficult to observe such events in fixed samples stained for endogenous proteins. Alternatively, specific effects of manipulating ESCRT-III proteins and VPS4 can be analyzed. The phenotypes of knocking down a few ESCRT-III proteins and VPS4A/B have been previously reported. Briefly, knocking down CHMP3 inhibits EGFR degradation and resulted in smaller MVBs with fewer ILVs (15). Knockdown of CHMP4B or CHMP3 leads to accumulation of autophagosomes (49, 50). CHMP6 knockdown inhibits degradation of EGFR and ferroportin but do not inhibit viral budding (17, 23). Knocking down VPS4A/B greatly reduces viral budding and EGF degradation but how it affects ILV formation has not been analyzed (16, 23). While these variable phenotypes support the idea of specific roles for individual ESCRT-III proteins and VPS4, the studies do not provide direct insight into the order of recruitment or how each protein functions at different stage of ILV formation and cargo sorting into ILVs. Such questions may be better answered by analyzing where the receptors accumulate, and how much and which ESCRT-III proteins and VPS4 colocalize after manipulating each protein. This can be examined by light and electron microscopic analyses of cells stained for endogenous ESCRT-III proteins, VPS4 and receptors after knocking down each protein followed by stimulating with ligands for the receptors. Such

analyses require good antibodies, efficient knockdown, defined cargo to engage the machinery and optimized times when most of the machinery is recruited to receptors, which are in part described in this chapter.

Based on the current model of sequential recruitment, knockdown of one ESCRT-III protein could result in more accumulation of some ESCRT-III proteins than others. For example, knockdown CHMP3 may lead to accumulation of CHMP4 and CHMP6 but not of CHMP2. Knockdown of VPS4 may result in accumulation of all core ESCRT-III proteins. It will be also interesting to determine where individual proteins accumulate relative to receptors and each other. In fact, such different localization of ESCRT-III proteins was observed in cells expressing VPS4B(E235Q); endogenous CHMP4A and CHMP2B accumulated on the rims of VPS4B containing endosomes (Fig. 4-1C and data not shown). Under a higher magnification, colocalization of CHMP2B with VPS4B on endosomes appeared to be better than that with CHMP4A supporting close relationship between CHMP2 and VPS4.

To learn about how individual ESCRT-III proteins and VPS4 contributes to specific stages of ILV formation, MVB morphology should be carefully analyzed in cells lacking one or more of these proteins by electron microscopy. It is conceivable that depleting different proteins may result in accumulation of ILVs at different stages of budding. ILV formation of cells lacking CHMP4 proteins is of particular interest because of their proposed roles in ESCRT-III polymer assembly and ILV formation (44, 46). It is possible that depleting all CHMP4 proteins in cells might almost completely block vesicle formation unlike that seen with CHMP3 knockdown (15). A challenge to study roles of CHMP4 in mammalian cells is the fact that there are three isoforms, and CHMP4C antibody is not available yet.

Several ESCRT-III proteins and VPS4 in mammalian cells have isoforms, and it is important to understand whether individual isoforms function redundantly or

specifically. In particular, studying CHMP2 proteins in this regard may provide insight for understanding pathophysiology of certain neurodegenerative diseases associated with mutations in CHMP2B (51, 52). It will be also interesting to examine specific roles of each isoform in different budding reactions. Recently, dominant negative mutant CHMP4C was shown to inhibit cytokinesis more than mutants of other CHMP4 proteins (53). To determine specific functions of CHMP4 proteins in different budding processes, effects of knockdown of each CHMP protein can be examined by various functional assays including receptor degradation assays, the virus-like particle (VLP) release assay, and counting multinucleated cells to measure interference with cell abscission during cytokinesis (Fig. 2-6, 4-4 and 4-5 and (54, 55)).

Finally, mechanisms for cargo sorting into ILVs by ESCRT machinery could vary for different cargo proteins. Unlike that seen in EGFR, ubiquitination of DOR is dispensable for its lysosomal degradation, and therefore it is possible that DOR might engage a different subset of ESCRT-III components. My preliminary data showed that CHMP6 and CHMP2A did not affect DOR degradation while CHMP3 inhibited degradation to some degree (data not shown). For CHMP2, CHMP2A and CHMP2B are likely to compensate for each others' function, because knocking down CHMP2B alone does not appear to have obvious effects on cells (49). Although further experiments are required to make a conclusion, it is tempting to think that CHMP6 may not be necessary for lysosomal degradation of DOR similar to that seen in viral budding. HIV budding is not affected by knockdown Eap20, a component of ESCRT-II and CHMP6 which is proposed to connect ESCRT-II and ESCRT-III (17). In fact, both viral Gag proteins and Cep55 which is important for midbody formation during cytokinesis can interact with CHMP4 proteins via their interaction with Alix (53, 55, 56). Whether CHMP4 proteins can assemble polymers without CHMP6 in cells, and whether DOR, Gag and Cep55 could engage such polymers deserve further investigation.

Assays to monitor ILV formation and receptor sorting into ILV

To study the roles of ESCRT machinery, I mostly used a functional assay to measure lysosomal degradation of EGFR and DOR, which allow for indirect monitoring of MVB biogenesis. For a more direct analysis, one can use the protease protection assay described in the Introduction. In this assay, the cytoplasmic domain of a receptor on the limiting membrane of the endosome will be degraded by proteases while the receptor internalized into ILVs will be protected from protease treatment. Thus, it will be useful to have a cell line expressing a receptor with an epitope tag at the cytoplasmic domain. I generated a HEK293 derived cell line expressing EGFR with GFP attached to the cytoplasmic domain. EGFR-GFP in this cell line was degraded efficiently upon EGF treatment (Fig. 4-3A and C). The DOR cell lines used here express DOR with a FLAG tag attached to the extracellular domain. Therefore, I have recently generated a HEK293 derived cell line expressing DOR with GFP at the cytoplasmic domain in addition to a FLAG at the extracellular domain. I confirmed that the double tagged DOR was efficiently degraded 4 hours after agonist treatment (data not shown). These EGFR and DOR cell lines will be used to directly monitor ILV formation and receptor sorting into ILV, and ultimately to establish an *in vitro* reconstitution using isolated endosomes (9).

In summary, tools and assays described here allow dissecting specific roles of ESCRT-III proteins and VPS4 in ILV formation, and sorting different receptors into ILVs. This will help understand mechanisms for this unusual budding process and downregulating receptors involved in critical cellular processes and pathological conditions.

REFERENCES

1. Wollert T, Wunder C, Lippincott-Schwartz J, Hurley JH. Membrane scission by the ESCRT-III complex. Nature 2009;458(7235):172-177.

2. Grandal MV, Madshus IH. Epidermal growth factor receptor and cancer: control of oncogenic signalling by endocytosis. J Cell Mol Med 2008;12(5A):1527-1534.

3. Rodahl LM, Stuffers S, Lobert VH, Stenmark H. The role of ESCRT proteins in attenuation of cell signalling. Biochem Soc Trans 2009;37(Pt 1):137-142.

4. Sorkin A, Goh LK. Endocytosis and intracellular trafficking of ErbBs. Exp Cell Res 2009;315(4):683-696.

5. Yarden Y, Sliwkowski MX. Untangling the ErbB signalling network. Nat Rev Mol Cell Biol 2001;2(2):127-137.

6. Hynes NE, Lane HA. ERBB receptors and cancer: the complexity of targeted inhibitors. Nat Rev Cancer 2005;5(5):341-354.

7. Raiborg C, Malerod L, Pedersen NM, Stenmark H. Differential functions of Hrs and ESCRT proteins in endocytic membrane trafficking. Exp Cell Res 2008;314(4):801-813.

8. Malerod L, Stuffers S, Brech A, Stenmark H. Vps22/EAP30 in ESCRT-II Mediates Endosomal Sorting of Growth Factor and Chemokine Receptors Destined for Lysosomal Degradation. Traffic 2007;8(11):1617-1629.

9. Luyet PP, Falguieres T, Pons V, Pattnaik AK, Gruenberg J. The ESCRT-I Subunit TSG101 Controls Endosome-to-Cytosol Release of Viral RNA. Traffic 2008.

10. White IJ, Bailey LM, Aghakhani MR, Moss SE, Futter CE. EGF stimulates annexin 1-dependent inward vesiculation in a multivesicular endosome subpopulation. Embo J 2006;25(1):1-12.

11. Gruenberg JS, H. The biogenesis of multivesicular endosomes. Nat Rev Mol Cell Biol 2004;5(4):317-323.

12. Piper RC, Luzio JP. Ubiquitin-dependent sorting of integral membrane proteins for degradation in lysosomes. Curr Opin Cell Biol 2007;19(4):459-465.

13. Raiborg C, Stenmark H. The ESCRT machinery in endosomal sorting of ubiquitylated membrane proteins. Nature 2009;458(7237):445-452.

14. Duan L, Miura Y, Dimri M, Majumder B, Dodge IL, Reddi AL, Ghosh A, Fernandes N, Zhou P, Mullane-Robinson K, Rao N, Donoghue S, Rogers RA, Bowtell D, Naramura M, *et al.* Cbl-mediated ubiquitinylation is required for lysosomal sorting of epidermal growth factor receptor but is dispensable for endocytosis. J Biol Chem 2003;278(31):28950-28960.

15. Bache KG, Stuffers S, Malerod L, Slagsvold T, Raiborg C, Lechardeur D, Walchli S, Lukacs GL, Brech A, Stenmark H. The ESCRT-III subunit hVps24 is required for degradation but not silencing of the epidermal growth factor receptor. Mol Biol Cell 2006;17(6):2513-2523.

16. Fraile-Ramos A, Pelchen-Matthews A, Risco C, Rejas MT, Emery VC, Hassan-Walker AF, Esteban M, Marsh M. The ESCRT machinery is not required for human cytomegalovirus envelopment. Cell Microbiol 2007;9(12):2955-2967.

17. Langelier C, von Schwedler UK, Fisher RD, De Domenico I, White PL, Hill CP, Kaplan J, Ward D, Sundquist WI. Human ESCRT-II complex and its role in human immunodeficiency virus type 1 release. J Virol 2006;80(19):9465-9480.

18. Bowers K, Piper SC, Edeling MA, Gray SR, Owen DJ, Lehner PJ, Luzio JP. Degradation of endocytosed epidermal growth factor and virally ubiquitinated major histocompatibility complex class I is independent of mammalian ESCRTII. J Biol Chem 2006;281(8):5094-5105.

19. Marchese A, Paing MM, Temple BR, Trejo J. G protein-coupled receptor sorting to endosomes and lysosomes. Annu Rev Pharmacol Toxicol 2008;48:601-629.

20. Jacob C, Cottrell GS, Gehringer D, Schmidlin F, Grady EF, Bunnett NW. c-Cbl mediates ubiquitination, degradation, and down-regulation of human protease-activated receptor 2. J Biol Chem 2005;280(16):16076-16087.

21. Hasdemir B, Bunnett NW, Cottrell GS. Hepatocyte growth factor-regulated tyrosine kinase substrate (HRS) mediates post-endocytic trafficking of protease-activated receptor 2 and calcitonin receptor-like receptor. J Biol Chem 2007;282(40):29646-29657.

22. Marchese A, Raiborg C, Santini F, Keen JH, Stenmark H, Benovic JL. The E3 ubiquitin ligase AIP4 mediates ubiquitination and sorting of the G protein-coupled receptor CXCR4. Dev Cell 2003;5(5):709-722.

23. Kieffer C, Skalicky JJ, Morita E, De Domenico I, Ward DM, Kaplan J, Sundquist WI. Two distinct modes of ESCRT-III recognition are required for VPS4 functions in lysosomal protein targeting and HIV-1 budding. Dev Cell 2008;15(1):62-73.

24. De Domenico I, Ward DM, Langelier C, Vaughn MB, Nemeth E, Sundquist WI, Ganz T, Musci G, Kaplan J. The molecular mechanism of hepcidin-mediated ferroportin down-regulation. Mol Biol Cell 2007;18(7):2569-2578.

25. Tanowitz M, Von Zastrow M. Ubiquitination-independent trafficking of G protein-coupled receptors to lysosomes. J Biol Chem 2002;277(52):50219-50222.

26. Cottrell GS, Padilla B, Pikios S, Roosterman D, Steinhoff M, Grady EF, Bunnett NW. Post-endocytic sorting of calcitonin receptor-like receptor and receptor activity-modifying protein 1. J Biol Chem 2007;282(16):12260-12271.

27. Gullapalli A, Wolfe BL, Griffin CT, Magnuson T, Trejo J. An essential role for SNX1 in lysosomal sorting of protease-activated receptor-1: evidence for retromer-, Hrs-, and Tsg101-independent functions of sorting nexins. Mol Biol Cell 2006;17(3):1228-1238.

28. Hislop JN, Marley A, Von Zastrow M. Role of mammalian vacuolar protein-sorting proteins in endocytic trafficking of a non-ubiquitinated G protein-coupled receptor to lysosomes. J Biol Chem 2004;279(21):22522-22531.

29. Bie B, Pan ZZ. Trafficking of central opioid receptors and descending pain inhibition. Mol Pain 2007;3:37.

30. Sharp BM. Multiple opioid receptors on immune cells modulate intracellular signaling. Brain Behav Immun 2006;20(1):9-14.

31. Shim S, Kimpler LA, Hanson PI. Structure/Function Analysis of Four Core ESCRT-III Proteins Reveals Common Regulatory Role for Extreme C-Terminal Domain. Traffic 2007;8(8):1068-1079.

32. Dalal S, Rosser MF, Cyr DM, Hanson PI. Distinct roles for the AAA ATPases NSF and p97 in the secretory pathway. Mol Biol Cell 2004;15(2):637-648.

33. Lin Y, Kimpler LA, Naismith TV, Lauer JM, Hanson PI. Interaction of the mammalian endosomal sorting complex required for transport (ESCRT) III protein hSnf7-1 with itself, membranes, and the AAA+ ATPase SKD1. J Biol Chem 2005;280(13):12799-12809.

34. Carthew RW, Sontheimer EJ. Origins and Mechanisms of miRNAs and siRNAs. Cell 2009;136(4):642-655.

35. Usami Y, Popov S, Popova E, Inoue M, Weissenhorn W, H GG. The ESCRT pathway and HIV-1 budding. Biochem Soc Trans 2009;37(Pt 1):181-184.

36. Morita E, Sundquist WI. Retrovirus budding. Annu Rev Cell Dev Biol 2004;20:395-425.

37. Garrus JE, von Schwedler UK, Pornillos OW, Morham SG, Zavitz KH, Wang HE, Wettstein DA, Stray KM, Cote M, Rich RL, Myszka DG, Sundquist WI. Tsg101 and the vacuolar protein sorting pathway are essential for HIV-1 budding. Cell 2001;107(1):55-65.

38. Ward DM, Vaughn MB, Shiflett SL, White PL, Pollock AL, Hill J, Schnegelberger R, Sundquist WI, Kaplan J. The role of LIP5 and CHMP5 in multivesicular body formation and HIV-1 budding in mammalian cells. J Biol Chem 2005;280(11):10548-10555.

39. Theos AC, Truschel ST, Tenza D, Hurbain I, Harper DC, Berson JF, Thomas PC, Raposo G, Marks MS. A lumenal domain-dependent pathway for sorting to intralumenal

vesicles of multivesicular endosomes involved in organelle morphogenesis. Dev Cell 2006;10(3):343-354.

40. Trajkovic K, Hsu C, Chiantia S, Rajendran L, Wenzel D, Wieland F, Schwille P, Brugger B, Simons M. Ceramide triggers budding of exosome vesicles into multivesicular endosomes. Science 2008;319(5867):1244-1247.

41. Babst M, Katzmann DJ, Estepa-Sabal EJ, Meerloo T, Emr SD. Escrt-III: an endosome-associated heterooligomeric protein complex required for mvb sorting. Dev Cell 2002;3(2):271-282.

42. Teo H, Perisic O, Gonzalez B, Williams RL. ESCRT-II, an endosome-associated complex required for protein sorting: crystal structure and interactions with ESCRT-III and membranes. Dev Cell 2004;7(4):559-569.

43. Yorikawa C, Shibata H, Waguri S, Hatta K, Horii M, Katoh K, Kobayashi T, Uchiyama Y, Maki M. Human CHMP6, a myristoylated ESCRT-III protein, interacts directly with an ESCRT-II component EAP20 and regulates endosomal cargo sorting. Biochem J 2005;387(Pt 1):17-26.

44. Saksena S, Wahlman J, Teis D, Johnson AE, Emr SD. Functional reconstitution of ESCRT-III assembly and disassembly. Cell 2009;136(1):97-109.

45. Teis D, Saksena S, Emr SD. Ordered assembly of the ESCRT-III complex on endosomes is required to sequester cargo during MVB formation. Dev Cell 2008;15(4):578-589.

46. Hanson PI, Roth R, Lin Y, Heuser JE. Plasma membrane deformation by circular arrays of ESCRT-III protein filaments. J Cell Biol 2008;180(2):389-402.

47. Lata S, Schoehn G, Jain A, Pires R, Piehler J, Gottlinger HG, Weissenhorn W. Helical structures of ESCRT-III are disassembled by VPS4. Science 2008;321(5894):1354-1357.

48. Ghazi-Tabatabai S, Saksena S, Short JM, Pobbati AV, Veprintsev DB, Crowther RA, Emr SD, Egelman EH, Williams RL. Structure and disassembly of filaments formed by the ESCRT-III subunit Vps24. Structure 2008;16(9):1345-1356.

49. Lee JA, Beigneux A, Ahmad ST, Young SG, Gao FB. ESCRT-III dysfunction causes autophagosome accumulation and neurodegeneration. Curr Biol 2007;17(18):1561-1567.

50. Rusten TE, Vaccari T, Lindmo K, Rodahl LM, Nezis IP, Sem-Jacobsen C, Wendler F, Vincent JP, Brech A, Bilder D, Stenmark H. ESCRTs and Fab1 regulate distinct steps of autophagy. Curr Biol 2007;17(20):1817-1825.

51. Parkinson N, Ince PG, Smith MO, Highley R, Skibinski G, Andersen PM, Morrison KE, Pall HS, Hardiman O, Collinge J, Shaw PJ, Fisher EM. ALS phenotypes with mutations in CHMP2B (charged multivesicular body protein 2B). Neurology 2006;67(6):1074-1077.

52. Skibinski G, Parkinson NJ, Brown JM, Chakrabarti L, Lloyd SL, Hummerich H, Nielsen JE, Hodges JR, Spillantini MG, Thusgaard T, Brandner S, Brun A, Rossor MN, Gade A, Johannsen P*, et al.* Mutations in the endosomal ESCRTIII-complex subunit CHMP2B in frontotemporal dementia. Nat Genet 2005;37(8):806-808.

53. Carlton JG, Agromayor M, Martin-Serrano J. Differential requirements for Alix and ESCRT-III in cytokinesis and HIV-1 release. Proc Natl Acad Sci U S A 2008;105(30):10541-10546.

54. Carlton JG, Martin-Serrano J. Parallels between cytokinesis and retroviral budding: a role for the ESCRT machinery. Science 2007;316(5833):1908-1912.

55. Morita E, Sandrin V, Chung HY, Morham SG, Gygi SP, Rodesch CK, Sundquist WI. Human ESCRT and ALIX proteins interact with proteins of the midbody and function in cytokinesis. Embo J 2007;26(19):4215-4227.

56. Usami Y, Popov S, Gottlinger HG. Potent rescue of human immunodeficiency virus type 1 late domain mutants by ALIX/AIP1 depends on its CHMP4 binding site. J Virol 2007;81(12):6614-6622.

FIGURE LEGENDS

Figure 4-1 Antibodies recognizing ESCRT-III proteins and other proteins in the ESCRT pathway.

(A-B) Endogenous ESCRT-III proteins (A) and other proteins in the ESCRT pathway (B) in HEK293 derived cell lines were visualized by immunoblotting with antibodies for indicated proteins. Samples shown here were prepared by lysis in 1% Triton X-100 or SDS sample buffer. Arrows point to the bands representing proteins of interest around expected sizes. For CHMP2A, there are two bands near the expected size, ~30 - 35KDa (left lane). The lower band in the pellet (P) likely represents endogenous CHMP2A protein. Supernatant (S) and pellet (P) were obtained by solubilizing HEK293 cells expressing the dominant negative mutant VPS4B (VPS4B(E235Q)) in 1% Triton X-100. (C) HEK293 cell line expressing VPS4B(E235Q)-GFP was immunostained with CHMP4A antibody and analyzed by confocal microscopy. GFP signal was visualized without staining. VPS4B(E235Q)-GFP and CHMP4A are shown in green and red respectively.

Table 4-1 List of antibodies for ESCRT-III proteins and other proteins in the ESCRT pathway.

Figure 4-2 Knockdown of ESCRT-III proteins and other proteins in the ESCRT pathway.

(A) Efficiency of knockdown by shRNAs. ESCRT-III proteins were knocked down by transduction with recombinant lentivirus expressing shRNAs while Tsg101 and LIP5 were knocked down by transfection with shRNA expressing plasmids. shRNAs were transduced in various HEK293 derived cell lines, and knockdown efficiency was

analyzed by visualizing endogenous proteins by immunoblotting. For CHMP6, knockdown by two different shRNAs was shown. Note that in the case of CHMP3, knockdown efficiency was tested against overexpressed CHMP3. To do this, cells transduced with CHMP3 shRNA were transfected with myc tagged CHMP3 construct a day before analysis. Con: cells expressing LacZ shRNA or no shRNAs, K/D: cells expressing with indicated shRNAs. (B) Efficiency of knockdown by siRNAs. Cells were transfected with 20nM siRNA for Tsg101, VPS4A or VPS4B, and knockdown efficiency was analyzed by immunoblotting for endogenous proteins. Con: untransfected control, K/D: cells transfected with indicated siRNAs.

Table 4-2 List of shRNAs and siRNAs to knock down ESCRT-III proteins and other proteins in the ESCRT pathway.

Figure 4-3 Trafficking and degradation of EGFR and EGF upon EGF treatment. (A) A stable HEK293 cell line expressing EGFR-GFP in a tetracyclin inducible manner (TRex-HEK293;EGFR-GFP) was incubated with 10ng/mL of tetracycline overnight to induce EGFR-GFP expression. Cells were stimulated with 100ng/mL EGF for 0, 1 or 2 hours. EGFR-GFP protein was visualized by immunoblotting with anti-GFP antibody. Equal loading of proteins was confirmed by Ponceau staining. (B) HeLa cells were incubated with 100ng/mL EGF for 0, 1 or 2 hours after starvation in serum free media for 3 hours. Endogenous EGFR was visualized by immunoblotting with anti-EGFR antibody. Equal loading of proteins was confirmed by Ponceau staining and immunoblotting for α-tubulin. (C) TRex-HEK293;EGFR-GFP cells were incubated with 10ng/mL tetracycline overnight to induce EGFR-GFP expression. Cells were then stimulated with 100ng/mL EGF for 0min, 10min or 2 hours and analyzed by epifluorescence microscopy. Nuclei were visualized by DAPI staining while GFP signal was visualized without staining.

Images were taken under the same exposure time. (D) HeLa cells were incubated with 200ng/mL of EGF conjugated with Alexa-555 fluorescent dye for 30min on ice. After washing unbound ligands, cells were transferred to 37ºC and incubated for 15min or 5 hours. Cells were stained with DAPI and analyzed by epifluorescence microscopy. Images were taken under the same exposure time.

Figure 4-4 EGFR degradation is inhibited by manipulating the ESCRT pathway. (A) HeLa cells transfected with GFP or VPS4B(E235Q)-GFP were stimulated with 100ng/mL EGF for 0, 1 and 2 hours after starvation for 3 hours. Endogenous EGFR was visualized by immunoblotting with anti-EGFR antibody. Equal loading of proteins was confirmed by Ponceau staining, and expression of GFP and VPS4B(E235Q)-GFP was determined by immunoblotting with anti-GFP antibody. (B) HeLa cells transfected with 20nM Tsg101 siRNA were simulated with EGF and analyzed as described above. Equal loading of proteins was confirmed by immunoblotting for α-tubulin. Knockdown efficiency of Tsg101 is shown in Figure 4-2(B).

Figure 4-5 Trafficking and degradation of DOR upon agonist treatment. (A) HEK293 cells stably expressing FLAG-DOR (HEK293;FLAG-DOR) were stimulated with 10μM DADLE for 0, 2 or 4 hours and analyzed by immunoblotting with anti-FLAG antibody. (B) HeLa cells stably expressing FLAG-DOR (HeLa;FLAG-DOR) were stimulated with DADLE and analyzed as described above. (A-B) Equal loading of protein was confirmed by immunoblotting for α-tubulin. (C) HEK293;FLAG-DOR cells stimulated with 10μM DADLE for 0min, 30min or 4 hours were immunostained for FLAG-DOR and EEA1 (early endosomal marker), and analyzed by confocal microscopy. Images were taken under the same confocal setting.

Figure 4-6 Internalized DOR transits through late endosomes.

HEK293;FLAG-DOR cells stimulated with 10μM DADLE for 30min were immunostained for FLAG-DOR and CD63, a marker for late endosomes/MVBs, and subsequently analyzed by confocal microscopy. FLAG-DOR and CD63 are shown in green and red respectively. DIC image is shown in gray.

Figure 4-7 Dominant negative mutant VPS4 inhibits degradation of DOR.

(A) HEK293;FLAG-DOR cells transfected with VPS4B-GFP (wild type or mutant (E235Q)) were incubated with 10μM DADLE for 0, 2 and 4 hours and analyzed by immunoblotting with anti-FLAG antibody. (B) TRex-HEK293 cells stably expressing VPS4B-GFP (wild type or mutant (E235Q)) in addition to FLAG-DOR were stimulated with DADLE and analyzed as described above. Expression of VPS4B was induced by treatment of 1μg/mL tetracycline overnight. (A and B) Equal loading of proteins and expression of VPS4 proteins were confirmed by immunoblotting with anti-α-tubulin antibody and anti-GFP antibody. (C) TRex-HEK293 cell line expressing both FLAG-DOR and VPS4(E235Q)-GFP was stimulated with 10μM DADLE for 1 hour, immunostained with anti-FLAG antibody and subsequently analyzed by confocal microscopy. Expression of VPS4B was induced by treatment of 1μg/mL tetracycline for 6 hours. GFP signal visualized without staining is shown in green and FLAG-DOR shown in red.

Figure 4-8 Knockdown of VPS4 inhibits degradation of DOR.

HEK293;FLAG-DOR (A) and HeLa;FLAG-DOR (B) cell lines transfected with 30nM control or VPS4 siRNAs (15nM/each) were stimulated with 10μM DADLE for 0, 2 and 4 hours and analyzed by immunoblotting with anti-FLAG antibody. Knockdown efficiency

for VPS4A and VPS4B was determined by immunoblotting for VPS4A and VPS4B respectively. Equal loading of proteins was confirmed by immunoblotting for α-tubulin.

Figure 4-9 Dominant negative ESCRT-III proteins inhibit degradation of DOR.
(A) HEK293;FLAG-DOR cells were transfected with FLAG-CHMP2A full-length or 1-180 (dominant negative mutant). Next day, cells were treated with 10μM DADLE for 0, 2 and 4 hours and analyzed by immunoblotting with anti-FLAG antibody. (B) TREx-HEK293 cells stably expressing Myc-CHMP2A (wild type or 1-180) in addition to FLAG-DOR were stimulated with DADLE and analyzed as described above. Expression of CHMP2A proteins was induced by treatment of 1μg/mL tetracycline overnight. (A - B) Equal loading of proteins and expression of CHMP2A proteins were confirmed by immunoblotting with anti-α-tubulin antibody and anti-FLAG antibody. (C) TREx-HEK293 cell line expressing both FLAG-DOR and Myc-CHMP2A (1-180) was stimulated with 10μM DADLE for 1 hour, immunostained with anti-FLAG antibody, and subsequently analyzed by confocal microscopy. Expression of CHMP2A 1-180 was induced by treatment of 1μg/mL tetracycline for 6 hours. GFP signal visualized without staining is shown in green and FLAG-DOR shown in red.

Figure 4-10 Knockdown of Tsg101 inhibits degradation of DOR.
HEK293;FLAG-DOR (A) and HeLa;FLAG-DOR (B) cell lines transfected with 20nM control or Tsg101 siRNA were stimulated with 10μM DADLE for 0, 2 or 4 hours and the level of DOR was visualized by immunoblotting with anti-FLAG antibody. Knockdown efficiency of Tsg101 and equal loading of proteins were confirmed by immunoblotting for Tsg101 and α-tubulin respectively.

Figure 4-1

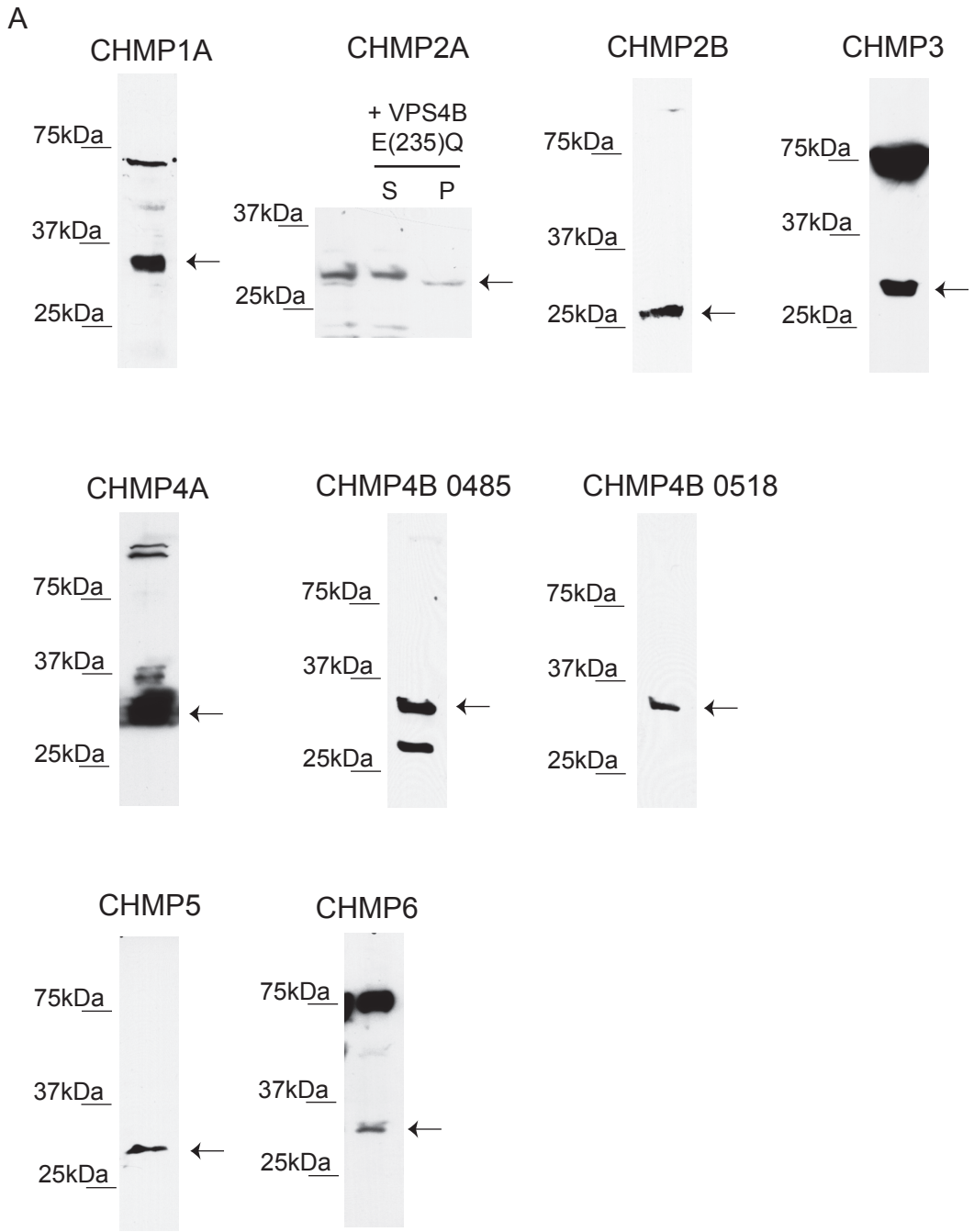
A
CHMP1A
75kDa
37kDa
25kDa
CHMP2A
+ VPS4B
E(235)Q
S
P
37kDa
25kDa
CHMP2B
75kDa
37kDa
25kDa
CHMP3
75kDa
37kDa
25kDa
CHMP4A
75kDa
37kDa
25kDa
CHMP4B 0485
75kDa
37kDa
25kDa
CHMP4B 0518
75kDa
37kDa
25kDa
CHMP5
75kDa
37kDa
25kDa
CHMP6
75kDa
37kDa
25kDa

Figure 4-1

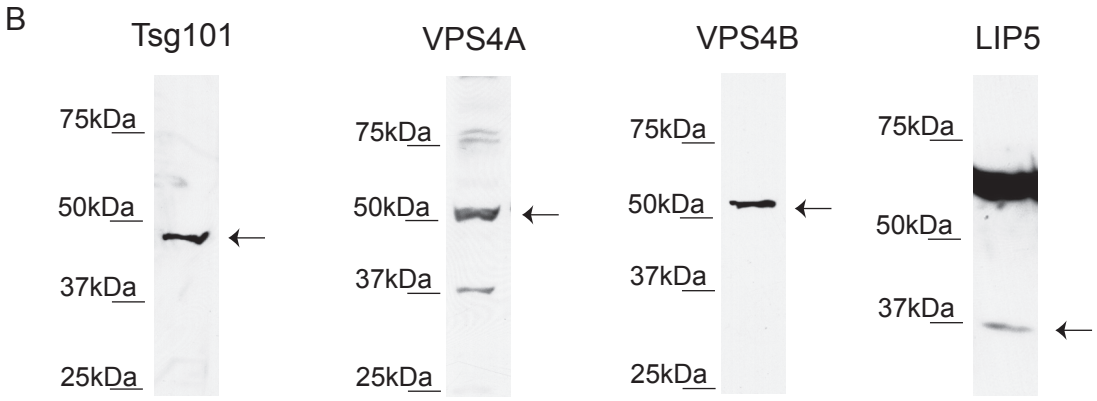
B
Tsg101
VPS4A
VPS4B
LIP5
75kDa
50kDa
37kDa
25kDa

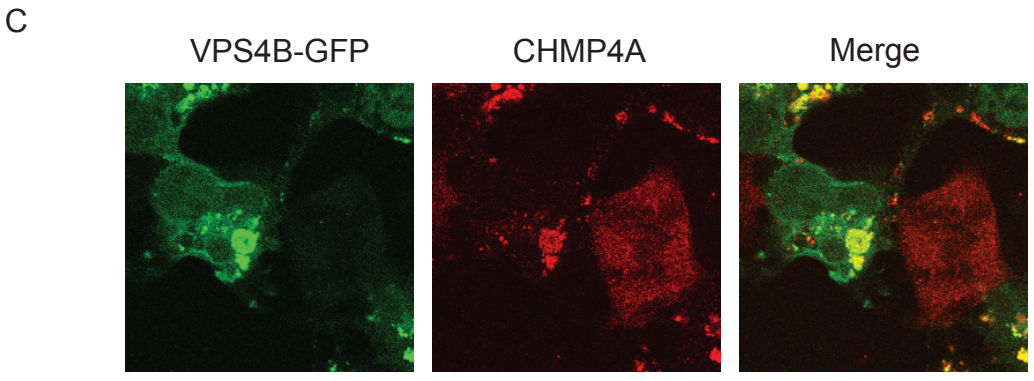
C
VPS4B-GFP
CHMP4A
Merge

Table 4-1

Antigen	Source		conc.	Detection of endogenous protein by IB	Detection of endogenous proteins by IF	comments
CHMP1A	Abcam ab55536	mouse monoclonal	1µg/µL	1-2µg/mL	cannot detect endogenous protein	
CHMP2A	Proteintech group BC-2 10477-1	rabbit polyclonal	0.55µg/µL	1-2µg/mL	cannot detect endogenous protein	not cross-react with CHMP2B
CHMP2B	Abcam ab33174	rabbit polyclonal	0.7µg/µL	1 - 1.5 µg/mL	3-5 µg/mL	not cross-react with CHMP2A
CHMP2	Santa Cruz sc-49905	goat polyclonal	0.2µg/µL	cannot detect endogenous protein/ 1µg/mL for overexpressed CHMP2A	not determined	not cross-react with CHMP2B / use PVDF for blotting
CHMP3	Hanson lab, affinity purified by LK	rabbit polyclonal	N/A	1:40	cannot detect endogenous protein	not stable
CHMP4A	Hanson lab, affinity purified by LK	rabbit polyclonal	N/A	1:50	1:20 - 1:50	not cross-react with CHMP4B or CHMP4C
CHMP4B	Shiels lab # 0485	rabbit polyclonal, affinity purified	N/A	1:2000	1:100 - 1:250	not cross-react with CHMP4A or CHMP4C
CHMP4B	Shiels lab # 0518	rabbit polyclonal, affinity purified	N/A	1:2000	1:100 - 1:250	not cross-react with CHMP4A or CHMP4C
CHMP5	Everst EB06716	goat polyclonal	0.5µg/µL	2µg/mL	cannot detect endogenous protein	
CHMP6	Santa Cruz sc-49922	goat polyclonal	0.2µg/µL	cannot detect the endogenous protein	not determined	
CHMP6	Sundquist Lab	rabbit polyclonal serum	N/A	1:500	1:300	
VPS4A	Sundquist Lab	rabbit polyclonal serum	N/A	1:1000	not determined	generally specific to VPS4A but cross-react little bit with VPS4B
VPS4B/SKD1	Hanson lab, affinity purified by YL	rabbit polyclonal, affinity purified	N/A	1:200	not determined	not cross-react with VPS4A
LIP5	Kaplan lab	rabbit polyclonal, serum	N/A	1:500	cannot detect endogenous protein	block in TBST containing 5% milk and 1% BSA for blotting
Tsg101	GeneTex, MS-TSG10-PX	mouse monoclonal	1µg/µL	2µg/µL	cannot detect endogenous protein	

LK: Lisa Kimpler
YL: Yuan Lin
N/A: not available

Figure 4-2

A. Knockdown by shRNAs

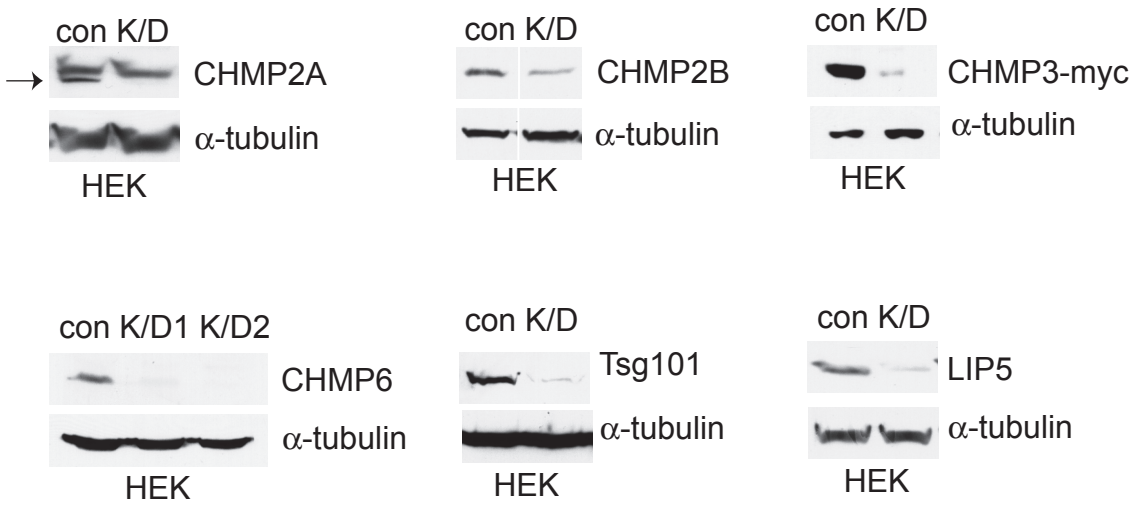

B. Knockdown by siRNAs

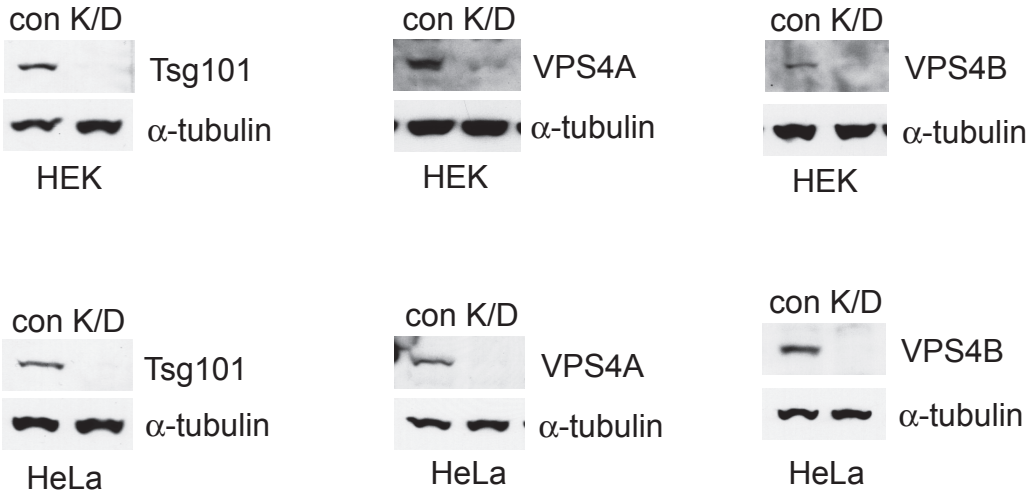

Table 4-2

Target protein	Type	targeting sequence	source	comment
LacZ	shRNA	CTACGCATAGAAGCCGGGATT	TRC1 A4	
CHMP2A	shRNA	GCAGGCAGAGATCATGGATAT	TRC1 C6	
CHMP2B	shRNA	GCAGCTTTAGAGAAACAAGAA	TRC1 C2	
CHMP3	shRNA	GTGAAACGATCTGTGAAAGAT	TRC1 D4	
CHMP6	shRNA	GCGCAATCACTCAGGAACAAA	TRC1 E1	
CHMP6	shRNA	GCTGCTCAAGAAGAAGCGATA	TRC1 E2	
LIP5	shRNA	CCTTCTATACTGCAAGTCTTT	TRC1 B9	
Tsg101	shRNA	GCAGAGCTCAATGCCTTGAAA	TRC1 A10	
Tsg101	siRNA	CCUCCAGUCUUCUCUCGUC	Dharmacon	dTdT to 3' end added
VPS4A	siRNA	CCGAGAAGCUGAAGGAUUA	Dharmacon	dTdT to 3' end added
VPS4B	siRNA	CCAAAGAAGCACUGAAAGA	Dharmacon	dTdT to 3' end added

Figure 4-3

A

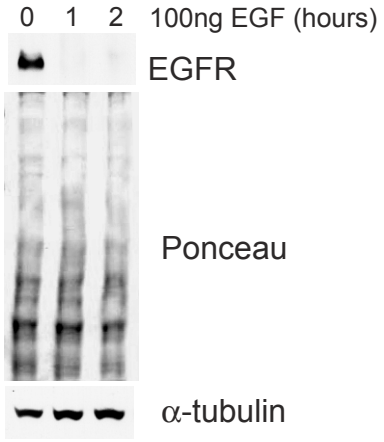
0 1 2 100ng EGF (hours)
EGFR
Ponceau
α-tubulin

B

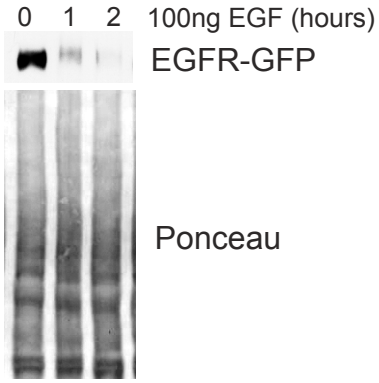
0 1 2 100ng EGF (hours)
EGFR-GFP
Ponceau

Figure 4-3

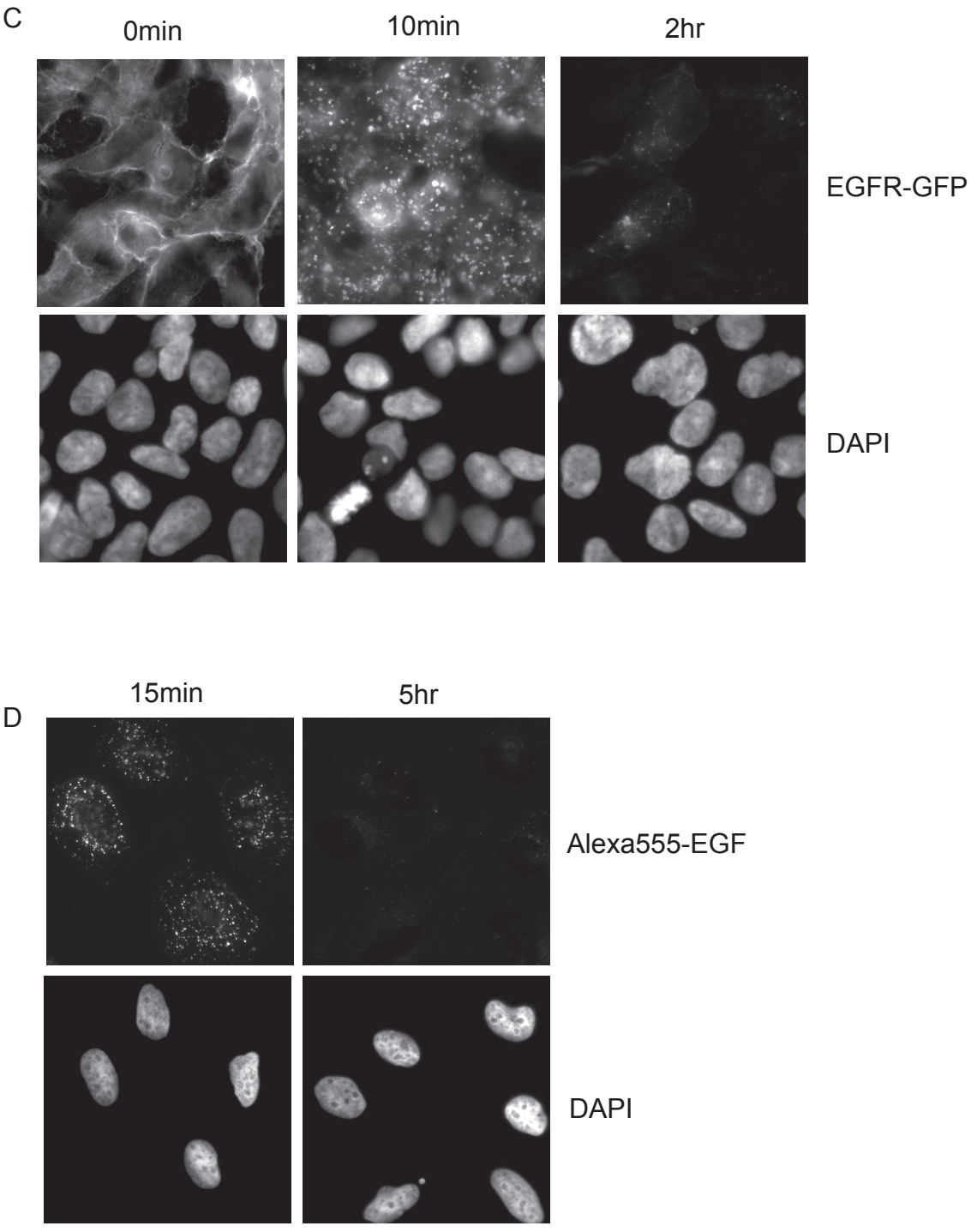

Figure 4-4

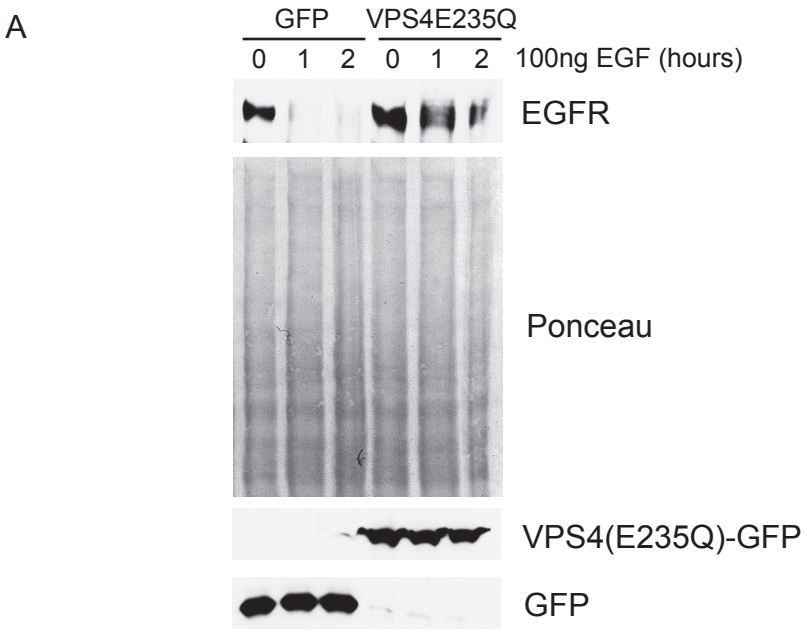
A
GFP
VPS4E235Q
0 1 2 0 1 2
100ng EGF (hours)
EGFR
Ponceau
VPS4(E235Q)-GFP
GFP

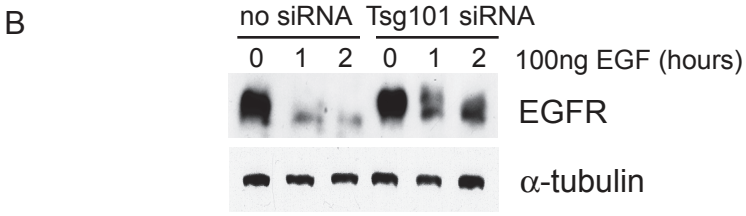
B
no siRNA
Tsg101 siRNA
0 1 2 0 1 2
100ng EGF (hours)
EGFR
α-tubulin

Figure 4-5

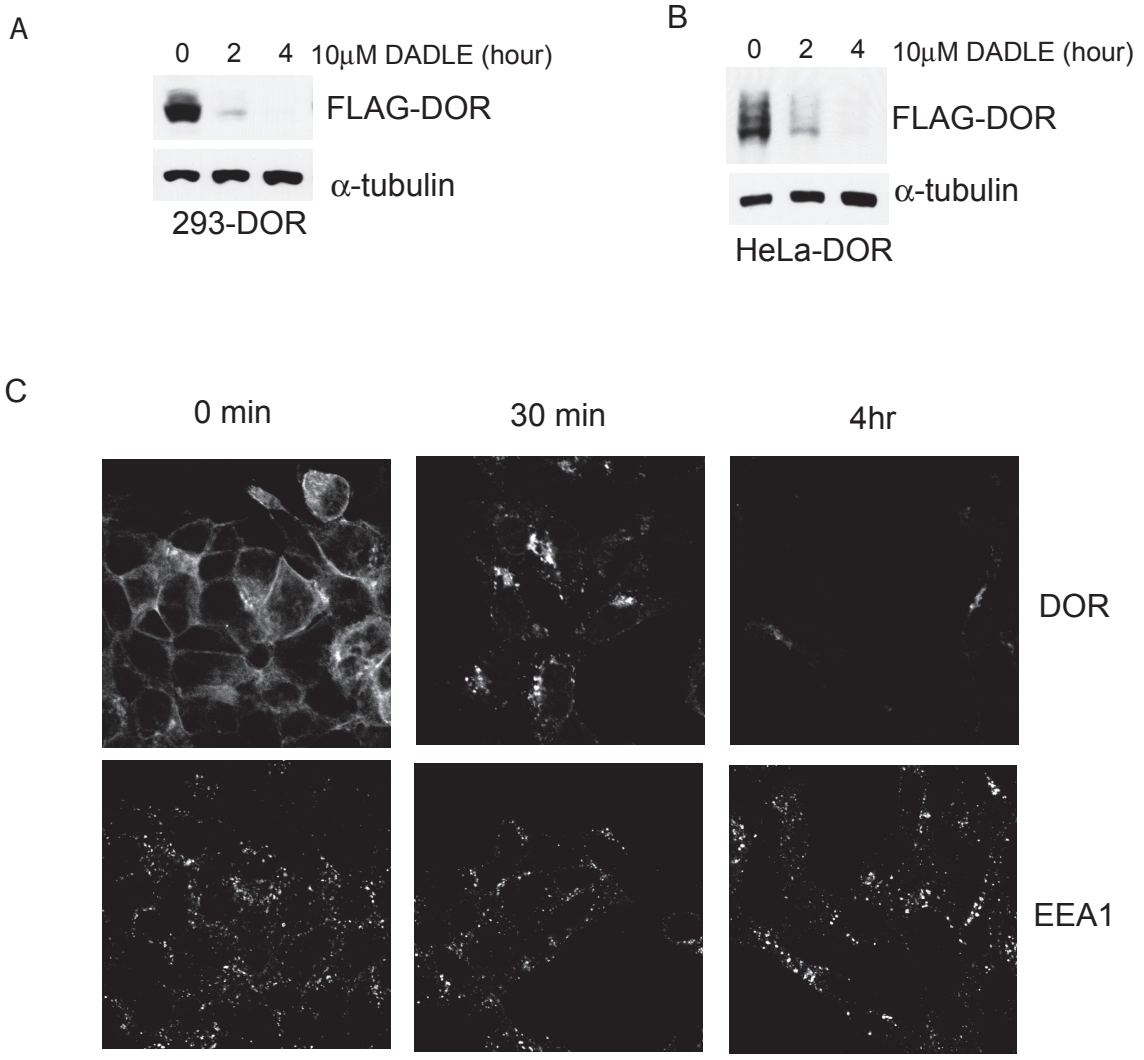
A
0 2 4 10μM DADLE (hour)
FLAG-DOR
α-tubulin
293-DOR
B
0 2 4 10μM DADLE (hour)
FLAG-DOR
α-tubulin
HeLa-DOR
C
0 min
30 min
4hr
DOR
EEA1

Figure 4-6

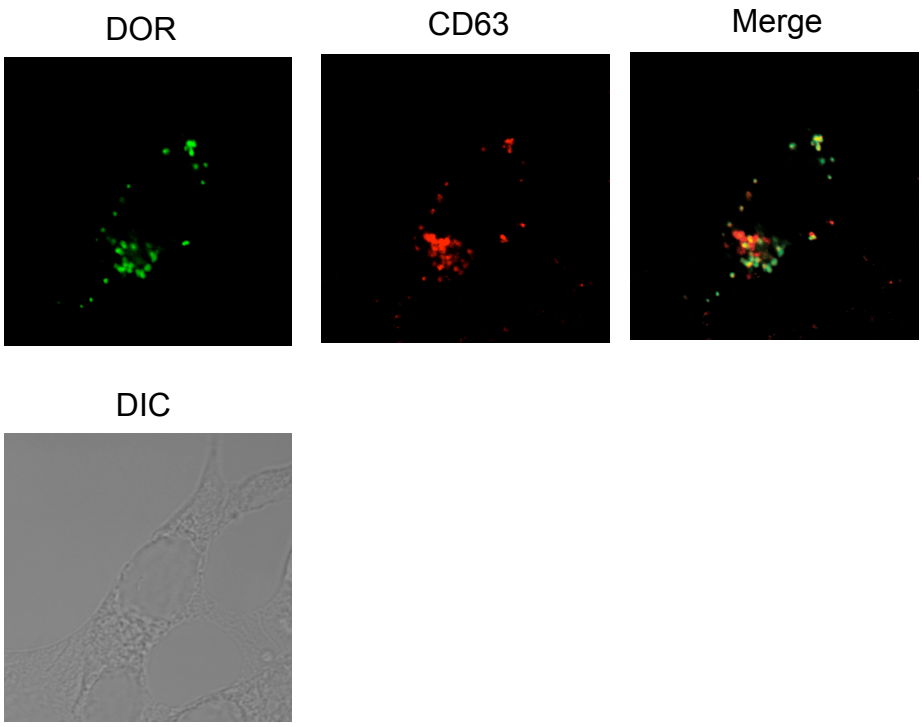

Figure 4-7

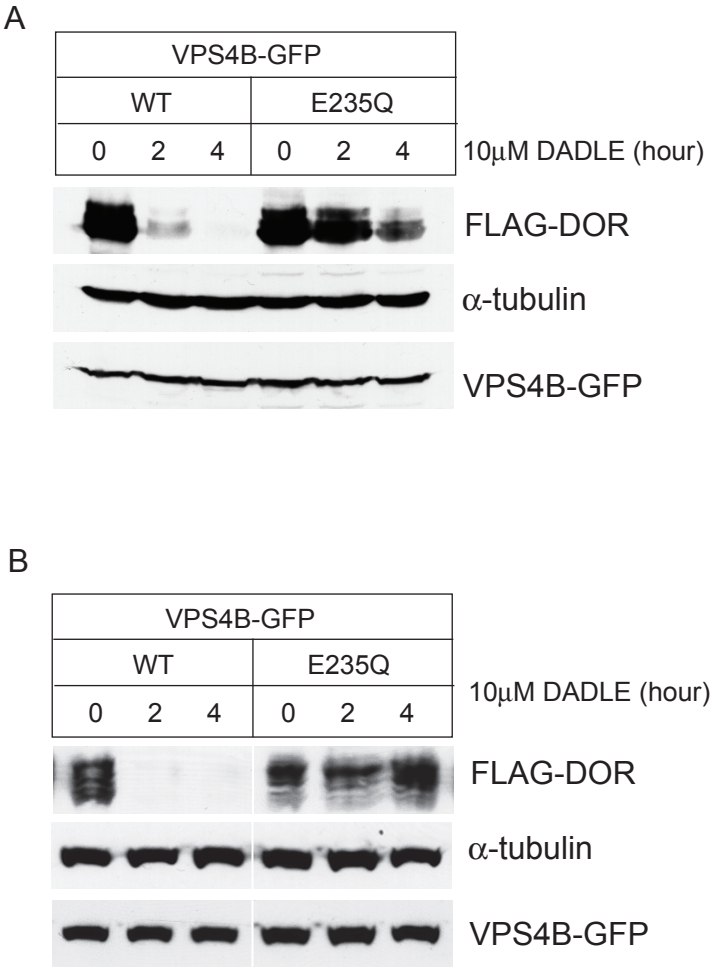
A
VPS4B-GFP
WT
E235Q
0 2 4 0 2 4
10μM DADLE (hour)
FLAG-DOR
α-tubulin
VPS4B-GFP
B
VPS4B-GFP
WT
E235Q
0 2 4 0 2 4
10μM DADLE (hour)
FLAG-DOR
α-tubulin
VPS4B-GFP
C
VPS4BE(235)Q
DOR
merge

Figure 4-8

A. 293-DOR

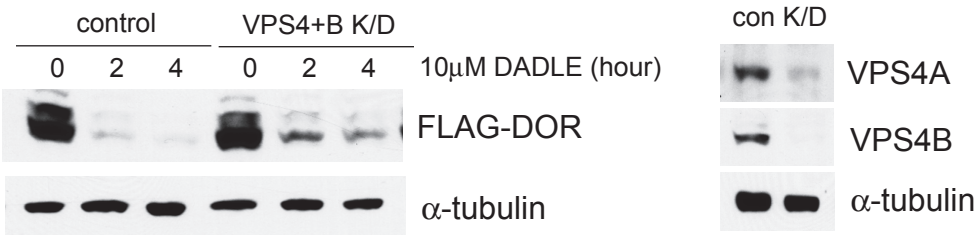

B. HeLa-DOR

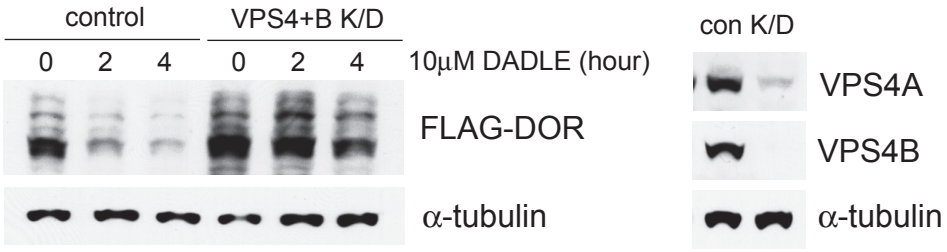

Figure 4-9

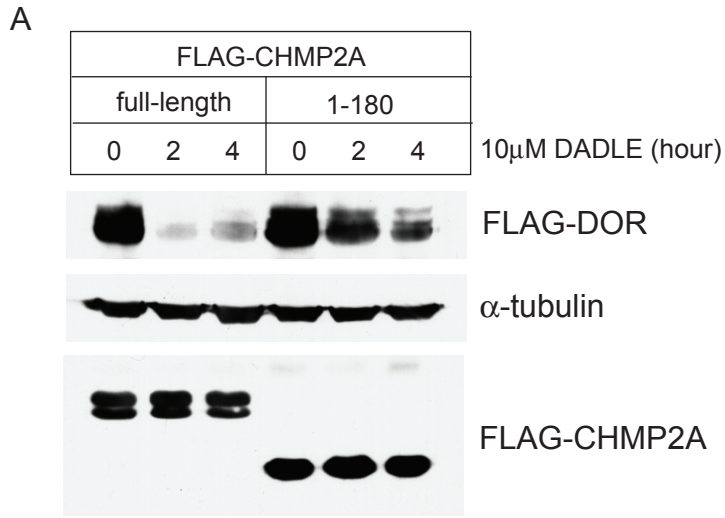
A
FLAG-CHMP2A
full-length
1-180
0 2 4 0 2 4
10μM DADLE (hour)
FLAG-DOR
α-tubulin
FLAG-CHMP2A

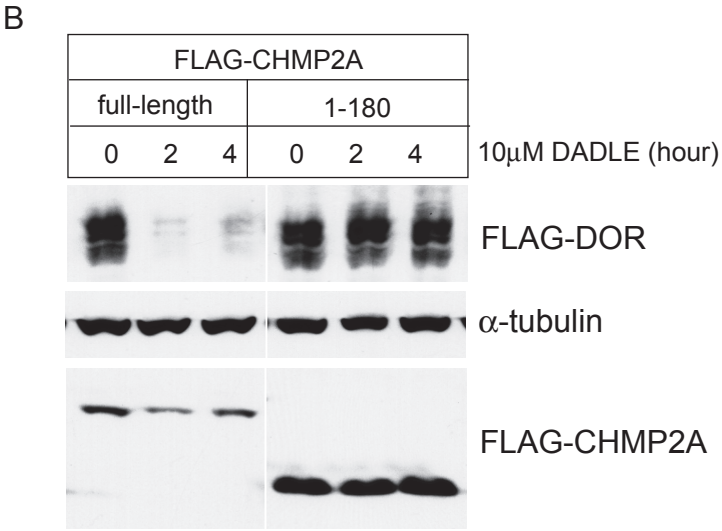
B
FLAG-CHMP2A
full-length
1-180
0 2 4 0 2 4
10μM DADLE (hour)
FLAG-DOR
α-tubulin
FLAG-CHMP2A

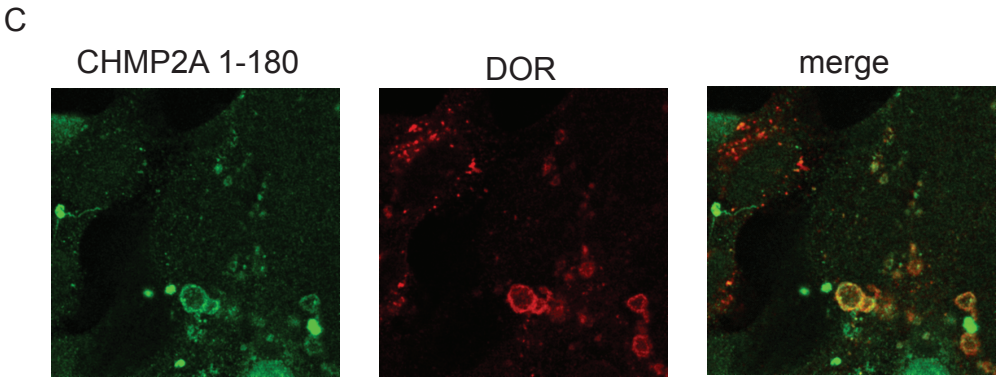
C
CHMP2A 1-180
DOR
merge

Figure 4-10

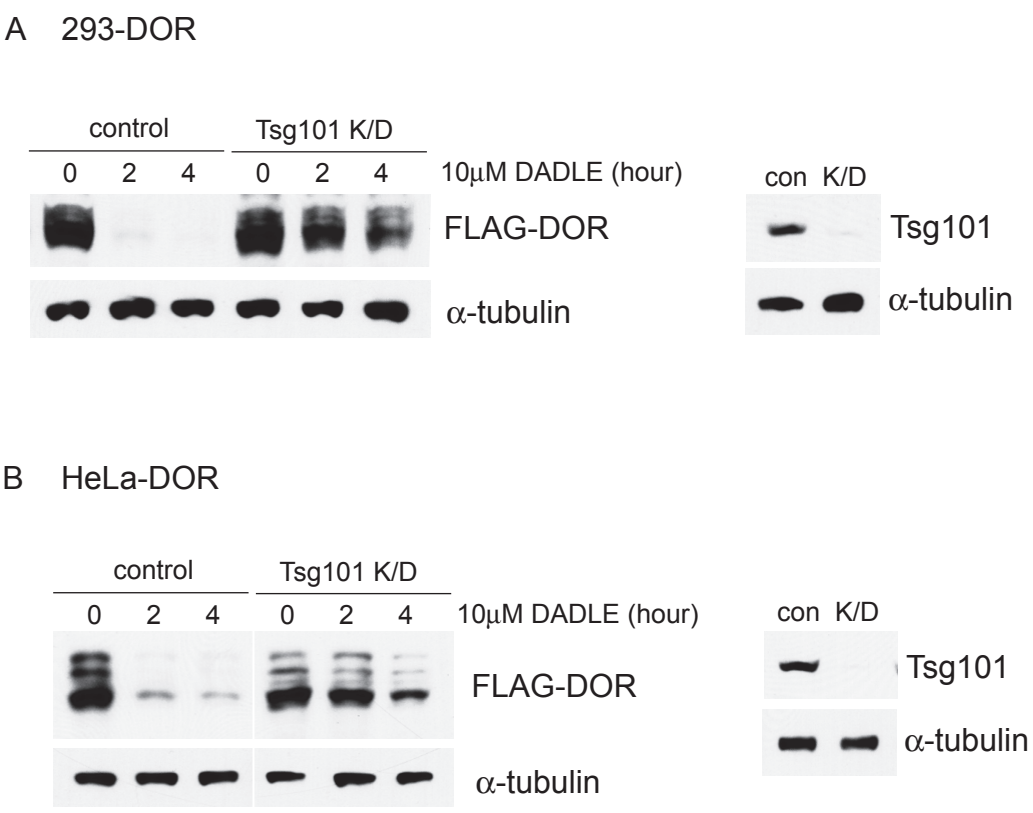
A 293-DOR
control
Tsg101 K/D
0 2 4 0 2 4
10μM DADLE (hour)
FLAG-DOR
α-tubulin
con K/D
Tsg101
α-tubulin
B HeLa-DOR
control
Tsg101 K/D
0 2 4 0 2 4
10μM DADLE (hour)
FLAG-DOR
α-tubulin
con K/D
Tsg101
α-tubulin

CHAPTER FIVE

DISCUSSION AND FUTURE DIRECTIONS

1. Summary

The studies described in this thesis focus on studying the regulation of ESCRT-III proteins and their functions in multivesicular body biogenesis. The work in Chapter 2 identified a common autoinhibitory domain in ESCRT-III proteins which controls the conformational states of these proteins. This solidified the model that ESCRT-III operates by switching between closed and open states, and confirmed the self-propagating property of ESCRT-III polymers. The work in Chapter 3 discovered an unexpected link between these ESCRT-III proteins and LIP5, a cofactor of VPS4. In Chapter 4, I described the study of the roles of endogenous ESCRT-III proteins in ILV formation and cargo sorting into ILVs. In this chapter, I discuss my current thinking about the role and regulation of ESCRT-III and remaining questions. I also describe some pieces of data and suggestions that may contribute to future studies.

2. Discussion

The ESCRT machinery has clearly established roles in cargo sorting to the MVB and creating intralumenal vesicles. A flurry of studies over the past several years has provided structural and mechanistic insight into the assembly and disassembly of ESCRTs and recruitment of cargo to the MVB. In particular, the molecular architecture of ESCRT-0, I and II and their roles in directing ubiquitinated cargo to the MVB have become fairly clear (1). One of the major challenges remaining in the ESCRT field is to understand how ESCRT-III assembles on the endosomal membrane and what roles it plays in generating ILVs (2, 3).

ESCRT-III polymers

Thanks to several recent reports, the molecular architecture of ESCRT-III polymers is beginning to come to light (4-8). Although the precise stoichiometry and structure of ESCRT-III polymers is still unclear, ESCRT-III polymers seem to be highly organized and membrane-associated structures that contain different ESCRT-III proteins. Snf7/CHMP4 is likely to be a main constituent of the polymers because Snf7 is a main protein present in ESCRT-III isolated from yeast (5). Furthermore, circular homopolymers formed by CHMP4 proteins in mammalian cells are able to induce membrane deformation (4).

Regulation of ESCRT-III polymer assembly

From the work of the past several years, including mine, it is quite clear that ESCRT-III proteins in the cytoplasm are maintained in a closed conformation by the C-terminal autoinhibitory domain (8-12). When ESCRT-III proteins are relieved from autoinhibition (or opened), they assemble on the endosomal membrane. There are two important steps in regulating ESCRT-III assembly. One is opening ESCRT-III proteins to expose their ability to associate with the membrane and form polymers. ESCRT-III proteins in an open conformation likely promote the opening of other ESCRT-III proteins, allowing propagation of ESCRT-III polymer assembly (9, 10). It has been proposed that there are cellular factors that bind to the autoinhibitory domain and help control conformational changes of ESCRT-III proteins (9-11). The other important step is targeting ESCRT-III proteins in the cytoplasm to the specific endosomal membrane. Many cytosolic proteins including components of upstream ESCRTs are recruited to the endosomal membrane by their interactions with specific phospholipids on endosomes (13, 14). I will discuss possible mechanisms for endosomal targeting of ESCRT-III proteins in Section 3.

VPS4 mediated ESCRT-III polymer disassembly

Several recent reports have shown that different variations of ESCRT-III polymers could be disassembled by VPS4 in the presence of ATP, confirming that VPS4 is indeed the disassembly machinery for ESCRT-III (6-8, 15). Whether or not VPS4 is directly involved in ILV formation remains to be determined. Nevertheless, it is clear that VPS4 mediated disassembly is a critical process for MVB biogenesis (16-19). Thanks to advances in structural biology, the structure of VPS4 and its interaction with ESCRT-III proteins have been fairly well characterized (20-22). However, the mechanistic basis for VPS4 mediated disassembly of ESCRT-III polymers is far from clear. One of the questions to be answered regarding VPS4 mediated disassembly is how VPS4 acts on a core of ESCRT-III polymers - CHMP4/Snf7, and I will discuss this issue in Section 3.

Regulators of ESCRT-III polymer disassembly

Given the importance of VPS4 in MVB biogenesis, it is not surprising that many proteins identified as regulators of the ESCRT pathway are proposed to control VPS4 mediated disassembly directly or indirectly. Such regulatory proteins include Vta1/LIP5, Ist1/IST1, Did2/CHMP1 and Vps60/CHMP5 (23-30). Although mutants of these regulators in yeast exhibit only mild phenotypes, knocking out CHMP5 in mice leads to embryonic lethality (24-26, 30). This suggests that roles of these proteins may be underappreciated. Furthermore, the regulators can interact with each other and are thought to function cooperatively or antagonistically. How exactly these proteins fine-tune VPS4 mediated disassembly, and thereby MVB biogenesis, is not clear yet. In Section 3, I will discuss one of these regulators, CHMP5, which may negatively regulate the ESCRT pathway via its interaction with LIP5, a proposed cofactor of VPS4.

Mechanisms for ILV formation by ESCRT-III polymers

Although we have begun to learn about the characteristics of ESCRT-III polymers and their ability to deform membranes, our current knowledge is not enough to understand the precise relationship between ESCRT-III polymers and ILV formation. The current speculative model is that ESCRT-III polymers may form circular filaments around concentrated cargo, push membranes into the lumen to form a vesicle and finally cut the neck of the vesicle (3, 4, 8, 15). Based on the currently available data, ESCRT-III proteins are not likely to be incorporated into ILVs; thus, ESCRT-III polymers could not provide a platform inside of a vesicle to deform the membrane. Instead, they might form a circular 'fence' inside the neck of a nascent vesicle (3, 4, 8, 12, 15).

Whether and how ESCRT-III polymers initiate the negative membrane curvature from a flat membrane remains enigmatic. Interestingly, this seems to be less problematic in other topologically related budding processes. In the case of HIV and other retroviral budding, Gag proteins comprising the core of a virus particle may provide a scaffold to deform the membrane (31, 32). Supporting this, when a late domain of a virus which recruits ESCRT machinery is mutated, viral budding is shown to be arrested at a late stage (33, 34). ESCRT machinery also plays a role in the final step of cytokinesis after the cleavage furrow is formed by actomyosin-based contraction (35-37). Therefore, it is conceivable that generating the initial membrane curvature for ILV formation may require help from other factors such as upstream ESCRTs, concentrated cargo proteins, and/or lipids. Alternatively and not exclusively, budding processes for viral budding and cytokinesis may require only part of the ESCRT-III machinery for a late stage of vesicle formation – perhaps narrowing and closing the neck of the vesicles.

Whether and how VPS4 contributes to the budding process also remains unclear. VPS4 might help ESCRT-III polymers contract the neck of a vesicle by inducing conformational changes in ESCRT-III proteins and/or disassembly of ESCRT-III

polymers concomitant with assembly (3, 4, 12). Alternatively, VPS4 might contribute to membrane scission analogous to dynamin, a GTPase functioning in endocytic vesicle formation (38). A recent *in vitro* reconstitution study using giant unilamellar vesicles, however, suggests that Vps20, Snf7 and Vps24 are sufficient for creating and detaching ILVs and the role of VPS4 mediated disassembly may be limited to the recycling of machinery (15). It should be noted that a significant number of vesicles were formed spontaneously in this reaction, implying that the synthetic membranes used in the assay might be prone to form vesicles. Therefore, it is necessary to determine exactly when and how ESCRT-III and VPS4 act on the ILV formation in a more physiological reaction, which is a goal of the work described in Chapter 4.

3. Preliminary data and future directions

Determine how ESCRT-III proteins are selectively targeted to the endosomal membrane

To gain insight into regulation of ESCRT-III, it will be critical to determine the molecular mechanisms governing ESCRT-III targeting to the endosomal membrane. Components of upstream ESCRTs contain phosphoinositide-3-phosphate (PI3P) binding domains, such as the FYVE and GLUE domains, which help them localize to the endosomal membrane; however, how ESCRT-III is targeted to the endosome is less clear (39-44). In the current model, ESCRT-III is thought to be targeted to the endosomal membrane by the interaction of CHMP6/Vps20 with a component of ESCRT-II (Eap20/Vps25). However, the data from my cell based experiments suggest that ESCRT-III proteins may have the ability to target themselves to the endosomal membrane (10). First, individual ESCRT-III proteins interact with the endosomal membrane when their C-terminal autoinhibitory domain is removed (Figure 2-2). Because each protein was highly overexpressed in cells, its interaction with membranes

is not likely to be mediated by association with endogenous proteins. Some ESCRT-III proteins like CHMP3 and CHMP4A were shown to have weak specificity to phosphoinositide-3,5-bisphosphate ($PI(3,5)P_2$), a phospholipid found in the endosome (9, 45). Additionally, C-terminally truncated CHMP2A co-localized well with the FYVE domain in cells cotransfected with CHMP2A 1-180 and 2x FYVE domain, suggesting that the ESCRT-III protein may have specificity to PI3P (Fig. 5-1). Furthermore, the crystal structure of CHMP3 suggests that an ESCRT-III protein contains a basic N-terminal helical core which could bind to acidic phosphoinositides concentrating on endosomal membranes (46). Taken together, I hypothesize that individual ESCRT-III proteins have an intrinsic ability to bind to endosomal membranes, and that this property contributes to restricting ESCRT-III assembly to these membranes.

CHMP2A may be a good ESCRT-III protein for testing this hypothesis. First, less is known about membrane binding and endosomal targeting of CHMP2/Vps2 compared to other core ESCRT-III proteins, and therefore it deserves more attention. Additionally, the striking difference between full-length (soluble) and α1-α5 (membrane-bound) proteins should make it possible to better understand how the interaction of the protein with membranes is regulated (Fig. 2-2 and 2-3). To test the direct interaction of CHMP2A with membranes and its lipid specificity, I would carry out an *in vitro* liposome binding assay with recombinant CHMP2A proteins (comparing full-length and α1-α5 mutant (1-180)) and liposomes containing different phosphoinositides. To distinguish lipid specificity from nonspecific electrostatic interactions between the basic surface of CHMP2A and acidic phosphoinositides, the interaction with other acidic lipids should be tested. If CHMP2A binds specifically to certain phosphoinositide(s), it would be interesting to define the domain responsible for this lipid specificity. In my cell based experiments, α1-α5 mutant CHMP2A was localized on the endosome while CHMP2A

with a deletion from the end of α4 (α1-α4 mutant; CHMP2A 1-144) was not found primarily on the endosome (Fig. 2-2). Similar trends were seen with other ESCRT-III proteins. Supporting this, the helical bundle formed by α1-α4 in the CHMP3 crystal structure does not have a notable feature that might provide lipid specificity (46) . Together, a specific determinant for targeting may lie within the region around helix 5 of an ESCRT-III protein. If deleting α5 changes lipid specificity, one could carry out alanine scanning within the α5 region to identify residues critical for endosomal targeting. The proposed work will provide insight into the molecular basis for endosomal targeting of ESCRT-III proteins, and also help set up systems to screen cellular factors to control ESCRT-III assembly on the endosomal membrane.

Determine mechanisms to disassemble the core of ESCRT-III polymers - interaction of VPS4 with CHMP4

ESCRT-III is disassembled by the AAA ATPase VPS4. A subset of ESCRT-III proteins contain the MIT domain interacting motif1 (MIM1) at their extreme C-termini (α6 region) while CHMP6/Vps20 has the MIM2 within the linker between α5 and α6 (20, 21, 47). It is less clear how CHMP4/Snf7 interacts with VPS4 although CHMP4/Snf7 is thought to be a main component of ESCRT-III polymers (5). It has been suggested that CHMP4 also has the MIM2 similar to CHMP6; however, binding affinity between the MIM2 and the MIT domain is very weak (47). In detail, the dissociation constants (Kd) for CHMP1B MIM1 and CHMP6 MIM2 to the VPS4A MIT domain are 5- 20μM, while Kd for CHMP4A MIM2 to the VPS4A MIT domain is about 250μM (47).

Interestingly, my preliminary data points to a more internal region than the MIM2 in CHMP4 as a potential VPS4 binding site. When the dominant negative mutant VPS4 (VPS4B(E235Q)) was coexpressed with CHMP4A 1-181 (α1-α5, lacking both MIM1 and

MIM2), the mutant VPS4B accumulated on the rim of the enlarged endosomal vesicles delineated by CHMP4A 1-181 (Fig. 5-2A). VPS4B(E235Q), however, was not recruited by CHMP4A 1-147 (α1-α4). The mutant VPS4B also co-localized well with CHMP4A 20-181 but not with 20-147 (Fig. 5-2A). Because the localization of CHMP4A 20-181 differs strikingly from that of 1-181 and from that of VPS4B(E235Q) expressed by itself, the colocalization of 20-181 and VPS4 must reflect an interaction between them (9). The interaction of CHMP4A 1-181 with VPS4B(E235Q) seen by light microscopy was further confirmed by deep-etch electron microscopy (data not shown). Interestingly, a sequence alignment of Snf7/CHMP4 from different species suggests that the α5 region is one of the most highly conserved regions, and contains a MIM-like motif (Fig. 5-2B). Finally, this helix in the CHMP3 crystal structure is packed perpendicular to the core of the protein in what seems likely to be an accessible and regulatory region (46). Together, the predicted α5 appears to be a likely candidate VPS4 binding site.

To define the VPS4 binding site, I would carry out site-directed mutagenesis within the α5 region of CHMP4A. The effects of mutations on CHMP4A binding to VPS4 can be determined by binding assays. I have attempted to carry out a GST pull down assay using bacterially expressed GST-CHMP4A proteins and VPS4B(E235Q). However, the binding between these proteins was too weak to detect their interaction under my assay conditions. One possible change to make would be using VPS4A rather than VPS4B because the binding affinity for CHMP4 to the VPS4A MIT domain is higher than that to the VPS4B MIT domain (47). Alternatively, I could use immunofluorescence analysis similar to that shown in Fig. 5-2A. I would introduce mutations in 20-181 constructs and examine the disruption of co-localization between mutant VPS4 and CHMP4A 20-181 by various mutations in α5 region of CHMP4A 20-181. Finally, The ATPase activity of VPS4 stimulated by different constructs of CHMP4A could be used as

an indicator of the interaction between VPS4 and CHMP4A. Sam Merrill, another student in our lab, has established an *in vitro* VPS4 ATPase assay and showed that CHMP4 could stimulate ATPase activity of VPS4. Characterizing the interaction between VPS4 and CHMP4, a main component of ESCRT-III polymers, will help us understand the precise mechanisms for VPS4 mediated ESCRT-III polymer disassembly.

Determine the role of CHMP5, a regulator in the ESCRT pathway

CHMP5/Vps60 is an ESCRT-III-like protein and proposed to be a regulator of the ESCRT pathway (24, 26, 27, 29, 30). Precisely how CHMP5/Vps60 regulates the ESCRT pathway is not clear. Because it tightly interacts with LIP5/Vta1, it has been suggested that CHMP5/Vps60 acts through LIP5/Vta1 (24, 26, 27, 29, 30, 48-50). Interestingly, cells from CHMP5 knockout mice have enlarged MVBs filled with a number of ILVs such that ILV formation seems to be almost facilitated without CHMP5 (25). Based on my work and from elsewhere, LIP5 interacts preferentially with soluble CHMP5 over polymerized CHMP5 (Fig. 3-8) (29, 48, 50). Together, I hypothesize that CHMP5 sequesters LIP5, a positive regulator of VPS4 in the cytoplasm and thereby functions as a negative regulator of the ESCRT pathway.

To test this hypothesis, I would first determine whether endogenous CHMP5 and LIP5 form a stable complex in the cytoplasm by chemical cross-linking and sucrose gradient analysis. I have characterized antibodies for CHMP5 and LIP5 which are necessary for the experiments (Fig. 4-1 and Table 4-1). To test whether CHMP5 functions via its interaction with LIP5, the specific interaction between CHMP5 and LIP5 should be characterized. In Chapter 3, I found that CHMP5 interacts with the N-terminus of LIP5 via its α5 region (Fig. 3-8) (48). In fact, a small fragment of CHMP5 (27 amino acids) was sufficient for LIP5 binding (Fig. 3-8C). Additionally, a recent crystal structure of Vta1, the yeast ortholog of LIP5, showed that there are two MIT domains at the N-

terminus of Vta1 (51). Thus, I tested the contribution of these MIT domains to interactions with two MIM1 containing ESCRT-III proteins (CHMP1B and CHMP2A) and CHMP5, and found that the MIT1 domain is important for interaction with MIM1 containing ESCRT-III proteins while the MIT2 domain is required for binding to CHMP5 (Fig. 5-3A-C). Interestingly, CHMP5 also contains an MIM-like motif within its α5 region, suggesting that CHMP5 interaction with LIP5 is a variation of MIT-MIM interaction (Fig. 5-3D). To further define the LIP5 binding site in CHMP5, I would examine the interaction of LIP5 with CHMP5 after mutating residues in the MIM-like motif of CHMP5 by site-directed mutagenesis.

To disrupt the interaction between CHMP5 and LIP5 specifically, I would treat cells with a peptide (27 amino acids) from the CHMP5 α5 region sufficient for LIP5 binding or express CHMP5 with mutations within its MIM-like motif in cells. Furthermore, because the MIT2 domain is important for the interaction with CHMP5 but not for binding to other ESCRT-III proteins, I would express LIP5 with mutations in the MIT2 domain in cells. I would then examine the effects of these manipulations on the ESCRT pathway with the various functional assays described in Chapters 2 and 4. I would also analyze the morphology of MVBs after disrupting the interaction of CHMP5 and LIP5, and compare the results to published data showing the effects of knockout of CHMP5 (25). Finally, one could also establish an ESCRT-III disassembly assay and test how CHMP5 affects VPS4 mediated disassembly in the presence of LIP5. Overall, this work will provide insight into the intricate regulation of the ESCRT pathway.

REFERENCES

1. Hurley JH, Im YJ, Lee HH, Ren X, Wollert T, Yang D. Piecing together the ESCRTs. Biochem Soc Trans 2009;37(Pt 1):161-166.

2. Hurley JH. ESCRT complexes and the biogenesis of multivesicular bodies. Curr Opin Cell Biol 2008;20(1):4-11.

3. Raiborg C, Stenmark H. The ESCRT machinery in endosomal sorting of ubiquitylated membrane proteins. Nature 2009;458(7237):445-452.

4. Hanson PI, Roth R, Lin Y, Heuser JE. Plasma membrane deformation by circular arrays of ESCRT-III protein filaments. J Cell Biol 2008;180(2):389-402.

5. Teis D, Saksena S, Emr SD. Ordered assembly of the ESCRT-III complex on endosomes is required to sequester cargo during MVB formation. Dev Cell 2008;15(4):578-589.

6. Ghazi-Tabatabai S, Saksena S, Short JM, Pobbati AV, Veprintsev DB, Crowther RA, Emr SD, Egelman EH, Williams RL. Structure and disassembly of filaments formed by the ESCRT-III subunit Vps24. Structure 2008;16(9):1345-1356.

7. Lata S, Schoehn G, Jain A, Pires R, Piehler J, Gottlinger HG, Weissenhorn W. Helical structures of ESCRT-III are disassembled by VPS4. Science 2008;321(5894):1354-1357.

8. Saksena S, Wahlman J, Teis D, Johnson AE, Emr SD. Functional reconstitution of ESCRT-III assembly and disassembly. Cell 2009;136(1):97-109.

9. Lin Y, Kimpler LA, Naismith TV, Lauer JM, Hanson PI. Interaction of the mammalian endosomal sorting complex required for transport (ESCRT) III protein hSnf7-1 with itself, membranes, and the AAA+ ATPase SKD1. J Biol Chem 2005;280(13):12799-12809.

10. Shim S, Kimpler LA, Hanson PI. Structure/Function Analysis of Four Core ESCRT-III Proteins Reveals Common Regulatory Role for Extreme C-Terminal Domain. Traffic 2007;8(8):1068-1079.

11. Zamborlini A, Usami Y, Radoshitzky SR, Popova E, Palu G, Gottlinger H. Release of autoinhibition converts ESCRT-III components into potent inhibitors of HIV-1 budding. Proc Natl Acad Sci U S A 2006;103(50):19140-19145.

12. Lata S, Roessle M, Solomons J, Jamin M, Gottlinger HG, Svergun DI, Weissenhorn W. Structural basis for autoinhibition of ESCRT-III CHMP3. J Mol Biol 2008;378(4):818-827.

13. Mulgrew-Nesbitt A, Diraviyam K, Wang J, Singh S, Murray P, Li Z, Rogers L, Mirkovic N, Murray D. The role of electrostatics in protein-membrane interactions. Biochim Biophys Acta 2006;1761(8):812-826.

14. Krauss M, Haucke V. Phosphoinositides: regulators of membrane traffic and protein function. FEBS Lett 2007;581(11):2105-2111.

15. Wollert T, Wunder C, Lippincott-Schwartz J, Hurley JH. Membrane scission by the ESCRT-III complex. Nature 2009;458(7235):172-177.

16. Babst M, Katzmann DJ, Estepa-Sabal EJ, Meerloo T, Emr SD. Escrt-III: an endosome-associated heterooligomeric protein complex required for mvb sorting. Dev Cell 2002;3(2):271-282.

17. Babst M, Katzmann DJ, Snyder WB, Wendland B, Emr SD. Endosome-associated complex, ESCRT-II, recruits transport machinery for protein sorting at the multivesicular body. Dev Cell 2002;3(2):283-289.

18. Babst M, Wendland B, Estepa EJ, Emr SD. The Vps4p AAA ATPase regulates membrane association of a Vps protein complex required for normal endosome function. Embo J 1998;17(11):2982-2993.

19. Bishop N, Woodman P. ATPase-defective mammalian VPS4 localizes to aberrant endosomes and impairs cholesterol trafficking. Mol Biol Cell 2000;11(1):227-239.

20. Obita T, Saksena S, Ghazi-Tabatabai S, Gill DJ, Perisic O, Emr SD, Williams RL. Structural basis for selective recognition of ESCRT-III by the AAA ATPase Vps4. Nature 2007;449(7163):735-739.

21. Stuchell-Brereton MD, Skalicky JJ, Kieffer C, Karren MA, Ghaffarian S, Sundquist WI. ESCRT-III recognition by VPS4 ATPases. Nature 2007;449(7163):740-744.

22. Scott A, Gaspar J, Stuchell-Brereton MD, Alam SL, Skalicky JJ, Sundquist WI. Structure and ESCRT-III protein interactions of the MIT domain of human VPS4A. Proc Natl Acad Sci U S A 2005;102(39):13813-13818.

23. Howard TL, Stauffer DR, Degnin CR, Hollenberg SM. CHMP1 functions as a member of a newly defined family of vesicle trafficking proteins. J Cell Sci 2001;114(Pt 13):2395-2404.

24. Shiflett SL, Ward DM, Huynh D, Vaughn MB, Simmons JC, Kaplan J. Characterization of Vta1p, a class E Vps protein in S. cerevisiae. J Biol Chem 2004;279(12):10982-10990.

25. Shim JH, Xiao C, Hayden MS, Lee KY, Trombetta ES, Pypaert M, Nara A, Yoshimori T, Wilm B, Erdjument-Bromage H, Tempst P, Hogan BL, Mellman I, Ghosh S. CHMP5 is essential for late endosome function and down-regulation of receptor signaling during mouse embryogenesis. J Cell Biol 2006;172(7):1045-1056.

26. Rue SM, Mattei S, Saksena S, Emr SD. Novel Ist1-Did2 Complex Functions at a Late Step in MVB Sorting. Mol Biol Cell 2008;19(2):475-484.

27. Dimaano C, Jones CB, Hanono A, Curtiss M, Babst M. Ist1 regulates Vps4 localization and assembly. Mol Biol Cell 2008;19(2):465-474.

28. Scott A, Chung HY, Gonciarz-Swiatek M, Hill GC, Whitby FG, Gaspar J, Holton JM, Viswanathan R, Ghaffarian S, Hill CP, Sundquist WI. Structural and mechanistic studies of VPS4 proteins. Embo J 2005;24(20):3658-3669.

29. Ward DM, Vaughn MB, Shiflett SL, White PL, Pollock AL, Hill J, Schnegelberger R, Sundquist WI, Kaplan J. The role of LIP5 and CHMP5 in multivesicular body formation and HIV-1 budding in mammalian cells. J Biol Chem 2005;280(11):10548-10555.

30. Azmi I, Davies B, Dimaano C, Payne J, Eckert D, Babst M, Katzmann DJ. Recycling of ESCRTs by the AAA-ATPase Vps4 is regulated by a conserved VSL region in Vta1. J Cell Biol 2006;172(5):705-717.

31. Bieniasz PD. Late budding domains and host proteins in enveloped virus release. Virology 2006;344(1):55-63.

32. Demirov DG, Freed EO. Retrovirus budding. Virus Res 2004;106(2):87-102.

33. Gottlinger HG, Dorfman T, Sodroski JG, Haseltine WA. Effect of mutations affecting the p6 gag protein on human immunodeficiency virus particle release. Proc Natl Acad Sci U S A 1991;88(8):3195-3199.

34. Demirov DG, Orenstein JM, Freed EO. The late domain of human immunodeficiency virus type 1 p6 promotes virus release in a cell type-dependent manner. J Virol 2002;76(1):105-117.

35. Barr FA, Gruneberg U. Cytokinesis: placing and making the final cut. Cell 2007;131(5):847-860.

36. Carlton JG, Martin-Serrano J. Parallels between cytokinesis and retroviral budding: a role for the ESCRT machinery. Science 2007;316(5833):1908-1912.

37. Morita E, Sandrin V, Chung HY, Morham SG, Gygi SP, Rodesch CK, Sundquist WI. Human ESCRT and ALIX proteins interact with proteins of the midbody and function in cytokinesis. Embo J 2007;26(19):4215-4227.

38. Praefcke GJ, McMahon HT. The dynamin superfamily: universal membrane tubulation and fission molecules? Nat Rev Mol Cell Biol 2004;5(2):133-147.

39. Komada M, Soriano P. Hrs, a FYVE finger protein localized to early endosomes, is implicated in vesicular traffic and required for ventral folding morphogenesis. Genes Dev 1999;13(11):1475-1485.

40. Misra S, Hurley JH. Crystal structure of a phosphatidylinositol 3-phosphate-specific membrane-targeting motif, the FYVE domain of Vps27p. Cell 1999;97(5):657-666.

41. Stahelin RV, Long F, Diraviyam K, Bruzik KS, Murray D, Cho W. Phosphatidylinositol 3-phosphate induces the membrane penetration of the FYVE domains of Vps27p and Hrs. J Biol Chem 2002;277(29):26379-26388.

42. Slagsvold T, Aasland R, Hirano S, Bache KG, Raiborg C, Trambaiolo D, Wakatsuki S, Stenmark H. Eap45 in mammalian ESCRT-II binds ubiquitin via a phosphoinositide-interacting GLUE domain. J Biol Chem 2005;280(20):19600-19606.

43. Teo H, Gill DJ, Sun J, Perisic O, Veprintsev DB, Vallis Y, Emr SD, Williams RL. ESCRT-I core and ESCRT-II GLUE domain structures reveal role for GLUE in linking to ESCRT-I and membranes. Cell 2006;125(1):99-111.

44. Im YJ, Hurley JH. Integrated structural model and membrane targeting mechanism of the human ESCRT-II complex. Dev Cell 2008;14(6):902-913.

45. Whitley P, Reaves BJ, Hashimoto M, Riley AM, Potter BV, Holman GD. Identification of mammalian Vps24p as an effector of phosphatidylinositol 3,5-bisphosphate-dependent endosome compartmentalization. J Biol Chem 2003;278(40):38786-38795.

46. Muziol T, Pineda-Molina E, Ravelli RB, Zamborlini A, Usami Y, Gottlinger H, Weissenhorn W. Structural basis for budding by the ESCRT-III factor CHMP3. Dev Cell 2006;10(6):821-830.

47. Kieffer C, Skalicky JJ, Morita E, De Domenico I, Ward DM, Kaplan J, Sundquist WI. Two distinct modes of ESCRT-III recognition are required for VPS4 functions in lysosomal protein targeting and HIV-1 budding. Dev Cell 2008;15(1):62-73.

48. Shim S, Merrill S, Hanson PI. Novel Interactions of ESCRT-III with LIP5 and VPS4 and their implications for ESCRT-III disassembly. Mol Biol Cell 2008;19(6):2661-2672.
49. Azmi IF, Davies BA, Xiao J, Babst M, Xu Z, Katzmann DJ. ESCRT-III family members stimulate Vps4 ATPase activity directly or via Vta1. Dev Cell 2008;14(1):50-61.
50. Ma YM, Boucrot E, Villen J, Affar el B, Gygi SP, Gottlinger HG, Kirchhausen T. Targeting of AMSH to endosomes is required for epidermal growth factor receptor degradation. J Biol Chem 2007;282(13):9805-9812.
51. Xiao J, Xia H, Zhou J, Azmi IF, Davies BA, Katzmann DJ, Xu Z. Structural basis of Vta1 function in the multivesicular body sorting pathway. Dev Cell 2008;14(1):37-49.

FIGURE LEGENDS

Figure 5-1 Co-localization of FYVE domain with C-terminally truncated CHMP2A.

COS7 cells transfected with 2x FYVE-GFP alone or cotransfected with 2xFYVE-GFP and FLAG-CHMP2A 1-180 (α1-α5) were immunostained with anti-FLAG antibody and analyzed by epifluorescence microscopy. GFP signal was visualized without staining. Subcellular localization 2x FYVE and CHMP2A are shown in the left (green) and middle (red) panel respectively. Merge image is shown in the right panel.

Figure 5-2 VPS4 binding site in CHMP4A.

(A) COS-7 cells co-transfected with VPS4B(EQ)-GFP and indicated FLAG-CHMP4A constructs were immunostained with anti-FLAG antibody and viewed by epifluorescence microscopy. GFP signal was visualized without staining. Subcellular localization of VPS4B(E235Q)-GFP and CHMP4A are shown in the left (green) and middle (red) panel respectively. Merged images are shown in the right panel. (B) Sequence alignment of α5 region of CHMP4/Snf7 from different species.

Figure 5-3 Differential contribution of two MIT domains in LIP5 to interaction of ESCRT-III proteins.

(A-B) Interaction of MIM1 containing ESCRT-III proteins (CHMP2A and CHMP1B) with LIP5 MIT domains. Shown is GST pull down with purified GST-CHMP2A C-terminal half (residue 117-222) or GST-CHMP1B C-terminal half (residue 106-199) and HEK293T cell lysate containing GFP-LIP5. Critical residues in MIT1 and MIT2 domains in LIP5 were mutated into alanine (Met64 in MIT1 domain, Lys148 in MIT2 domain). (C) Interaction of CHMP5 with LIP5 MIT domains. GFP-LIP5 was immunoprecipitated from soluble lysate

of HEK293T cells cotransfected with FLAG-CHMP5 and GFP-LIP5. Bound proteins and lysate were analyzed by immunoblotting. (D) Sequence alignment of α5 region of human CHMP5 and yeast Vps60.

Figure 5-1

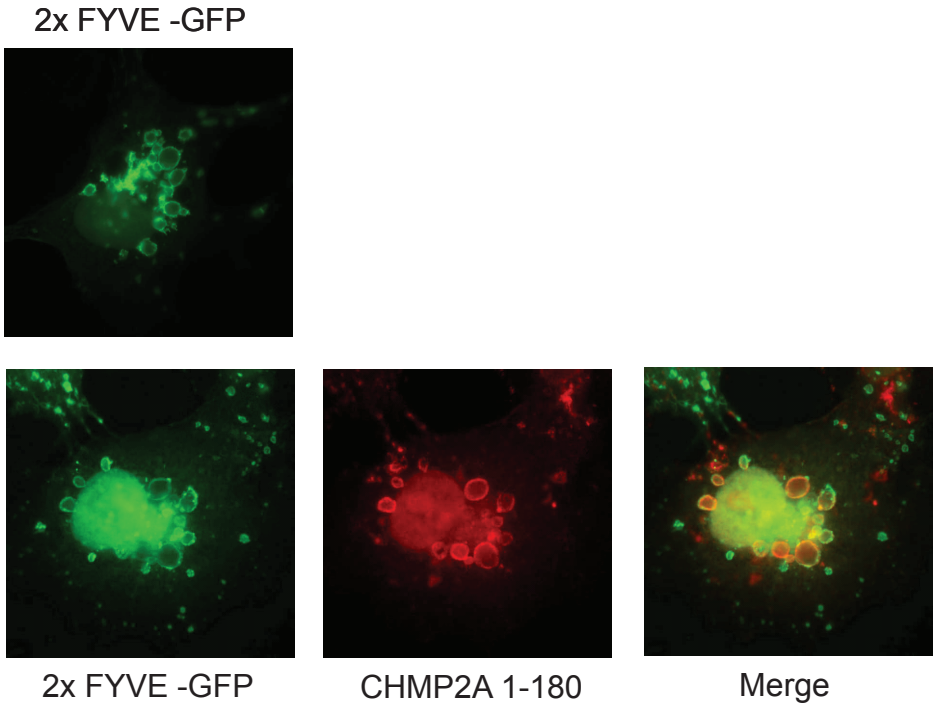

Figure 5-2

A

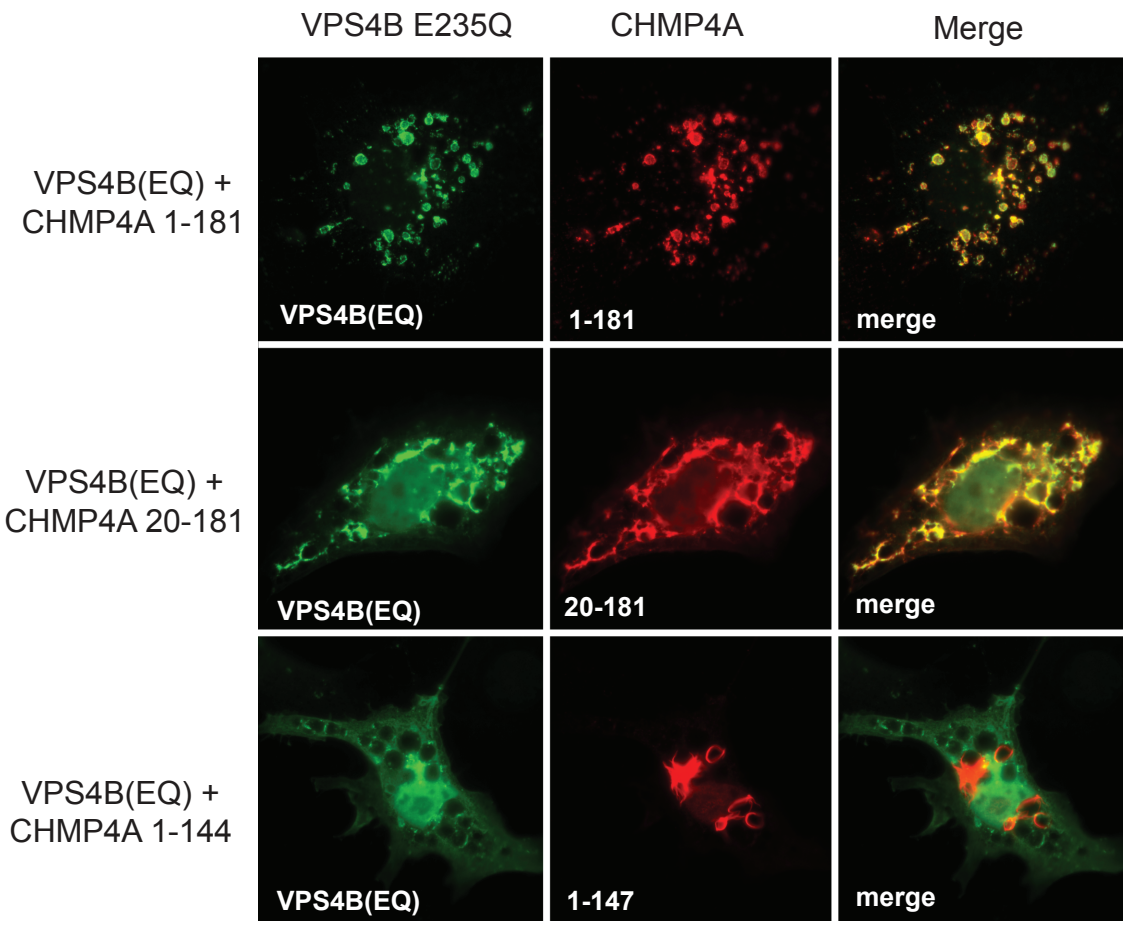

B

```
          MIM1          ---LxxRLAAL+
     consensus        DEDELxxEL-ELEQ
       Sc-Snf7  TGANEVDEDELDEELDMLAQENANQET
     hu-CHMP4A  GFGDDVDEDELLEELEELEQEELAQEL
     hu-CHMP4B  GFGEEFDEDELMAELEELEQEELDKNL
     hu-CHMP4C  GFGDDFDEDELMAELEELEQEELNKKM
     AraCHMP4A  GAAADFDEDELAAELDELESEELESQL
     AraCHMP4B  GAN-DFDEDELEAELDELEGAELEEQL
     Fly-Shurb  AFGADLDDEDLERELDELEQENFDKEI
                          α5
```

Figure 5-3

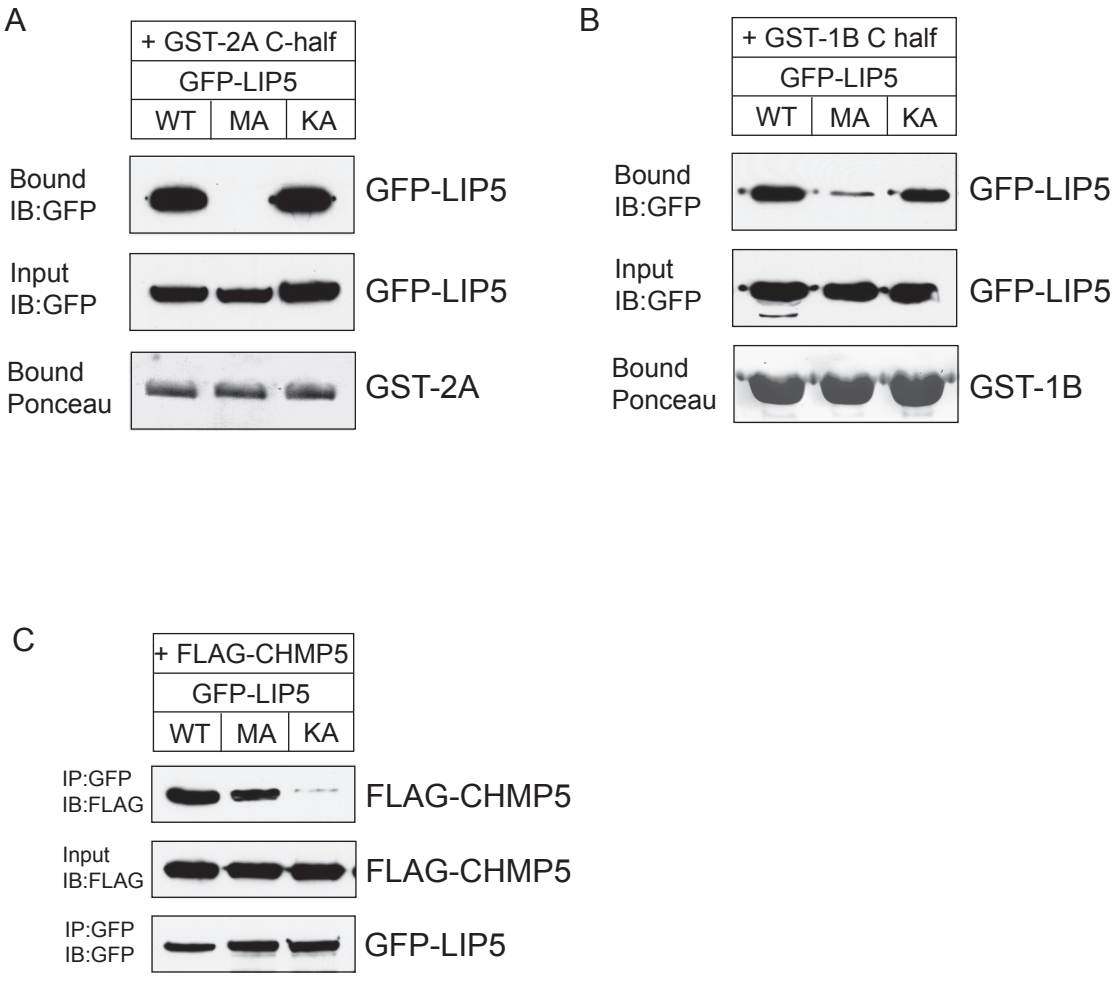
A
+ GST-2A C-half
GFP-LIP5
WT
MA
KA
Bound IB:GFP
GFP-LIP5
Input IB:GFP
GFP-LIP5
Bound Ponceau
GST-2A
B
+ GST-1B C half
GFP-LIP5
WT
MA
KA
Bound IB:GFP
GFP-LIP5
Input IB:GFP
GFP-LIP5
Bound Ponceau
GST-1B
C
+ FLAG-CHMP5
GFP-LIP5
WT
MA
KA
IP:GFP IB:FLAG
FLAG-CHMP5
Input IB:FLAG
FLAG-CHMP5
IP:GFP IB:GFP
GFP-LIP5
D
MIM1 ---LxxRLAAL+
ScVps60 GELDDISDAELDAELDALQEDFTLPTSENS
huCHMP5 YGTPELDEDDLEAELDALGDELLADEDSSY
α5

Appendix 1

CHMP4B, a novel gene for autosomal dominant cataracts linked to chromosome 20q (Am J. Hum. Genet., 2007 81(3):596-606).

REPORT

CHMP4B, a Novel Gene for Autosomal Dominant Cataracts Linked to Chromosome 20q

Alan Shiels, Thomas M. Bennett, Harry L. S. Knopf, Koki Yamada, Koh-ichiro Yoshiura, Norio Niikawa, Soomin Shim, and Phyllis I. Hanson

Cataracts are a clinically diverse and genetically heterogeneous disorder of the crystalline lens and a leading cause of visual impairment. Here we report linkage of autosomal dominant "progressive childhood posterior subcapsular" cataracts segregating in a white family to short tandem repeat (STR) markers *D20S847* (LOD score [*Z*] 5.50 at recombination fraction [θ] 0.0) and *D20S195* ($Z = 3.65$ at $\theta = 0.0$) on 20q, and identify a refined disease interval (*rs2057262*–(3.8 Mb)–*rs1291139*) by use of single-nucleotide polymorphism (SNP) markers. Mutation profiling of positional-candidate genes detected a heterozygous transversion (c.386A→T) in exon 3 of the gene for chromatin modifying protein-4B (*CHMP4B*) that was predicted to result in the nonconservative substitution of a valine residue for a phylogenetically conserved aspartic acid residue at codon 129 (p.D129V). In addition, we have detected a heterozygous transition (c.481G→A) in exon 3 of *CHMP4B* cosegregating with autosomal dominant posterior polar cataracts in a Japanese family that was predicted to result in the missense substitution of lysine for a conserved glutamic acid residue at codon 161 (p.E161K). Transfection studies of cultured cells revealed that a truncated form of recombinant D129V-CHMP4B had a different subcellular distribution than wild type and an increased capacity to inhibit release of virus-like particles from the cell surface, consistent with deleterious gain-of-function effects. These data provide the first evidence that *CHMP4B,* which encodes a key component of the endosome sorting complex required for the transport-III (ESCRT-III) system of mammalian cells, plays a vital role in the maintenance of lens transparency.

Hereditary forms of cataracts are usually diagnosed at birth (congenital), during infancy, or during childhood and are clinically important as a cause of impaired form vision development.[1] In addition to being found in >50 genetic syndromes involving other ocular defects (e.g., microphthalmia [MIM 212550]) and systemic abnormalities (e.g., galactokinase deficiency [MIM 230200]), cataracts may be inherited as an isolated lens phenotype, most frequently by autosomal dominant transmission.[2] So far, genetic linkage studies of >60 families worldwide have mapped at least 25 independent loci for clinically diverse forms of nonsyndromic cataracts on 15 human chromosomes, involving some 17 lens-abundant genes.[2] The majority of associated mutations have been identified in 10 crystallin genes (*CRYAA* [MIM 123580], *CRYAB* [MIM 123590], *CRYBB1* [MIM 600929], *CRYBB2* [MIM 123620], *CRYBB3* [MIM 123630], *CRYBA1* [MIM 123610], *CRYBA4* [MIM 123631], *CRYGC* [MIM 123680], *CRYGD* [MIM 123690], and *CRYGS* [MIM 123730]),[3–11] which encode the major "refractive" proteins of the lens. The remaining mutations have been identified in seven functionally diverse genes, including those coding for gap-junction connexin proteins (*GJA3* [MIM 121015], *GJA8* [MIM 600897]),[12,13] a heat-shock transcription factor (*HSF4* [MIM 602438]),[14] an aquaporin water channel (*MIP* [MIM 154050])[15] a claudin-like cell-junction protein (*LIM2* [MIM 154045]),[16] and intermediate-filament-like cytoskeletal proteins (*BFSP1* [MIM 603307], *BFSP2* [MIM 603212]).[17,18] In addition to the known genes, at least 10 novel genes for autosomal dominant or recessive forms of nonsyndromic cataracts remain to be identified at loci on chromosomes 1 (CCV [MIM 115665], CTPP1 [MIM 116600]), 2 (PCC [MIM 601286], CCNP [MIM 607304, MIM 115800]), 3 (CATC2 [MIM 610019]), 9 (CAAR [MIM 605749]), 15 (CCSSO [MIM 605728]), 17 (CTAA2 [MIM 601202], CCA1 [MIM 115660]), 19 (CATCN1 [MIM 609376]), and 20 (CPP3 [MIM 605387]).[19–32] Here we have fine-mapped a locus for autosomal dominant cataracts on chromosome 20q and, subsequently, have identified underlying missense mutations in the gene for chromatin modifying protein-4B (*CHMP4B* [MIM 610897]), also known as charged multivesicular body protein-4B, which has not previously been associated with human disease.

Linkage studies.—We investigated a six-generation white family from the United States (family Sk) segregating autosomal dominant progressive childhood posterior subcapsular cataracts (PCPSC) in the absence of other ocular or systemic abnormalities (fig. 1*A*). Ophthalmic records indicated that the cataracts presented in both eyes as disc-shaped posterior subcapsular opacities, progressing with age to affect the nucleus and anterior subcapsular regions of the lens (fig. 1*B*). The age at diagnosis varied from 4 to

From the Departments of Ophthalmology and Visual Sciences (A.S.; T.M.B.; H.L.S.K.), Genetics (A.S.), and Cell Biology and Physiology (S.S.; P.I.H.), Washington University School of Medicine, St. Louis, MO; and the Departments of Ophthalmology and Visual Sciences (K.Y.), and Human Genetics (K-i.Y.; N.N), Nagasaki University Graduate School of Biomedical Sciences, Nagasaki, Japan

Received March 9, 2007; accepted for publication May 9, 2007; electronically published July 27, 2007.

Address for correspondence and reprints: Dr. Alan Shiels, Department of Ophthalmology and Visual Sciences, Campus Box 8096, Washington University School of Medicine, 660 South Euclid Avenue, St. Louis, MO 63110. E-mail: shiels@vision.wustl.edu

Am. J. Hum. Genet. 2007;81:596–606. 0002-9297/2007/8103-0017$15.00
DOI: 10.1086/519980

20 years, and the age at surgery ranged from 4 to 40 years. Postsurgical corrected visual acuity varied from 20/20 to 20/200 in the better eye. Blood samples were obtained from 27 family members, and leukocyte genomic DNA was purified and quantified using standard techniques (Qiagen). Ethical approval for this study was obtained from the Washington University Human Research Protection Office, and written informed consent was provided by all participants prior to enrollment, in accordance with the tenets of the Declaration of Helsinki.

For linkage analysis, 15 affected individuals, 8 unaffected individuals, and 4 spouses from family Sk were genotyped using STR markers from the combined Généthon, Marshfield, and deCODE genetic linkage maps (National Center for Biotechnology Information [NCBI]), as described elsewhere.[33] Following exclusion of linkage to known loci for autosomal dominant cataracts on chromosomes 1–3, 10–13, 15–17, 19, 21, and 22 (table 1), we obtained significant evidence of linkage (table 2) for markers *D20S847* ($Z = 5.50$ and $\theta = 0$), *D20S195* ($Z = 3.65$ and $\theta = 0$), and *D20S870* ($Z = 3.11$ and $\theta = 0$).

Haplotype analysis detected seven recombinant individuals within the Sk pedigree (fig. 1*A*). First, two affected females, VI:4 and VI:6, were obligate recombinants, proximally at *D20S885* and distally at *D20S855,* respectively. Second, three affected females (IV:1, IV:4, and V:3) and one affected male (VI:1) were obligate recombinants distally at *D20S834.* Third, one affected female (V:3) and her affected son (VI:1) were obligate recombinants proximally at *D20S837.* However, with the exception of individual V:5 (see below), no further recombinant individuals were detected at four other intervening STR markers, suggesting that the cataract locus lay in the physical interval, *D20S837*–(4.7 Mb)–*D20S834.*

At the time of our study, individual V:5 was 17 years of age and phenotypically unaffected; however, he inherited the complete disease haplotype (fig. 1*A*), suggesting that he was either nonpenetrant or presymptomatic for cataracts. The two-point LOD scores shown in table 2 were calculated with the assumption of unaffected status for individual V:5 and 95% penetrance in family Sk; however, even when 100% penetrance was assumed, we still retained significant evidence of linkage proximally at *D20S195* ($Z_{max} = 4.31$ at $\theta_{max} = 0.04$) and distally at *D20S847* ($Z_{max} = 5.08$ at $\theta_{max} = 0.04$). Conversely, if individual V:5 developed cataracts later in life, perhaps extending the age-at-onset range in family Sk, and was included with the assumption of preaffected status and 100% penetrance, we would obtain enhanced evidence for linkage (*D20S195,* $Z_{max} = 5.12$ at $\theta_{max} = 0.0$; *D20S847,* $Z_{max} = 6.97$ at $\theta_{max} = 0.0$). However, regardless of whether individual V:5 was included or excluded, we found no evidence of linkage at other candidate genes or loci for autosomal dominant cataracts (table 1).

To further refine the disease interval, we genotyped family Sk with biallelic SNP markers (NCBI) located within the STR interval using conventional dye-terminator cycle-sequencing chemistry (Applied Biosystems). Critical affected individuals IV:1, IV:4, and V:3 were also found to be recombinant at SNP marker *rs1291139* (A/T), which lies ~0.5 Mb centromeric to *D20S834.* Similarly, critical affected individuals V:3, and VI:1 were also recombinant at marker *rs2057262* (A/C) located ~0.4 Mb telomeric to *D20S837* (fig. 1*A*). However, individual V:5 excepted, no further recombination events were detected at intervening SNP markers, indicating that the cataract locus lay in the reduced (~0.9 Mb) physical interval, *rs2057262*–(3.8 Mb)–*rs1291139* (fig. 1*C*).

Mutation analysis.—The refined SNP interval contained ~80 positional-candidate genes, none of which were obvious functional candidates for cataracts in family Sk (NCBI Map Viewer). We prioritized genes for mutation analysis of exons and intron boundaries (splice sites) on the basis of three main criteria.

1. NCBI reference sequence status, with those genes designated "reviewed" or "provisional" selected over those designated "model" or "pseudogene."
2. Evidence of expression in (fetal) eye, from the UniGene EST database.
3. Number of exons or amplicons required for coverage of the coding region, starting with smaller genes first.

Resequencing analysis of individuals IV:5, V:6, V:10, and VI:6 from the Sk pedigree (fig. 1*A*) excluded the presence of coding or splice-site mutations in eight genes (data not shown), including *EPB41L1* (MIM 602879), *E2F1* (MIM 189971), *ZNF341, PXMP4, ITGB4BP* (MIM 602912), *APBA2BP, SCAND1* (MIM 610416), and *DYNLRB1* (MIM 607167). However, resequencing of a 5-exon gene symbolized *CHMP4B* (GeneID: 128866) identified a heterozygous c.386A→T transversion in exon 3 that was not present in wild type (fig. 2*B*). This single-nucleotide change did not result in the gain or loss of a convenient restriction site; therefore, we designed allele-specific (A/T) PCR analysis to confirm that the mutant "T" allele cosegregated with affected but not unaffected members of family Sk, with the exception of individual V:5 (fig. 2*C*). Furthermore, when we tested the c.386A→T transversion as a biallelic marker, with a notional allelic frequency of 1%, in a two-point LOD score analysis of the cataract locus (table 2) we obtained further compelling evidence of linkage ($Z = 6.52$ at $\theta = 0$). In addition, we confirmed that the c.386A→T transversion was not listed in the NCBI SNP database (dbSNP), and we excluded it as a SNP in a panel of 192 normal, unrelated individuals (i.e., 384 chromosomes), using the allele-specific PCR analysis described in fig. 2*C* (data not shown). Although it is possible that an undetected mutation lay elsewhere within the disease-haplotype interval (3.8 Mb), our genotype data strongly suggested that the c.386A→T transversion in exon 3 of *CHMP4B* represented a causative mutation rather than a benign SNP in linkage disequilibrium with the cataract phenotype.

To verify that the c.386A→T transversion in *CHMP4B*

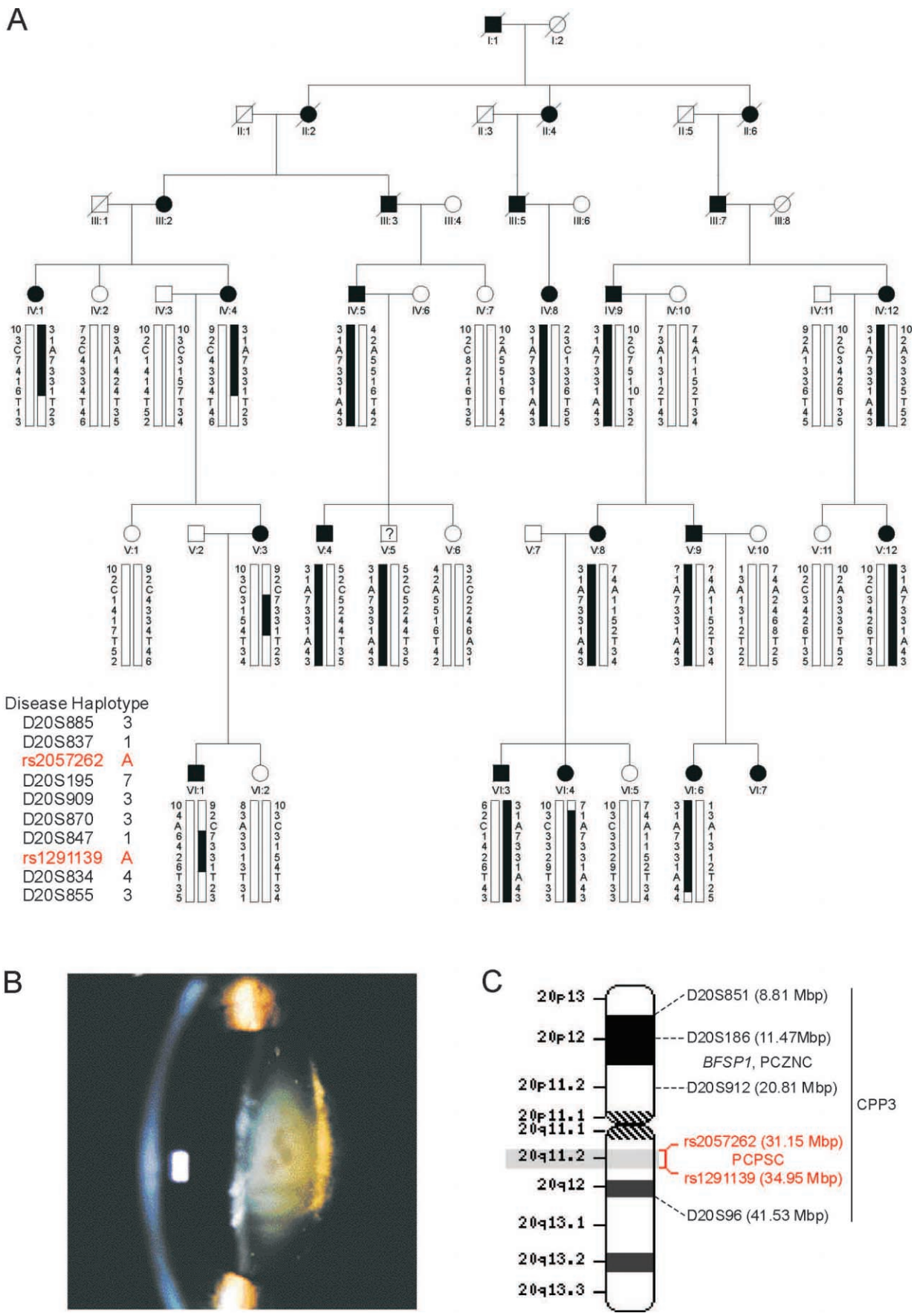
A
I:1
I:2
II:1
II:2
II:3
II:4
II:5
II:6
III:1
III:2
III:3
III:4
III:5
III:6
III:7
III:8
IV:1
IV:2
IV:3
IV:4
IV:5
IV:6
IV:7
IV:8
IV:9
IV:10
IV:11
IV:12
V:1
V:2
V:3
V:4
V:5
V:6
V:7
V:8
V:9
V:10
V:11
V:12
VI:1
VI:2
VI:3
VI:4
VI:5
VI:6
VI:7
Disease Haplotype
D20S885 3
D20S837 1
rs2057262 A
D20S195 7
D20S909 3
D20S870 3
D20S847 1
rs1291139 A
D20S834 4
D20S855 3
B
C
20p13
20p12
20p11.2
20p11.1
20q11.1
20q11.2
20q12
20q13.1
20q13.2
20q13.3
D20S851 (8.81 Mbp)
D20S186 (11.47Mbp)
BFSP1, PCZNC
D20S912 (20.81 Mbp)
rs2057262 (31.15 Mbp)
PCPSC
rs1291139 (34.95 Mbp)
D20S96 (41.53 Mbp)
CPP3

was present at the RNA transcript level in family Sk, we performed allele-specific RT-PCR analysis of peripheral blood leukocytes (PBLs), which have been shown to express *CHMP4B*.[35] PCR primers (table 3) were designed to amplify the entire coding region of *CHMP4B* (codons 1–224) in the presence of a nested mutant (T allele) primer to detect heterozygosity in three consenting relatives, including individual V:5 (fig. 3*A*). The affected father (IV:5) and his son (V:5) were heterozygous for the wild-type (A allele) and mutant (T allele) transcripts, whereas his unaffected daughter (V:6) was homozygous for the wild-type (A allele) transcript. To gain a more accurate comparison of wild-type versus mutant CHMP4B transcript levels in PBL RNA, we then performed quantitative (q)RT-PCR with SYBR Green-1 in real time (fig. 3*B*), using a sense anchor primer paired with either a mutant (T allele) or wild-type (A allele) primer (table 3). When standardized against transcript levels for the midabundance ribosomal protein-L19 (RPL19), the ratio of wild-type to mutant CHMP4B transcripts was estimated to be 60(A):40(T), suggesting decreased expression and/or increased turnover of the mutant transcript in affected individuals. Overall, the transcript and genotype data are consistent for these individuals (fig. 1*A* and fig. 3*A*) and support the view that the clinically unaffected son (V:5) is either presymptomatic or nonpenetrant for the cataract phenotype. Moreover, the ability to amplify the intact coding region of CHMP4B transcripts from affected individuals was consistent with correct mRNA splicing, suggesting that the c.386A→T transversion, which is located near the beginning of exon 3, did not activate a cryptic splice site.[36] Finally, we also confirmed that the intact coding region of CHMP4B transcripts could be amplified from human and mouse post mortem lenses (fig. 3*C*), consistent with a functional role for CHMP4B in lens biology.

CHMP4B is cytogenetically distinct from *BFSP1* and an interval on 20p (fig. 1*C*) that was linked recently with autosomal dominant progressive congenital zonular nuclear cataract (PCZNC) segregating in a Chinese family.[32] However, *CHMP4B* is located within a much larger region spanning 20p12–20q12 that was previously linked with autosomal dominant posterior polar cataract (CPP3 [MIM 605387]) segregating in a Japanese family.[31] Like the cataracts in family Sk, CPP3 was characterized by a juvenile onset and progressive disc-shaped posterior subcapsular opacities along with some cortical opacification.[37] To investigate the possibility of allelism, we performed a similar mutation screen of *CHMP4B* in the CPP3 family and identified a heterozygous c.481G→A transition in exon 3 that was not present in wild type (fig. 4*A* and 4*B*) or in the SNP database. This single-nucleotide change removed an adjacent *Mnl*1 restriction enzyme-site, and restriction fragment length analysis confirmed that the heterozygous A allele cosegregated with affected members of the CPP3 family but was not present in unaffected relatives or our control panel (fig. 4*C* and data not shown). The identification of a second coding nucleotide change in a geographically and ethnically distinct family provided strong supporting evidence for *CHMP4B* as the causative gene for cataracts linked to 20q. In addition, the locus for lens opacity-4 (*Lop4*)[38] has been linked to a region of murine chromosome 2 that is syntenic with human 20q11.2 raising the possibility of a mouse model for the cataracts described here.

CHMP4B encodes a highly charged helical protein (~25 kDa) with N-terminal basic and C-terminal acidic halves (fig. 5*B*). The c.386A→T transversion in exon 3 occurred at the second base of codon 129 (G<u>A</u>T→G<u>T</u>T), and is predicted to result in the missense substitution of aspartic acid to valine (p.D129V) at the level of translation. Similarly, the c.481G→A transition occurred at the first base of codon 161 (<u>G</u>AG→<u>A</u>AG) of exon 3, and is predicted to translate as a missense substitution of glutamic acid to lysine (p.E161K). Cross-species alignment of the amino acid sequences for CHMP4B present in the Entrez Protein database, performed by means of ClustalW, revealed that p.D129 and p.E161 are phylogenetically conserved from yeast to man (fig. 5*C*). Moreover, the predicted p.D129V and p.E161K substitutions represented nonconservative amino acid changes, with the acidic side-group ($-CH_2COOH$) of aspartic acid replaced by the neutral, hydrophobic side-group ($-CH-C_2H_6$) of valine, and the acidic side-group ($-C_2H_4COOH$) of glutamic acid replaced by the basic side-group ($-C_4H_8NH_2$) of lysine, respectively, suggestive of functional consequences.

Functional expression studies.—Eleven CHMP genes have been identified in the human genome and, on the basis of phylogenetic analyses, have been divided into seven subfamilies, some with multiple members.[39,40] CHMP4B is one of three human orthologs of yeast Snf7/Vps32 (<u>s</u>ucrose <u>n</u>on-<u>f</u>ermenting-7 or <u>v</u>acuolar <u>p</u>rotein <u>s</u>orting-32), which functions in protein sorting and transport in the endosome-lysosome pathway.[39] In the current model, CHMP4B is a core subunit of the endosomal-sorting com-

Figure 1. Autosomal dominant PCPSC in a six-generation family (Sk). *A,* Pedigree and haplotype analysis showing segregation of eight STR markers and two SNP markers on 20q, listed in descending order from the centromere. Squares and circles denote males and females, respectively. Filled symbols and bars denote affected status and haplotypes, respectively. Individual V:5 is marked with a question mark (?) to denote unknown status. Pedigree and haplotype data were managed using Cyrillic 2.1 software (FamilyGenetix). *B,* Slit-lamp image of lens from affected female V:12 (age 40 years) showing posterior subcapsular, nuclear, and anterior subcapsular opacities. *C,* Ideogram of chromosome 20, comparing the cytogenetic location of SNP markers defining the PCPSC locus in this study (*red*) with those of STR markers defining loci for CPP3 and PCZNC.[31,32]

Table 1. Two-point LOD scores (*Z*) Showing Exclusion of Linkage between the Autosomal Dominant Cataract Locus and STR Markers near Candidate Genes or Loci on Chromosomes Other Than 20

Marker	Z^a	θ	Chromosome	Gene/Locus
D1S243	−2.77	.10	1p36	CCV, CPP1
D1S214	−2.93	.10		
D1S2748	−2.14	.20	1p32	*FOXE3*[MIM 601094]
D1S305	−2.01	.20	1q21	*GJA8*
D2S2333	−2.35	.20	2p12	CCNP
D2S128	−3.19	.05	2q32-q36	*CRYGC*, *CRYGD*, *CRYBA2*
D2S2248	−2.75	.20		
D3S1768	−∞	.00	3p21.1-p21.3	CATC2
D3S3564	−2.34	.05		
D3S1292	−1.76	.05	3q22.1	*BFSP2*
D3S3686	−4.04	.10	3q27.2	*CRYGS*
D5S2014	−2.05	.05	5q33.1	*SPARC* [MIM 182120]
D6S1710	−2.37	.05	6q12	*GLULD1*
D9S303	−1.31	.05	9q21.31	CAAR
D9S1120	−1.28	.05		
D10S566	−2.94	.10	10q24-q25	*PITX3*[MIM 602669]
D10S1697	−3.01	.10		
D11S4154	−2.63	.05	11p13	*PAX6* [MIM 607108]
D11S4192	−2.55	.10	11q23.1	*CRYAB*
D11S1347	−3.28	.05		
D12S368	−1.94	.10	12q13.3	*MIP*
D13S175	−2.34	.05	13q11	*GJA3*
D14S1047	−2.12	.05	14q24.3	*CHX10*[MIM 142993]
D15S209	−3.14	.05	15q21-q22	CCSSO
D15S1036	−2.41	.20		
D16S412	−2.51	.10	16p12.3	*CRYM*[MIM 123740]
D16S3095	−2.99	.10	16q22.1	*HSF4*
D17S1840	−2.45	.05	17p13	CTAA2
D17S796	−2.13	.10		
D17S799	−1.79	.05	17q11.2	*CRYBA1*
D17S798	−1.18	.05		
D17S785	−2.14	.10	17q24	*GALK1*[MIM 604313]
D17S802	−1.91	.05	17q24	CCA1
D17S784	−2.67	.10		
D19S412	−2.41	.15	19q13	*LIM2*
D20S112	2.58	.08	20p11.23	*BFSP1*
D20S885	2.71	.10	20p12–20q12	CPP3
D20S847	5.08	.04		
D21S1259	−2.78	.10	21q22.3	*CRYAA*
D21S1885	−.81	.00		
D22S1154	−2.20	.15	22q11.23-q21.1	*CRYBA4*, *CRYBB1-4*

[a] A gene frequency of 0.0001 and a penetrance of 100% were assumed for the disease locus.

plex required for transport-III (ESCRT-III), which facilitates the biogenesis of multivesicular bodies (MVBs).[39] The only CHMP gene so far implicated in human disease is *CHMP2B* (yeast ortholog Vps2/Did4 [MIM 609512]), which has been reported to harbor mutations infrequently associated with frontotemporal dementia (FTD [MIM 600795]) and amyotropic lateral sclerosis (ALS [MIM 609512]).[41–43]

CHMP4B is found diffusely throughout the cytoplasm and/or in association with endosome-like compartments when expressed in cultured mammalian cells.[44,45] To determine the effect of the p.D129V substitution on the subcellular distribution of CHMP4B, we transfected African green monkey kidney (COS-7) cells with expression plasmids[46] encoding either wild-type or mutant forms of CHMP4B tagged at the N-terminus with the FLAG epitope. Immunofluorescence microscopy with FLAG antibody revealed that full-length wild-type (FLAG-CHMP4B) and mutant protein (FLAG-D129V-CHMP4B) were diffusely distributed (fig. 6*A* and 6*B*). At higher expression levels, both were associated with endosome-like compartments (data not shown). Overall, there were no notable differences in the subcellular localization of wild type and

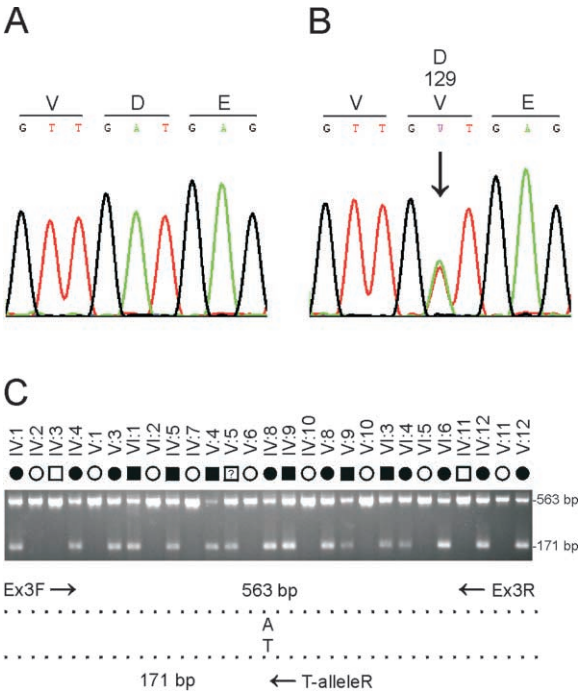

Figure 2. Mutation analysis of *CHMP4B* in family Sk. *A,* Sequence trace of the wild-type allele, showing translation of aspartic-acid (D) at codon 129 (GAT). *B,* Sequence trace of the mutant allele, showing the heterozygous c.386A→T transversion (denoted as W by the International Union of Pure and Applied Chemistry [IUPAC] code) that is predicted to result in the missense substitution of valine (GTT) for aspartate at codon 129 (p.D129V). Exons and flanking intron regions were amplified with gene-specific primers (M13-tailed) by use of the AmpliTaq PCR Master Mix in a GeneAmp 9700 thermal-cycler (Applied Biosystems). Resulting amplicons were purified using the QIAquick gel-extraction kit (Qiagen) and then direct sequenced in both directions with M13-primers and the BigDye Terminator (v.3.1) cycle sequencing kit on a 3130xl genetic analyzer running SeqScape mutation-profiling software (Applied Biosystems). *C,* Allele-specific PCR analysis using the three primers (table 3) indicated by arrows in the schematic diagram; exon 3 was amplified as above with the sense (anchor) primer located in intron 2 (Ex3F), the anti-sense primer located in intron 3 (Ex3R), and the nested mutant primer specific for the T allele in codon 129 (T-alleleR). PCR products were visualized (302 nm) on 2% agarose gels stained with ethidium bromide (EtBr). Note that only affected members of family Sk are heterozygous for the T allele (171 bp), with the exception of individual V:5, who is believed to be presymptomatic or nonpenetrant for cataracts.

Table 2. Two-Point LOD Scores (Z) for Linkage between the Cataract Locus and Markers on Chromosome 20q Listed in Physical Order (Mb) from the Short-Arm Telomere (p-tel)

Marker	Distance from p-tel		Z[a] at θ =							
	cM	Mb	.00	.05	.10	.20	.30	.40	Z_{max}	θ_{max}
D20S885	39.9	17.91	−7.79	2.51	2.72	2.35	1.60	.74	2.72	.10
D20S111	49.2	29.94	−2.82	1.14	1.17	.91	.54	.19	1.18	.08
D20S837	50.7	30.73	−.81	4.15	3.98	3.18	2.14	1.01	4.15	.05
rs2057262		31.15	−4.03	−.02	.14	.16	.09	.03	.17	.15
D20S195	50.2	31.29	3.65	4.17	3.88	2.96	1.90	.87	4.20	.03
CHMP4B (A>T)		31.90	6.24	5.87	5.37	4.19	2.82	1.36	6.24	.00
D20S909	50.7	33.92	1.89	1.88	1.72	1.25	.73	.33	1.91	.02
D20S896	50.2	34.16	2.88	2.60	2.30	1.68	1.05	.46	2.88	.00
D20S870	50.7	34.16	3.11	2.93	2.63	1.94	1.23	.59	3.11	.00
D20S847	50.2	34.32	5.50	5.18	4.72	3.60	2.33	1.05	5.50	.00
rs1291139		34.95	−1.85	.99	1.10	.96	.66	.30	1.10	.11
D20S834	50.7	35.43	−1.08	2.07	1.91	1.30	.65	.19	2.07	.05
D20S607	54.9	38.23	−1.61	1.85	2.02	1.81	1.30	.66	2.03	.11
D20S855	56.0	39.08	−.29	3.26	3.19	2.58	1.71	.77	3.27	.06

NOTE.—STR marker allele frequencies used for linkage analysis were those calculated by Généthon/Marshfield/deCODE. A gene frequency of .0001 and a penetrance of 95% were assumed for the disease locus.

[a] Z values were calculated using the MLINK subprogram from the LINKAGE (5.1) package of programs.[34]

p.D129V mutant protein. In contrast, similar expression studies of a splicing mutation in *CHMP2B* underlying FTD, which resulted in truncation (36 amino acids) and miscoding (29 amino acids) at the C-terminus of the full-length protein (residues 1–213), has been associated with redistribution of CHMP2B and the formation of dysmorphic organelles of the late endosomal pathway.[41]

The p.D129V missense substitution was predicted to be located centrally in CHMP4B and to result in the net loss of a negatively charged residue (fig. 5*B*). Domain expression studies have revealed that the N-terminal half of CHMP4A (MIM 610051), an isoform of CHMP4B, is responsible for self-association into polymers and binding to membrane phospholipids.[46] To better appreciate the effects of the p.D129V substitution, we compared the subcellular localization of wild-type and mutant N-terminal fragments of CHMP4B (residues 1–150) comparable to those previously studied.[46,47] As expected, the distribution of the truncated wild-type fragment (FLAG-CHMP4B$_{1–150}$) differed from that of the full-length wild-type protein; the former appeared to be in large polymers and sometimes associated with vacuolar structures (fig. 6*C*), whereas the latter was diffuse (fig. 6*A*). Similarly, the truncated mutant fragment (FLAG-D129V-CHMP4B$_{1–150}$) differed from the full-length mutant protein; the former was concentrated on a punctate perinuclear structure (fig. 6*D*), and the latter was again diffuse (fig. 6*B*). Consistently, however, the truncated mutant fragment (fig. 6*D*) displayed a different subcellular distribution pattern from that of the truncated wild-type fragment (fig. 6*C*).

In addition to MVB formation, CHMP4B is thought to participate in the budding of a number of RNA viruses, including human immunodeficiency virus type-1 (HIV-1), from the surface of infected cells.[45] To further investigate the effect of the p.D129V substitution on CHMP4B activity in a functional assay, we compared the effect of expressing wild-type and mutant protein on release of HIV-1 virus-like-particles (VLPs). To monitor VLP production, human embryonic kidney (HEK 293T) cells were cotransfected with a plasmid encoding the HIV-1 Gag polyprotein (Pr55) and a plasmid encoding wild-type or mutant CHMP4B. HIV-1 Gag forms VLPs in the absence of other viral proteins,[48] and expression of Gag and CHMP4B

Table 3. PCR Primers for Mutation Screening and Transcript Analysis of *CHMP4B*

Primer	Location	Strand	Sequence (5′→3′)[a]
Ex1F	Exon 1	Sense	gtagtcagtggcgcgttg
Ex1R	Intron 1	Antisense	aggcgagtctgatgaaggtg
Ex2F	Intron 1	Sense	cactagaacctcaccctgtgc
Ex2R	Intron 2	Antisense	aaacaaactcaggtgctcgaa
Ex3F	Intron 2	Sense	tcacagggagtcattgcaggg
Ex3R	Intron 3	Antisense	cccaccctggaaaggtgcag
Ex3R2	Intron 3	Antisense	agggacagcctcagggtatcattt
Ex4F	Intron 3	Sense	cacagggtctggaacctggaa
Ex4R	Intron 4	Antisense	tgggcaagctcaggacacaga
Ex5F1	Intron 4	Sense	aacatgttgaacgcaccagtc
Ex5R1	Exon 5	Antisense	AGGTCATTTCAACTGCAACCA
Ex5F2	Exon 5	Sense	CGCTGACTCCACTGCTGAATCC
Ex5R2	Exon 5	Antisense	ctggaaagggtcagctcccg
StartF	Exon 1	Sense	caccATGTCGGTGTTCGGGAAGCT
EndR	Exon 5	Antisense	CATGGATCCAGCCCAGTTCTCCAA
A-alleleR	Exon 3	Antisense	CAGCAATGTCCTGCATTAACTCAT
T-alleleR	Exon 3	Antisense	CAGCAATGTCCTGCATTAACTCAA

[a] Noncoding sequence is shown in lowercase, coding sequence in uppercase.

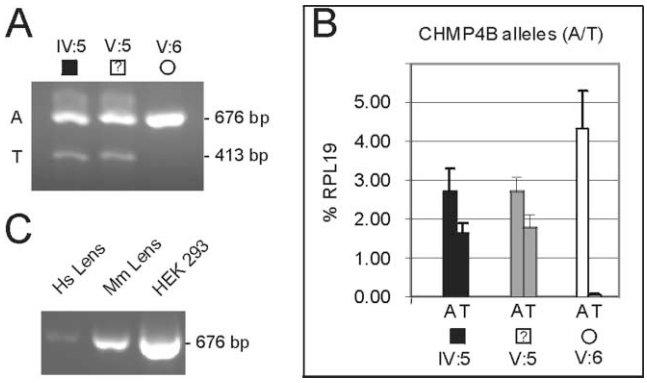

Figure 3. RT-PCR analysis of *CHMP4B* transcripts in peripheral blood leukocytes (PBLs) and eye lens. *A,* Agarose-gel electrophoresis showing nested amplification products of *CHMP4B* transcripts in PBL RNA from family Sk, confirming that individuals IV:5 and V:5 are heterozygous for the mutant T allele (413 bp), whereas individual V:6 is homozygous for the wild-type A allele (676 bp). PBL RNA was purified using the Versagene kit (Gentra), reverse transcribed with the iScript cDNA synthesis kit (Bio-Rad), and PCR amplified as above with three primers (StartF, nested T-alleleR, and EndR) (table 3). *B,* Quantitative amplification of *CHMP4B* transcripts from PBL RNA with allele-specific primers (StartF + A-alleleR, or StartF + T-alleleR) (table 3) showing the relative levels of wild-type (A allele) and mutant (T allele) transcripts in individuals IV:5, V:5, and V:6 from family Sk. RT-PCR products were amplified in a 10-fold dilution series (in triplicate) by use of the iQ SYBR Green Supermix in an iCycler fitted with a MyiQ single-color real-time PCR detection system (Bio-Rad). Allele-specific *CHMP4B* transcripts were detected by melt-curve analysis and standardization against control RPL19 transcript, which was amplified separately in a similar 10-fold dilution series of the same PBL RT-PCR products by use of RPL19 forward (5′-catccgcaagcctgtgac-3′) and reverse (5′-gtgaccttctctggcattcg-3′) primers. *C,* Agarose-gel electrophoresis showing amplicons containing the entire coding region (codons 1–224) of *CHMP4B* transcripts (676 bp) from human (Hs) lens (~30 years old), mouse (Mm) lens (postnatal day 6), and HEK 293 cells. Post mortem human lenses were obtained from the Lions Eye Bank of Oregon, and RNA was extracted using TRIzol reagent (Invitrogen). Following euthanasia (CO_2 gas), mouse lenses were dissected into RNA*later* tissue preservative, and RNA was extracted using the RNAqueous kit (Ambion). RNA was extracted from cultured HEK 293 cells as for mouse lenses. RT-PCR of lens and HEK 293 RNA was performed as for PBL RNA above, with use of StartF and EndR primers (table 3), and the resulting amplicons were verified by sequencing.

within cells and release of Gag into the media as VLPs was detected by immunoblotting (fig. 6*E*). As expected on the basis of previous results,[49] expression of the truncated wild-type fragment (FLAG-CHMP4B$_{1–150}$) inhibited VLP release. Interestingly, the truncated mutant fragment (FLAG-D129V-CHMP4B$_{1–150}$) was a more potent inhibitor than truncated wild type allowing release of only 53% ± 7% (average ± SD) as much Gag in VLPs. Correspondingly, the level of Gag expression in cells expressing the mutant fragment was 1.4 ± 0.3 times that of cells expressing the wild-type fragment. In contrast, neither the wild type nor the mutant forms of full-length CHMP4B significantly inhibited Gag production or VLP release (data not shown).

Precisely how the p.D129V substitution affects the function of CHMP4B is unclear. In this study, we found that the p.D129V substitution changed the subcellular distribution and effects of CHMP4B on VLP release when the protein's acidic C-terminus was removed. Previous studies suggest that the acidic C-termini of CHMPs are regulatory domains that interact specifically with their cognate N-terminal basic domains in an auto-inhibitory manner.[46,49,50] Thus, it is possible that when CHMP4B is relieved from auto-inhibition (mimicked here by truncation), the p.D129V substitution is exposed resulting in deleterious gain-of-function effects. On the basis of expression anal-

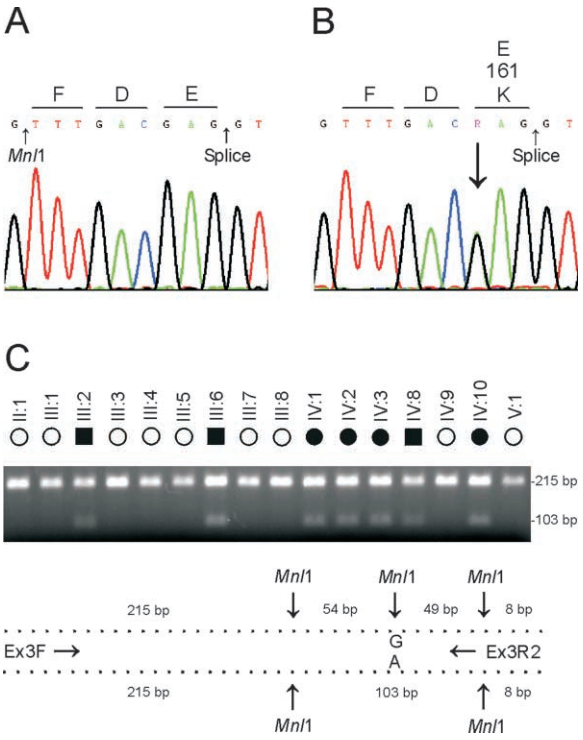

Figure 4. Mutation analysis of *CHMP4B* in the CPP3 family. *A,* Sequence trace of the wild-type allele showing translation of glutamic-acid (E) at codon 161 (GAG). *B,* Sequence trace of the mutant allele showing the heterozygous c.481G→A transition (denoted R by the IUPAC code) that is predicted to result in the missense substitution of lysine (AAG) for glutamate at codon 161 (p.E161K). *C,* Restriction-fragment–length analysis showing loss of an *Mnl*1 site (3′-GGAGN$_6$) that cosegregates only with affected individuals from the Japanese family[31] heterozygous for the c.481G→A transversion (103 bp). Exon 3 was amplified with PCR primers (table 3) shown in the schematic diagram and resulting amplicons (326 bp) digested (at 37°C for 1 h) with *Mnl*1 (5 U; New England BioLabs). Restriction fragments (>75 bp) were visualized on 2% agarose-EtBr gels.

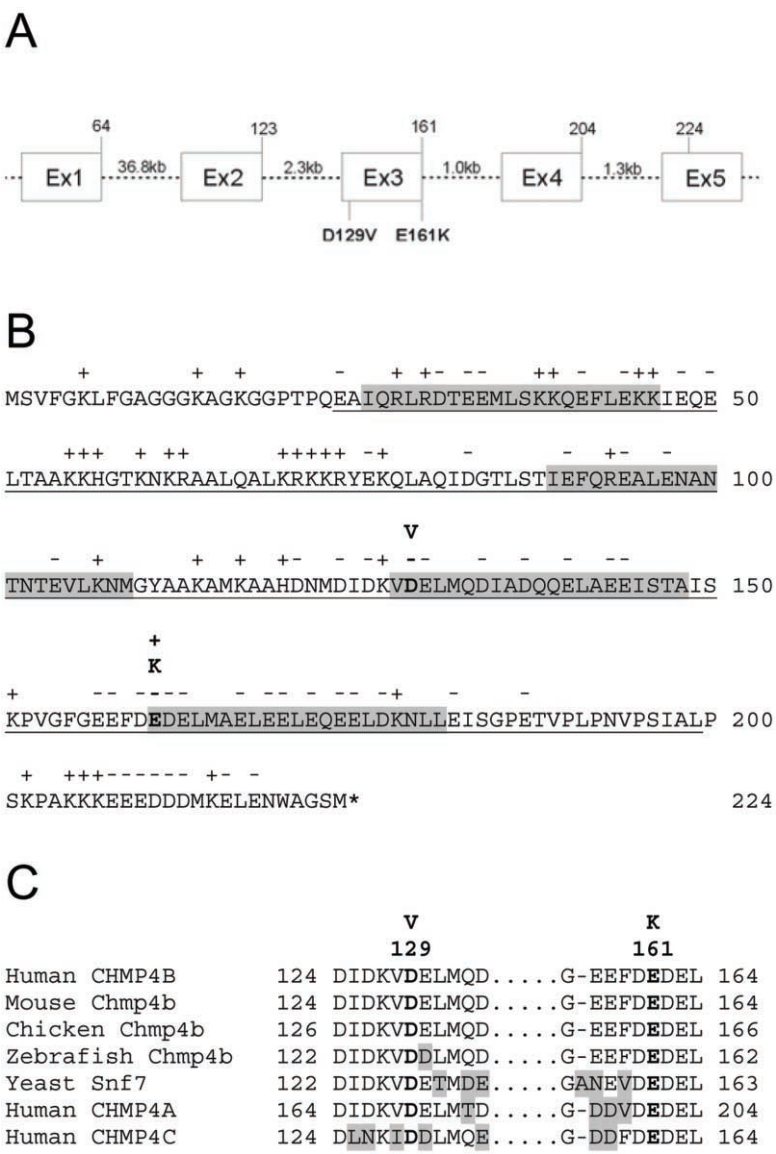

Figure 5. Gene structure and protein domains of CHMP4B. *A,* Exon organization and mutation profile of *CHMP4B*. Intron sizes are indicated (kb), and codons are numbered above each exon. *B,* Amino acid sequence of CHMP4B, showing the conserved SNF7 domain (*underlined*) of this protein family (Conserved Domain Databse, pfam03357) containing at least four predicted helical domains (*grey*). The proposed p.D129V and p.E161K substitutions are predicted to be located in the C-terminal acidic half of the protein, near the start of adjacent helices within the SNF7 domain. Charged amino acids (+, −) and the translation stop codon (*) are also indicated. *C,* Amino acid sequence alignment of human CHMP4B and orthologs from other species, showing phylogenetic conservation of D129 and E161.

ysis of the N-terminal region of CHMP4A,[46] we speculate that, once unmasked, the p.D129V substitution alters the polymerization and/or membrane-binding properties of CHMP4B; however, other mechanisms cannot be excluded. Further work will be required to understand how the p.D129V change affects the behavior of intact CHMP4B. Functional expression studies are also underway to determine how the p.E161K substitution affects CHMP4B. Although little is known about the role of CHMP proteins in lens development, endosome-like compartments have been observed in the newborn mouse lens.[51] Further characterization of endosomal pathways in the lens should provide insight into the pathogenetic mechanisms linking CHMP4B dysfunction with cataractogenesis.

In conclusion, our data identify the first mutations (p.D129V, p.E161K) in a novel gene (*CHMP4B*) for inherited cataracts linked to 20q, and they suggest that gain-of-function defects in an endosome-sorting complex (ESCRT-III) subunit triggers loss of lens transparency.

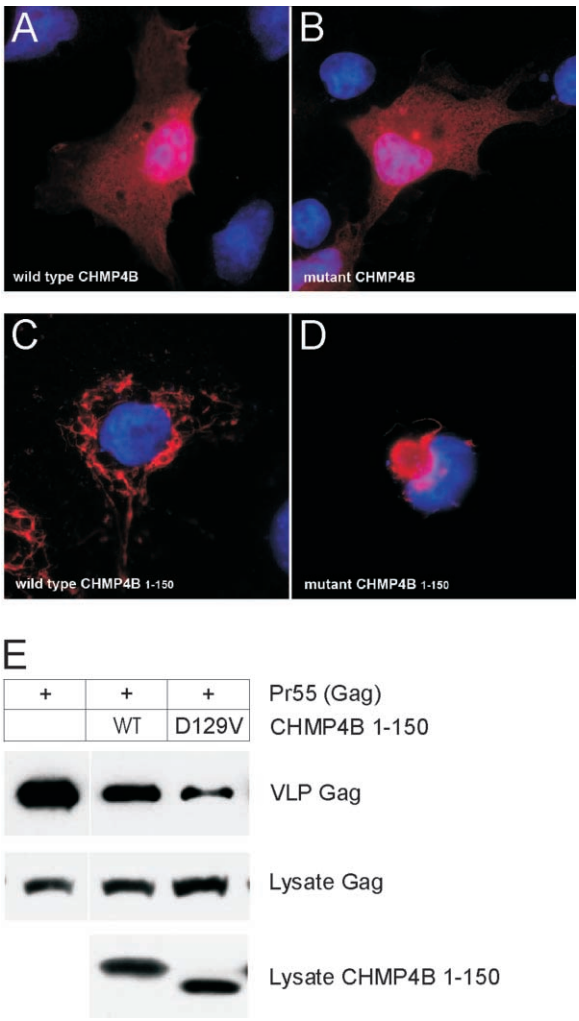

Figure 6. Transient expression of CHMP4B in cultured cells. *A–D,* Subcellular localization of CHMP4B proteins in COS-7 cells, visualized by immunostaining with FLAG antibody and epifluorescence microscopy. *A,* Full-length wild-type FLAG-CHMP4B. *B,* Full-length mutant FLAG-D129V-CHMP4B. *C,* Truncated wild-type FLAG-CHMP4B$_{1-150}$. *D,* Truncated mutant FLAG-D129V-CHMP4B$_{1-150}$. For full-length constructs, the coding sequence (codons 1–224) of human CHMP4B was PCR amplified from HeLa cDNA (Clontech) with forward (5′-gtagatctatgtcggtgt-tcgggaagctgttcgg-3′) and reverse (5′-cactcgagttacatggatccagcccagttctcc-3′) primers and then subcloned into the *Bam*HI and *Xho*I restriction sites in the poly-linker of pcDNA3.1-FLAG.[46] The D129V substitution was generated using the QuickChange mutagenesis kit (Stratagene). For truncated CHMP4B constructs, amplicons corresponding to codons 1–150 were amplified using the full-length constructs as templates and were subcloned into pcDNA3.1-FLAG as above. Plasmid DNA was prepared using the QIAprep spin kit (Qiagen), and inserts were verified by sequencing using the T7 primer. For transient expression, cells were cultured in Dulbecco's modified Eagle's medium (Gibco-BRL) containing 5% fetal bovine serum (Gibco-BRL), 5% supplemented calf serum (Hyclone Laboratories), and 2 mM glutamine. Cells were transfected with expression plasmids by use of Lipofectamine 2000 reagent (Invitrogen). At 18–24 h after transfection, COS-7 cells grown on glass cover slips were fixed in 3.5% paraformaldehyde, permeabilized in 0.2% Triton X-100, and immunostained with rabbit FLAG antibody (Sigma) followed by Alexa Fluor 488 goat anti-rabbit IgG (Molecular Probes). Cell nuclei were counterstained (*blue*) with DAPI (4′,6-Diamidino-2-phenylindole [Molecular Probes]). *E,* Immunoblot analysis of VLPs produced by HEK 293T cells cotransfected with plasmids encoding Gag (p24 antibody) and CHMP4B$_{1-150}$ (FLAG antibody). Top blot shows Gag recovered in VLPs, and middle blot shows Gag in cell lysates. Bottom blot shows that the levels of CHMP4B$_{1-150}$ were similar in cell lysates; however, the D129V substitution increased the electrophoretic mobility of the mutant fragment on SDS (sodium dodecyl sulfate) polyacrylamide gels compared with its wild-type counterpart. For VLPs, HEK 293T cells were transfected with 4 μg pCMV55 encoding HIV Gag, alone or together with 1μg of the indicated CHMP4B construct. At 18–24 h after transfection, media containing VLPs was harvested and clarified by passing through a 0.45 μm filter. VLPs were pelleted by centrifugation (3 h) through a 20% sucrose cushion at 26,000 rpm in SW41 Ti rotor (Beckman Coulter). VLPs and cell lysates were resuspended in sodium dodecyl sulfate (SDS) sample buffer, were separated by SDS-polyacrylamide gel electrophoresis, and then were analyzed by immunoblotting using rabbit antibody against p24, the capsid domain of HIV Gag, horseradish peroxidase (HRP)-conjugated goat anti-rabbit IgG, and the SuperSignal West Pico chemiluminescence detection kit (Pierce). Immunoblot signals were quantified using the Odyssey Infrared Imaging System (Li-Cor Bioscience).

Acknowledgments

We thank family members for participating in this study, Dr. Olivera Boskovska for help with ascertaining family Sk, and Dr. Donna Mackay for preliminary linkage analysis. Dr. Kenneth Johnson kindly provided the pcDNA3.1-FLAG plasmid, and Dr. Lee Ratner kindly provided the HIV GAG expression plasmid (pCMV55) and p24 antibody. This work was supported by National Institutes of Health/National Eye Institute grants EY012284 (to A.S.) and EY02687, and American Heart Association grants 0550148Z and 0750178Z (to P.I.H.).

Web Resources

Accession numbers and URLs for data presented herein are as follows:

ClustalW multiple sequence alignment, http://www.ebi.ac.uk/clustalw/http
Conserved Domain Database (CDD), http://www.ncbi.nlm.nih.gov/Structure/cdd/cdd.shtml
Entrez Protein database, http://www.ncbi.nlm.nih.gov/entrez/query.fcgi?db=Protein
Généthon, Marshfield, and deCODE genetic linkage maps, http://www.ncbi.nlm.nih.gov/genome/guide/human/
LINKAGE/MLINK, http://linkage.rockefeller.edu/soft/
NCBI, http://www.ncbi.nlm.nih.gov/index.html
NCBI Map Viewer, http://www.ncbi.nlm.nih.gov/mapview/
Online Mendelian Inheritance in Man (OMIM), http://www.ncbi.nlm.nih.govOMIM
SNP database (dbSNP), http://www.ncbi.nlm.nih.gov/projects/SNP/
UniGene, http://www.ncbi.nlm.nih.gov/entrez/query.fcgi?db=unigene

References

1. Zetterstrom C, Lundvall A, Kugelberg M (2005) Cataracts in children. J Cataract Refract Surg 31:824–840
2. Shiels A, Hejtmancik JF (2007) Genetic origins of cataract. Arch Ophthalmol 125:165–173
3. Litt M, Kramer P, LaMorticella DM, Murphey W, Lovrien EW, Weleber RG (1998) Autosomal dominant congenital cataract associated with a missense mutation in the human alpha crystallin gene CRYAA. Hum Mol Genet 7:471–474
4. Berry V, Francis P, Reddy MA, Collyer D, Vithana E, MacKay I, Dawson G, Carey AH, Moore A, Bhattacharya SS, et al (2001) Alpha-B crystallin gene (CRYAB) mutation causes dominant congenital posterior polar cataract in humans. Am J Hum Genet 69:1141–1145
5. Mackay DS, Boskovska OB, Knopf HL, Lampi KJ, Shiels A (2002) A nonsense mutation in CRYBB1 associated with autosomal dominant cataract linked to human chromosome 22q. Am J Hum Genet 71:1216–1221
6. Litt M, Carrero-Valenzuela R, LaMorticella DM, Schiltz DW, Mitchell TN, Kramer P, Maumenee IH (1997) Autosomal dominant cerulean cataract is associated with a chain termination mutation in the human β-crystallin gene CRYBB2. Hum Mol Genet 6:665–668
7. Riazuddin SA, Yasmeen A, Yao W, Sergeev YV, Zhang Q, Zulfigar F, Riaz A, Riazuddin S, Hejtmancik JF (2005) Mutations in βB3-crystallin associated with autosomal recessive cataract in two Pakistani families. Invest Ophthalmol Vis Sci 46:2100–2106
8. Kannabiran C, Rogan PK, Olmos L, Basti S, Rao GN, Kaiser-Kupfer M, Hejtmancik JF (1998) Autosomal dominant zonular cataract with sutural opacities is associated with a splice mutation in the βA3/A1-crystallin gene. Mol Vis 4:21
9. Billingsley G, Santhiya ST, Paterson AD, Ogata K, Wodak S, Hosseni SM, Manisastry SM, Vijayalakshmi P, Gopinath PM, Graw J, et al (2006) *CRYBA4* a novel human cataract gene is also involved in microphthalmia. Am J Hum Genet 79:702–709
10. Santhiya ST, Shyam Manohar M, Rawlley D, Vijayalakshmi P, Namperumalsamy P, Gopinath PM, Loster J, Graw J (2002) Novel mutations in the γ-crystallin genes cause autosomal dominant congenital cataracts. J Med Genet 39:352–358
11. Sun H, Ma Z, Li Y, Liu B, Li Z, Ding X, GaoY, Ma W, Tang X, Li X, et al (2005) Gamma-S crystallin gene (CRYGS) mutation causes dominant progressive cortical cataract in humans. J Med Genet 42:706–710
12. Mackay D, Ionides A, Kibar Z, Rouleau G, Berry V, Moore A, Shiels A, Bhattacharya S (1999) Connexin46 mutations in autosomal dominant congenital cataract. Am J Hum Genet 64:1357–1364
13. Shiels A, Mackay D, Ionides A, Berry V, Moore A, Bhattacharya S (1998) A missense mutation in the human connexin50 gene (*GJA8*) underlies autosomal dominant zonular pulverulent cataract on chromosome 1q. Am J Hum Genet 62:526–532
14. Bu L, Jin Y, Shi Y, Chu R, Ban A, Eiberg H, Andres L, Jiang H, Zheng G, Qian M, et al (2002) Mutant DNA binding domain of HSF4 is associated with autosomal dominant lamellar and Marner cataract. Nat Genet 31:276–278
15. Berry V, Francis P, Kaushal S, Moore A, Bhattacharya S (2000) Missense mutations in *MIP* underlie autosomal dominant polymorphic and lamellar cataracts linked to 12q. Nat Genet 25:15–17
16. Pras E, Levy-Nissenbaum E, Bakhan T, Lahat H, Assia E, Geffin-Carmi N, Frydman M, Goldman B, Pras E (2002) A missense mutation in the *LIM2* gene is associated with autosomal recessive presenile cataract in an inbred Iraqi Jewish family. Am J Hum Genet 70:1363–1367
17. Ramachandran RD, Perumalsamy V, Hejtmancik JF (2007) Autosomal recessive juvenile onset cataract associated with mutation in *BFSP1*. Hum Genet 121:475–482
18. Conley YP, Erturk D, Keverline A, Mah TS, Keravala A, Barnes LR, Bruchis A, Hess JF, FitzGerald PG, Weeks DE, et al (2000) A juvenile-onset progressive cataract locus on chromosome 3q21-q22 is associated with a missense mutation in the beaded filament structural protein-2. Am J Hum Genet 66:1426–1431
19. Eiberg H, Lund AM, Warburg M, Rosenberg T (1995) Assignment of congenital cataract Volkmann type (CCV) to chromosome 1p36. Hum Genet 96:33–38
20. Ionides ACW, Berry V, Mackay DS, Moore AT, Bhattacharya SS, Shiels A (1997) A locus for autosomal dominant posterior polar cataract on chromosome 1p. Hum Mol Genet 6:47–51
21. McKay JD, Patterson B, Craig JE, Russell-Eggitt IM, Wirth MG, Burdon KP, Hewitt AW, Cohn AC, Kerdraon Y, Mackey DA (2005) The telomere of human chromosome 1p contains at least two independent autosomal dominant congenital cataract genes. Br J Ophthalmol 89:831–834
22. Rogaev EI, Rogaeva EA, Korovaitseva GI, Farrer LA, Petrin AN, Keryanov SA, Turaeva S, Chumakov I, St George-Hyslop P, Ginter EK (1996) Linkage of polymorphic congenital cataract

to the gamma-crystallin gene locus on human chromosome 2q33–35. Hum Mol Genet 5:699–703
23. Khaliq S, Hameed A, Ismail M, Anwar K, Mehdi SQ (2002) A novel locus for autosomal dominant nuclear cataract mapped to chromosome 2p12 in a Pakistani family. Invest Ophthalmol Vis Sci 43:2083–2087
24. Gao L, Qin W, Cui H, Feng G, Liu P, Gao W, Ma L, Li P, He L, Fu S (2005) A novel locus of coralliform cataract mapped to chromosome 2p24-pter. J Hum Genet 50:305–310
25. Pras E, Pras E, Bakhan T, Levy-Nissenbaum E, Lahat H, Assia EI, Garzozi HJ, Kastner DL, Goldman B, Frydman M (2001) A gene causing autosomal recessive cataract maps to the short arm of chromosome 3. Isr Med Assoc J 3:559–562
26. Heon E, Paterson AD, Fraser M, Billingsley G, Priston M, Balmer A, Schorderet DF, Verner A, Hudson TJ, Munier FL (2001) A progressive autosomal recessive cataract locus maps to chromosome 9q13-q22. Am J Hum Genet 68:772–777
27. Vanita, Singh JR, Sarhadi VK, Singh D, Reis A, Rueschendorf F, Becker-Follmann J, Jung M, Sperling K (2001) A novel form of central pouchlike cataract with sutural opacities maps to chromosome 15q21-22. Am J Hum Genet 68:509–514
28. Armitage MM, Kivlin JD, Ferrell RE (1995) A progressive early onset cataract gene maps to human chromosome 17q24. Nat Genet 9:37–40
29. Berry V, Ionides AC, Moore AT, Plant C, Bhattacharya SS, Shiels A (1996) A locus for autosomal dominant anterior polar cataract on chromosome 17p. Hum Mol Genet 5:415–419
30. Riazuddin SA, Yasmeen A, Zhang Q, Yao W, Sabar MF, Ahmed Z, Riazuddin S, Hejtmancik JF (2005) A new locus for autosomal recessive nuclear cataract mapped to chromosome 19q13 in a Pakistani family. Invest Ophthalmol Vis Sci 46: 623–626
31. Yamada K, Tomita H, Yoshiura K, Kondo S, Wakui K, Fukushima Y, Ikegawa S, Nakamura Y, Amemiya T, Niikawa N (2000) An autosomal dominant posterior polar cataract locus maps to human chromosome 20p12-q12. Eur J Hum Genet 8:535–539
32. Li N, Yang Y, Bu J, Zhao C, Lu S, Zhao J, Yan L, Cui L, Zheng R, Li J, et al (2006) An autosomal dominant progressive congenital zonular nuclear cataract linked to chromosome 20p12.2-p11.23. Mol Vis 12:1506–1510
33. Mackay DS, Andley UP, Shiels A (2003) Cell death triggered by a novel mutation in the alphaA-crystallin gene underlies autosomal dominant cataract linked to chromosome 21q. Eur J Hum Genet 11:784–793
34. Lathrop GM, Lalouel JM, Julier C, Ott J (1984) Strategies for multilocus linkage analysis in humans. Proc Natl Acad Sci USA 81:3443–3446
35. Katoh K, Shibata H, Hatta K, Maki M (2004) CHMP4b is a major binding partner of the ALG-2-interacting protein Alix among the three CHMP4 isoforms. Arch Biochem Biophys 421:159–165
36. Cartegni L, Chew SL, Krainer AR (2002) Listening to silence and understanding nonsense: exonic mutations that affect splicing. Nat Rev Genet 3:285–298
37. Yamada K, Tomita HA, Kanazawa S, Mera A, Amemiya T, Niikawa N (2000) Genetically distinct autosomal dominant posterior polar cataract in a four-generation Japanese family. Am J Ophthalmol 129:159–165
38. West JD, Fisher G (1986) Further experience of the mouse dominant cataract mutation test from an experiment with ethylnitrosourea. Mutat Res 164:127–136
39. Hurley JH, Emr SD (2006) The ESCRT complexes: structure and mechanism of a membrane-trafficking network. Annu Rev Biophys Biomol Struct 35:277–298
40. Horii M, Shibata H, Kobayashi R, Katoh K, Yorikawa C, Yasuda J, Maki M (2006) CHMP7 a novel ESCRT-III related protein associates with CHMP4b and functions in the endosomal sorting pathway. Biochem J 400:23–32
41. Skibinski G, Parkinson NJ, Brown JM, Chakrabarti L, Lloyd SL, Hummerich H, Nielsen JE, Hodges JR, Spillantini MG, Thursgaard T, et al (2005) Mutations in the endosomal ESCRT-III complex subunit CHMP2B in frontotemporal dementia. Nat Genet 37:806–808
42. Parkinson N, Ince PG, Smith MO, Highley R, Skibinski G, Andersen PM, Morrison KE, Pall HS, Hardiman O, Collinge J, et al (2006) ALS phenotypes with mutations in CHMP2B (charged multivesicular body protein 2B). Neurology 67: 1074–1077
43. Talbot K, Ansorge O (2006) Recent advances in the genetics of amyotrophic lateral sclerosis and frontotemporal dementia: common pathways in neurodegenerative disease. Hum Mol Genet 15:R182–R187
44. Katoh K, Shibata H, Suzuki H, Nara A, Ishidoh K, Kominami E, Yoshimori T, Maki M (2003) The ALG-2-interacting protein Alix associates with CHMP4b a human homologue of yeast Snf7 that is involved in multivesicular body sorting. J Biol Chem 278:39104–39113
45. von Schwedler UK, Stuchell M, Muller B, Ward DM, Chung HY, Morita E, Wang HE, Davis T, He GP, Cimbora DM, et al (2003) The protein network of HIV budding. Cell 114:701–713
46. Lin Y, Kimpler LA, Naismith TV, Lauer JM, Hanson PI (2005) Interaction of the mammalian endosomal sorting complex required for transport (ESCRT) III protein hSnf7-1 with itself membranes and the AAA+ ATPase SKD1. J Biol Chem 280: 12799–12809
47. Muziol T, Pineda-Molina E, Ravelli RB, Zamborlini A, Usami Y, Gottlinger H, Weissenhorn W (2006) Structural basis for budding by the ESCRT-III factor CHMP3. Dev Cell 10:821–830
48. Accola MA, Strack B, Gottlinger HG (2000) Efficient particle production by minimal Gag constructs which retain the carboxy-terminal domain of human immunodeficiency virus type 1 capsid-p2 and a late assembly domain. J Virol 74:5395–5402
49. Zamborlini A, Usami Y, Radoshitzky SR, Popova E, Palu G, Gottlinger H (2006) Release of autoinhibition converts ESCRT-III components into potent inhibitors of HIV-1 budding. Proc Natl Acad Sci USA 103:19140–19145
50. Whitley P, Reaves BJ, Hashimoto M, Riley AM, Potter BVL, Holman GD (2003) Identification of mammalian Vps24p as an effector of phosphatidylinositol 3,5-bisphosphate-dependent endosome compartmentalization. J Biol Chem 278: 38786–38795
51. Beebe D, Garcia C, Wang X, Rajagopal R, Feldmeier M, Kim J-Y, Chytil A, Moses H, Ashery-Padan R, Rauchman M (2004) Contributions by members of the TGFbeta superfamily to lens development. Int J Dev Biol 48:845–856

Appendix 2

List of plasmids

Name of plasmid	Key word	Expression type	Antibiotics	Orignal DNA Source	Primers (Fwd/Rev)	Restriction enzyme (5'/3')	backbone vector
pET11a Alix 1-716	**Alix**	bacterial	Amp	Sundquist lab	N/A	N/A	pET11a
pET11a Alix 1-868	**Alix**	bacterial	Amp	Sundquist lab	N/A	N/A	pET11a
pET11a Alix 1-876	**Alix**	bacterial	Amp	Sundquist lab	N/A	N/A	pET11a
pCI FLAG Alix 1-868	**Alix**	mammalian	Amp	Sundquist lab	N/A	N/A	pCI
pCI FLAG Alix 1-868	**Alix**	mammalian	Amp	Sundquist lab	N/A	N/A	pCI
AMSH GFP	**AMSH**	mammalian	Kan	Stahl Lab	N/A	N/A	N/A
pGEX CHMP1B 106-136	**CHMP1B**	bacterial	Amp	Cloned by SS	PHA903/PHA899	BamHI/XhoI	pGEX 4T1
pGEX CHMP1B 106-168	**CHMP1B**	bacterial	Amp	Cloned by SS	PHA903/PHA900	BamHI/XhoI	pGEX 4T1
pGEX CHMP1B 106-181	**CHMP1B**	bacterial	Amp	Cloned by SS	PHA903/PHA901	BamHI/XhoI	pGEX 4T1
pGEX CHMP1B 106-199 (C-term half)	**CHMP1B**	bacterial	Amp	Cloned by SS	PHA903/PHA820	BamHI/XhoI	pGEX 4T1
pGEX CHMP1B 1-168	**CHMP1B**	bacterial	Amp	Cloned by SS	PHA898/PHA900	BamHI/XhoI	pGEX 4T1
pGEX CHMP1B 1-181	**CHMP1B**	bacterial	Amp	Cloned by SS	PHA898/PHA901	BamHI/XhoI	pGEX 4T1
pcDNA3.1 FLAG CHMP1B	**CHMP1B**	mammalian	Amp	Cloned by SS	PHA819/PHA820	BamHI/XhoI	pcDNA3.1 FLAG
pcDNA3.1 FLAG CHMP1B 1-105	**CHMP1B**	mammalian	Amp	Cloned by SS	PHA898/PHA902	BamHI/XhoI	pcDNA3.1 FLAG
pcDNA3.1 FLAG CHMP1B 1-136	**CHMP1B**	mammalian	Amp	Cloned by SS	PHA898/PHA899	BamHI/XhoI	pcDNA3.1 FLAG
pcDNA3.1 FLAG CHMP1B 1-168	**CHMP1B**	mammalian	Amp	Cloned by SS	PHA898/PHA900	BamHI/XhoI	pcDNA3.1 FLAG
pcDNA3.1 FLAG CHMP1B 1-181	**CHMP1B**	mammalian	Amp	Cloned by SS	PHA898/PHA901	BamHI/XhoI	pcDNA3.1 FLAG
pcDNA3.1 FLAG CHMP1B 1-181 DE158,159AA	**CHMP1B**	mammalian	Amp	Quickchanged by TN/SS	PHA928/PHA929	BamHI/XhoI	pcDNA3.1 FLAG
pcDNA3.1 FLAG CHMP1B FL DE158,159AA	**CHMP1B**	mammalian	Amp	Quickchanged by TN/SS	PHA928/PHA929	BamHI/XhoI	pcDNA3.1 FLAG
pcDNA4TO CHMP1B myc	**CHMP1B**	mammalian	Amp	Cloned by SS	PHA819/PHA886	BamHI/XhoI	pcDNA4TO myc
pcDNA4TO Vps2-1(CHMP2A) 1-206 myc	**CHMP2A**	bacterial	Amp	Cloned by SS	PHA802/PHA836	BamHI/XhoI	pGEX 4T1
pET28a Vps2-1(CHMP2A) 1-144	**CHMP2A**	bacterial	Kan	Cloned by SS	cut and paste	BamHI/XhoI	pET28a
pET28a Vps2-1(CHMP2A) 1-180	**CHMP2A**	bacterial	Kan	Cloned by SS	cut and paste	BamHI/XhoI	pET28a
pET28a Vps2-1(CHMP2A) FL	**CHMP2A**	bacterial	Kan	Cloned by SS	PHA802/PHA792	BamHI/XhoI	pET28a
pGEX Vps2-1(CHMP2A) 1-144	**CHMP2A**	bacterial	Amp	Cloned by SS	cut and paste	BamHI/XhoI	pGEX 4T1
pGEX Vps2-1(CHMP2A) 1-144	**CHMP2A**	bacterial	Amp	Cloned by SS	cut and paste	BamHI/XhoI	pGEX 4T1
pGEX Vps2-1(CHMP2A) 1-180	**CHMP2A**	bacterial	Amp	Cloned by SS	cut and paste	BamHI/XhoI	pGEX 4T1
pGEX Vps2-1(CHMP2A) 1-193	**CHMP2A**	bacterial	Amp	Cloned by SS	PHA802/PHA833	BamHI/XhoI	pGEX 4T1
pGEX Vps2-1(CHMP2A) 1-203	**CHMP2A**	bacterial	Amp	Cloned by SS	PHA802/PHA851	BamHI/XhoI	pGEX 4T1
pGEX Vps2-1(CHMP2A) 1-206	**CHMP2A**	bacterial	Amp	Cloned by SS	PHA802/PHA837	BamHI/XhoI	pcDNA3.1 FLAG
pGEX Vps2-1(CHMP2A) 1-216	**CHMP2A**	bacterial	Amp	Cloned by SS	PHA802/PHA852	BamHI/XhoI	pGEX 4T1
pGEX Vps2-1(CHMP2A) 1-219	**CHMP2A**	bacterial	Amp	Cloned by SS	PHA802/PHA837	BamHI/XhoI	pGEX 4T1
pGEX Vps2-1(CHMP2A) 56-144	**CHMP2A**	bacterial	Amp	Cloned by SS	PHA791/ PHA792	BamHI/XhoI	pGEX 4T1
pGEX Vps2-1(CHMP2A) 56-180	**CHMP2A**	bacterial	Amp	Cloned by SS	PHA791/ PHA772	BamHI/XhoI	pGEX 4T1
pGEX Vps2-1(CHMP2A) 56-222	**CHMP2A**	bacterial	Amp	Cloned by SS	PHA791/ PHA773	BamHI/XhoI	pGEX 4T1
pGEX Vps2-1(CHMP2A) C-half (117-222)	**CHMP2A**	bacterial	Amp	Cloned by SS	PHA792/PHA904	BamHI/XhoI	pGEX 4T1
pGEX Vps2-1(CHMP2A) FL	**CHMP2A**	bacterial	Amp	Cloned by SS	cut and paste	BamHI/XhoI	pGEX 4T1
pGEX Vps2-1(CHMP2A) L216A	**CHMP2A**	bacterial	Amp	Cloned by SS	PHA802/PHA792	BamHI/XhoI	pGEX 4T1
pGEX Vps2-1(CHMP2A) S203A	**CHMP2A**	bacterial	Amp	Cloned by SS	PHA802/PHA792	BamHI/XhoI	pGEX 4T1
Lenti CHMP2A shRNA C6	**CHMP2A**	mammalian	Amp	TRC1	N/A	N/A	pLKO
Lenti CHMP2A shRNA C8	**CHMP2A**	mammalian	Amp	TRC1	N/A	N/A	pLKO
pcDNA3.1 FLAG Vps2-1(CHMP2A) C-half (117-222)	**CHMP2A**	mammalian	Amp	Cloned by SS	PHA792/PHA904	BamHI/XhoI	pcDNA3.1 FLAG
pcDNA3.1 FLAG Vps2-1(CHMP2A) 1-116	**CHMP2A**	mammalian	Amp	Cloned by SS	PHA730/PHA771	BamHI/XhoI	pcDNA3.1 FLAG
pcDNA3.1 FLAG Vps2-1(CHMP2A) 1-144	**CHMP2A**	mammalian	Amp	Cloned by SS	PHA730/PHA772	BamHI/XhoI	pcDNA3.1 FLAG
pcDNA3.1 FLAG Vps2-1(CHMP2A) 1-180	**CHMP2A**	mammalian	Amp	Cloned by SS	PHA730/PHA773	BamHI/XhoI	pcDNA3.1 FLAG

pcDNA3.1 FLAG Vps2-1(CHMP2A) 1-193	**CHMP2A**	mammalian	Amp	Cloned by SS	PHA802/PHA833	BamHI/XhoI	pGEX 4T1
pcDNA3.1 FLAG Vps2-1(CHMP2A) 1-206	**CHMP2A**	mammalian	Amp	Cloned by SS	PHA802/PHA835	BamHI/XhoI	pcDNA3.1 FLAG
pcDNA3.1 FLAG Vps2-1(CHMP2A) 1-206 DE153,154	**CHMP2A**	mammalian	Amp	Quickchanged by TN/SS	PHA930/PHA931	BamHI/XhoI	pcDNA3.1 FLAG
pcDNA3.1 FLAG Vps2-1(CHMP2A) 1-206 DE169,170	**CHMP2A**	mammalian	Amp	Quickchanged by SS	PHA825/PHA826	BamHI/XhoI	pcDNA3.1 FLAG
pcDNA3.1 FLAG Vps2-1(CHMP2A) 1-206 DE177,178	**CHMP2A**	mammalian	Amp	Quickchanged by TN/SS	PHA932/PHA933	BamHI/XhoI	pcDNA3.1 FLAG
pcDNA3.1 FLAG Vps2-1(CHMP2A) 1-219	**CHMP2A**	mammalian	Amp	Cloned by SS	PHA802/PHA837	BamHI/XhoI	pcDNA3.1 FLAG
pcDNA31. FLAG Vps2-1(CHMP2A) 56-180	**CHMP2A**	mammalian	Amp	Cloned by SS	PHA791/PHA773	BamHI/XhoI	pcDNA3.1 FLAG
pcDNA3.1 FLAG Vps2-1(CHMP2A) 56-203	**CHMP2A**	mammalian	Amp	Cloned by SS	PHA791/PHA851	BamHI/XhoI	pcDNA3.1 FLAG
pcDNA3.1 FLAG Vps2-1(CHMP2A) 56-222	**CHMP2A**	mammalian	Amp	Cloned by SS	PHA791/PHA792	BamHI/XhoI	pcDNA4TO myc
pcDNA3.1 FLAG Vps2-1(CHMP2A) FL	**CHMP2A**	mammalian	Amp	Cloned by SS	cut and paste	BamHI/XhoI	pcDNA3.1 FLAG
pcDNA3.1 FLAG Vps2-1(CHMP2A) FL DE169,170 AA	**CHMP2A**	mammalian	Amp	Quickchanged by SS	PHA825/PHA826	BamHI/XhoI	pcDNA3.1 FLAG
pcDNA4TO FLAG Vps2-1(CHMP2A) 1-180	**CHMP2A**	mammalian	Amp	cloned by SS	cut and paste	HindIII-FLAG-BamHI-cDNA-Xho	pcDNA4TO
pcDNA4TO FLAG Vps2-1(CHMP2A) FL	**CHMP2A**	mammalian	Amp	cloned by SS	cut and paste	HindIII-FLAG-BamHI-cDNA-Xho	pcDNA4TO
pcDNA4TO N-myc CHMP2A 1-180	**CHMP2A**	mammalian	Amp	Cloned by SS	cut and paste	BamHI/XhoI	pcDNA4TO N-myc
pcDNA4TO N-myc CHMP2A FL	**CHMP2A**	mammalian	Amp	Cloned by SS	cut and paste	BamHI/XhoI	pcDNA4TO N-myc
pcDNA4TO Vps2-1(CHMP2A) myc 1-144	**CHMP2A**	mammalian	Amp	Cloned by SS	PHA802/PHA804	BamHI/XhoI	pcDNA4 TO myc
pcDNA4TO Vps2-1(CHMP2A) myc 1-180	**CHMP2A**	mammalian	Amp	Cloned by SS	PHA802/PHA803	BamHI/XhoI	pcDNA4 TO myc
pcDNA4TO Vps2-1(CHMP2A) myc FL	**CHMP2A**	mammalian	Amp	Cloned by SS	PHA802/PHA793	BamHI/XhoI	pcDNA4 TO myc
pcDNA4TO Vps2-1(CHMP2A) myc FL(DE169,170AA	**CHMP2A**	mammalian	Amp	Quickchanged by TN/SS	PHA825/PHA826	BamHI/XhoI	pcDNA4 TO myc
pcDNA4TO Vps2-1(CHMP2A) myc FL(L216A)	**CHMP2A**	mammalian	Amp	Quickchanged by TN/SS	PHA831/PHA832	BamHI/XhoI	pcDNA4 TO myc
pcDNA4TO Vps2-1(CHMP2A) myc FL(S203A)	**CHMP2A**	mammalian	Amp	Quickchanged by TN/SS	PHA827/PHA828	BamHI/XhoI	pcDNA4 TO myc
pcDNA4TO Vps2-1(CHMP2A) myc FL(S203D)	**CHMP2A**	mammalian	Amp	Quickchanged by TN/SS	PHA829/PHA830	BamHI/XhoI	pcDNA4 TO myc
pCR blunt Vps2-1(CHMP2A) FL	**CHMP2A**	mammalian	N/A	Cloned by LK	N/A	N/A	pCR blunt
Lenti CHMP2B shRNA C2	**CHMP2B**	mammalian	Amp	TRC1	N/A	N/A	pLKO
Lenti CHMP2B shRNA C4	**CHMP2B**	mammalian	Amp	TRC1	N/A	N/A	pLKO
pcDNA3.1 FLAG CHMP2B	**CHMP2B**	mammalian	Amp	Cloned by SS	PHA950/PHA951	EcoRV/XhoI	pcDNA3.1 FLAG
pcDNA4TO CHMP2B myc	**CHMP2B**	mammalian	Amp	Cloned by SS	PHA944/PHA945	Blunt (BamHI-BglI)/XhoI	pcDNA4TO myc
pcDNA4TO N-myc CHMP2B 1-179	**CHMP2B**	mammalian	Amp	Cloned by SS	cut and paste	BamHI/XhoI	pcDNA4TO N-myc
pcDNA4TO N-myc CHMP2B FL	**CHMP2B**	mammalian	Amp	Cloned by SS	cut and paste	Blunt (BamHI-BglI)/XhoI	pcDNA4TO N-myc
pcDNA4TO N-myc CHMP2B intron5	**CHMP2B**	mammalian	Amp	Cloned by SS	cut and paste	BamHI/XhoI	pcDNA4TO N-myc
pET28a hVps24(CHMP3) FL (with PCR mutations)	**CHMP3**	bacterial	Kan	Cloned before 2005	N/A	N/A	pET28a
pGEX Vps24(CHMP3) FL (mutations corrected)	**CHMP3**	bacterial	Amp	Cloned by SS	PHA805/PHA806	BamHI/XhoI	pGEX 4T1
pGEX hVps24(CHMP3) FL (with PCR mutations)	**CHMP3**	bacterial	Amp	Cloned before 2005	N/A	N/A	pGEX 4T1
hVps24(CHMP3)-GFP	**CHMP3**	mammalian	Kan	Cloned before 2005	N/A	N/A	N/A
hVps24(CHMP3)-GFP N half	**CHMP3**	mammalian	Kan	Cloned before 2005	N/A	N/A	N/A
hVps24(CHMP3)-myc (PCR mutations)	**CHMP3**	mammalian	Amp	Cloned before 2005	N/A	N/A	N/A
Lenti CHMP3 shRNA D4	**CHMP3**	mammalian	Amp	TRC1	N/A	N/A	pLKO
pcDNA3.1 hVps24(CHMP3) myc FL (G149E)	**CHMP3**	mammalian	Amp	Quickchanged by TN/SS	PHA798/PHA799	HindIII/XbaI	pcDNA3.1(-) myc his
pcDNA3.1 hVps24(CHMP3) myc FL (WT, no mutatio	**CHMP3**	mammalian	Amp	Quickchanged by TN/SS	PHA800/PHA801	XhoI/BamHI	pcDNA3.1(-) myc his
pcDNA4TO hVps24(CHMP3) myc 1-119	**CHMP3**	mammalian	Amp	Cloned by TN/SS	PHA774/PHA775	BamHI/XhoI	pcDNA4 TO myc
pcDNA4TO hVps24(CHMP3) myc 1-150	**CHMP3**	mammalian	Amp	Cloned by TN/SS	PHA774/PHA776	BamHI/XhoI	pcDNA4 TO myc
pcDNA4TO hVps24(CHMP3) myc 1-178(WT; G149E)	**CHMP3**	mammalian	Amp	Quickchanged by TN/SS	PHA798/PHA799	BamHI/XhoI	pcDNA4 TO myc
pET28a hSnf7-1(CHMP4A) FL	**CHMP4A**	bacterial	Kan	Cloned before 2005	N/A	N/A	pET28a
pET28a hSnf7-1(CHMP4A) C half	**CHMP4A**	bacterial	Kan	Cloned before 2005	N/A	N/A	pET28a
pET28a hSnf7-1(CHMP4A) N half	**CHMP4A**	bacterial	Kan	Cloned before 2005	N/A	N/A	pET28a
pGEX hSnf7-1(CHMP4A) FL	**CHMP4A**	bacterial	Amp	Cloned before 2005	N/A	N/A	pGEX 4T1
pGEX hSnf7-1(CHMP4A) C half	**CHMP4A**	bacterial	Amp	Cloned before 2005	N/A	N/A	pGEX 4T1

pGEX hSnf7-1(CHMP4A) N half	**CHMP4A**	bacterial	Amp	Cloned before 2005	N/A	N/A	pGEX 4T1
pGEX Snf7-1(CHMP4A) 60-147	**CHMP4A**	bacterial	Amp	Cloned by SS	cut and paste	BamHI/XhoI	pGEX 4T1
pGEX Snf7-1(CHMP4A) 60-181	**CHMP4A**	bacterial	Amp	Cloned by SS	cut and paste	BamHI/XhoI	pGEX 4T1
pGEX Snf7-1(CHMP4A) 60-222	**CHMP4A**	bacterial	Amp	Cloned by SS	cut and paste	BamHI/XhoI	pGEX 4T1
hSnf7-1(CHMP4A) N half monoGFP	**CHMP4A**	mammalian	N/A	Cloned before 2005	N/A	N/A	N/A
hSnf7-1(CHMP4A) monoGFP	**CHMP4A**	mammalian	N/A	Cloned before 2005	N/A	N/A	N/A
hSnf7-1(CHMP4A) myc	**CHMP4A**	mammalian	N/A	Cloned before 2005	N/A	N/A	N/A
hSnf7-1(CHMP4A) myc	**CHMP4A**	mammalian	N/A	Cloned before 2005	N/A	N/A	N/A
hSnf7-1(CHMP4A) no Tag	**CHMP4A**	mammalian	N/A	Cloned before 2005	N/A	N/A	N/A
hSnf7-1(CHMP4A) no Tag	**CHMP4A**	mammalian	N/A	Cloned before 2005	N/A	N/A	N/A
hSnf7-1(CHMP4A)-GFP	**CHMP4A**	mammalian	N/A	Cloned before 2005	N/A	N/A	N/A
hSnf7-1(CHMP4A)-monoGFP	**CHMP4A**	mammalian	N/A	Cloned before 2005	N/A	N/A	N/A
pCAF FLAG hSnf7-1(CHMP4A)	**CHMP4A**	mammalian	N/A	N/A	N/A	N/A	N/A
pcDNA 3.1 FLAG Snf7-1(CHMP4A) 1-147	**CHMP4A**	mammalian	Amp	Cloned by SS	PHA289/PHA711	BamHI/XhoI	pcDNA3.1 FLAG
pcDNA 3.1 FLAG Snf7-1(CHMP4A) 1-181	**CHMP4A**	mammalian	Amp	Cloned by SS	PHA289/PHA712	BamHI/XhoI	pcDNA3.1 FLAG
pcDNA 3.1 FLAG Snf7-1(CHMP4A) 1-209	**CHMP4A**	mammalian	Amp	Cloned by SS	PHA289/PHA713	BamHI/XhoI	pcDNA3.1 FLAG
pcDNA 3.1 FLAG Snf7-1(CHMP4A) 1-48	**CHMP4A**	mammalian	Amp	Cloned by SS	PHA289/PHA708	BamHI/XhoI	pcDNA3.1 FLAG
pcDNA 3.1 FLAG Snf7-1(CHMP4A) 1-58	**CHMP4A**	mammalian	Amp	Cloned by SS	PHA289/PHA709	BamHI/XhoI	pcDNA3.1 FLAG
pcDNA 3.1 FLAG Snf7-1(CHMP4A) 1-80	**CHMP4A**	mammalian	Amp	Cloned by SS	PHA289/PHA710	BamHI/XhoI	pcDNA3.1 FLAG
pcDNA 3.1 FLAG Snf7-1(CHMP4A) 20-116	**CHMP4A**	mammalian	Amp	Cloned by SS	PHA714/PHA634	BamHI/XhoI	pcDNA3.1 FLAG
pcDNA 3.1 FLAG Snf7-1(CHMP4A) 20-147	**CHMP4A**	mammalian	Amp	Cloned by SS	PHA714/PHA711	BamHI/XhoI	pcDNA3.1 FLAG
pcDNA 3.1 FLAG Snf7-1(CHMP4A) 20-181	**CHMP4A**	mammalian	Amp	Cloned by SS	PHA714/PHA712	BamHI/XhoI	pcDNA3.1 FLAG
pcDNA 3.1 FLAG Snf7-1(CHMP4A) 20-222	**CHMP4A**	mammalian	Amp	Cloned by SS	PHA714/PHA290	BamHI/XhoI	pcDNA3.1 FLAG
pcDNA 3.1 FLAG Snf7-1(CHMP4A) 60-116	**CHMP4A**	mammalian	Amp	Cloned by SS	PHA715/PHA634	BamHI/XhoI	pcDNA3.1 FLAG
pcDNA 3.1 FLAG Snf7-1(CHMP4A) 60-147	**CHMP4A**	mammalian	Amp	Cloned by SS	PHA715/PHA711	BamHI/XhoI	pcDNA3.1 FLAG
pcDNA 3.1 FLAG Snf7-1(CHMP4A) 60-181	**CHMP4A**	mammalian	Amp	Cloned by SS	PHA715/PHA712	BamHI/XhoI	pcDNA3.1 FLAG
pcDNA 3.1 FLAG Snf7-1(CHMP4A) 60-222	**CHMP4A**	mammalian	Amp	Cloned by SS	PHA715/PHA290	BamHI/XhoI	pcDNA3.1 FLAG
pcDNA3.1 FLAG hSnf7-1(CHMP4A)	**CHMP4A**	mammalian	Amp	Cloned before 2005	N/A	N/A	pcDNA3.1 FLAG
pcDNA3.1 FLAG hSnf7-1(CHMP4A) C half	**CHMP4A**	mammalian	Amp	Cloned before 2005	N/A	N/A	pcDNA3.1 FLAG
pcDNA3.1 FLAG hSnf7-1(CHMP4A) C half	**CHMP4A**	mammalian	Amp	Hanson lab	N/A	BamHI/XhoI	pcDNA3.1 FLAG
pcDNA3.1 FLAG hSnf7-1(CHMP4A) D126V	**CHMP4A**	mammalian	Amp	Quickchanged by SS	PHA778/PHA781	BamHI/XhoI	pcDNA3.1 FLAG
pcDNA3.1 FLAG hSnf7-1(CHMP4A) D126V 1-147	**CHMP4A**	mammalian	Amp	Quickchanged by SS	PHA778/PHA781	BamHI/XhoI	pcDNA3.1 FLAG
pcDNA3.1 FLAG hSnf7-1(CHMP4A) FL	**CHMP4A**	mammalian	Amp	Cloned before 2005	N/A	N/A	pcDNA3.1 FLAG
pcDNA3.1 FLAG hSnf7-1(CHMP4A) N(S2C)	**CHMP4A**	mammalian	Amp	Cloned before 2005	N/A	BamHI/XhoI	pcDNA3.1 FLAG
pcDNA3.1 FLAG hSnf7-1(CHMP4A) N(WT)	**CHMP4A**	mammalian	Amp	Quickchange by LK	N/A	BamHI/XhoI	pcDNA3.1 FLAG
pcDNA3.1 FLAG Snf7-1(CHMP4A) EE177,178AA	**CHMP4A**	mammalian	Amp	Quickchanged by TN/SS	N/A	BamHI/XhoI	pcDNA3.1 FLAG
pcDNA3.1 hSnf7-1(CHMP4A) myc-his D126V	**CHMP4A**	mammalian	Amp	Quickchanged by SS	PHA778/PHA781	HindIII/XbaI	pcDNA3.1(-) myc his
pcDNA3.1 N-myc hSnf7-1(CHMP4A) 1-181	**CHMP4A**	mammalian	Amp	Cloned by SS	cut and paste	BamHI/XhoI	pcDNA3.1 N-myc
pcDNA3.1 N-myc hSnf7-1(CHMP4A) 1-209	**CHMP4A**	mammalian	Amp	Cloned by SS	cut and paste	BamHI/XhoI	pcDNA3.1 N-myc
pcDNA3.1 N-myc hSnf7-1(CHMP4A) 20-222	**CHMP4A**	mammalian	Amp	Cloned by SS	cut and paste	BamHI/XhoI	pcDNA3.1 N-myc
pcDNA4TO N-myc hSnf7-1(CHMP4A) 1-181	**CHMP4A**	mammalian	Amp	cloned by SS	cut and paste	HindIII-Myc-BamHI-cDNA-XhoI	pcDNA4TO
pcDNA4TO N-myc Snf7-1(CHMP4A) FL	**CHMP4A**	mammalian	Amp	cloned by SS	cut and paste	BamHI/XhoI	pcDNA4TO N-myc
pcDNA3.1 FLAG hSnf7-2(CHMP4B) 1-150	**CHMP4B**	mammalian	Amp	Cloned by SS	PHA789/PHA790	BamHI/XhoI	pcDNA3.1 FLAG
pcDNA3.1 FLAG hSnf7-2(CHMP4B) 1-150	**CHMP4B**	mammalian	Amp	Cloned by SS	PHA789/PHA790	BamHI/XhoI	pcDNA3.1 FLAG
pcDNA3.1 FLAG hSnf7-2(CHMP4B) 1-185 DV	**CHMP4B**	mammalian	Amp	Cloned by SS	PHA789/PHA797	BamHI/XhoI	pcDNA3.1 FLAG
pcDNA3.1 FLAG hSnf7-2(CHMP4B) 1-185 WT	**CHMP4B**	mammalian	Amp	Cloned by SS	PHA789/PHA797	BamHI/XhoI	pcDNA3.1 FLAG
pcDNA3.1 FLAG hSnf7-2(CHMP4B) D129V	**CHMP4B**	mammalian	Amp	Quickchanged by SS	PHA779/PHA782	BamHI/XhoI	pcDNA3.1 FLAG

pcDNA3.1 FLAG hSnf7-2(CHMP4B) D129V 1-150	**CHMP4B**	mammalian	Amp	Cloned by SS	PHA789/PHA790	BamHI/XhoI	pcDNA3.1 FLAG
pcDNA3.1 FLAG hSnf7-2(CHMP4B) D129V 1-150	**CHMP4B**	mammalian	Amp	Cloned by SS	PHA789/PHA790	BamHI/XhoI	pcDNA3.1 FLAG
pcDNA3.1 FLAG hSnf7-2(CHMP4B) FL	**CHMP4B**	mammalian	Amp	Cloned before 2005	N/A	N/A	pcDNA3.1 FLAG
pCAF FLAG hSnf7-3(CHMP4C)	**CHMP4C**	mammalian	N/A	Cloned before 2005	N/A	N/A	pCAF FLAG
pGEX CHMP5 121-149	**CHMP5**	bacterial	Amp	Cloned by SS	PHA870/PHA896	BamHI/XhoI	pGEX 4T1
pGEX CHMP5 121-149	**CHMP5**	bacterial	Amp	Cloned by SS	PHA870/PHA896	BamHI/XhoI	pGEX 4T1
pGEX CHMP5 121-158	**CHMP5**	bacterial	Amp	Cloned by SS	PHA870/PHA897	BamHI/XhoI	pGEX 4T1
pGEX CHMP5 121-175	**CHMP5**	bacterial	Amp	Cloned by SS	PHA870/PHA877	BamHI/XhoI	pGEX 4T1
pGEX CHMP5 121-175	**CHMP5**	bacterial	Amp	Cloned by SS	PHA870/PHA896	BamHI/XhoI	pGEX 4T1
pGEX CHMP5 121-175	**CHMP5**	bacterial	Amp	Cloned by SS	PHA870/PHA896	BamHI/XhoI	pGEX 4T1
pGEX CHMP5 121-205	**CHMP5**	bacterial	Amp	Cloned by SS	PHA870/PHA878	BamHI/XhoI	pGEX 4T1
pGEX CHMP5 149-175	**CHMP5**	bacterial	Amp	Cloned by SS	PHA905/PHA907	BamHI/XhoI	pGEX 4T1
pGEX CHMP5 149-183	**CHMP5**	bacterial	Amp	Cloned by SS	PHA905/PHA908	BamHI/XhoI	pGEX 4T1
pcDNA3 mouse CHMP5-FLAG	**CHMP5**	mammalian	Amp	Ghosh Lab	N/A	HindIII-cDNA-KpnI-FLAG-XhoI	pcDNA3
pcDNA3.1 FLAG CHMP5 1-175	**CHMP5**	mammalian	Amp	Cloned by SS	PHA817/PHA876	BamHI/XhoI	pcDNA3.1 FLAG
pcDNA3.1 FLAG CHMP5 1-205	**CHMP5**	mammalian	Amp	Cloned by SS	PHA817/PHA878	BamHI/XhoI	pcDNA3.1 FLAG
pcDNA3.1 FLAG CHMP5 149-175	**CHMP5**	mammalian	Amp	Cloned by SS	PHA905/PHA907	BamHI/XhoI	pcDNA3.1 FLAG
pcDNA3.1 FLAG CHMP5 149-183	**CHMP5**	mammalian	Amp	Cloned by SS	PHA905/PHA908	BamHI/XhoI	pcDNA3.1 FLAG
pcDNA3.1 FLAG CHMP5 FL	**CHMP5**	mammalian	Amp	Cloned by SS	PHA817/PHA818	BamHI/XhoI	pcDNA3.1 FLAG
pcDNA3.1 N-Myc CHMP5 121-149	**CHMP5**	mammalian	Amp	Cloned by SS	PHA870/PHA896	BamHI/XhoI	pcDNA3.1 N-myc
pcDNA3.1 N-Myc CHMP5 149-175	**CHMP5**	mammalian	Amp	Cloned by SS	PHA905/PHA907	BamHI/XhoI	pcDNA3.1 N-myc
pcDNA3.1 N-Myc CHMP5 149-183	**CHMP5**	mammalian	Amp	Cloned by SS	PHA905/PHA908	BamHI/XhoI	pcDNA3.1 N-myc
pcDNA4TO CHMP5 1-205 myc	**CHMP5**	mammalian	Amp	Cloned by SS	PHA817/PHA879	BamHI/XhoI	pcDNA4TO myc
pcDNA4TO CHMP5 FL myc	**CHMP5**	mammalian	Amp	Cloned by SS	PHA817/PHA857	BamHI/XhoI	pcDNA4TO myc
pGEX Vps20(CHMP6)	**CHMP6**	bacterial	Amp	Cloned by SS	PHA808/PHA809	EcoRIXhoI	pGEX 4T1
pGEX Vps20(CHMP6)	**CHMP6**	bacterial	Amp	Cloned by SS	PHA808/PHA809	EcoRIXhoI	pGEX 4T1
pcDNA4TO hVps20(CHMP6)-myc-his	**CHMP6**	mammalian	Amp	Cloned by LK	N/A	N/A	pcDNA4TO myc
pcDNA4TO hVps20(CHMP6)-myc-his 1-115	**CHMP6**	mammalian	Amp	Cloned by LK	N/A	N/A	pcDNA4TO myc
pcDNA4TO hVps20(CHMP6)-myc-his 1-147	**CHMP6**	mammalian	Amp	Cloned by LK	N/A	N/A	pcDNA4TO myc
pcDNA4TO hVps20(CHMP6)-myc-his 1-167	**CHMP6**	mammalian	Amp	Cloned by LK	N/A	N/A	pcDNA4TO myc
pcDNA4TO Vps20(CHMP6) no tag T55S	**CHMP6**	mammalian	Amp	Cloned by LK	N/A	N/A	pcDNA4TO myc
pcDNA-Vps20(CHMP6)-myc (deltaQ26)	**CHMP6**	mammalian	Amp	Burbelo lab	N/A	N/A	pcDNA4TO myc
Clathrin-GFP	**clathrin**	mammalian	N/A	N/A	N/A	N/A	pcDNA4TO myc
pcDNA3 FLAG-DOR 0K-HA (all lysine mutated)	**DOR**	mammalian	Amp	von Zastrow lab	N/A	N/A	pcDNA3
pcDNA3 FLAG-DOR-HA	**DOR**	mammalian	Amp	von Zastrow lab	N/A	N/A	pcDNA3
pcDNA3.0 FLAG-DOR	**DOR**	mammalian	Amp	von Zastrow lab	N/A	N/A	pcDNA3.0
pEGFP N1 FLAG-DOR (FLAG-DOR-GFP)	**DOR**	mammalian	Kan	cloned by SS	cut and paste	HindIII/blunt (EcoRV-SmaI)	pEGFP N1
pcDNA4TO EGFR-GFP	**EGFR**	mammalian	Amp	cloned by SS	cut and paste	Blunt/NotI	pcDNA4/TO myc
pN1 EGFP-EGFR(EGFR-GFP)	**EGFR**	mammalian	Kan	From Pike lab	N/A	N/A	pN1 EGFP
pCMV M1-10 (GAG)	**Gag**	mammalian	Amp	Ratner lab	N/A	N/A	N/A
Hrs V5 His pcDNA	**Hrs**	mammalian	Amp	From Stahl Lab	N/A	N/A	N/A
pSPORT6 human Ist1	**Ist1**	mammalian	Amp	purchased from ATCC	N/A	N/A	pSPORT6
Lenti LacZ shRNA A4	**LacZ**	mammalian	Amp	TRC1	N/A	N/A	pLKO
LC3-GFP	**LC3**	mammalian	Kan	Weihl Lab	N/A	N/A	N/A
pCMV 8.2 delta R (Lenti-packaging)	**Lenti**	mammalian	Amp	Stewart Lab	N/A	N/A	pCMV
pCMV VSV-G	**Lenti**	mammalian	Amp	Stewart Lab	N/A	N/A	pCMV
pRRL-GFP (Lenti-GFP)	**Lenti**	mammalian	Amp	Stewart Lab	N/A	N/A	pRRL

pET16b LIP5	**LIP5**	bacterial	Amp	Kaplan Lab	N/A	BamHI/XhoI	pET16b
pET28a LIP5	**LIP5**	bacterial	Kan	Cloned by SS	N/A	NdeI-XhoI/BamHI	pET28a
Lenti LIP5 shRNA B10	**LIP5**	mammalian	Amp	TRC1	N/A	N/A	pLKO
Lenti LIP5 shRNA B9	**LIP5**	mammalian	Amp	TRC1	N/A	N/A	pLKO
Lenti LIP5 shRNA E10	**LIP5**	mammalian	Amp	TRC1	N/A	N/A	pLKO
pEGFP C1- LIP5	**LIP5**	mammalian	Kan	Kaplan Lab	N/A	BglII/KpnI	pEGFP C1
pEGFP C1 LIP5 K148A	**LIP5**	mammalian	Kan	Quickchanged by SS	PHA942/PHA943	KpnI/BamHI	pEGFP C1
pEGFP C1 LIP5 M64A	**LIP5**	mammalian	Kan	Quickchanged by SS	PHA940/PHA941	KpnI/BamHI	pEGFP C1
pEGP C1 LIP5 delta C	**LIP5**	mammalian	Kan	Cloned by SS	PHA855/PHA856	BglII/HindIII	pEGFP C1
pEGFP C1 Rab5 Q79L	**Rab5**	mammalian	Kan	Stahl Lab	N/A	HindIII/XhoI	pEGFP C1
STAM PM1WHA	**STAM**	mammalian	N/A	Stahl Lab	N/A	N/A	N/A
Lenti Tsg101 shRNA A10	**Tsg101**	mammalian	Amp	TRC1	N/A	N/A	pLKO
Lenti Tsg101 shRNA A9	**Tsg101**	mammalian	Amp	TRC1	N/A	N/A	pLKO
pLLEXP Tsg101 FLAG -WT	**Tsg101**	mammalian	N/A	Cohen lab	N/A	N/A	pLLEXP
UBPY GFP	**UBPY**	mammalian	Kan	Stahl Lab	N/A	N/A	N/A
pET28a	**vector**	bacterial	Kan	Hanson lab	N/A	N/A	pET28a
pBS SK+	**vector**	mammalian	N/A	Hanson Lab	N/A	N/A	pBS SK+
pcDNA3.1 FLAG3NK3B (vector + insert)	**vector**	mammalian	Amp	Kornfeld Lab	N/A	N/A	pcDNA3.1 FLAG
pcDNA3.1 Zeo (+)	**vector**	mammalian	Amp	Hanson Lab	N/A	N/A	pcDNA3.1
pcDNA4TO-myc-his A	**vector**	mammalian	Amp	Hanson lab	N/A	N/A	pcDNA4/TO myc
pEGFP N1	**vector**	mammalian	Kan	Hanson lab	N/A	N/A	pN1 EGFP
pEGFP C1 Vps4A	**VPA4A**	mammalian	Kan	Sundquist lab	N/A	EcoRI/BamHI	pEGFP C1
pEGFP C1 VPS4A E258A	**VPS4A**	mammalian	Kan	Quickchanged by TN/SS	PHA954/PHA955	EcoRI/BamHI	pEGFP C1
pEGFP C1 VPS4A E228Q	**VPS4A**	mammalian	Kan	Quickchanged by TN/SS	PHA823/PHA924	EcoRI/BamHI	pEGFP C1
pEGFP C1 VPS4A L202A	**VPS4A**	mammalian	Kan	Quickchanged by TN/SS	PHA952/PHA953	EcoRI/BamHI	pEGFP C1
pEGFP C1 VPS4A R254A	**VPS4A**	mammalian	Kan	Quickchanged by TN/SS	PHA927/PHA973	EcoRI/BamHI	pEGFP C1
pEGFP C1 VPS4A E228Q, E258A	**VPS4A**	mammalian	Kan	Quickchanged by TN/SS	PHA954/PHA955	EcoRI/BamHI	pEGFP C1
pEGFP C1 VPS4A E228Q, L202A	**VPS4A**	mammalian	Kan	Quickchanged by TN/SS	PHA952/PHA953	EcoRI/BamHI	pEGFP C1
pEGFP C1 VPS4A E228Q, R254A	**VPS4A**	mammalian	Kan	Quickchanged by TN/SS	PHA927/PHA973	EcoRI/BamHI	pEGFP C1
pGEX VPS4B/SKD1EQ	**VPS4B**	bacterial	Amp	Cloned by SS	N/A	BamHI/XhoI	pGEX 4T1
pGEX VPS4B/SKD1WT	**VPS4B**	bacterial	Amp	Cloned by SS	N/A	BamHI/XhoI	pGEX 4T1
pHO 2d VPS4B/SKD1 WT	**VPS4B**	bacterial	Amp	Cloned before 2005	N/A	NcoI/EcoRI	pHO 2d
PHO 4d VPS4B/SKD1 EQ	**VPS4B**	bacterial	Amp	Cloned by SS	N/A	NcoI/EcoRI	pHO 4d
pHO 4d VPS4B/SKD1 WT	**VPS4B**	bacterial	Amp	Cloned by SS	N/A	NcoI/EcoRI	pHO 4d
pcDNA4 TO VPS4B/SKD1 EQ myc-his	**VPS4B**	mammalian	Amp	Cloned before 2005	N/A	N/A	pcDNA4TO myc
pcDNA4 TO VPS4B/SKD1 WT myc-his	**VPS4B**	mammalian	Amp	Cloned before 2005	N/A	N/A	pcDNA4TO myc
pcDNA4TO VPS4B/SKD1 EQ-GFP	**VPS4B**	mammalian	Amp	Cloned before 2005	N/A	N/A	pcDNA4TO
pcDNA4TO VPS4B/SKD1 WT-GFP	**VPS4B**	mammalian	Amp	Cloned before 2005	N/A	N/A	pcDNA4TO
pEGFP N1 VPS4B/SKD1 EQ	**VPS4B**	mammalian	Kan	Cloned before 2005	N/A	N/A	pEGFP N1
pEGFP N1 VPS4B/SKD1 WT	**VPS4B**	mammalian	Kan	Cloned before 2005	N/A	N/A	pEGFP N1
VPS4B/SKD1 EQ momeric GFP	**VPS4B**	mammalian	Kan	Quickchanged by LK	N/A	N/A	N/A
VPS4B/SKD1 WT momeric GFP	**VPS4B**	mammalian	Kan	Quickchanged by LK	N/A	N/A	N/A

N/A : information is not available
SS: Soomin Shim
LK: Lisa Kimpler
TN: Teri Naismith